UNIVERSITY OF AGDER

Investigation of Stabilization Method for Hydraulically Actuated Boom

Confidential

Rune Husveg
Sondre Nordås

Supervisor:
Ilya Tyapin

Co-Supervisor:
Michael Rygaard Hansen

This master's thesis is carried out as a part of the education at the
University of Agder and is therefore approved as a part of this education.
However, this does not imply that the University answers for the methods
that are used or the conclusions that are drawn.

University of Agder, 2015
Faculty of Engineering and Science
Department of Engineering Sciences

Abstract

It is well known that a counterbalance valve (CBV) tend to introduce instability in load holding systems like cranes and winches, especially when the flow supply is pressure compensated. It is a problem in presents day hydraulic to design stable load lowering systems containing a CBV and a pressure compensated flow supply without compromising system efficiency and response.

This thesis investigates a novel stabilization method, developed by the University of Agder, for stabilizing a hydraulic actuated boom. This method has for its object to assign a low pass filtrated version of its original pressure into the pilot area for the CBV and/or to the pressure compensator. This stabilization method is investigated by means of linearized models, time domain simulations and physical testings.

Based on the work done in this thesis, it can be concluded that this new stabilization method provides a stable system. A first order low pass filter is used for filtration. The break frequency have to be adjusted for each system. Further work should include other filters and hydraulic systems with motors.

Keywords: Counterbalance valve, pressure compensated directional control valve, load holding systems, instability, linearization, time domain simulation, prototyping

Preface

This Master's Thesis in Mechatronics is carried out as a part of the education at the University of Agder Faculty of Engineering and Science Department of Engineering Sciences, spring 2015. The purpose of the project is to investigate a novel method of stabilizing pressure compensated systems containing counterbalance valves.

Counterbalance valves plays an important safety role in load carrying applications e.g. load holding at pipe burst and ensures that no drop occurs before lift. On the other hand is it also known that they tend to introduce instabilities in the system, especially if the flow supply is pressure compensated. A pressure compensation of the flow supply is desired as it provides constant volume flow corresponding to the opening of the control valve, regardless of the load. A method of stabilizing such systems is therefore in the greatest interest of the University, the machine development industry in general and everyone working with hydraulic load holding systems where safety and precision plays important roles.

In this aspect was two potential master projects and a bachelor project presented by the University of Agder in the fall of 2014. The scope of the master projects was to investigate two different methods of stabilizing such a system and to perform physical testing of the stabilizing methods. The scope of the bachelor project was to compose a simulation model of the test rig used for the physical testing so that future stabilization methods can be developed by virtual prototyping. The participants of the second master project are Christian Høgeli Solvik and Thomas Børseth who investigated a stabilization method where the control valve compensates for oscillations using pressure feedback. The participants of the bachelor group are Sondre Efjestad Fjereide, Joao Pedro Ferreira da Costa Pires, Kjetil Bakkelund Omholt and Bjørnar Lie Aas.

The test rig was originally designed by the University of Agder in the fall of 2014, and the construction started early 2015 at the University. The structure was assembled and the hydraulics put together before the rig was handed over to the students. The students received the test rig mid-March due delays in the delivery of some components. The electric cabinet was then assembled by the bachelor group, who followed instructions given by the designer. By the end of March was the rig assembled, but never tested. Several problems with the electric arrangement, and dimensions of the cylinder brackets were discovered and mended during the start-up phase. Also problems in the hydraulics occurred. One of the control valves was not correctly assembled and a wiring diagram, given by the designer, for one of the control valves was not in agreement with the ordered valve. The master groups did, in addition of handling these initial problems, complete the instrumentation of the test rig, including measurement and data logging program development.

The authors would like to express their greatest gratitude to Senior Engineer Jan Andreas Holm, Senior Engineer Eivind Arne Johansen and Staff Engineer Carl Thomas Duus at the University of Agder for outstanding guidance and assistance in the Mechanical Laboratory. We would also like to send our thanks to Senior Engineer Steve Schading and Senior Engineer Jan Andreas Holm for the interviews regarding manual operation of the stabilized test rig.

Grimstad, 2015

Rune Husveg   Sondre Nordås

Contents

Chapter 1

Introduction

1.1   Motivation

Counterbalance valves are widely used in crane and winch applications, on-shore and off-shore. It is well known that they tend to introduce instability when handling negative loads, especially when the flow supply is pressure compensated.

The counterbalance valves possesses qualities which is highly desirable considering safety and system efficiency e.g. prevent cavitation at load lowering, prevent negative loads from dropping in case of pipe or hose failure, ensure no drop before lift, ensure leak tight at load holding, and as shock absorption.

A pressure compensated directional control valve is equipped with an internal compensator in series with the main spool. The compensator ensures a constant volume flow corresponding to position of the main spool, regardless of load. In cases where several actuators are connected to the same flow source is the pressure compensation used to ensures that all actuators receives their designated share of the total available pump flow.

It is a major problem in present day hydraulics to design stable load lowering systems containing counterbalance valve without compromising the effect and response. The main goal of this thesis is therefore to investigate a novel method of stabilizing pressure compensated systems containing counterbalance valves.

1.2   Literature Review

Counter balance valves tends to introduce undesired oscillation while load lowering due to insufficient damping. The degree of oscillations is affected by many variables among which are the effective mass on the actuator, the viscosity of the fluid, the oil flow, the input of the operator and the fluctuation of the pilot signal. Due to the pilot ratio, fluctuation in the pilot pressure will fluctuate the opening of the CBV and the system will oscillate.

The most common solution is to smoothen the pilot pressure. Bosch Rexroth Oil Control has developed modules including CBV and fixed or adjustable restrictions to smoothen the pilot pressure[1]. Four of the most commonly used modules from Bosch are illustrated in Figure 1.1 and Figure 1.2.

A fixed or adjustable damping screw is used to create a smooth and stable pressure acting on the pilot area. As a safety function, a check valve is normally added in parallel with the damping screw in order to reduce the pilot pressure quickly when the pressure drops in the system. The systems illustrated in Figure 1.1 are sensitive to changes in viscosity.

A system which handle the delay problem is shown in Figure 1.2. A small normally open by-pass (VEM) has been added in parallel with the damper screw. When the system pressure reaches crack pressure of the VEM, the valve closes, and the final pressurization is achieved through the damping screw. When a quick closing of the CBV is required, the pilot oil can be discharged through the VEM. It is hard to adjust the orifices in all of the systems shown above. The systems tend to be sensitive for the effective mass acting on the actuator. In [9] a method for optimize the parameters in the damping network in the pilot line is investigated. Numbers of articles regarding the instability of a pressure compensated system including a
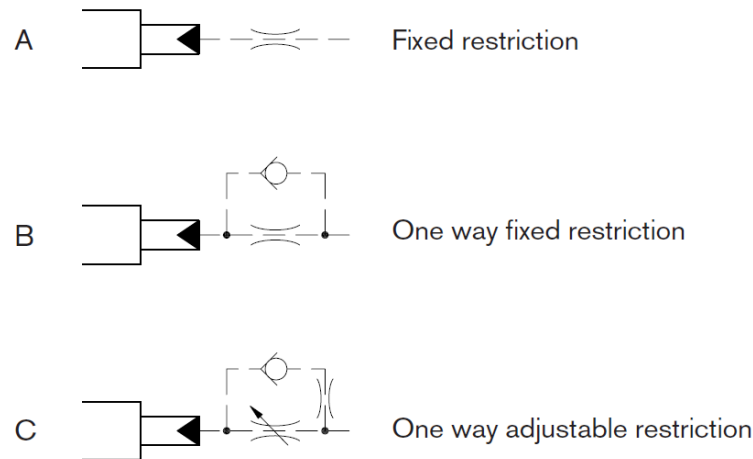
Figure 1.1: Module A, Module B and Module C from Bosch [1]
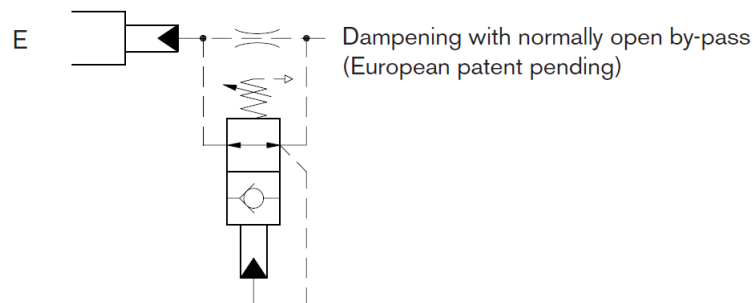
Figure 1.2: Modul E from Bosch [1]

CBV are already published. Even though many aspects of the problem are already investigated is there yet no simple general solution to the problem, meaning that investigations are still ongoing in this field. An example is [12] where a proposition of a design where the main throttling ability is moved from the CBV to the return orifice of the DCV are presented. The CBV is in this proposition piloted open during the lowering, resulting in a stable, but inefficient system with limitations regarding load variation. Further, in [11], is the pressure compensated DCV replaced by a electronic hydraulically actuated DCV with a electronic pressure compensation control system. The control system utilizes a position feedback and velocity feed forward to stabilize the lowering motion. In [10] is a different pressure feedback system investigated. The pilot pressure is measured and filtered by a high pass filter to extract the pressure gradients. Further, is the goal to maintain low, or zero, pressure gradients by regulating the DCV.

1.3   Target of investigation

The main object of the stabilizing method investigated in this thesis is to use a separate circuit, in which the pressure is adjusted as desired, to generate the pressure assigned to the pilot line of the counter balance valve or the compensator in series with the DCV, either separately or simultaneously. The intention of this is to investigate if a filtration of the pressure originally assigned to the components will stabilize the system. The pressure in the separate circuit is therefore adjusted according to a low pass filtration of the pressure originally assigned to the components. The method introduces three different settings which all are investigated in this thesis. The settings are:

Setting 1
      The filtered pressure is only assigned to the pilot line of counterbalance valve.

Setting 2
      The filtered pressure is only assigned to the compensator in series with the DCV.

Setting 3
    The filtered pressure is assigned both to the pilot line of counterbalance valve and the compensator in series with the DCV

1.4 Problem Statement

In order to investigate the stabilizing effect of the three settings is the study divided into the following objectives:

Objective 1
    Theoretically investigate the stabilizing effect of each setting

Objective 2
    Investigate by means of time domain simulation the stabilizing effect of each setting

Objective 3
    Investigate by means of experimental work the stabilizing effect of each setting

If time allows:

Objective 4:
    Investigate the generality and robustness of the stabilizing method

Objective 5:
    Investigate other methods of stabilizing the system

1.5 Report Outline

Chapter 2 introduces the original circuit and provides the main equations used in the investigations. The instability of the original circuit is studied based on the provided equations.

Chapter 3 introduces the test rig used for experimental work. The mechanic and hydraulic aspects of the test rig are described and analyzed. The chapter also presents the electric aspect of the test rig.

Chapter 4 provides a detailed description of the stabilizing method, including a description of the three settings and a description of the separate circuit used for pressure generation.

Chapter 5 presents the theoretical stability investigation of the three settings based on the main equations and the structure of the test rig.

Chapter 6 presents the time domain simulation of each of the three settings.

Chapter 7 presents the physical testing of the settings performed on the test rig.

Chapter 8 discusses the findings and the stabilizing method.

Chapter 9 presents the conclusion and suggestions for further work.

Chapter 2

Theoretical Background

This chapter provides an introduction of the circuit which this thesis is based on. Namely a circuit containing a pressure compensated directional control valve that delivers flow to an actuator on which a counterbalance valve is mounted. Further are the main equations describing each component of the circuit introduced. Also a section containing miscellaneous equations are included. These equations are the basis for the theoretical investigations and simulations through out the thesis. Lastly is the instability, introduced by the combination of a CBV and a pressure compensated DCV, investigated by means of theoretical investigation inspired by [10] and [12].

2.1   Circuit Description

The original circuit consists of three main components, a cylinder, a counterbalance valve (CBV) and a pressure compensated directional control valve (DCV), as shown in Figure 2.1.
The main purpose of this circuit is to lift, or lower a load in a controlled manner. The DCV is used to control the rate of flow which enters the circuit, hence control the speed at which the load is lifted or lowered. The DCV is pressure compensated, meaning the pressure drop across the valve is kept constant. This leaves the rate of flow through the valve only dependent of the discharge area, $A(x)$, see the orifice equation, eq. 2.1.

$$Q = C_D \cdot A(x) \cdot \sqrt{\frac{2}{\rho} \cdot \Delta p} \tag{2.1}$$

where

Q	Volume flow	$\frac{\mathrm{m}^3}{s \cdot \sqrt{\mathrm{Pa}}}$
C_D	Discharge coefficient	-
A	Discharge area	m^2
x	Ball/poppet travel	m
ρ	Mass density	$\frac{\mathrm{kg}}{\mathrm{m}^3}$
Δp	Pressure drop	Pa

The CBV is included in the circuit for several reasons.

- Prevent the load from dropping in case of pipe burst

- Secure a leak tight load holding

- Prevent the load from dropping before lifting

- Prevent cavitation in the circuit during load lowering

5
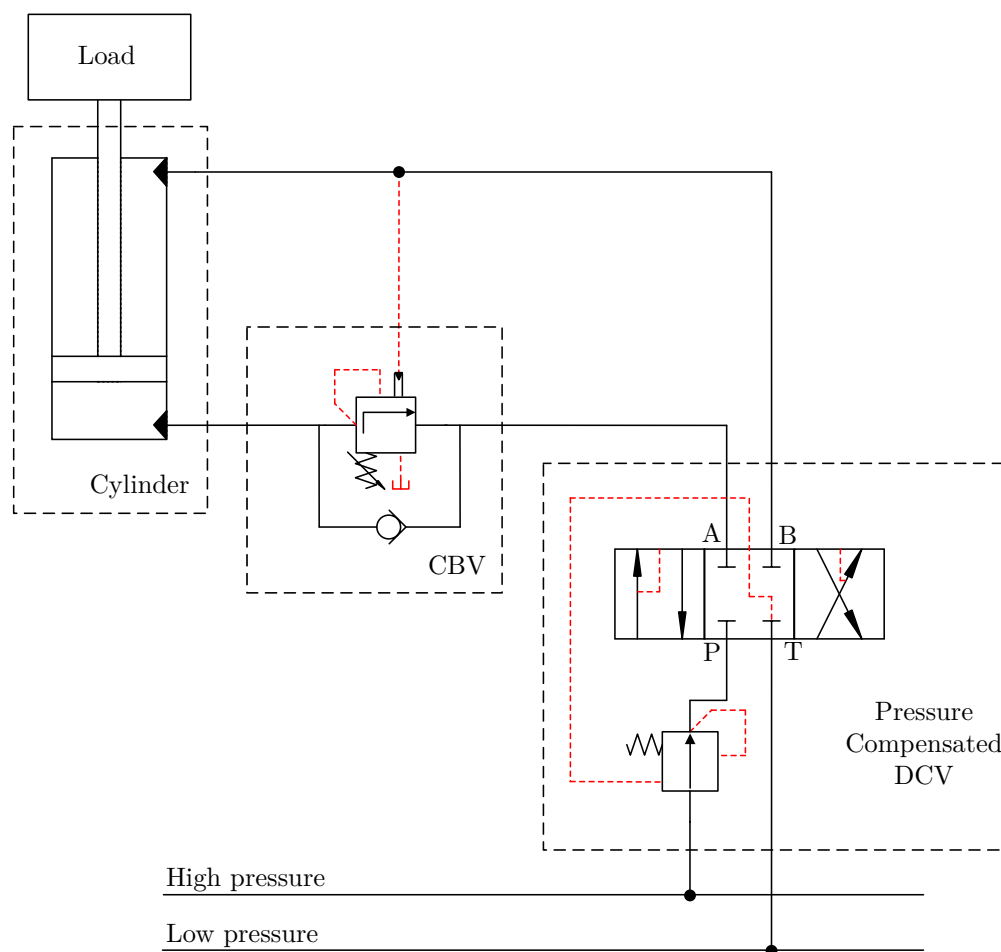
Figure 2.1: Illustration original circuit

- Absorb shocks in the circuit

The CBV is mounted directly to the cylinder, leaving no exposed tubes between the cylinder and the valve. This connection is thereby secured from bursting. The valve prevents the load from dropping in case pipes elsewhere in the circuit should burst. The valve is leak tight, and will therefore prevent creeping of the load. The CBV ensures sufficient pressure build-up between the CBV and the DCV before load lifting is carried out. This ensures no drop of the load before lifting. At normal conditions, a certain pressure level on the ring side of the cylinder (chamber B) is required in order to open the valve. This prevent cavitation in this line during load lowering. If the circuit is left dormant, but pressurized, and exposed for temperature changes, a higher temperature may rise the pressure to a critical level. The CBV will prevent a critical pressure build up by slightly open before the pressure reaches a critical level.

2.2   Component Simplification and Description

Only the lowering of the load is of interest in this thesis. The circuit shown in Figure 2.1 is therefore simplified as shown in Figure 2.2. Note that this circuit is a simplification, and does not represent the complete circuit needed to fully operate the load. The simplified circuit is the basis for the investigation in this thesis and the components described in this section are based on this circuit.

2.2.1   Pressure Compensated Directional Control Valve

The pressure compensated DCV is simplified and represented as a flow control valve (FCV) and an adjustable orifice. The adjustable orifice represents the opening of the main spool in one direction, and the FCV provides
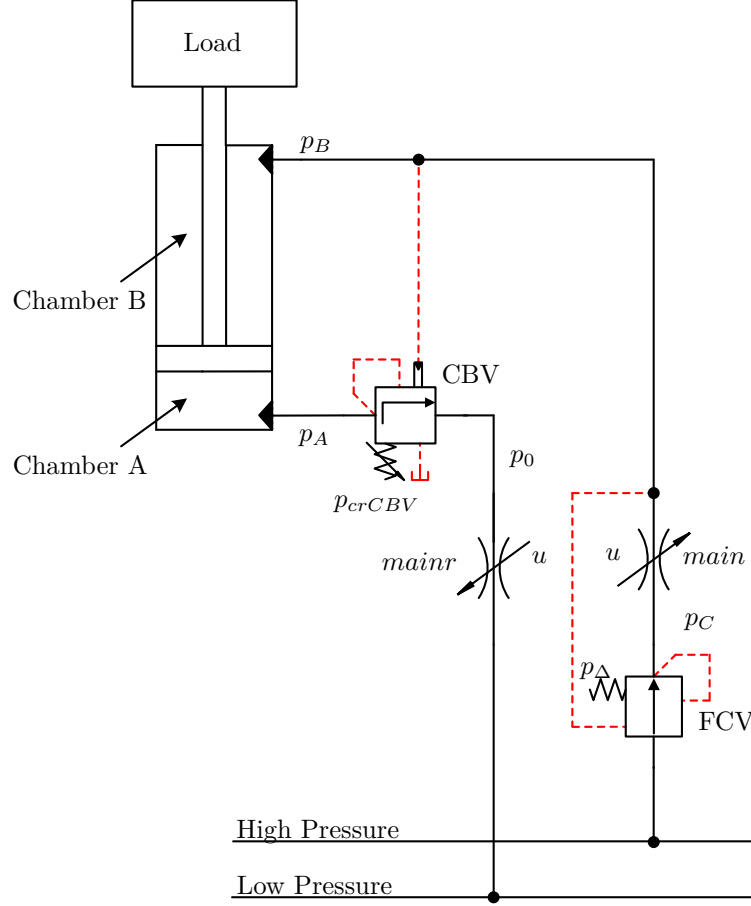
Figure 2.2: Simplified circuit showing the three main components: cylinder, CBV and pressure compensated DCV

the characteristics of the pressure compensation. This simplification is illustrated in Figure 2.3. Note that this figure only illustrates some of the functions of the valve and is therefore not a technical drawing.

The flow through the FCV is calculated based on the orifice equation, eq. 2.1, although some changes in the expression is made. The new expression is based on the rate of opening of the valve, rather than the travel of the ball/poppet. The rate of opening is found by comparing the total pressure acting on the poppet and the pressure needed to fully open the valve. The equation describing the flow through the FCV is shown in eq. 2.2.

$$Q_{FCV} = k_{vFCV} \cdot u_{FCV} \cdot \sqrt{\Delta p_{FCV}} \tag{2.2}$$

where

Q_{FCV}	Volume flow, FCV	$\frac{\text{m}^3}{\text{s}}$
k_{vFCV}	Flow coefficient, FCV	$\frac{\text{m}^3}{\text{s} \cdot \sqrt{\text{Pa}}}$
u_{FCV}	Rate of opening, FCV	-
Δp_{FCV}	Pressure drop, FCV	Pa

The flow coefficient, k_v, can be estimated from a physical test of the valve. The valve is set fully open ($u = 1$) and the pressure drop versus flow characteristics is investigated. This test is usually carried out by the supplier and a curve can be found in the data sheet. k_v is calculated as shown in eq. 2.3, where Q_{ref} and Δp_{ref} are respectively the flow and the corresponding pressure drop found from the curve in the data sheet or by performing a physical test.

7
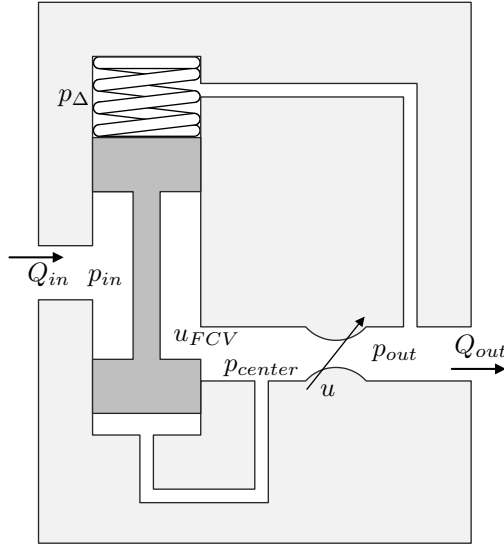
Figure 2.3: Illustration of the pressure compensated DCV

$$k_v = \frac{Q_{ref}}{\sqrt{\Delta p_{ref}}} \tag{2.3}$$

By comparing eq. 2.1 and a general representation of eq. 2.2, shown in eq. 2.4, is it seen that the flow coefficient, k_v, in some extent, takes into account for the parameters C_d, A and ρ and is therefore a representation of the physical attributes of the valve based on a performance test.

$$Q = k_v \cdot u \cdot \sqrt{\Delta p} \tag{2.4}$$

An expression for the rate of the opening of the FCV is found based on the illustration of the valve in Figure 2.3. In this expression is the pressures acting on the spool summed and divided by the total pressure needed to fully open the valve. The expression is shown in eq. 2.5.

$$u_{FCV} = \begin{cases} 1, & u_{FCV} > 1 \\ \frac{p_{back} + p_\Delta - p_{center}}{\Delta p_{open_{FCV}}}, & 0 \leq u_{FCV} \leq 1 \\ 0, & u_{FCV} < 0 \end{cases} \tag{2.5}$$

where

p_{out}	Back pressure	Pa
p_{center}	Pressure between FCV and main spool	Pa
p_Δ	Desired pressure drop across the main valve	Pa
$\Delta p_{open_{FCV}}$	Pressure needed to fully open the FCV	Pa

As mentioned, the purpose of the FCV is to keep the pressure drop across the main valve constant and known. This is done in order to easily control the volume flow through the circuit, hence easily control the speed of the cylinder. It is seen from eq. 2.5 that the FCV keeps an opening, by regulating the spool, which results in a pressure drop across the DCV equal to the desired pressure drop p_Δ. The magnitude of p_Δ is set by adjusting the spring shown in Figure 2.3.

The flow through the main spool is calculated from the expression shown in eq. 2.8.

$$Q_{main} = k_{v_{main}} \cdot u \cdot \sqrt{\Delta p_{main}} \tag{2.6}$$

where

Q_{main}	Volume flow, main spool	$\frac{\text{m}^3}{\text{s}}$
$k_{v_{main}}$	Flow coefficient, main spool	$\frac{\text{m}^3}{\text{s}\cdot\sqrt{\text{Pa}}}$
u	Rate of opening, main spool	-
Δp_{main}	Pressure drop, main spool	Pa

As the pressure drop, Δp_{main}, is controlled by the FCV and therefore known, is the volume flow through the main spool only dependent on the rate of opening of the main valve, u. The return flow trough the compensated DCV is calculated from the expression shown in eq. 2.7.

$$Q_{mainr} = k_{v_{mainr}} \cdot u \cdot \sqrt{\Delta p_{mainr}} \tag{2.7}$$

where

$$Q_{main} = k_{v_{main}} \cdot u \cdot \sqrt{\Delta p_{main}} \tag{2.8}$$

where

Q_{mainr}	Return flow trough the DCV	$\frac{\text{m}^3}{\text{s}}$
$k_{v_{mainr}}$	Flow coefficient, main return spool	$\frac{\text{m}^3}{\text{s}\cdot\sqrt{\text{Pa}}}$
u	Rate of opening, main return spool	-
Δp_{mainr}	Pressure drop, main return spool	Pa

Note that u represents the rate of opening for the compensated DCV, meaning both the main spool and the main return spool. The rate of opening is an input signal given by the operator.

2.2.2 Counterbalance Valve

The flow through the CBV is described by a rephrasing of the orifice equation, eq. 2.1, analogous to the rephrasing done to describe the flow through the FCV, eq. 2.2. The equation describing the flow through the CBV is shown in eq. 2.9.

$$Q_{CBV} = k_{v_{CBV}} \cdot u_{CBV} \cdot \sqrt{\Delta p_{CBV}} \tag{2.9}$$

where

Q_{CBV}	Volume flow, CBV	$\frac{\text{m}^3}{\text{s}}$
$k_{v_{CBV}}$	Flow coefficient, CBV	$\frac{\text{m}^3}{\text{s}\cdot\sqrt{\text{Pa}}}$
u_{CBV}	Rate of opening, CBV	-
Δp_{CBV}	Pressure drop, CBV	Pa

The flow coefficient, $k_{v_{CBV}}$, is calculated in the same manner as done for the FCV, recall eq. 2.3. The rate of opening of the CBV, u_{CBV}, is calculated as shown in eq. 2.10. This equation is found based on the illustration of the CBV shown in Figure 2.4. Note that this figure only illustrates some of the functions of the valve and is therefore not a technical drawing.

$$u_{CBV} = \begin{cases} 1, & u_{CBV} > 1 \\ \frac{p_{in} + p_{pilot} \cdot \rho_p - p_{cr_{CBV}}}{\Delta p_{open_{CBV}}}, & 0 \leq u_{CBV} \leq 1 \\ 0, & u_{CBV} < 0 \end{cases} \tag{2.10}$$

where
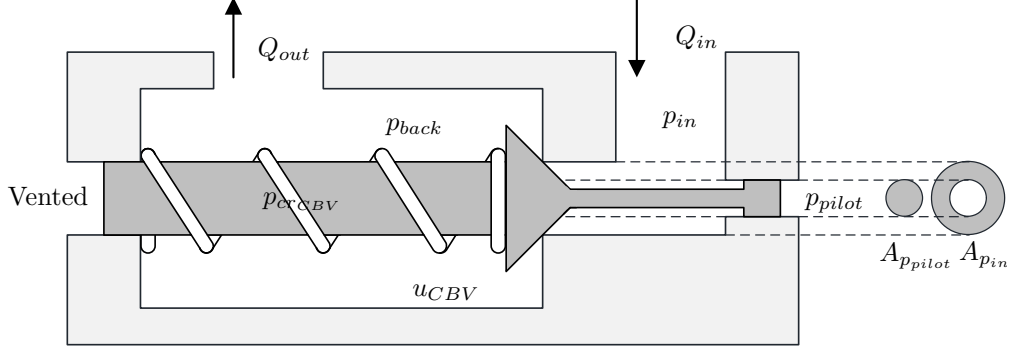
Figure 2.4: Illustration of the CBV

p_{in}	Pressure in to the CBV	Pa
p_{pilot}	Pressure acting on the pilot area	Pa
$p_{cr_{CBV}}$	Crack pressure, CBV	Pa
ρ_p	Pilot ratio, CBV	-
$\Delta p_{open_{CBV}}$	Pressure needed to fully open the CBV	Pa

The pilot ratio, ρ_p, is usually given by the supplier in the data sheet, but is also calculated as shown in eq. 2.11, based on Figure 2.4, where $A_{p_{pilot}}$ and $A_{p_{in}}$ are the areas on which p_{pilot} and p_{in} acts, respectively.

$$\rho_p = \frac{A_{p_{pilot}}}{A_{p_{in}}} \tag{2.11}$$

It is seen from eq. 2.10 that the CBV will not open before $p_{in} + p_{pilot} \cdot \rho_p > p_{crCBV}$. This is what gives the CBV the functionalities described in Section 2.1.

2.2.3   Pressure Relief Valve

The pressure relief valve is not used in neither the circuit shown in Figure 2.1 nor the circuit in Figure 2.2, but is required in order to implement the stability method investigated in this thesis. The valve is therefore described in this section, for the sake of clarity. The flow through the pressure relief valve (PRV) is described in eq. 2.12 by rephrasing the orifices equation, eq. 2.1, analogous to the rephrasing done to describe the flow through the FCV in eq. 2.2.

$$Q_{PRV} = k_{v_{PRV}} \cdot u_{PRV} \cdot \sqrt{\Delta p_{PRV}} \tag{2.12}$$

where

Q_{PRV}	Volume flow, PRV	$\frac{\text{m}^3}{\text{s}}$
$k_{v_{PRV}}$	Flow coefficient, PRV	$\frac{\text{m}^3}{\text{s}\cdot\sqrt{\text{Pa}}}$
u_{PRV}	Rate of opening, PRV	-
Δp_{PRV}	Pressure drop, PRV	Pa

The flow coefficient, $k_{v_{PRV}}$, is calculated in the same manner as done for the FCV, recall eq. 2.3. The rate of opening is calculated as shown in eq. 2.13. This equation is found based on the illustration in Figure 2.5. Note that this figure only illustrates some of the functions of the valve and is therefore not a technical drawing.

$$u_{PRV} = \begin{cases} 1, & u_{PRV} > 1 \\ \frac{p_{in} - p_{cr_{PRV}}}{\Delta p_{open_{PRV}}}, & 0 \leq u_{PRV} \leq 1 \\ 0, & u_{PRV} < 0 \end{cases} \tag{2.13}$$
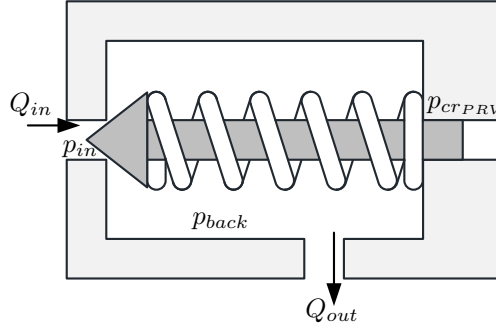
Figure 2.5: Illustration of the PRV

where

p_{in}	Pressure in to the PRV	Pa
p_{back}	Back pressure, PRV	Pa
$p_{cr_{PRV}}$	Crack pressure, PRV	Pa
$\Delta p_{open_{PRV}}$	Pressure needed to fully open the PRV	Pa

2.3 Miscellaneous Equations

This section presents miscellaneous equations needed to investigate the effect of the stabilization method. The equations are described in this section and further used throughout the thesis.

2.3.1 Newton's Second Law

When a force is applied to a mass, will the mass begin to accelerate. Newton's second law describes the relationship between mass, force and acceleration. Two different versions are used. The version in eq. 2.14 describes the acceleration of the cylinder piston in the linear models. The presented version in eq. 2.15 describes the rotational acceleration of the crane arm in the time domain simulations.

$$\Sigma F = m \cdot \ddot{x}_c \tag{2.14}$$

where

F	Force	N
m	Mass	kg
$\ddot{x}_c$	Acceleration	$\frac{m}{s^2}$

$$\Sigma \overset{\curvearrowright}{M} = I \cdot \ddot{\theta} \tag{2.15}$$

where

M	Moment	Nm
$\ddot{\theta}$	Acceleration of rotation	$\frac{1}{s^2}$
I	Mass moment of inertia	kgm^2

11

2.3.2 Pressure Gradient

Time domain simulations are often characterized by including compressible fluid and acceleration. When considering a compressible fluid, the pressure gradient in a given volume can be calculated from eq. 2.16. The re-phrasing shown in eq. 2.17 is used in the linear models.

$$\dot{p} = \frac{\beta \cdot (Q - \dot{V})}{V} \tag{2.16}$$

$$C \cdot \dot{p} = Q - \dot{V} \tag{2.17}$$

where

$$C = \frac{V}{\beta} \tag{2.18}$$

and

$\dot{p}$	Pressure gradient	$\frac{\text{Pa}}{\text{s}}$
V	Total volume	m^3
β	Bulk modulus	Pa
Q	Net-flow, positive if flow enters the volume V	$\frac{\text{m}^3}{\text{s}}$
$\dot{V}$	Volume expansion, positive if volume is expanding	$\frac{\text{m}^3}{\text{s}}$
C	Capacitance of a volume	$\frac{\text{m}^3}{Pa}$

2.3.3 1. Order Low Pass Filter

A low pass filter is a filter that passes signals with a frequency below a certain value, a so called break frequency or cutoff frequency. All frequencies higher then the break frequency are attenuated. The order of the filter determines the amount of the attenuation. In this thesis is a first order low pass filter used to filtrate a measured pressure. The differential equation in eq. 2.19 describes a low pass filter in time domain.

$$\dot{\nu}_{LPF} = \frac{K \cdot \nu - \nu_{LPF}}{\tau} \tag{2.19}$$

where

$\dot{\nu}_{LPF}$	Gradient of filtrated signal	[-]
ν_{LPF}	Filtrated signal	[-]
ν	Signal to be filtrated	[-]
τ	Time constant low pass filter	$\frac{\text{s}}{\text{rad}}$
K	Gain low pass filter	[-]

Where the break frequency, f_c, in Hz can be calculated as shown in eq. 2.20.

$$f_c = \frac{1}{2\pi \cdot \tau} \tag{2.20}$$

2.3.4 PI Controller

A PI controller is widely used in the industry to day. It is used in systems where a feed back signal is measured. A PI controller consists of two terms, a gain and an integrator. The gain will give the system a

fast response, and the integrator will minimize the steady state error between the measured value and the desired value. The differential equation for a PI controller in time domain is shown in eq. 2.21.

$$\dot{\nu}_{PI} = G \cdot \left(\dot{\nu} + \frac{\nu}{Ti} \right) \tag{2.21}$$

where

$\dot{\nu}_{PI}$	Gradient of output signal	[-]
ν	Input signal	[-]
$\dot{\nu}$	Gradient of the input signal	[-]
G	Gain	[-]
Ti	Integral time	s

2.3.5 Linearization

Linearization involves finding a linear approximation for a function at a given point. It is used on non-linear systems in order to investigate local stability. The general equation of a linearized function $f(x, y)$ at a given point is shown in eq. 2.22

$$f(x, y) \approx f(x^{(ss)}, y^{(ss)}) + \frac{\partial f(x, y)}{\partial x}\bigg|_{\left(x^{(ss)}, y^{(ss)}\right)} \cdot \left(x - x^{(ss)}\right) + \frac{\partial f(x, y)}{\partial y}\bigg|_{\left(x^{(ss)}, y^{(ss)}\right)} \cdot \left(y - y^{(ss)}\right) \tag{2.22}$$

where

$x^{(ss)}$	Steady state value of x
$y^{(ss)}$	Steady state value of y

The general expression can be redefined where the variables are deviations from the linearization point. This form is shown in eq. 2.23 and further used in this thesis.

$$\tilde{f} = \frac{\partial f(x, y)}{\partial x}\bigg|_{\left(x^{(ss)}, y^{(ss)}\right)} \cdot \tilde{x} + \frac{\partial f(x, y)}{\partial y}\bigg|_{\left(x^{(ss)}, y^{(ss)}\right)} \cdot \tilde{y} \tag{2.23}$$

where

$$\tilde{f} = f(x, y) - f(x^{(ss)}, y^{(ss)}) \tag{2.24}$$
$$\tilde{x} = x - x^{(ss)} \tag{2.25}$$
$$\tilde{y} = y - y^{(ss)} \tag{2.26}$$

2.3.6 State Space Model

A state space model is model of a physical system. It is build up by a set of first-order differential equations ordered in matrixes and vectors. The general formulation is shown in eq. 2.27 and eq. 2.28.

$$\dot{\mathbf{x}} = \mathbf{A} \cdot \mathbf{x} + \mathbf{B} \cdot \mathbf{u} \tag{2.27}$$
$$\mathbf{y} = \mathbf{C} \cdot \mathbf{x} + \mathbf{D} \cdot \mathbf{u} \tag{2.28}$$

where

A	System matrix
B	Input matrix
C	Output matrix
D	Direct transmission matrix (usually not involved)
x	State vector
y	Output vector
u	Input vector

2.3.7 Transfer Function

A transfer function describes the output signal as a function of the input signal, in Laplace domain. Knowing the transfer function the response of the system is known and a controller can be designed to meet desired response. The transfer function can be converted from a state space model as shown in eq. 2.29.

$$G(s) = \frac{Y(s)}{U(s)} = \mathbf{C} \cdot \phi(s) \cdot \mathbf{B} \tag{2.29}$$

where

A	System matrix
B	Input matrix
C	Output matrix
I	Identity matrix
$G(s)$	Transfer function
$Y(s)$	Output signal Laplace domain
$U(s)$	Input signal Laplace domain
$\phi(s)$	Transmission matrix
s	Laplace variable

The transmission matrix is calculated as shown in eq. 2.30.

$$\phi(s) = [s \cdot \mathbf{I} - \mathbf{A}]^{-1} \tag{2.30}$$

were

I	Identity matrix
s	Laplace variable

2.3.8 Routh Hurwitz

Roth hurwitz stability criterion is a mathematical test which is used to determine stability of linear time invariant systems. Linear time invariant system is a system that dose not depend explicitly on time. Three different versions of Routh Hurwitz stability criterion are used For a third-order polynomial the Routh-Hurwitz criterion is as shown in eq. 2.32 and eq. 2.33.

$$D_3 \cdot s^3 + D_2 \cdot s^2 + D_1 \cdot s + D_0 \tag{2.31}$$

$$D_j > 0 \qquad for \quad j = 0...3 \tag{2.32}$$

$$D_2 \cdot D_1 > D_3 \cdot D_0 \tag{2.33}$$

For a fourth-order polynomial the criterion is expanded. Three inequalities shown in eq. 2.35, eq. 2.36 and eq. 2.37 have to be met in order for the system to be stable.

$$D_4 \cdot s^4 + D_3 \cdot s^3 + D_2 \cdot s^2 + D_1 \cdot s + D_0 \tag{2.34}$$

Table 2.1: General Routh Array

D_n	D_{n-2}	D_{n-4}	D_{n-6}
D_{n-1}	D_{n-3}	D_{n-5}	0
b_1	b_2	b_3	b_3
c_1	c_2	c_3	c_3
d_1	d_2	d_3	d_4
e_1	e_2	e_3	e_4
f_1	f_2	f_3	f_4

$$D_j > 0 \qquad for \quad j = 0...4 \tag{2.35}$$

$$D_3 \cdot D_2 > D_4 \cdot D_1 \tag{2.36}$$

$$D_3 \cdot D_2 \cdot D_1 > D_4 \cdot D_1{}^2 + D_3{}^2 \cdot D_0 \tag{2.37}$$

Routh-array have to be used to investigate polynomial of a higher order. Table 2.1 shows the Routh-array for a sixth-order polynomial. The system is stable if all the rows in the first column have the same sign. Number of sign changes corresponds to the number of roots in the right half plane.

$$D_6 \cdot s^6 + D_5 \cdot s^5 + D_4 \cdot s^4 + D_3 \cdot s^3 + D_2 \cdot s^2 + D_1 \cdot s + D_0 \tag{2.38}$$

where b_i, c_i, d_i, e_i and f_i are as shown in eq. 2.39, eq. 2.40, eq. 2.41, eq. 2.42 and eq. 2.43.

$$b_i = \frac{D_{n-1} \cdot D_{n-2i} - D_n \cdot a_{n-2i-1}}{a_{n-1}} \tag{2.39}$$

$$c_i = \frac{b_1 \cdot a_{n-2i-1} - a_{n-1} \cdot b_{i+1}}{b_1} \tag{2.40}$$

$$d_i = \frac{c_1 \cdot b_{i+1} - b_1 \cdot c_{i+1}}{c_1} \tag{2.41}$$

$$e_i = \frac{d_1 \cdot c_{i+1} - c_1 \cdot d_{i+1}}{d_1} \tag{2.42}$$

$$f_i = \frac{e_1 \cdot d_{i+1} - d_1 \cdot e_{i+1}}{e_1} \tag{2.43}$$

2.4 Stability Analysis Background

"The most important asset of a hydraulic system is stability, and therefor stability should be based on hard quantities. Quantities that can be easily identified and determined with fair precision and whose values remain relative constant" [8, p. 53]. This section gives a theoretical understanding of the instability problem when handling negative loads with circuits containing a CBV in series with a pressure compensated DCV . A simplified hydraulic circuit is presented and a state space model is designed based on this simplified circuit. Finally is Routh Hurwiz stability criterion used to investigate stability of the system. This investigation and the theoretical investigations in chapter 5 are inspired by[10] and [12].
Figure 2.6 shows a simplified circuit of the standard system shown in Figure 2.2. The pressure compensated DCV which has as main object to give a flow that is proportional to the rate of opening is modeled as a flow source. The pressure drop over the *mainr* valve is small and has been neglected together with the valve dynamic for the CBV. The cylinder is also assumed ideal with no friction and no internal leakage.

15
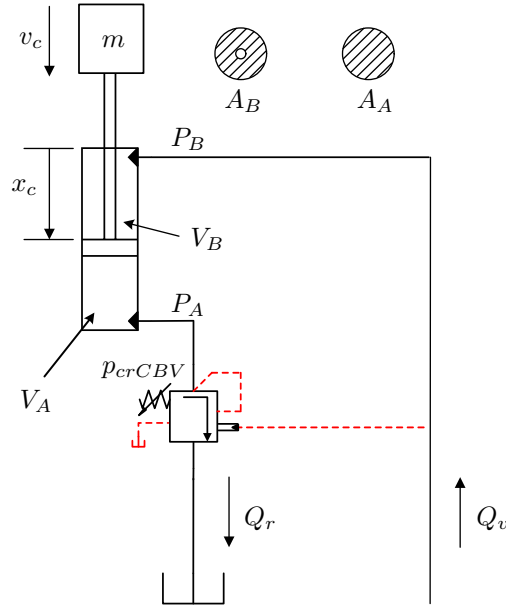
Figure 2.6: Simplified hydraulic circuit general system

2.4.1 Basic Equations

In order to arrange a state space model is a set of 1. order differential equations describing the system shown in Figure 2.6 needed. Equation 2.44 describes the cylinder acceleration and is based on Newton's second law from eq. 2.14. Equation 2.46 and eq. 2.48 describes respectively the pressure build up in chamber A and chamber B and are based on eq. 2.17.

$$m \cdot \dot{v}_c = p_B \cdot A_B - p_A \cdot \rho_c \cdot A_B + m \cdot g \tag{2.44}$$

where

$$\rho_c = \frac{A_A}{A_B} \tag{2.45}$$

and

m	Mass	kg
g	Acceleration of gravity	$\frac{m}{s^2}$
$\dot{v}_c$	Piston acceleration	$\frac{m}{s}$
A_A	Piston area in chamber A	m^2
A_B	Piston area in chamber B	m^2
ρ_c	Area ratio cylinder	[-]
p_A	Pressure in chamber A	bar
p_B	Pressure in chamber B	bar

$$C_A \cdot \dot{p}_A = \rho_c \cdot A_B \cdot v_c - Q_r \tag{2.46}$$

Where C_A is the capacitance of the volume in cylinder chamber A, and is calculated as shown in eq. 2.47

$$C_A = \frac{V_A}{\beta}$$
$$= \frac{(l_{cyl.stroke} - x_c) \cdot A_A + V_{A0}}{\beta} \tag{2.47}$$

16

V_A	Total volume in chamber A	m^3
V_{A0}	Dead volume in chamber A, including cylinder, hose and tubing	m^3
C_A	Capacitance V_A	$\frac{\mathrm{m}^3}{\mathrm{Pa}}$
$l_{cyl.stroke}$	Total cylinder stroke length	m
β	Bulk modulus	Pa
Q_r	Return flow	$\frac{\mathrm{m}^3}{\mathrm{s}}$
x_c	Cylinder piston position	m

$$C_B \cdot \dot{p}_B = Q_v - A_B \cdot v_c \tag{2.48}$$

Where C_B is the capacitance of the volume in cylinder chamber B, and is calculated as shown in eq. 2.49.

$$\begin{aligned} C_B &= \frac{V_B}{\beta} \\ &= \frac{x_c \cdot A_B + V_{B0}}{\beta} \end{aligned} \tag{2.49}$$

V_B	Total volume in chamber B	m^2
V_{B0}	Dead volume in chamber B, including cylinder hose and tubing	m^3
C_B	Capacitance V_B	$\frac{\mathrm{m}^3}{\mathrm{Pa}}$
β	Bulk modulus	Pa
Q_v	Inlet flow	$\frac{\mathrm{m}^3}{s}$
x_c	Cylinder piston position	m

Equation 2.50 describes the flow trough the CBV and is based on eq. 2.9. Equation 2.51 describes the rate of opening of the CBV and is based on eq. 2.10.

$$Q_r = k_{v_{CBV}} \cdot u_{CBV} \cdot \sqrt{p_A} \tag{2.50}$$

where

Q_r	Return flow	$\frac{\mathrm{m}^3}{\mathrm{s}}$
$k_{v_{CBV}}$	Flow coefficient CVB	$\frac{\mathrm{m}^3}{\mathrm{s}\cdot\sqrt{\mathrm{Pa}}}$
u_{CBV}	Rate of opening CBV	[-]
p_A	Pressure in camber A	Pa

$$u_{CBV} = \frac{p_B \cdot \rho_p + p_A - p_{cr_{CBV}}}{\Delta p_{open_{CBV}}} \tag{2.51}$$

where

u_{CBV}	Rate of opening CBV	[-]
p_B	Pressure in camber B	Pa
p_A	Pressure in camber A	Pa
ρ_p	Pilot ratio CBV	[-]
$p_{cr_{CBV}}$	Crack pressure CBV	Pa
$\Delta p_{open_{CBV}}$	Pressure to fully open CBV	Pa

The set of basic equations needed to describe the system in Figure 2.6 is derived and is repeated as:

$$m \cdot \dot{v}_c = p_B \cdot A_B - p_A \cdot \rho_c \cdot A_B + m \cdot g \tag{2.44}$$

$$C_A \cdot \dot{p}_A = \mu_c \cdot A_B \cdot v_c - Q_r \tag{2.46}$$

$$C_B \cdot \dot{p}_B = Q_v - A_B \cdot v_c \tag{2.48}$$

$$Q_r = k_{v_{CBV}} \cdot u_{CBV} \cdot \sqrt{p_A} \tag{2.50}$$

$$u_{CBV} = \frac{p_B \cdot \rho_p + p_A - p_{cr_{CBV}}}{\Delta p_{open_{CBV}}} \tag{2.51}$$

2.4.2 Linearization

In order to design a state space model, the equations which are to be used have to be linear. The non-linear orifices equation, here eq. 2.50, must therefore be linearized. The set of basic equations is linearized based on eq. 2.23 in Section 2.3.5. The linearized version is shown in eq. 2.52 - 2.56.

$$m \cdot \dot{\tilde{v}}_c = \tilde{p}_B \cdot A_B - \tilde{p}_A \cdot \rho_c \cdot A_B \tag{2.52}$$

$$C_A \cdot \dot{\tilde{p}}_A = \rho_c \cdot A_B \cdot \tilde{v}_c - \tilde{Q}_r \tag{2.53}$$

$$C_B \cdot \dot{\tilde{p}}_B = \tilde{Q}_v - A_B \cdot \tilde{v}_c \tag{2.54}$$

$$\tilde{Q}_r = k_{qu_{CBV}} \cdot \tilde{u}_{CBV} + k_{qp_{CBV}} \cdot \tilde{p}_A \tag{2.55}$$

$$\tilde{u}_{CBV} = \frac{\tilde{p}_B \cdot \rho_p + \tilde{p}_A}{\Delta p_{open_{CBV}}} \tag{2.56}$$

Equation 2.55 is derived as shown in eq. 2.57.

$$\tilde{Q}_r = \left.\frac{\partial Q_r}{\partial u_{CBV}}\right|_{ss} \cdot \tilde{u}_{CBV} + \left.\frac{\partial Q_r}{\partial p_A}\right|_{ss} \cdot \tilde{p}_A$$

$$\tilde{Q}_r = k_{qu_{CBV}} \cdot \tilde{u}_{CBV} + k_{qp_{CBV}} \cdot \tilde{p}_A \tag{2.57}$$

where

$$k_{qu_{CBV}} = \left.\frac{\partial Q_r}{\partial u_{CBV}}\right|_{ss} = k_{v_{CBV}} \cdot \sqrt{p_A^{(ss)}} \tag{2.58}$$

$$k_{qp_{CBV}} = \left.\frac{\partial Q_r}{\partial p_A}\right|_{ss} = \frac{k_{v_{CBV}} \cdot u_{CBV}^{(ss)}}{2 \cdot \sqrt{p_A^{(ss)}}} \tag{2.59}$$

2.4.3 State Space Model

Based on the three linearized differential equations in eq. 2.52 - 2.54 is a state space model arranged. The system is a single input, single output system (SISO-system) with three states. The states are $\tilde{v}_c$, $\tilde{p}_A$ and $\tilde{p}_B$. Q_v is the input signal and $A_B \cdot v_c$ is the output signal. In order to arrange the state space model similar to the description in eq. 2.27 and eq. 2.28, the linearized differential equations are re-organized as shown in eq. 2.60 - 2.62.

$$\dot{\tilde{v}}_c = \frac{A_B}{m} \cdot \tilde{p}_B - \frac{\rho_c \cdot A_B}{m} \cdot \tilde{p}_A \tag{2.60}$$

$$\dot{\tilde{p}}_A = \frac{\rho_c \cdot A_B}{C_A} \cdot \tilde{v}_c - \frac{\rho_p \cdot k_{qu_{CBV}}}{\Delta p_{open_{CBV}} \cdot C_A} \cdot \tilde{p}_B - \left(\frac{k_{qu_{CBV}}}{\Delta p_{open_{CBV}} \cdot C_A} + \frac{k_{qp_{CBV}}}{C_A}\right) \cdot \tilde{p}_A \tag{2.61}$$

$$\dot{\tilde{p}}_B = \frac{1}{C_B} \cdot \tilde{Q}_v - \frac{A_B}{C_B} \cdot \tilde{v}_c \tag{2.62}$$

Finally is the state space model arranged in eq. 2.63 and eq. 2.64, based on eq. 2.60 - 2.62.

$$\begin{bmatrix} \dot{\tilde{v}}_c \\ \dot{\tilde{p}}_A \\ \dot{\tilde{p}}_B \end{bmatrix} = \begin{bmatrix} 0 & -\frac{\rho_c \cdot A_B}{m} & \frac{A_B}{m} \\ \frac{\rho_c \cdot A_B}{C_A} & -\left(\frac{k_{qu_{CBV}}}{\Delta p_{open_{CBV}} \cdot C_A} + \frac{k_{qp_{CBV}}}{C_A}\right) & -\frac{\rho_p \cdot k_{qu_{CBV}}}{\Delta p_{open_{CBV}} \cdot C_A} \\ -\frac{A_B}{C_B} & 0 & 0 \end{bmatrix} \cdot \begin{bmatrix} \tilde{v}_c \\ \tilde{p}_A \\ \tilde{p}_B \end{bmatrix} + \begin{bmatrix} 0 \\ 0 \\ \frac{1}{C_B} \end{bmatrix} \cdot \tilde{Q}_v \tag{2.63}$$

$$y = \begin{bmatrix} A_B & 0 & 0 \end{bmatrix} \cdot \begin{bmatrix} \tilde{v}_c \\ \tilde{p}_A \\ \tilde{p}_B \end{bmatrix} \tag{2.64}$$

2.4.4 Transfer Function

The state space model in eq. 2.63 and 2.64 is re-arrange as a transfer function using eq. 2.29. The transfer function is shown in eq. 2.65 and is used to evaluate stability for the system.

$$G(s) = \frac{N_1 \cdot s + N_0}{D_3 \cdot s^3 + D_2 \cdot s^2 + D_1 \cdot s + D_0} \tag{2.65}$$

where

$$N_0 = A_B{}^2 \left(\frac{k_{qu_{CBV}}}{\Delta p_{open_{CBV}}} \cdot (1 + \rho_p \cdot \rho_c) + k_{qp_{CBV}} \right) \tag{2.66}$$

$$N_1 = C_A \cdot A_B{}^2 \tag{2.67}$$

$$D_0 = A_B{}^2 \cdot \left(\frac{k_{qu_{CBV}}}{\Delta p_{open_{CBV}}} \cdot (1 + \rho_p \cdot \rho_c) + k_{qp_{CBV}} \right) \tag{2.68}$$

$$D_1 = A_B{}^2 \cdot \left(C_A + C_B \cdot \rho_c{}^2 \right) \tag{2.69}$$

$$D_2 = C_B \cdot m \cdot \left(\frac{k_{qu_{CBV}}}{\Delta p_{open_{CBV}}} + k_{qp_{CBV}} \right) \tag{2.70}$$

$$D_3 = C_A \cdot C_B \cdot m \tag{2.71}$$

$$\tag{2.72}$$

2.4.5 Routh-Hurwitz Stability Criterion

Bode plots and step response are widely used to investigate response of the system. In this case, only the stability is of interest. In order for the system to be stable, must the polynomial in the denominator of the transfer function only consist of roots with negative real part. This is investigated by means of Routh-Hurwitz stability criterion. As the denominator of the transfer function is a third-order polynomial, must the inequalities shown in eq. 2.32 and eq. 2.33 be met.

The inequality in eq. 2.33 is always fulfilled as none of the constants D_j can ever be negative. The second criterion has to be further investigated in order to decide if the inequality is met. In eq. 2.73 are the D_j-terms from eq. 2.32 substituted by the corresponding terms from eq. 2.68 - 2.71.

$$D_2 \cdot D_1 > D_3 \cdot D_0 \tag{2.33}$$

$$C_B \cdot m \cdot \left(\frac{k_{qu_{CBV}}}{\Delta p_{open_{CBV}}} + k_{qp_{CBV}} \right) \cdot A_B{}^2 \cdot (C_A + C_B \cdot \rho_c{}^2) > C_A \cdot C_B \cdot m \cdot A_B{}^2 \cdot \left(\frac{k_{qu_{CBV}}}{\Delta p_{open_{CBV}}} \cdot (1 + \rho_p \cdot \rho_c) + k_{qp_{CBV}} \right)$$

$$\frac{C_B}{C_A} > \frac{\rho_p}{\rho_c} \cdot \frac{\frac{k_{qu_{CBV}}}{\Delta p_{open_{CBV}}}}{\frac{k_{qu_{CBV}}}{\Delta p_{open_{CBV}}} + k_{qp_{CBV}}}$$

$$\frac{V_B}{V_A} > \frac{\rho_p}{\rho_c} \cdot \frac{2 \cdot p_A}{2 \cdot p_A + u_{CBV} \cdot \Delta p_{open_{CBV}}} \tag{2.73}$$

The inequality in 2.73 can not be fulfilled for all cylinder positions. The system is unstable if the criteria listed below are met.

- $V_A >> V_B$,   which happens when the cylinder is fully extended

- $\rho_p > \rho_c$, $\rho_p = 2...8$ and ρ_c is normally not greater then 2

- $\frac{2 \cdot p_A}{2 \cdot p_A + u_{CBV} \cdot \Delta p_{open_{CBV}}} \approx 1$,   which happens with a high load and a small volume flow

$$(2 \cdot p_A >> u_{CBV} \cdot \Delta p_{open_{CBV}})$$

The system will not be stable for the cylinder fully extended, with a high pressure in chamber A and a small volume flow.

Chapter 3

Test Rig

In this chapter is the physical structure of the rig used for testing introduced. The test rig consists of a hinged arm actuated by a cylinder. The chapter includes a general description of the structure and manner of operation of the rig, and mechanical calculations such as: estimation of the center of gravity and mass moment of inertia. The chapter also includes a description of the hydraulic installation, steady state calculations of the hydraulics through out the field of operation of the rig, and a description of the instrumentation of the rig.

3.1 Description

An overview of the test rig is shown in Figure 3.1. The rig consists of the main body, a cylinder, an arm and a ballast stack. The hydraulic system is made up of several components with quick release couplings. The hydraulic circuit can therefore easily be changed. The test rig is build by the University of Agder (UiA). The rig was completed in March 2015 and is located at UiAs laboratory in Grimstad. The purpose of the rig is for students to conduct projects in connection with lectures, bachelor or master thesis. The test rig is oversized and bolted to the floor in order to withstand rough treatment. Figure 3.1 shows an overview of the test rig where the ballast stack, beam and cylinder are marked. Figure 3.2 shows external dimensions.
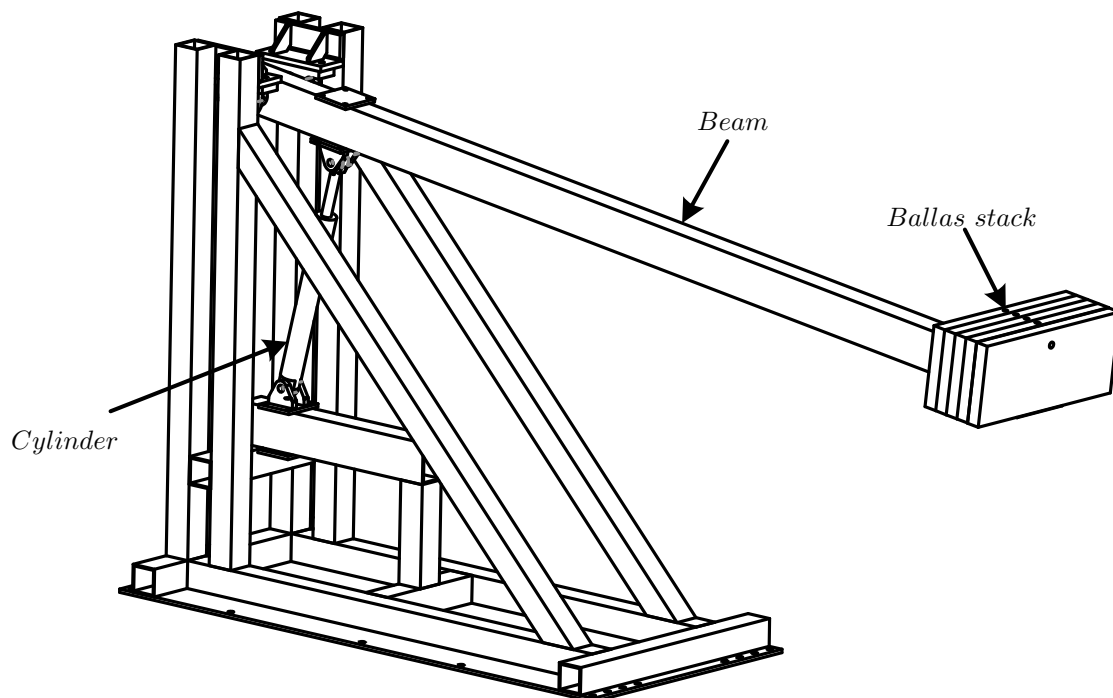
Figure 3.1: Overview test rig
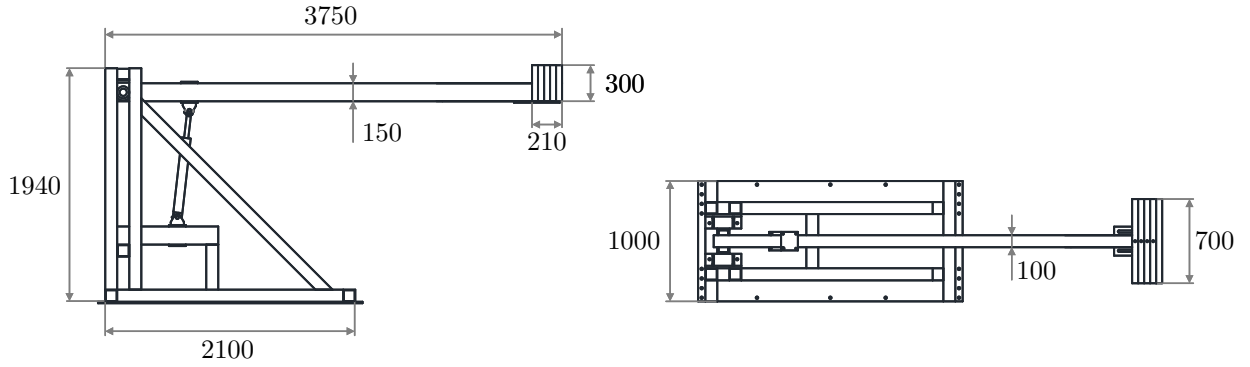
Figure 3.2: External dimensions of the test rig. All dimensions in [mm]

The hydraulic system is well equipped and consists of a flow meter, six pressure gauges, a cylinder, a CBV and two blocks of DCVs. This gives several opportunities for controlling and observing the test rig.

3.2 Mechanical Analysis

A mechanical analysis of the rig were carried out in order to determine quantities such as: center of gravity, mass moment of inertia and cylinder force in steady state.

3.2.1 Mass and Center of Gravity

The mass and the center of gravity of the rotating arm are important quantities. In order to acquire them are some assumptions made.

- The beam is assumed to be made of steel with uniformly distributed density, $\rho_{Steel} = 7850 \ \frac{\text{kg}}{\text{m}^3}$

- The ballast stack is assumed to be one solid block with uniformly distributed mass.
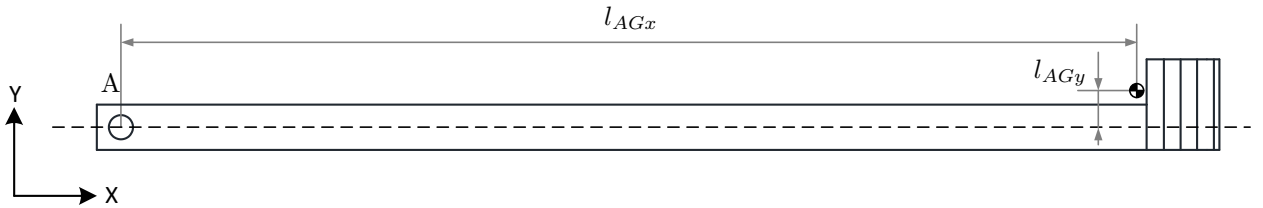
Figure 3.3: Center of gravity arm

The distance from the rotation point, A, to the center of mass, see Figure 3.3, and the total mass of the arm are needed in order to calculate the steady state cylinder force. Prior to the installation were all the plates of the ballast stack weighed. The ballast stack consists of five plates stacked together, where four of them are main ballast plates and the last plate an endplate. The main ballast plates weighs 76 kg each, while the endplate weighs 16 kg. The total mass for the ballast stack is calculated in eq. 3.1.

$$m_{Ballast\ stack} = 4 \cdot 76 \text{ kg} + 16 \text{ kg} = \underline{320 \text{ kg}} \tag{3.1}$$

The weight of the beam was not determined prior to the assembly and is therefore calculated. The dimensions of the beam is shown in Figure 3.4. The volume and mass of the beam is calculated as shown in eq. 3.2 and eq. 3.3 where the density is assumed to be $\rho_{steel} = 7850 \ \frac{\text{kg}}{\text{m}^3}$, and the mass uniformly distributed.

22

Section A-A, beam   Section B-B, ballast stack
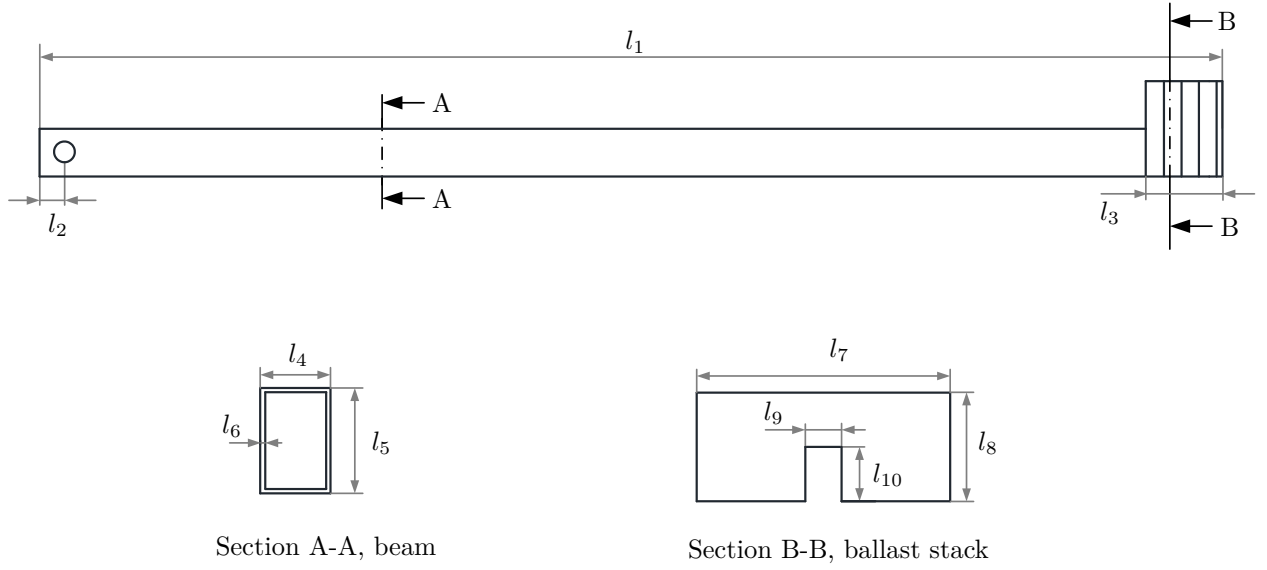
Figure 3.4: Dimensions arm

$$l_1 = 3680 \text{ mm}$$
$$l_2 = 80 \text{ mm}$$
$$l_3 = 215 \text{ mm}$$
$$l_4 = 100 \text{ mm}$$
$$l_5 = 150 \text{ mm}$$
$$l_6 = 6 \text{ mm}$$
$$l_7 = 700 \text{ mm}$$
$$l_8 = 300 \text{ mm}$$
$$l_9 = 100 \text{ mm}$$
$$l_{10} = 150 \text{ mm}$$
$$r_1 = 40 \text{ mm}$$

$$V_{Beam} = l_1 \cdot l_4 \cdot l_5 - l_1 \cdot (l_4 - 2 \cdot l_6) \cdot (l_5 - 2 \cdot l_6) - 2 \cdot \pi \cdot r_1^2 \cdot l_6 = \underline{0.01045 \text{ m}^3} \tag{3.2}$$

$$m_{Beam} = V_{beam} \cdot \rho_{Steel} = \underline{82 \text{ kg}} \tag{3.3}$$

In order to calculate the center of gravity for the crane arm, must the center of gravity of the beam and the center of gravity of the ballast stack first be calculated. Figure 3.5 is an illustration of the crane arm which illustrates where to find the center of mass for the beam and ballast stack.
Due to symmetry is the center of mass for the arm relative to point A calculated as shown in eq. 3.4 and eq. 3.5.

$$l_{AGx,Beam} = \frac{l_1}{2} - l_2 = \underline{1760 \text{ mm}} \tag{3.4}$$

$$l_{AGy,Beam} = \underline{0 \text{ mm}} \tag{3.5}$$

When determining center of gravity of the ballast stack relative to point A is the stack face divided as shown in Figure 3.6. The center of gravity in y-direction is at the same position as the center of area of the stack face due to the assumption of uniformly distributed density.
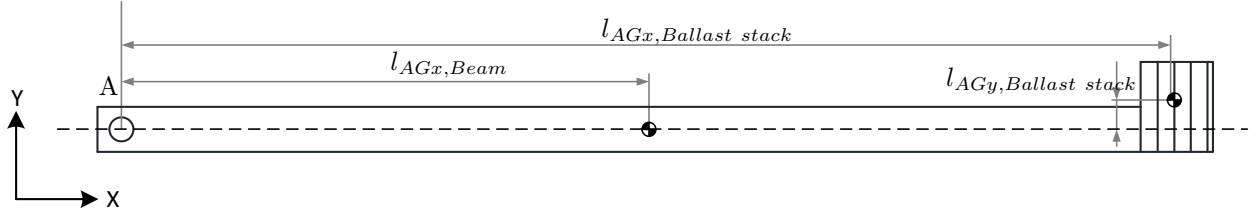
Figure 3.5: Center of gravity beam and ballast stack
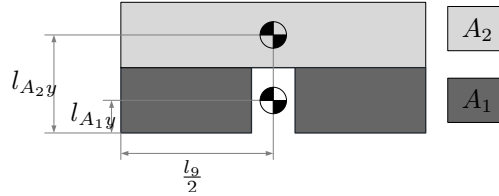
Figure 3.6: Center of area

The center of gravity of the ballast plates relative to point A is therefore calculated as shown in Equation 3.6 and 3.7.

$$l_{AGx,Ballast\ stack} = l_1 - l_2 - \frac{l_3}{2} = \underline{3492.5\ \text{mm}} \tag{3.6}$$

$$
\begin{aligned}
l_{AGy,Ballast\ stack} &= \frac{l_{A_1y} \cdot A_1 + l_{A_2y} \cdot A_2}{A_1 + A_2} - \frac{l_5}{2} \\
&= \frac{\frac{l_{10}}{2} \cdot l_{10} \cdot (l_7 - l_9) + \left(l_{10} + \frac{l_8 - l_{10}}{2}\right) \cdot (l_8 - l_{10}) \cdot l_7}{l_7 \cdot l_8 - l_9 \cdot l_{10}} - \frac{l_5}{2} \\
&= \underline{80.8\ \text{mm}}
\end{aligned}
\tag{3.7}
$$

Finally is the center of gravity of the assembly, consisting of the beam and the ballast stack, relative to point A calculated as shown in eq. 3.8 and eq. 3.9.

$$l_{AGx} = \frac{m_{Beam} \cdot l_{AGx,Beam} + m_{Ballast\ stack} \cdot l_{AGx,Ballast\ stack}}{m_{beam} + m_{Ballast\ stack}} = \underline{3139\ \text{mm}} \tag{3.8}$$

$$l_{AGy} = \frac{m_{Beam} \cdot l_{AGy,Beam} + m_{Ballast\ stack} \cdot l_{AGy,Ballast\ stack}}{m_{beam} + m_{Ballast\ stack}} = \underline{64\ \text{mm}} \tag{3.9}$$

3.2.2 Mass Moment of Inertia

The mass moment of inertia for the crane arm must be known in order to perform a dynamic simulation of the test rig. The crane arm is therefore divided into two parts, namely the beam and the ballast stack, as shown in Figure 3.7. The mass moment of inertia for each part is first determined relative to the mass center. The parallel axis theorem, also known as Huygens-Steiner theorem, is then applied in order to determine the mass moment of inertia for each part relative to point A. Finally is the inertia of each part summed in order to obtain the total mass moment of inertia.

The mass moment of inertia relative to the center of mass for the beam and the ballast stack are calculated in eq. 3.10 and eq. 3.11.

$$I_{CG,Beam} = \frac{m_{Beam} \cdot l_1^2}{12} = \underline{92.54\ \text{kgm}^2} \tag{3.10}$$

$$I_{CG,Ballast\ stack} = \frac{1}{12} \cdot m_{Ballast\ stack} \cdot \left(l_3^2 + l_4^2\right) = \underline{1.50\ \text{kgm}^2} \tag{3.11}$$
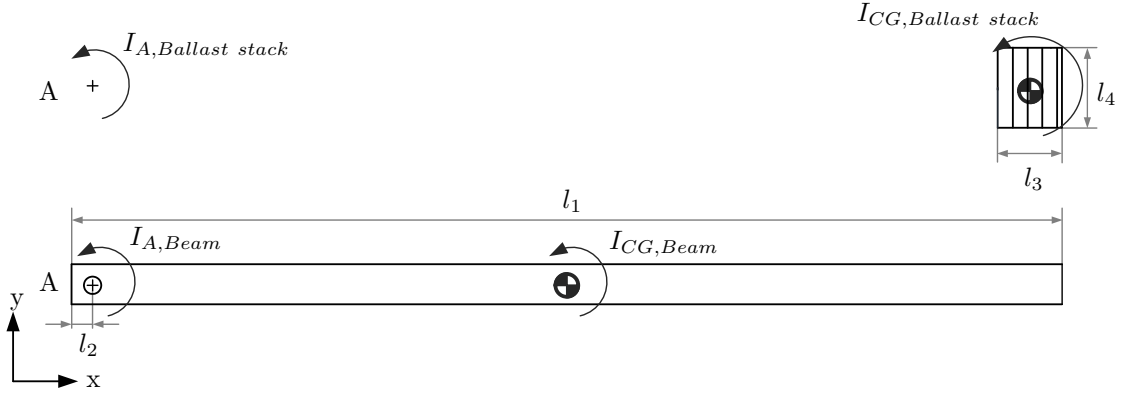
Figure 3.7: Mass moment of inertia

The mass moment of inertia relative to point A for the beam and the ballast stack are then calculated by using the parallel axial theorem. The calculations are shown in eq. 3.12 and eq. 3.13, respectively.

$$I_{A,Beam} = I_{CG,Beam} + m_{Beam} \cdot \left(\frac{l_1}{2} - l_2\right)^2 = \underline{346.5 \text{ kgm}^2} \tag{3.12}$$

$$I_{A,Ballast\ stack} = I_{CG,Ballast\ stack} + m_{Ballast\ stack} \cdot \left(l_1 - l_2 - \frac{l_3}{2}\right)^2 = \underline{3904.7 \text{ kgm}^2} \tag{3.13}$$

The mass moment of the assembled crane arm is calculated in eq. 3.14

$$I_A = I_{A,Beam} + I_{A,Ballast\ stack} = \underline{4251.2 \text{ kgm}^2} \tag{3.14}$$

3.2.3 Steady State Reaction Forces

Lengths and angles used to calculate the steady state reaction forces in cylinder and in bearings at point A are shown in Figure 3.8.
The magnitude of the lengths shown in Figure 3.8 are:

$$l_{ACx} = 550 \text{ mm}$$
$$l_{ACy} = 130 \text{ mm}$$
$$l_{ABx} = 420 \text{ mm}$$
$$l_{ABy} = 1055 \text{ mm}$$
$$l_{AGx} = 3139 \text{ mm}$$
$$l_{AGy} = 64 \text{ mm}$$

The angle θ in Figure 3.8 is the angle of the beam relative to the horizontal line and φ is the angle of the cylinder. The angles α_0, α_1 and α_2 are constant angles, and are calculated as shown in eq. 3.15, eq. 3.16 and eq. 3.17.

$$\alpha_0 = \tan^{-1}\left(\frac{l_{ACy}}{l_{ACx}}\right) = \underline{13.3°} \tag{3.15}$$

$$\alpha_1 = \tan^{-1}\left(\frac{l_{AGy}}{l_{AGx}}\right) = \underline{1.2°} \tag{3.16}$$

$$\alpha_2 = \tan^{-1}\left(\frac{l_{ABy}}{l_{ABx}}\right) = \underline{68.3°} \tag{3.17}$$

The lengths l_{AB}, l_{AC} and l_{AG} are constant and calculated as shown in eq. 3.18, eq. 3.19 and eq. 3.20.
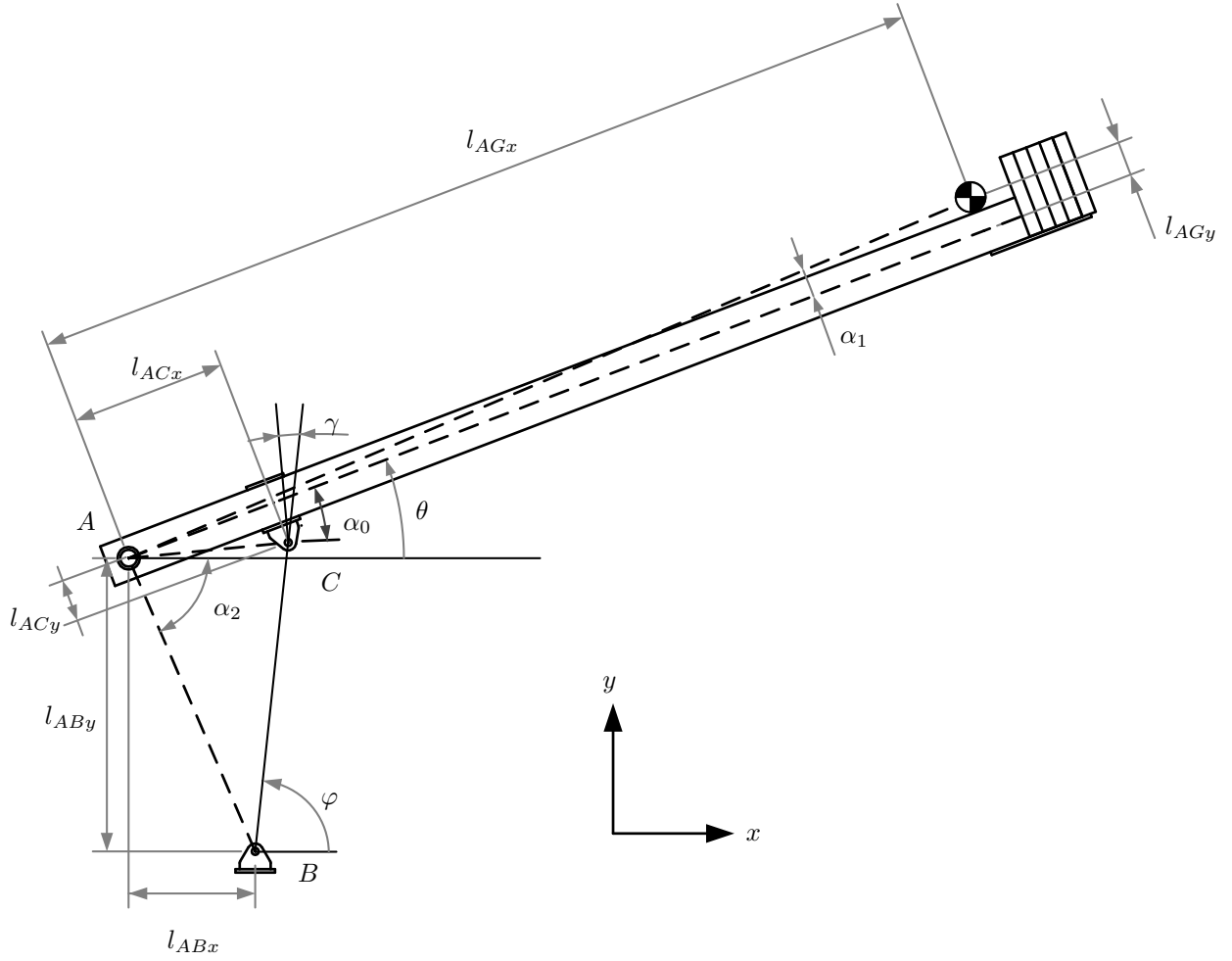
Figure 3.8: Assistance figure for steady state calculations

$$l_{AB} = \sqrt{l_{ABx}{}^2 + l_{ABy}{}^2} = \underline{1136 \text{ mm}} \tag{3.18}$$

$$l_{AC} = \sqrt{l_{ACx}{}^2 + l_{ACy}{}^2} = \underline{565 \text{ mm}} \tag{3.19}$$

$$l_{AG} = \sqrt{l_{AGx}{}^2 + l_{AGy}{}^2} = \underline{3126 \text{ mm}} \tag{3.20}$$

In order to determine the angle of the cylinder, φ, must the lengths l_{BCx} and l_{BCy} be know. l_{BCx} is the horizontal distance between point B and point C, while l_{BCy} is the vertical distance. These lengths are calculated as shown in eq. 3.21 and eq. 3.22.

$$l_{BCx} = l_{AC} \cdot \cos(\theta - \alpha_0) - l_{ABx} \tag{3.21}$$
$$l_{BCy} = l_{AC} \cdot \sin(\theta - \alpha_0) + l_{ABy} \tag{3.22}$$

φ is then calculated as shown in eq. 3.23.

$$\varphi = \tan^{-1}\left(\frac{l_{BCy}}{l_{BCx}}\right) \tag{3.23}$$

γ is calculated from eq. 3.24.

$$\gamma = \theta - \alpha_0 + \frac{\pi}{2} - \varphi \tag{3.24}$$

Figure 3.9 shows a kinetic diagram (KD) and a free body diagram (FBD) of the beam. The center of gravity is shown in the figure and the mass of the crane arm, m, is 402 kg, calculated from eq. 3.25. The steady state reaction forces in the bearings and in the cylinder are calculated based on the FBD. All accelerations are therefore zero ($\ddot{\theta} = 0 \; a_x = 0 \; a_y = 0$). Recall Figure 3.8 for geometric description.

$$m = m_{Ballast\ stack} + m_{Beam} = \underline{402\ kg} \tag{3.25}$$
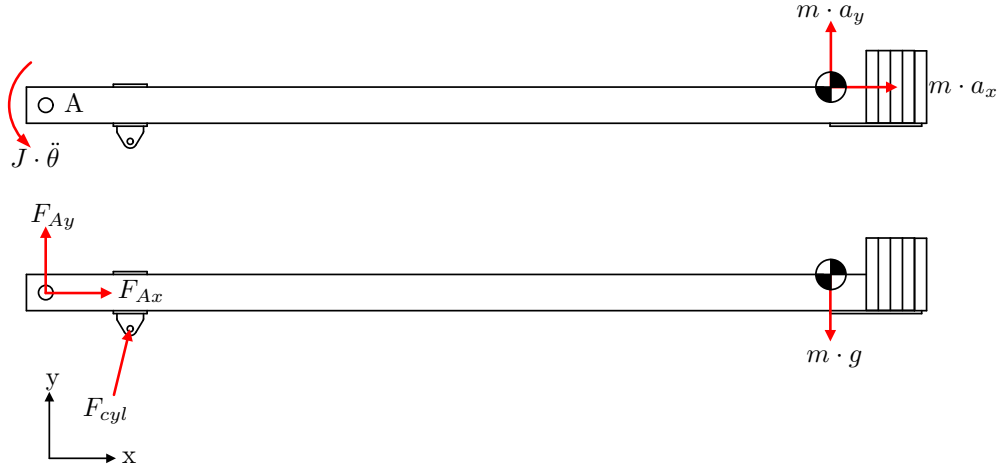
Figure 3.9: KD and FBD of the beam

For a system with constant velocity (in steady state) is the sum of all forces equal to zero. The force equilibrium, shown in Equation 3.26, is used to determine the forces in the bearing, namely F_{Ax} and F_{Ay}.

$$\sum \mathbf{F} = \begin{bmatrix} F_{Ax} \\ F_{Ay} \end{bmatrix} + F_{cyl} \begin{bmatrix} \cos(\varphi) \\ \sin(\varphi) \end{bmatrix} + \begin{bmatrix} 0 \\ -m \cdot g \end{bmatrix} = \mathbf{0} \tag{3.26}$$

Equation 3.27 and eq. 3.28 are used to determine F_{Ax} and F_{Ay} respectively.

$$F_{Ax} = -F_{cyl} \cdot \cos(\varphi) \tag{3.27}$$

$$F_{Ay} = -F_{cyl} \cdot \cos(\varphi) + m \cdot g \tag{3.28}$$

The moment equilibrium is shown in eq. 3.29 and is used to determine the cylinder force, F_{cyl}.

$$\sum \overset{\curvearrowleft}{M_A} = l_{AC} \begin{bmatrix} \cos(\theta - \alpha_0) \\ \sin(\theta - \alpha_0) \end{bmatrix} \times F_{cyl} \begin{bmatrix} \cos(\varphi) \\ \sin(\varphi) \end{bmatrix} + l_{ACG} \begin{bmatrix} \cos(\theta + \alpha_1) \\ \sin(\theta + \alpha_1) \end{bmatrix} \times \begin{bmatrix} 0 \\ -m \cdot g \end{bmatrix} = 0 \tag{3.29}$$

Equation 3.29 is rephrased to give the cylinder force, F_{cyl}, as a function of θ.

$$F_{cyl} = \frac{m \cdot g \cdot l_{ACG} \cdot \cos(\theta + \alpha_1)}{l_{AC} \left(\cos(\theta - \alpha_0) \cdot \sin(\varphi) - \sin(\theta - \alpha_0) \cdot \cos(\varphi) \right)} \tag{3.30}$$

As the cylinder force is a function of θ will its magnitude vary as the angle of the crane arm is altered. It is further advantageous to determine a relation between the cylinder piston position, x_c as shown in figure 2.6, and the angle of the beam, θ, to determine the cylinder force relative to the cylinder piston position. The

cylinder used on the test rig got a stroke length of $500mm$ and a total compressed length of $772mm$. This means that l_{BC} varies between $772mm$ and $1272mm$, and is calculated as shown in eq. 3.31.

$$l_{BC} = 1.272 - x_c \tag{3.31}$$

θ is then found as a function of l_{BC} by applying the law of cosines, as shown in eq. 3.32.

$$\theta = \cos^{-1}\left(\frac{l_{AB}^2 + l_{AC}^2 - l_{BC}^2}{2 \cdot l_{AB} \cdot l_{AC}}\right) - \theta_2 + \theta_0 \tag{3.32}$$

In Figure 3.10 is the cylinder force plotted relative to cylinder piston position, and in Figure 3.11 is the reaction forces in the bearing plotted as a function of the cylinder piston position.
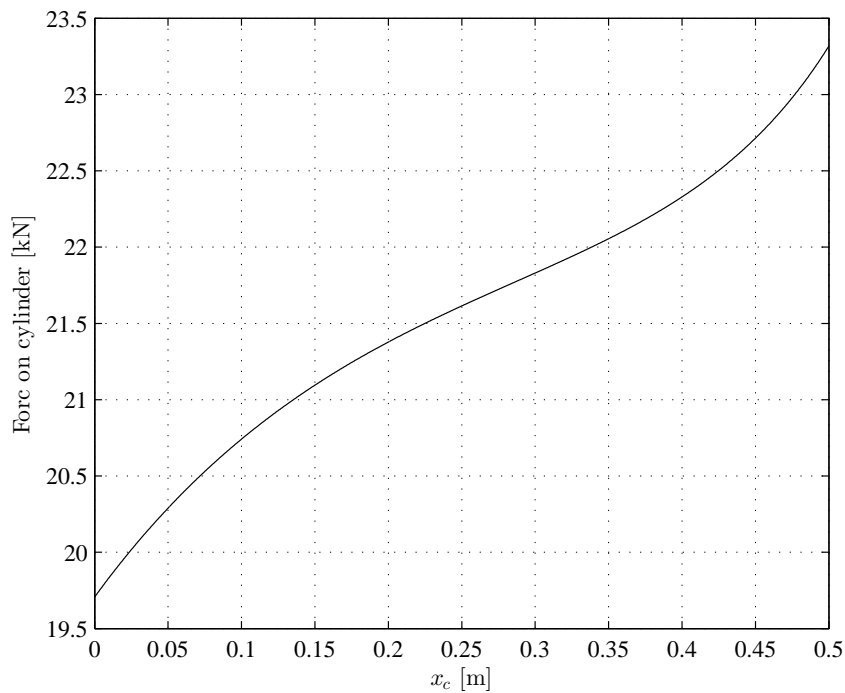
Figure 3.10: Steady state cylinder force
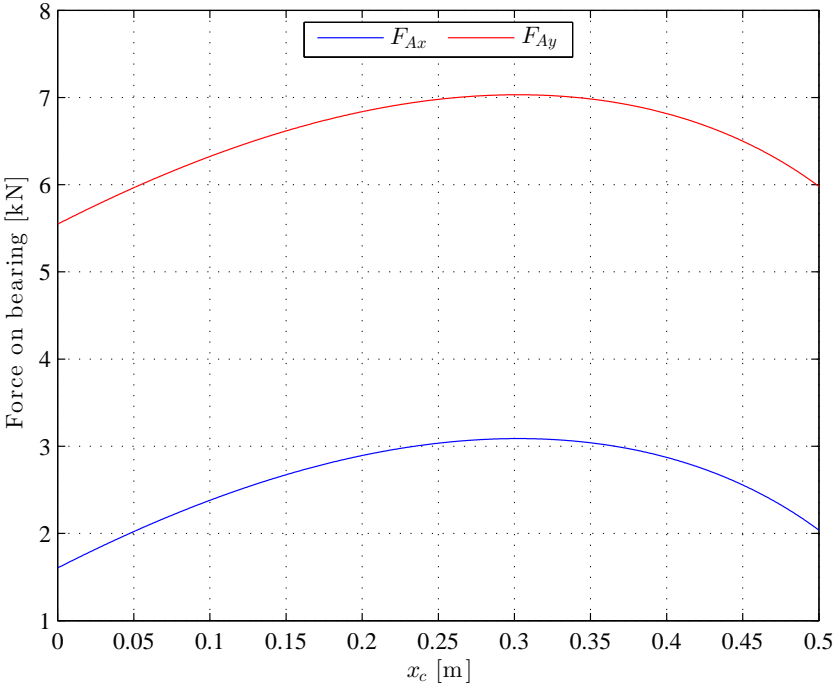
Figure 3.11: Steady state reaction force on bearings in point A

3.3 Hydraulics

This section provides a description of the hydraulic circuits and components of the test rig. These circuits are used when performing physical tests of the stabilizing method, and are the basis of the theoretical investigations and simulations. Constants used in the investigations, which are based on the hydraulic components, are therefore introduced in this section. Please note that a full list of the constants used in the calculations and simulations are to be found in Appendix A.

3.3.1 The Circuits

The hydraulics of the test rig consists of two circuits, namely a main circuit and an external pressure circuit. Figure 3.12 shows an illustration of the hydraulic circuits and the components, including sensors.
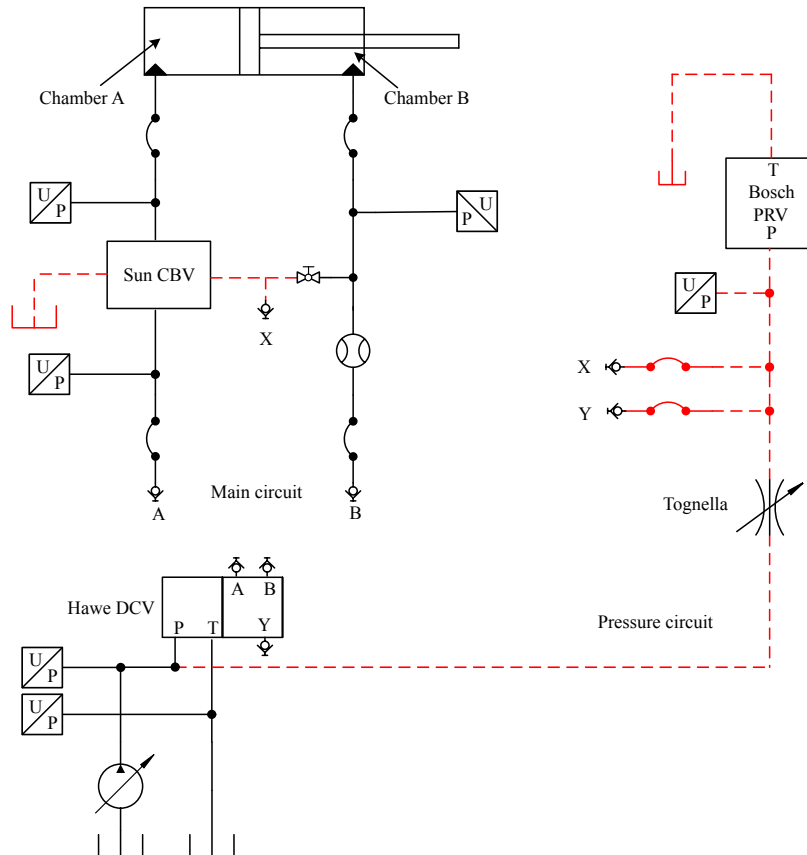
Figure 3.12: Hydraulic installation test rig

Main circuit

The main circuit, shown to the left in Figure 3.12, is used to actuate the test rig. This circuit mainly consist of a cylinder and a CBV. Pressure sensors are located as shown in the figure and are used to measure pressures during testing. The pressure sensor on the ring side of the cylinder is also used in the stabilization method. A flow sensor is placed in the main circuit as shown in the figure. The main circuit is supplied by the pump, via the Hawe DCV, through connector A and B. The pressure in the external pressure circuit can be assigned to the pilot line of the CBV through connector X and to the load sensing (LS) line of the compensated DCV through connector Y.

Pressure Circuit

The circuit shown to the right in Figure 3.12 is called the pressure circuit or external pressure circuit. This circuit is used to design a pressure for the stabilization method. An adjustable orifice is placed in series with

the Bosch PRV. The adjustable orifice is adjusted to provide a high pressure drop, meaning that the pressure in between the orifice and the PRV is low when the PRV is fully open. The Bosch PRV is a proportional pressure relief valve with adjustable crack pressure. The crack pressure is adjusted by means of a solenoid. The pressure in between the adjustable orifice and the PRV is therefore controlled by adjusting the crack pressure of the PRV, and are accessible through connector X and Y. Connector X is used to assign the pressure in the pressure circuit to the pilot line of the CBV, and connector Y is used to assign the pressure to the pressure compensated DCV. A control loop is used to continuously adjust the crack pressure of the PRV, hence control the pressure in the pressure circuit.

3.3.2 The Components

Further are the components used in the circuits introduced. Constants used in the investigations, which are based on the hydraulic components, are listed for each component. Some constants are estimates and are therefore not to be found in the data sheets. These constants are market with *. Each constant and its usage are either described here or in Chapter 2. In addition is a complete list of constants used in the calculations and simulations to be found in Appendix A.

DCV

The directional control valve used for testing is a pressure compensated proportional directional spool valve delivered by Hawe Hydraulik. The test rig is equipped with a valve bank consisting of three spool valves. As only one of the spool valves is used, is only this described here. A technical description of the valve bank is available in Appendix B.1. The ordering code of the valve used for testing is: PSV 31/D250-2-A 2 O 25/16 A 200 B 200S 1/EAWA/2 -E 1-G 24. Meaning, among other things, that the main spool pattern is open-center, the valve can provide a maximum flow of 25 $\frac{l}{min}$ at connector A and 16 $\frac{l}{min}$ at connector B, and that the valve got electro-hydraulic and manual actuation with integrated travel indicator. The constants used in the investigations of the stabilization method, which are based on the DCV, are listed in Table 3.1.

Table 3.1: Constants based on the DCV

Parameter	Value	Unit
$Q_{ref_{main}}$	16	$\frac{l}{min}$
$\Delta p_{ref_{main}}$	6	bar
$k_{v_{main}}$	$3.44 \cdot 10^{-7}$	$\frac{m^3}{s \cdot \sqrt{Pa}}$
$Q_{ref_{mainr}}$	50	$\frac{l}{min}$
$\Delta p_{ref_{mainr}}$	7	bar
$k_{v_{mainr}}$	$9.96 \cdot 10^{-7}$	$\frac{m^3}{s \cdot \sqrt{Pa}}$
$Q_{ref_{FCV}}$	210*	$\frac{l}{min}$
$\Delta p_{ref_{FCV}}$	5*	bar
$k_{v_{FCV}}$	$4.95 \cdot 10^{-7}$	$\frac{m^3}{s \cdot \sqrt{Pa}}$
p_Δ	6	bar
$\Delta p_{open_{FCV}}$	6*	bar
V_{C0}	$1.0 \cdot 10^{-7*}$	m^3

V_{C0} is the internal volume in between the pressure compensator and the main spool. The rest of the constants presented in Table 3.1 are described in Section 2.2.1. $Q_{ref_{FCV}}$, $\Delta p_{ref_{FCV}}$, $\Delta p_{open_{FCV}}$ and V_{C0} are based on experience, as the data sheet of the DCV do not provide detailed information about the internal pressure compensator.

CBV

The counter balance valve is delivered by Sun Hydraulics, and the ordering code is: CWCA-LHN. The CBV is an adjustable 4-port vented valve with a pilot ratio of 3:1. The crack pressure of the valve is kept at its

standard setting, 210 bar. Further information about the valve is available in Appendix B.2. The constants used in the investigations of the stabilization method, which are based on the CBV, are listed in Table 3.2.

Table 3.2: Constants based on the CBV

Parameter	Value	Unit
ρ_p	3	-
$Q_{ref_{CBV}}$	60	$\frac{l}{min}$
$\Delta p_{ref_{CBV}}$	16	bar
$k_{v_{CBV}}$	$7.906 \cdot 10^{-7}$	$\frac{m^3}{s \cdot \sqrt{Pa}}$
$\Delta p_{open_{CBV}}$	400*	bar
$p_{cr_{CBV}}$	210	bar

The constants presented in Table 3.2 are described in Section 2.2.2. $\Delta p_{open_{CBV}}$ are based on experience, as the data sheet of the CBV do not provide information about the pressure needed to fully open the valve. Please note that the CBV normally is mounted directly to the cylinder for safety reasons. As this test rig, on the other hand, is placed in a safe environment is the CBV in this case not mounted directly to the cylinder for the sake of simplicity.

Cylinder

The hydraulic cylinder is delivered by PMC Cylinders, and the ordering code is: 25CAL-65/35-0500/85. Meaning, among other things, that the piston diameter is 65 mm, the rod diameter is 35 mm and that the stroke length is 500 mm. This cylinder also got an internal sensor for piston position feedback. Further information about the cylinder is available in Appendix B.3, and Appendix B.9 for the cylinder piston position sensor. The constants used in the investigations of the stabilization method, which are based on the cylinder, are listed in Table 3.3.

Table 3.3: Constants based on the Cylinder

Parameter	Value	Unit
d_p	65	mm
d_r	35	mm
V_{A0}	$0.2 \cdot 10^{-3}$	m^3
V_{B0}	$0.25 \cdot 10^{-3}$	m^3
A_A	0.0033	m^2
A_B	0.0024	m^2
ρ_c	1.4083	-

where

d_c Piston diameter

d_r Rod diameter

V_{A0} Dead volume chamber A including tubes and hoses

V_{B0} Dead volume chamber B including tubes and hoses

A_A Piston area in chamber A

A_B Piston area in chamber B

ρ_c Area ratio

PRV

The pressure relief valve is a proportional pressure relief valve with integrated electronics delivered by Bosch Rexroth, and the ordering code is: DBETE-61/315G24K31A1V. The valve is actuated by proportional solenoid to vary the system pressure in dependence upon the electrical command value [5]. For more information about the valve see Appendix B.4. The constants used in the investigations of the stabilization method, which are based on the PRV, are listed in Table 3.4.

Table 3.4: Constants based on the PRV

Parameter	Value	Unit
$Q_{ref_{PRV}}$	2	$\frac{1}{\min}$
$\Delta p_{ref_{PRV}}$	5.75	bar
$k_{v_{PRV}}$	$4.4 \cdot 10^{-8}$	$\frac{\mathrm{m}^3}{\mathrm{s} \cdot \sqrt{\mathrm{Pa}}}$
$\Delta p_{open_{PRV}}$	280	bar

The constants presented in Table 3.4 are described in Section 2.2.3.

Adjustable orifice

The adjustable orifice is a double-acting control valve delivered by Tognella, and the ordering code is: FT 1251/2-01-14. For more information about the valve see Appendix B.5. The constants used in the investigations of the stabilization method, which are based on the adjustible orifice, are listed in Table 3.5.

Table 3.5: Constants based on the adjustable orifice

Parameter	Value	Unit
$Q_{ref_{AO}}$	2^*	$\frac{1}{\min}$
$\Delta p_{ref_{AO}}$	200^*	bar
$k_{v_{AO}}$	$7.45 \cdot 10^{-9}$	$\frac{\mathrm{m}^3}{\mathrm{s} \cdot \sqrt{\mathrm{Pa}}}$

The constants presented in Table 3.5 are described in eq. 2.3. The adjustable orifice is hardly opened to obtain the highest possible pressure drop across the orifice. Q_{ref_X} and Δp_{ref_X} are based on experience, as the data sheet of the adjustable orifice do not provide information for the valve characteristics with an opening smaller than two turns on the knob.

HPU

The test rig is connected to a Hydraulic Power Unit (HPU) with adjustable supply pressure. The constants used in the investigations of the stabilization method, which are based on the HPU, are listed in Table 3.6.

Table 3.6: Constants based on the HPU

Parameter	Value	Unit
p_S	200	bar
β	1.5^*	GPa

The oil used during testing is: MOBIL DTE 25 ISO VG 46, more information available at [4]. The bulk modulus, β, is assumed constant.

Tubes and Hoses

The test rig is equipped with a combination of hoses and tubes, as shown in Figure 3.12. For the sake of simplicity are their volume assumed constant. The constants used in the investigations of the stabilization method, which are based on tubes and hoses, are listed in Table 3.7.
V_0 is the estimated volume between the DCV and the CBV, and V_X is the estimated volume between the adjustable orifice and the PRV.

Table 3.7: Constants based on the tubes and hoses

Parameter	Value	Unit
V_0	$0.1 \cdot 10^{-3*}$	m^3
V_X	$0.1 \cdot 10^{-3*}$	m^3

Ball Valve

The ball valve is delivered by Pister, and the ordering code is: BKHG1/4 06 1113 0 PN500. The valve is used to separate the pilot line of the CBV from the pressure in chamber B. No investigation constants are based on this valve.

Sensors

The test rig is equipped with sensors monitoring the pressures throughout the circuits, the cylinder elongation, the flow on the rod side of the cylinder and the spool position of the directional control valves. A complete list of sensors are shown in Table 3.8.

Table 3.8: Test rig sensors: type and amount

Type	Amount	Further information
Pressure sensor	6	Appendix B.7
Flow sensor	1	Appendix B.8
Cylinder position sensor (Potentiometer)	1	Appendix B.9
Spool position sensor (Hall-sensor)	1	Appendix B.1

3.4 Steady State Calculations

In this section are steady state calculations for pressures in the main circuit, recall Figure 3.12, presented. The calculations are based on Figure 3.13 where the compensated DCV is illustrated as two adjustable orifices, *main* and *mainr*, and one compensator, FCV. The steady state calculations will always apply for the main circuit independent of stabilization method.
The steady state calculation is based on the following statements:

- no losses in cylinder (no friction and no leakage in cylinder)

- constant actuator speed

- constant pump pressure

- incompressible fluid

- all mechanical parts in valves are stationary

Equations for the flow trough all valves illustrated in Figure 3.13 are sat up in eq. 3.33 - 3.36. Equation for flow continuity for the cylinder is set up in eq. 3.37. Equations for the rate of valve openings are set up in eq. 3.38 and eq. 3.39, and actuator equilibrium is sat up in eq. 3.40.

$$Q_{in} - k_{v_{FCV}} \cdot u_{FCV} \cdot SIGN\left(p_S - p_C{}^{(ss)}\right) \cdot \sqrt{\left|p_S - p_C{}^{(ss)}\right|} = 0 \tag{3.33}$$

$$Q_{in} - k_{v_{main}} \cdot u \cdot SIGN\left(p_C{}^{(ss)} - p_B{}^{(ss)}\right) \cdot \sqrt{\left|p_C{}^{(ss)} - p_B{}^{(ss)}\right|} = 0 \tag{3.34}$$

$$Q_{out} - k_{v_{CBV}} \cdot u_{CBV} \cdot SIGN\left(p_A{}^{(ss)} - p_0{}^{(ss)}\right) \cdot \sqrt{\left|p_A{}^{(ss)} - p_0{}^{(ss)}\right|} = 0 \tag{3.35}$$

$$Q_{out} - kv_{mainr} \cdot u \cdot SIGN\left(p_0{}^{(ss)}\right) \cdot \sqrt{\left|p_0{}^{(ss)}\right|} = 0 \tag{3.36}$$
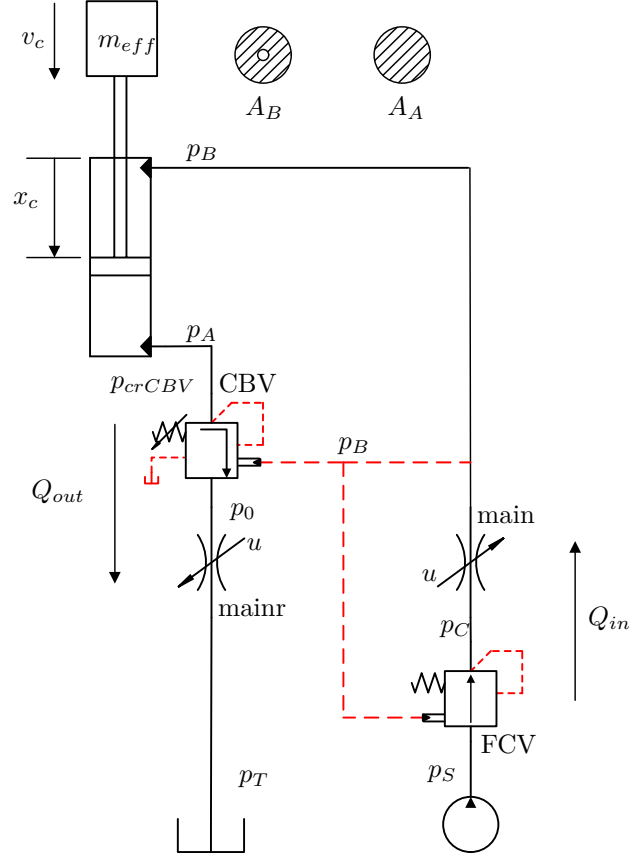
Figure 3.13: Auxiliary figure steady state calculations

$$Q_{out} - \frac{A_A}{A_B} \cdot Q_{in} = 0 \tag{3.37}$$

$$u_{FCV} - \frac{p_B{}^{(ss)} + p_{cr_{FCV}} - p_C{}^{(ss)}}{\Delta p_{open_{FCV}}} = 0 \tag{3.38}$$

$$u_{CBV} - \frac{p_B{}^{(ss)} \cdot \rho + p_A{}^{(ss)} - p_{cr_{CBV}}}{\Delta p_{open_{CBV}}} = 0 \tag{3.39}$$

$$p_A{}^{(ss)} \cdot A_A - p_B{}^{(ss)} \cdot A_B - m_{eff} \cdot g = 0 \tag{3.40}$$

The values for the flow coefficients are presented in section 3.3.2 and are also listed in Table A.1 in Appendix A. The effective mass is calculated as shown in eq. 3.41 , where F_{cyl} is calculated in eq. 3.30 from section 3.2.3.

$$m_{eff} = \frac{F_{cyl}}{g} \tag{3.41}$$

The set of equations presented in eq. 3.33 - 3.40 are non-linear due to the orifice equations. The set of equations are therefore solved numerically by fsolve in MATLAB, which uses Newton-Raphson iteration. Figure 3.14 shows the steady state pressures in p_A, p_B, p_C and p_0 as a function of cylinder piston position whit an opening of the main valve at $u = 0.1$.

Figure 3.14: Steady state pressures

3.5 Electric system

This section deals with instrumentation of the test rig and structure of the information flow between the sensors, the NI CompactRio and the PC.

3.5.1 Instrumentation

The test rig is equipped with several sensors. These sensors are used for controlling the rig and for documentation. The amount and type of the different sensors used on the rig are listed in Table 3.8 in Section 3.3.2. A compressed data sheet is made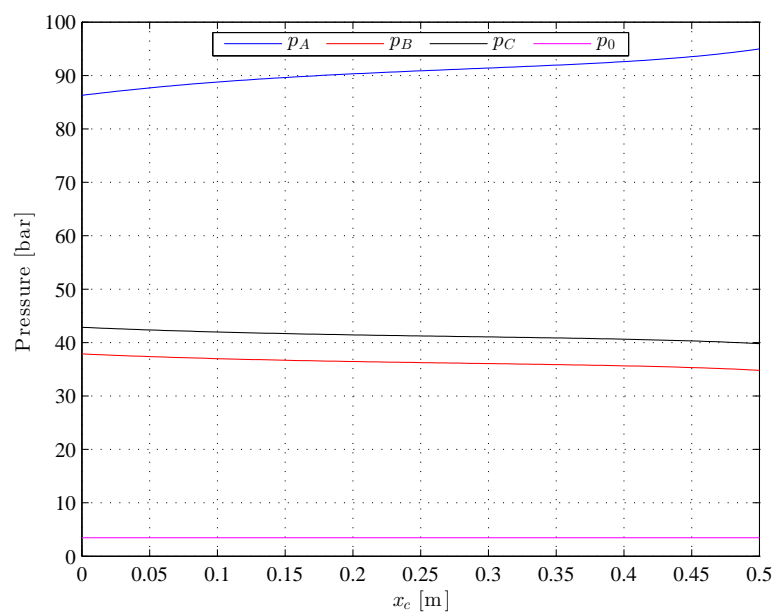 for each of the different sensors which are used, and is to be fount in Appendix B. The pressure sensors and the flow sensor are placed in the hydraulic circuit as shown in Figure 3.12. The potentiometer measuring the cylinder piston displacement and the Hall-sensor measuring the DCV spool position are not shown in the figure. These sensors are installed onto the components by the supplier.

3.5.2 Information Flow

The sensors are transducers which converts the measured value to a voltage. The voltage is then read by the cRio. An illustration of the information flow is shown in Figure 3.15.
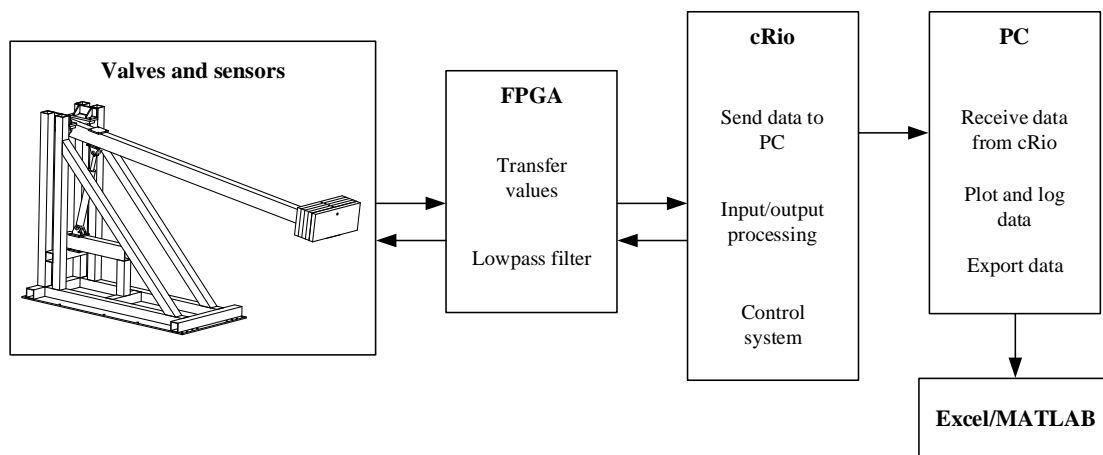
Figure 3.15: Illustration of the communication setup between the rig, FPGA, cRio and PC

FPGA

The FPGA (Field-programmable gate array) is "an integrated circuit designed to be configured by a customer or a designer after manufacturing" [7] which is a part of the cRio. The FPGA can be execute with high rate and precision due to its construction, and is therefore used for sensor reading and noise filtering.

cRio

As mentioned is the FPGA physically a part of the cRio, but is in this context regarded a separate component. A program executed on the cRio itself will not have the same low cycling time as for programs on the FPGA, but more functionalities are available. The cRio is therefore used for the processing of the values received and send from the FPGA, and for the control system. The processing is the conversion of the readings done by the sensors from a voltage to a value suitable for the control system on the cRio, and the reverse conversion of the control system values to a voltage which is send to the actuators. The control system is explained in detail in Section 4.4.

PC

The processed sensor readings are, if desired, stored on the cRio during the operation of the rig. These stored reading are then send to the PC which saves them on the hard-drive in a desired file format. This allows the sensor readings to be read and plotted by program such as Microsoft Excel and MATLAB.

Chapter 4

Stabilizing Method

This chapter introduces the method of stabilizing which are to be investigated in this thesis. Namely applying an externally produced pressure to the pilot line of the CBV or apply the external pressure to the pressure compensated DCV or, lastly, a combination. This chapter also includes a description of how the external pressure is produced.

4.1 Main Idea

It is mainly the counter balance valve that introduces oscillations in the system, especially when the flow supply is pressure compensated. The introduced oscillations causes oscillations in the pilot pressure for the CBV and in the pressure sensed by the pressure compensator for the DCV, which then starts a ring effect. The opening for the CBV and the compensator begins alter and introducing even worse oscillations of the system.

The main idea of the stabilizing method is to brake this ring effect by removing the oscillations in the pilot pressure for the CBV and the pressure sensed by the compensator. Either by assigning a low pass filtered pilot pressure to the CBV or filter the pressure sensed by the pressure compensated DCV.

4.2 Instability Description

At first, when the pressure compensated directional control valve opens and oil enters the system, is the counter balance valve closed. This is illustrated in the first window of Figure 4.1, where a stable, but increasing pilot pressure is assigned to the CBV. A smooth arrow illustrates a stable and smooth pressure, while a jagged arrow illustrates an oscillating pressure.
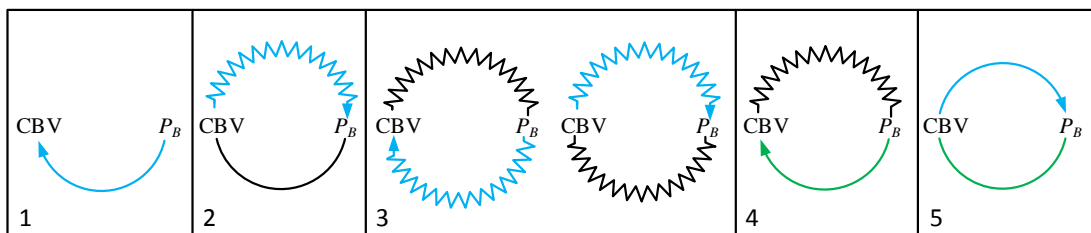
Figure 4.1: Illustration of the stabilizing principle

The fact that oil enters the system while the CBV is closed leads to a pressure built-up in the cylinder. The cylinder pressure continues to rise until it reaches a level which opens the CBV. When CBV is open, will the excess energy stored in the cylinder force the cylinder to contract quicker than first intended by the sizes of the opening of the DCV. This leads to a pressure drop on the ring side of the cylinder and is illustrated by a blue arrow in the second window of Figure 4.1. The pressure which is reduced by the quick cylinder contraction, p_B, is the pressure piloted to the CBV and sensed by the compensator, meaning that the CBV will close due to reduced pilot pressure. The pressure in the cylinder will then again rise as the CBV is

closed and the cycle will repeat itself, as illustrated in the third window in Figure 4.1. It is this stressed relationship between the counter balance valve and flow entering the circuit which causes the cylinder to contract in a jagged, or unstable, manner.

4.3 Settings Description

The intentions of the stabilizing method is, as mentioned, to calm the CBV by calming the pilot pressure, as illustrated in the fourth and fifth window in Figure 4.1, or by calming the pressure sensed by the compensator. A calmed CBV will not introduce oscillations and the cylinder will be contracted smoothly. Three methods for calming the CBV is investigated in this thesis. These three methods are called Setting 1, Setting 2 and Setting 3.

Setting 1

In Setting 1 is the pilot line of the CBV connected to the external pressure circuit introduced in Section 3.3.2. The pressure in the external pressure circuit is a low pass filtered version of pressure p_B, the original pilot pressure. This will ensure that the pilot pressure assign to the CBV is smooth and will thereby calm the CBV.

Setting 2

In Setting 2 is the pilot line of the CBV connected at its original pressure, namely the pressure between the ring side of the cylinder and the DCV. On the other hand is the pressure sensing line for the compensator connected to the external pressure circuit. The pressure in the external pressure circuit is a low pass filtered version of the pressure p_B, as this is the pressure originally sensed by the compensator. This will calm the compensator inside the DCV and, presumably, calm the pressure upstream of the DCV which is assigned to the pilot area for the CBV.

Setting 3

In Setting 3 is both the pilot line of the CBV and the pressure sensing line of the compensator connected to the external pressure circuit. This way is the CBV calmed both by ensuring a smooth pressure in the pilot line and by calming the pressure on the ring side of the cylinder.

4.4 Control System

As mentioned is the main idea of the stabilizing method to remove the oscillations in the pilot pressure of the CBV. In order to achieve this is an external pressure circuit used. The pressure in this circuit is controlled by means of a pressure relief valve (PRV). The magnitude of the pressure in front of the PRV is set by adjusting the crack pressure (the pressure required to open the PRV). The controlled pressure is then connected either to the CBV, the DCV or both. The crack pressure of the PRV is continuously regulated by the control system showed in Figure 4.2.
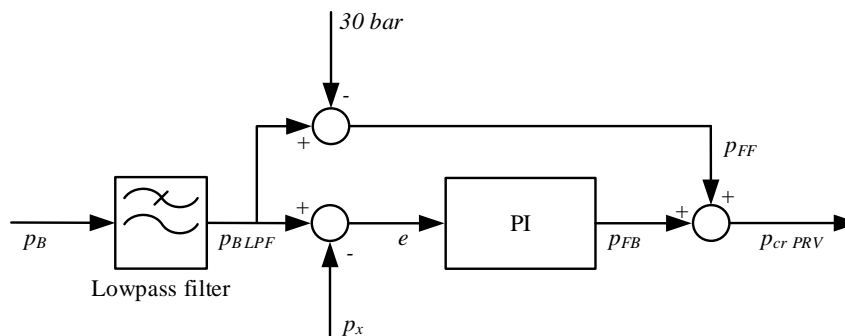

Figure 4.2: The controller used to regulate $p_{cr\,PRV}$

The pressure on the ring side of the cylinder, p_B, is first measured by a pressure sensor. The readings from the sensor is then low pass filtered to remove the undesired oscillations introduced by the CBV. This low pass filtered version of the pressure p_B, named $p_{B\,LPF}$, is the pressure desired to recreate in the external

pressure circuit by means of the PRV and the control system. The control system consist of a feedforward, a feedback and a PI controller, as shown in Figure 4.2.

4.4.1 Feedfoward

A pressure drop across the PRV of $30 bar$ is assumed. This pressure drop is subtracted from $p_{B_{LPF}}$ and the difference is used as a feedforward signal, called p_{FF}.

4.4.2 Feedback

In addition to the feedforward signal is a feedback loop added. The actual pressure in front of the PRV, p_x, is measured by a pressure sensor. The error, e, is the difference between the desired pressure, $p_{B_{LP}}$, and the produced pressure, p_x. This error is then send through a PI controller and the result, p_{FB}, is added to to the feed forward signal, p_{FF}. This sum is then converted to a voltage signal which is send to the PRV.

4.4.3 Tuning

An academic PI controller is used. This is tuned by trail and error, and the values $K_c = 2$ and $T_i = 1$ are found.

4.5 The Full Circuit

Figure 4.3 shows an illustration of the circuit considered in this thesis with the external pressure circuit and the control system added to the illustration.
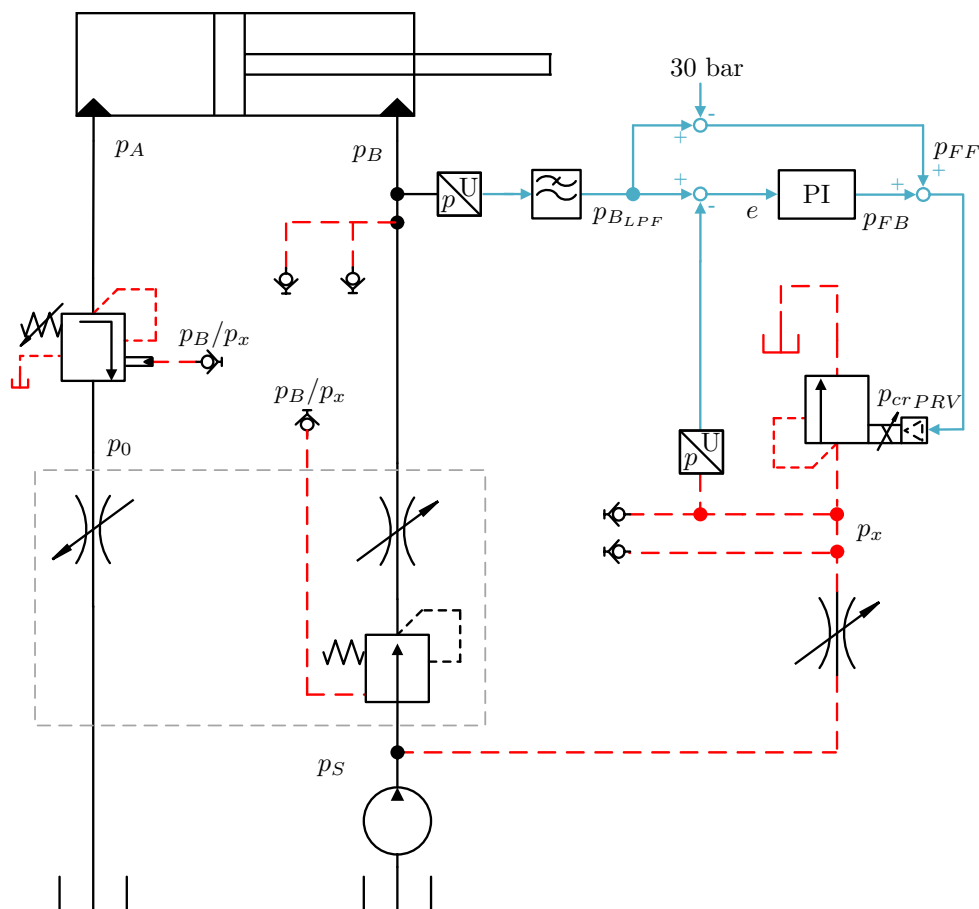

Figure 4.3: Hydraulic circuit with control system

Chapter 5

Theoretical Investigation

In this chapter is the theoretical investigation of the stability for each of the three settings presented. The investigation is carried out by first presenting each setting in an individual state space model. The state space models are then transformed into transfer functions from which the stability is investigated by Routh Hurwitz stability criterion.

In the first section is the pressure compensated DCV assumed ideal, by this is the supply flow considered constant. Setting 1 alone is investigated in the first section, as the assumption only applies for this setting. In the latter sections are the pressure compensated DCV included in the investigation in order to investigate Setting 2 and Setting 3. A second investigation of Setting 1 is preformed as well, this time with the pressure compensation included. The inclusion of the compensator enlarges the state space models and transfer functions due to the inclusion of more states. The investigation is therefore performed partly analytically and partly by the inclusion of parameter values in order to shorten the expressions.

5.1 Simplified Investigation of Setting 1

In this section is the first investigation of the stability of Setting 1 presented. The investigation is based on the same assumptions and equations used for the investigation of the original circuit, preformed in Section 2.4. The supply flow considered constant and the externally designed pressure, p_x, is assumed equal to a low pass filtration of the pressure in cylinder chamber B, p_B. Figure 5.1 shows an illustration of the circuit investigated in this section.

5.1.1 Basic Equations

In order to arrange the state space model is a set of equations describing the system needed. Four differential equations is found based on Figure 5.1. Equation 5.1 describes the cylinder acceleration. This equation is based on eq. 2.14 from Section 2.3.1. Equation 5.2 and eq. 5.3 describes the pressure gradient in cylinder chamber A and B, respectively. These equations are based on eq. 2.17 from Section 2.3.2. Equation 5.4 describes the low pass filter. This equation is based on eq. 2.19 from Section 2.3.3.

$$m_{eff} \cdot \dot{v}_c = p_B \cdot A_B - p_A \cdot \rho_c \cdot A_B + m_{eff} \cdot g \tag{5.1}$$

$$C_A \cdot \dot{p}_A = \rho_c \cdot A_B \cdot v_c - Q_r \tag{5.2}$$

$$C_B \cdot \dot{p}_B = Q_v - A_B \cdot v_c \tag{5.3}$$

$$\tau \cdot \dot{p}_x = p_B \cdot K - p_x \tag{5.4}$$

For the low pass filter in eq. 5.4 is τ the time constant and K the filter gain. Q_v is the volume flow entering cylinder chamber B. The return flow, Q_r, and the rated opening of the CBV, u_{CBV}, is calculated in eq. 5.5 and eq. 5.6, respectively. These equations are based on eq. 2.9 and eq. 2.10 from Section 2.2.2.

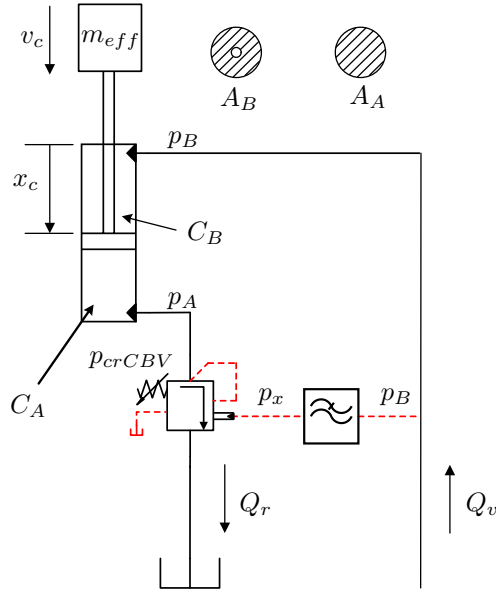$$Q_r = k_{vCBV} \cdot u_{CBV} \cdot \sqrt{p_A} \tag{5.5}$$

Figure 5.1: Simplified hydraulic circuit for Setting 1 including the low pass filter

where

$$u_{CBV} = \frac{p_x \cdot \rho_p + p_A - p_{crCBV}}{\Delta p_{openCBV}} \tag{5.6}$$

5.1.2 Linearization

Equations, which are to be arranged in a state space model, must be linear. The orifice equation, here eq. 5.5, is non-linear and must therefore be linearized. The basic equations are linearized around a certain steady state point by the use of eq. 2.23 from Section 2.3.5. Before being arranged in the state space model are the linearized equations organized as presented in eq. 5.7 - 5.12.

$$m_{eff} \cdot \dot{\tilde{v}}_c = \tilde{p}_B \cdot A_B - \tilde{p}_A \cdot \rho_c \cdot A_B \tag{5.7}$$

$$C_A \cdot \dot{\tilde{p}}_A = \rho_c \cdot A_B \cdot \tilde{v}_c - \tilde{Q}_r \tag{5.8}$$

$$C_B \cdot \dot{\tilde{p}}_B = \tilde{Q}_v - A_B \cdot \tilde{v}_c \tag{5.9}$$

$$\tau \cdot \dot{\tilde{p}}_x = \tilde{p}_B \cdot K - \tilde{p}_x \tag{5.10}$$

$$\tilde{Q}_r = k_{qu_{CBV}} \cdot \tilde{u}_{CBV} + k_{qp_{CBV}} \cdot \tilde{p}_A \tag{5.11}$$

$$\tilde{u}_{CBV} = \frac{\tilde{p}_x \cdot \rho_p + \tilde{p}_A}{\Delta p_{open_{CBV}}} \tag{5.12}$$

where

$$k_{qu_{CBV}} = \left. \frac{\partial Q_r}{\partial u_{CBV}} \right|_{ss} = k_{v_{CBV}} \cdot \sqrt{p_A{}^{(ss)}} \tag{5.13}$$

$$k_{qp_{CBV}} = \left. \frac{\partial Q_r}{\partial p_A} \right|_{ss} = \frac{k_{v_{CBV}} \cdot u_{CBV}{}^{(ss)}}{2 \cdot \sqrt{p_A{}^{(ss)}}} \tag{5.14}$$

5.1.3 State Space Model

The state space model is arranged based on the linearized differential equations, eq. 5.7 - 5.10. This is performed as in eq. 2.27 and eq. 2.28 from Section 2.3.6. The state space model is a SISO-system with four states. The states are $\tilde{p}_A$, $\tilde{p}_B$, $\tilde{p}_x$ and $\tilde{v}_c$. $\tilde{Q}_v$ is the input signal and $A_B \cdot \tilde{v}_c$ is the output signal. In order to be arranged in the state space model are the linearized differential equations re-organized as shown in eq. 5.15 - 5.18.

$$\tilde{\dot{v}}_c = \frac{A_B}{m_{eff}} \cdot \tilde{p}_B - \frac{\rho_c \cdot A_B}{m_{eff}} \cdot \tilde{p}_A \tag{5.15}$$

$$\tilde{\dot{p}}_A = \frac{\rho_c \cdot A_B}{C_A} \cdot \tilde{v}_c - \frac{k_{qu_{CBV}} \cdot \rho_p}{\Delta p_{open_{CBV}} \cdot C_A} \cdot \tilde{p}_x - \left(\frac{k_{qu_{CBV}}}{\Delta p_{open_{CBV}} \cdot C_A} + \frac{k_{qp_{CBV}}}{C_A} \right) \cdot \tilde{p}_A \tag{5.16}$$

$$\tilde{\dot{p}}_B = \frac{1}{C_B} \cdot \tilde{Q}_v - \frac{A_B}{C_B} \cdot \tilde{v}_c \tag{5.17}$$

$$\tilde{\dot{p}}_x = \frac{K}{\tau} \cdot \tilde{p}_B - \frac{1}{\tau} \cdot \tilde{p}_x \tag{5.18}$$

The state space model is finally arranged in eq. 5.19 and eq. 5.20, based on eq. 5.15 - 5.18.

$$\begin{bmatrix} \tilde{\dot{v}}_c \\ \tilde{\dot{p}}_A \\ \tilde{\dot{p}}_B \\ \tilde{\dot{p}}_x \end{bmatrix} = \begin{bmatrix} 0 & -\frac{\rho_c \cdot A_B}{m_{eff}} & \frac{A_B}{m_{eff}} & 0 \\ \frac{\rho_c \cdot A_B}{C_A} & -\left(\frac{k_{qu_{CBV}}}{\Delta p_{open_{CBV}} \cdot C_A} + \frac{k_{qp_{CBV}}}{C_A} \right) & 0 & -\frac{\rho_p \cdot k_{qu_{CBV}}}{\Delta p_{open_{CBV}} \cdot C_A} \\ -\frac{A_B}{C_B} & 0 & 0 & 0 \\ 0 & 0 & \frac{K}{\tau} & -\frac{1}{\tau} \end{bmatrix} \begin{bmatrix} \tilde{v}_c \\ \tilde{p}_A \\ \tilde{p}_B \\ \tilde{p}_x \end{bmatrix} + \begin{bmatrix} 0 \\ 0 \\ \frac{1}{C_B} \\ 0 \end{bmatrix} \cdot \tilde{Q}_v \tag{5.19}$$

$$y = \begin{bmatrix} A_B & 0 & 0 & 0 \end{bmatrix} \begin{bmatrix} \tilde{v}_c \\ \tilde{p}_A \\ \tilde{p}_B \\ \tilde{p}_x \end{bmatrix} \tag{5.20}$$

5.1.4 Transfer Function

The transfer function is calculated based on the state space model as shown in eq. 2.29 from Section 2.3.7. The calculated transfer function is presented in eq. 5.21.

$$\frac{Y(s)}{U(s)} = \frac{N_2 \cdot s^2 + N_1 \cdot s + N_0}{D_4 \cdot s^4 + D_3 \cdot s^3 + D_2 \cdot s^2 + D_1 \cdot s + D_0} \tag{5.21}$$

where

$$N_0 = A_B{}^2 \cdot \left(\frac{k_{qu_{CBV}}}{\Delta p_{open_{CBV}}} \cdot (1 + \rho_p \cdot \rho_c \cdot K) + k_{qp_{CBV}} \right) \tag{5.22}$$

$$N_1 = A_B{}^2 \cdot \left(C_A + \tau \cdot \left(\frac{k_{qu_{CBV}}}{\Delta p_{open_{CBV}}} + k_{qp_{CBV}} \right) \right) \tag{5.23}$$

$$N_2 = A_B{}^2 \cdot C_A \cdot \tau \tag{5.24}$$

$$D_0 = A_B{}^2 \cdot \left(\frac{k_{qu_{CBV}}}{\Delta p_{open_{CBV}}} \cdot (1 + \rho \cdot \rho_c \cdot K) + k_{qp_{CBV}} \right) \tag{5.25}$$

$$D_1 = A_B{}^2 \left(C_A + C_B \cdot \rho_c{}^2 + \tau \cdot \left(\frac{k_{qu_{CBV}}}{\Delta p_{open_{CBV}}} + k_{qp_{CBV}} \right) \right) \tag{5.26}$$

$$D_2 = C_B \cdot m_{eff} \cdot \left(\frac{k_{qu_{CBV}}}{\Delta p_{open_{CBV}}} + k_{qp_{CBV}} \right) + A_B{}^2 \cdot \tau \cdot (C_A + C_B \cdot \rho_c{}^2) \tag{5.27}$$

$$D_3 = C_B \cdot m_{eff} \cdot \left(C_A + \tau \cdot \left(\frac{k_{qu_{CBV}}}{\Delta p_{open_{CBV}}} + k_{qp_{CBV}} \right) \right) \tag{5.28}$$

$$D_4 = C_A \cdot C_B \cdot m_{eff} \cdot \tau \tag{5.29}$$

5.1.5 Routh-Hurwitz Stability Criterion

The stability of the circuit presented in Figure 5.1 is investigated based on its transfer function. In order for the system to be stable, must polynomial in the denominator only consist of roots with negative real part. This is investigated by means of Routh-Hurwitz stability criterion. The influence of τ on the stability

is of great interest in this investigation. As the denominator of the transfer function from eq. 5.21 is a 4th order polynomial, must it meet the inequalities presented in eq. 2.35 - 2.37 in Section 2.3.8 in order to be considered stable by the stability criterion.

First Criterion

The inequality in eq. 2.35 is always fulfilled for this circuit as none of the constants in the D_j-terms can ever be negative. The inequality in eq. 2.36 and eq. 2.37, on the other hand, must be further investigated in order to determine the stability of the system.

Second Criterion

The terms of eq. 2.36 are substituted by eq. 5.25 - 5.29 as shown in eq. 5.30.

$$D_3 \cdot D_2 > D_4 \cdot D_1 \tag{2.36}$$

$$C_B \cdot m_{eff} \cdot \left(C_A + \tau \cdot \left(\frac{k_{qu_{CBV}}}{\Delta p_{open_{CBV}}} + k_{qp_{CBV}} \right) \right) \cdot \left(C_B \cdot m_{eff} \cdot \left(\frac{k_{qu_{CBV}}}{\Delta p_{open_{CBV}}} + k_{qp_{CBV}} \right) + A_B{}^2 \cdot \tau \cdot \left(C_A + C_B \cdot \rho_c{}^2 \right) \right) \ \rangle$$
$$C_A \cdot C_B \cdot m_{eff} \cdot \tau \cdot A_B{}^2 \left(C_A + C_B \cdot \rho_c{}^2 + \tau \cdot \left(\frac{k_{qu_{CBV}}}{\Delta p_{open_{CBV}}} + k_{qp_{CBV}} \right) \right) \tag{5.30}$$

Further is k_{CBV} defined as shown in eq. 5.31 in order to simplify eq. 5.30.

$$k_{CBV} = \frac{k_{qu_{CBV}}}{\Delta p_{open_{CBV}}} + k_{qp_{CBV}} \tag{5.31}$$

Equation 5.30 is then re-arranged as shown in eq. 5.32

$$G_2 \cdot \tau^2 + G_1 \cdot \tau + G_0 > 0 \tag{5.32}$$

where

$$G_0 = C_A \cdot C_B \cdot m_{eff} \cdot k_{CBV} \tag{5.33}$$
$$G_1 = C_B \cdot m_{eff} \cdot k_{CBV} \tag{5.34}$$
$$G_2 = C_B \cdot A_B{}^2 \cdot \rho_c \cdot k_{CBV} \tag{5.35}$$
$$\tag{5.36}$$

None of the terms of eq. 5.33 - 5.35 will ever be negative. The second order system in eq. 5.32 is therefore positive as long as τ is a positive value. The inequality in eq. 2.36 is therefore met.

Third Criterion

The terms of eq. 2.37 is substituted by eq. 5.25 - 5.29 as shown in eq. 5.37.

$$D_3 \cdot D_2 \cdot D_1 > D_4 \cdot D_1{}^2 + D_3{}^2 \cdot D_0 \tag{2.37}$$

$$m_{eff} \cdot C_B \cdot \left(C_A + \tau \cdot \left(\frac{k_{qu_{CBV}}}{\Delta p_{open_{CBV}}} + k_{qp_{CBV}} \right) \right) \cdot \left(m_{eff} \cdot C_B \cdot \left(\frac{k_{qu_{CBV}}}{\Delta p_{open_{CBV}}} + k_{qp_{CBV}} \right) + A_B{}^2 \cdot \tau \cdot \left(C_A + C_B \cdot \rho_c{}^2 \right) \right) \cdot$$
$$A_B{}^2 \cdot \left(C_A + C_B \cdot \rho_c{}^2 + \tau \cdot \left(\frac{k_{qu_{CBV}}}{\Delta p_{open_{CBV}}} + k_{qp_{CBV}} \right) \right) \ \rangle \ m_{eff} \cdot C_A \cdot C_B \cdot \tau \cdot A_B{}^4 \cdot$$
$$\left(C_A + C_B \cdot \rho_c{}^2 + \tau \cdot \left(\frac{k_{qu_{CBV}}}{\Delta p_{open_{CBV}}} + k_{qp_{CBV}} \right) \right)^2 \cdot m_{eff}{}^2 \cdot C_B{}^2 \cdot \left(C_A + \tau \cdot \left(\frac{k_{qu_{CBV}}}{\Delta p_{open_{CBV}}} + k_{qp_{CBV}} \right) \right)^2 \cdot A_B{}^2 \cdot$$
$$\left(\frac{k_{qu_{CBV}}}{\Delta p_{open_{CBV}}} + k_{qp_{CBV}} + \frac{k_{qu_{CBV}}}{\Delta p_{open_{CBV}}} \cdot \rho_p \cdot \rho_c \cdot K \right) \tag{5.37}$$

Further is k_{ρ_c} defined as shown in eq. 5.38 in order to simplify eq. 5.37.

$$k_{\rho_c} = \frac{k_{qu_{CBV}}}{\Delta p_{open_{CBV}}} \cdot \rho_p \cdot \rho_c \cdot K \tag{5.38}$$

Equation 5.37 is then re-arranged as shown in eq. 5.39

$$H_3 \cdot \tau^3 + H_2 \cdot \tau^2 + H_1 \cdot \tau + H_0 > 0 \tag{5.39}$$

where

$$H_0 = C_A \cdot C_B \cdot m_{eff} \cdot \left(C_B \cdot \rho_c^2 \cdot k_{CBV} - C_A \cdot k_{\rho_c}\right) \tag{5.40}$$

$$H_1 = C_B \cdot m_{eff} \cdot k_{CBV} \left(C_B \cdot \rho_c^2 \cdot k_{CBV} - 2 \cdot C_A \cdot k_{\rho_c}\right) \tag{5.41}$$

$$H_2 = C_B \cdot k_{CBV} \cdot \left(C_B \cdot A_B^2 \cdot \rho_c^4 + C_A \cdot A_B^2 \cdot \rho_c^2 - m_{eff} \cdot k_{\rho_c} \cdot k_{CBV}\right) \tag{5.42}$$

$$H_3 = C_B \cdot A_B^2 \cdot \rho_c^2 \cdot k_{CBV}^2 \tag{5.43}$$

Equation 5.40 - 5.42 may be negative and are therefore further investigated.

5.1.6 Evaluation of the Stability

The first and second criterion is always fulfilled. The third criterion, on the other hand, may not be fulfilled as H_0, H_1 and H_2 contains negative terms.
H_0 is positive if:

$$C_B \cdot \rho_c^2 \cdot k_{CBV} > C_A \cdot k_{\rho_c}$$
$$\Downarrow$$
$$\frac{C_B}{C_A} \cdot \frac{\rho_c}{\rho_p \cdot K} \left(1 + \frac{\Delta p_{open_{CBV}} \cdot u_{CBV}^{(ss)}}{2 \cdot p_A^{(ss)}}\right) > 1 \tag{5.44}$$

H_1 is positive if:

$$C_B \cdot \rho_c^2 \cdot k_{CBV} > 2 \cdot C_A \cdot k_{\rho_c}$$
$$\Downarrow$$
$$\frac{C_B}{2 \cdot C_A} \cdot \frac{\rho_c}{\rho_p \cdot K} \left(1 + \frac{\Delta p_{open_{CBV}} \cdot u_{CBV}}{2 \cdot p_A}\right) > 1 \tag{5.45}$$

H_2 is positive if:

$$C_B \cdot A_B^2 \cdot \rho_c^4 + C_A \cdot A_B^2 \cdot \rho_c^2 > m_{eff} \cdot k_{\rho_c} \cdot k_{CBV}$$
$$\Downarrow$$
$$C_B \cdot A_B^2 \cdot \rho_c^3 + C_A \cdot A_B^2 \cdot \rho_c > m_{eff} \cdot k_{v_{CBV}}^2 \rho_p \cdot K \cdot \left(\frac{p_A}{\Delta p_{open_{CBV}}} + \frac{u_{CBV}}{2}\right) \tag{5.46}$$

Evaluation of H_0 and H_1

H_0 and H_1 is negative if all the criteria listed below are fulfilled.

- The low pass filter gain, K, is equal 1

- $\frac{\rho_c}{\rho_p \cdot K} < 1$, which may happen as ρ_p usually is greater than ρ_c

- $\frac{\Delta p_{open_{CBV}} \cdot u_{CBV}}{2 \cdot p_A} << 1$, which happens with a high pressure in p_A and a small opening of the CBV

- $C_A >> C_B$, which happens when the cylinder is fully extended

47

Evaluation of H_2

If $\rho_p \cdot K \cdot \left(\frac{p_A}{\Delta p_{open_{CBV}}} + \frac{u_{CBV}}{2} \right) \approx 1$, and the cylinder is fully extended can eq. 5.46 be written as:

$$C_A \cdot A_B{}^2 \cdot \rho_c > m_{eff} \cdot k_{v_{CBV}}{}^2 \tag{5.47}$$

If $\rho_p \cdot K \cdot \left(\frac{p_A}{\Delta p_{open_{CBV}}} + \frac{u_{CBV}}{2} \right) \approx 1$, and the cylinder is fully retracted can eq. 5.46 be written as:

$$C_B \cdot A_B{}^2 \cdot \rho_c{}^3 > m_{eff} \cdot k_{v_{CBV}}{}^2 \tag{5.48}$$

H_2 may therefore be negative for systems with a high load pressure.

Discussion

H_0, H_1 and H_2 may all be negative if the cylinder is fully extended and the load pressure is to high. The system will then be unstable for low values of τ. H_0 and H_1 may be positive if the cylinder is fully retracted. H_2 will, on the other hand, still be negative for systems with high load pressure. A minimum value of τ is therefore required for the system to be stable in all positions.

5.1.7   Estimation of τ

Further is τ estimated by calculating eq. 5.39 with parameters from the test rig presented in Chapter 3. τ is estimated for five positions, namely $x_c = 50$ mm, $x_c = 150$ mm, $x_c = 250$ mm, $x_c = 350$ mm and $x_c = 450$ mm. The input flow is $2.4\frac{l}{\min}$ which is considered a small flow and would cause oscillations in the original system. Three different cases are investigated to map their effect on the value of τ. First is τ estimated with the parameters presented in Chapter 3. This is shown in Figure 5.2. Further is the load pressure kept constant in order to clarify the effect of the cylinder piston position. The results of this investigation is shown in Figure 5.3. Lastly is the effect of an increase in the load investigated, shown in Figure 5.4. Two graphs are presented for each investigation. The fist graph shows the pressure in chamber A, p_A, and chamber B, p_B compared to x_c. The second graph shows the calculated value of $H_3 \cdot \tau^3 + H_2 \cdot \tau^2 + H_1 \cdot \tau + H_0$ compared to τ for the five cylinder piston positions. Recall that the system is stable if $H_3 \cdot \tau^3 + H_2 \cdot \tau^2 + H_1 \cdot \tau + H_0 > 0$.

Discussion

Please recall that a higher value of τ means that a lower cutoff frequency of the low pass filter is required. On the other hand, a very low value of τ means that a low pass filter is almost unnecessary. Figure 5.2 shows that the highest value of τ is required when the cylinder is fully extended, and that the value decreases as the cylinder is contracted. Figure 5.3 verifies this as the characteristics are the same even if the load pressure is kept constant. An increase in the load increases the load pressure and will affect the requirements of τ. Figure 5.4 shows that the requirements of τ if increased if the weight of the ballast stack is increased from 320 kg to 800 kg.
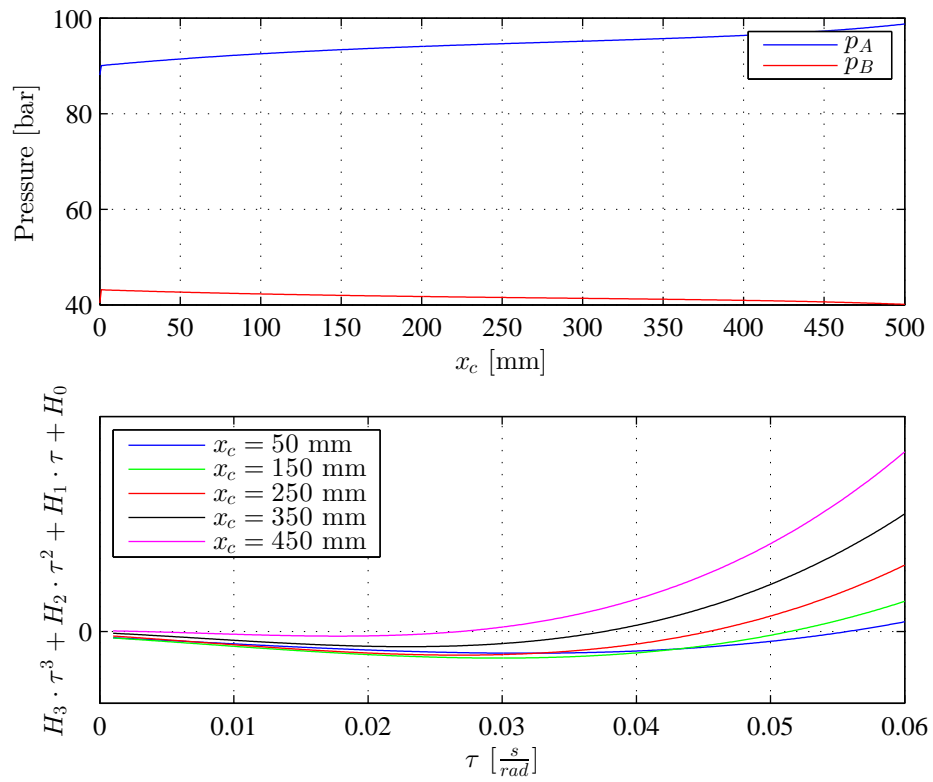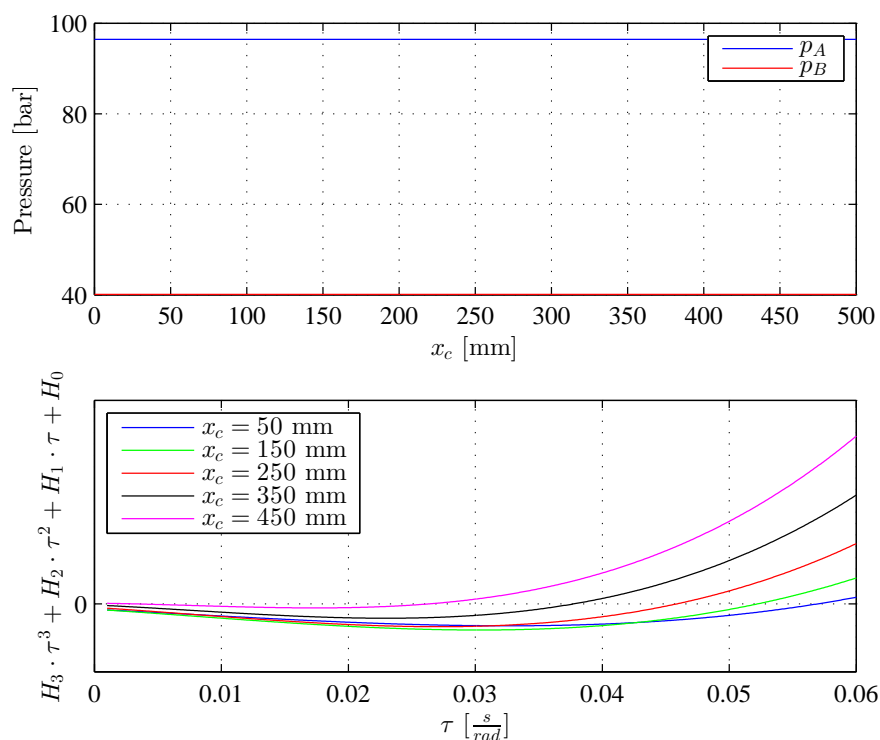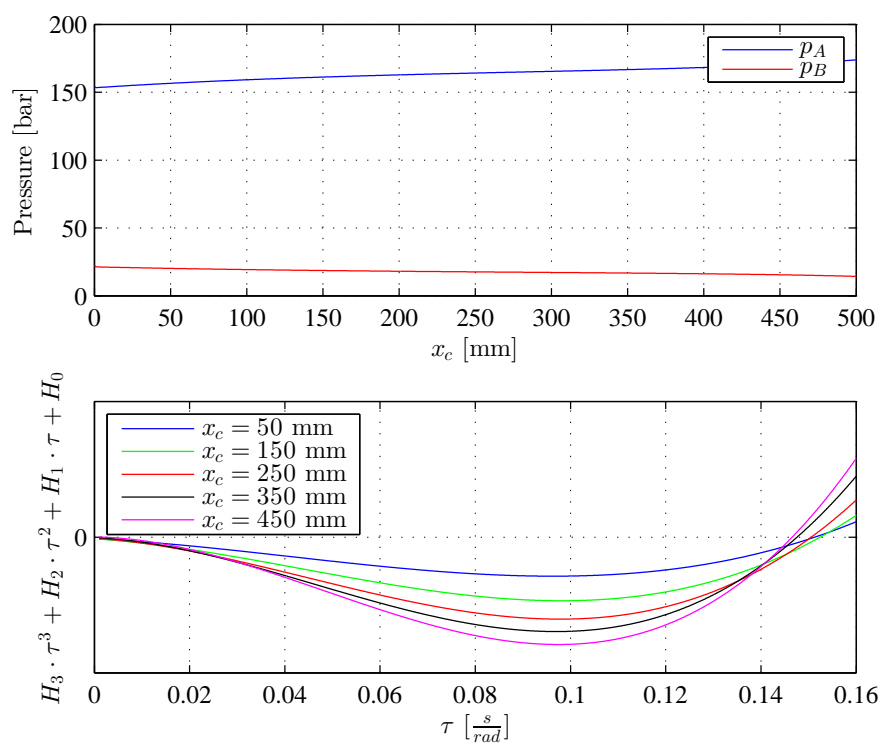
Figure 5.2: System pressures and estimated values of τ for the test rig

Figure 5.3: System pressures and estimated values of τ with a constant load pressure

Figure 5.4: System pressures and estimated values of τ for the test rig with an increase in the load

5.2 Investigation of Setting 1

In this section is a more complex investigation of Setting 1 preformed. The complexity is increased as the pressure compensated DCV is included, instead of being assumed ideal. The purposes of this investigation are to verify the simplification made in the simplified investigation of Setting 1, and to present investigations of all settings at the same complexity level. An illustration of the circuit investigated in this section is shown in Figure 5.5.
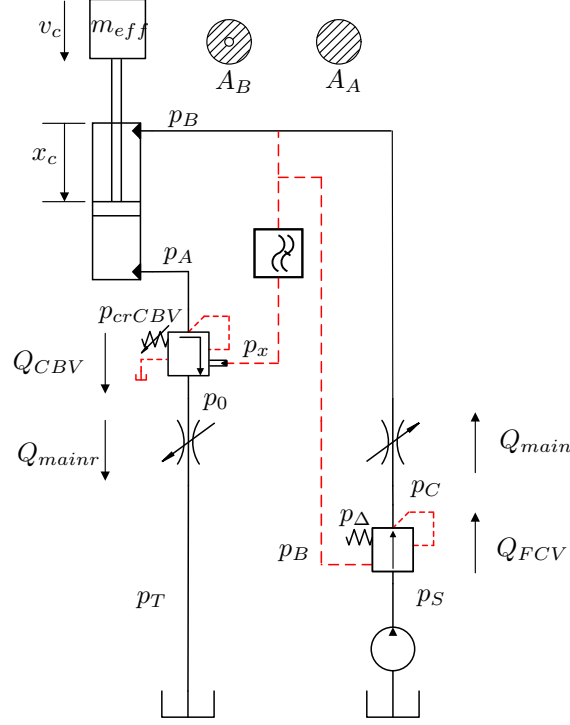

Figure 5.5: Simplified hydraulic circuit, p_x connected to CBV

The pressure compensated directional control valve is illustrated and modeled as two adjustable orifices, *main* and *mainr*, which represents the main spool, and a flow control valve that controls the pressure drop across *main*.

5.2.1 Basic Equations

Six differential equations are found based on Figure 5.5. Equation 5.49 describes the cylinder acceleration. This equation is based on eq. 2.14 from Section 2.3.1. Equation 5.50 - 5.53 describes the pressure gradient in cylinder chamber A and B, the volume between the main spool and the FCV, and the volume between the main spool and the CBV, respectively. These equations are based on eq. 2.17 from Section 2.3.2. Equation 5.54 describes the low pass filter. This equation is based on eq. 2.19 from Section 2.3.3.

$$m_{eff} \cdot \dot{v}_c = p_B \cdot A_B - p_A \cdot \rho_c \cdot A_B + m_{eff} \cdot g \tag{5.49}$$

$$C_A \cdot \dot{p}_A = \rho_c \cdot A_B \cdot v_c - Q_{CBV} \tag{5.50}$$

$$C_B \cdot \dot{p}_B = Q_{main} - A_B \cdot v_c \tag{5.51}$$

$$C_C \cdot \dot{p}_C = Q_{FCV} - Q_{main} \tag{5.52}$$

$$C_0 \cdot \dot{p}_0 = Q_{CBV} - Q_{mainr} \tag{5.53}$$

$$\tau \cdot \dot{p}_x = p_B \cdot K - p_x \tag{5.54}$$

51

The flows indicated in Figure 5.5 are calculated as shown in eq. 5.55 - 5.58. The rate of opening of the CBV and the FCV are calculated as shown in eq. 5.59 and eq. 5.60, based on Section 2.2.2 and Section 2.2.1, respectively. u is the rated opening of the main spool.

$$Q_{mainr} = k_{v_{mainr}} \cdot u \cdot \sqrt{p_0} \tag{5.55}$$

$$Q_{CBV} = k_{v_{CBV}} \cdot u_{CBV} \cdot \sqrt{p_A - p_0} \tag{5.56}$$

$$Q_{main} = k_{v_{main}} \cdot u \cdot \sqrt{p_C - p_B} \tag{5.57}$$

$$Q_{FCV} = k_{v_{FCV}} \cdot u_{FCV} \cdot \sqrt{p_S - p_C} \tag{5.58}$$

where

$$u_{CBV} = \frac{p_x \cdot \rho_p + p_A - p_{cr_{CBV}}}{\Delta P_{open_{CBV}}} \tag{5.59}$$

$$u_{FCV} = \frac{p_B + p_\Delta - p_C}{\Delta P_{open_{FCV}}} \tag{5.60}$$

5.2.2 Linearization

Further are the basic equations linearized around a certain steady state point. The linearization is performed as described in eq. 2.22 in Section 2.3.5. The linearized basic equations are presented in eq. 5.61 - 5.72.

$$m_{eff} \cdot \tilde{v}_c = \tilde{p}_B \cdot A_B - \tilde{p}_A \cdot \rho_c \cdot A_B \tag{5.61}$$

$$C_A \cdot \dot{\tilde{p}}_A = \rho_c \cdot A_B \cdot \tilde{v}_c - \tilde{Q}_{CBV} \tag{5.62}$$

$$C_B \cdot \dot{\tilde{p}}_B = \tilde{Q}_{main} - A_B \cdot \tilde{v}_c \tag{5.63}$$

$$C_C \cdot \dot{\tilde{p}}_C = \tilde{Q}_{FCV} - \tilde{Q}_{main} \tag{5.64}$$

$$C_0 \cdot \dot{\tilde{p}}_0 = \tilde{Q}_{CBV} - \tilde{Q}_{mainr} \tag{5.65}$$

$$\tau \cdot \dot{\tilde{p}}_x = \tilde{p}_B \cdot K - \tilde{p}_x \tag{5.66}$$

$$\tilde{Q}_{mainr} = k_{qu_{mainr}} \cdot \tilde{u} + k_{qp_{mainr}} \cdot \tilde{p}_0 \tag{5.67}$$

$$\tilde{Q}_{CBV} = k_{qu_{CBV}} \cdot \tilde{u}_{CBV} + k_{qp_{CBV}} \cdot (\tilde{p}_A - \tilde{p}_0) \tag{5.68}$$

$$\tilde{Q}_{FCV} = k_{qu_{FCV}} \cdot \tilde{u}_{FCV} - k_{qp_{FCV}} \cdot \tilde{p}_C \tag{5.69}$$

$$\tilde{Q}_{main} = k_{qu_{main}} \cdot \tilde{u} + k_{qp_{mian}} \cdot (\tilde{p}_C - \tilde{p}_B) \tag{5.70}$$

$$\tilde{u}_{CBV} = \frac{\tilde{p}_x \cdot \rho_p + \tilde{p}_A}{\Delta p_{open_{CBV}}} \tag{5.71}$$

$$\tilde{u}_{FCV} = \frac{\tilde{p}_B - \tilde{p}_C}{\Delta p_{open_{FCV}}} \tag{5.72}$$

where

$$k_{qu_{mainr}} = k_{v_{mainr}} \cdot \sqrt{p_0^{(ss)}} \tag{5.73}$$

$$k_{qp_{mainr}} = \frac{k_{v_{mainr}} \cdot u^{(ss)}}{2 \cdot \sqrt{p_0^{(ss)}}} \tag{5.74}$$

$$k_{qu_{CBV}} = k_{v_{CBV}} \cdot \sqrt{p_A^{(ss)} - p_0^{(ss)}} \tag{5.75}$$

$$k_{qp_{CBV}} = \frac{k_{v_{CBV}} \cdot u_{CBV}^{(ss)}}{2 \cdot \sqrt{p_A^{(ss)} - p_0^{(ss)}}} \tag{5.76}$$

$$k_{qu_{FCV}} = k_{v_{FCV}} \cdot \sqrt{p_S - p_C^{(ss)}} \tag{5.77}$$

$$k_{qp_{FCV}} = \frac{k_{v_{FCV}} \cdot u_{FCV}^{(ss)}}{2 \cdot \sqrt{p_S - p_C^{(ss)}}} \tag{5.78}$$

5.2.3 State Space Model

The state space model is arranged based on the linearized differential equations, eq. 5.61 - 5.66. This is performed as in eq. 2.27 and eq. 2.28 in Section 2.3.6. The state space model is a SISO-system with six states. The states are $\tilde{p}_A$, $\tilde{p}_B$, $\tilde{p}_C$, $\tilde{p}_x$, $\tilde{p}_0$ and $\tilde{v}_c$. $\tilde{u}$ is the input signal and $A_B \cdot \tilde{v}_c$ is the output signal. In order to be arranged in the state space model are the linearized differential equations re-organized as shown in eq. 5.79 - 5.84.

$$\dot{\tilde{v}}_c = -\frac{\rho_c \cdot A_B}{m_{eff}} \cdot \tilde{p}_A + \frac{A_B}{m_{eff}} \cdot \tilde{p}_B \tag{5.79}$$

$$\dot{\tilde{p}}_A = \frac{\rho_c \cdot A_B}{C_A} \cdot \tilde{v}_c - \left(\frac{k_{qp_{CBV}}}{C_A} + \frac{k_{qu_{CBV}}}{\Delta p_{open_{CBV}} \cdot C_A} \right) \cdot \tilde{p}_A + \frac{k_{qp_{CBV}}}{C_A} \cdot \tilde{p}_0 - \frac{k_{qu_{CBV}} \cdot \rho_p}{\Delta p_{open_{CBV}} \cdot C_A} \cdot \tilde{p}_x \tag{5.80}$$

$$\dot{\tilde{p}}_B = -\frac{A_B}{C_B} \cdot \tilde{v}_c - \frac{k_{qp_{main}}}{C_B} \cdot \tilde{p}_B + \frac{k_{qp_{main}}}{C_B} \cdot \tilde{p}_C + \frac{k_{qu_{main}}}{C_B} \cdot \tilde{u} \tag{5.81}$$

$$\dot{\tilde{p}}_C = \left(\frac{k_{qp_{main}}}{C_C} + \frac{k_{qu_{FCV}}}{\Delta p_{open_{FCV}} \cdot C_C} \right) \cdot \tilde{p}_B - \left(\frac{k_{qp_{main}}}{C_C} + \frac{k_{qp_{FCV}}}{C_C} + \frac{k_{qu_{FCV}}}{\Delta p_{open_{FCV}} \cdot C_C} \right) \cdot \tilde{p}_C - \frac{k_{qu_{main}}}{C_C} \cdot \tilde{u} \tag{5.82}$$

$$\dot{\tilde{p}}_0 = \left(\frac{k_{qp_{CBV}}}{C_0} + \frac{k_{qu_{CBV}}}{\Delta p_{open_{CBV}} \cdot C_0} \right) \cdot \tilde{p}_A - \left(\frac{k_{qp_{CBV}}}{C_0} + \frac{k_{qp_{mainr}}}{C_0} \right) \cdot \tilde{p}_0 + \frac{k_{qu_{CBV}} \cdot \rho_p}{\Delta p_{open_{CBV}} \cdot C_0} \cdot \tilde{p}_x - \frac{k_{qu_{mainr}}}{C_0} \cdot \tilde{u} \tag{5.83}$$

$$\dot{\tilde{p}}_x = \frac{K}{\tau} \cdot \tilde{p}_B - \frac{1}{\tau} \cdot \tilde{p}_x \tag{5.84}$$

The state space model is finally arranged in eq. 5.85 and eq. 5.86, based on eq. 5.79 - 5.84.

$$\begin{bmatrix} \dot{\tilde{v}}_c \\ \dot{\tilde{p}}_A \\ \dot{\tilde{p}}_B \\ \dot{\tilde{p}}_C \\ \dot{\tilde{p}}_0 \\ \dot{\tilde{p}}_x \end{bmatrix} = \begin{bmatrix} 0 & -\dfrac{\rho_c \cdot A_B}{m_{eff}} & \dfrac{A_B}{m_{eff}} & 0 & 0 & 0 \\[2ex] \dfrac{\rho_c \cdot A_B}{C_A} & -\left(\dfrac{k_{qp_{CBV}}}{C_A}+\dfrac{k_{qu_{CBV}}}{\Delta p_{open_{CBV}} \cdot C_A}\right) & 0 & 0 & \dfrac{k_{qp_{CBV}}}{C_A} & -\dfrac{k_{qu_{CBV}} \cdot \rho_p}{\Delta p_{open_{CBV}} \cdot C_A} \\[2ex] -\dfrac{A_B}{C_B} & 0 & -\dfrac{k_{qp_{main}}}{C_B} & \dfrac{k_{qp_{main}}}{C_B} & 0 & 0 \\[2ex] 0 & 0 & \dfrac{k_{qp_{main}}}{C_C}+\dfrac{k_{qu_{FCV}}}{\Delta p_{open_{FCV}} \cdot C_C} & -\left(\dfrac{k_{qp_{main}}}{C_C}+\dfrac{k_{qu_{FCV}}}{\Delta p_{open_{FCV}} \cdot C_C}\right) & 0 & 0 \\[2ex] 0 & \dfrac{k_{qp_{CBV}}}{C_0}+\dfrac{k_{qu_{CBV}}}{\Delta p_{open_{CBV}} \cdot C_0} & 0 & 0 & -\left(\dfrac{k_{qp_{CBV}}}{C_0}+\dfrac{k_{qp_{mainr}}}{C_0}\right) & \dfrac{k_{qu_{CBV}} \cdot \rho_p}{\Delta p_{open_{CBV}} \cdot C_0} \\[2ex] 0 & 0 & \dfrac{K}{\tau} & 0 & 0 & -\dfrac{1}{\tau} \end{bmatrix} \cdot \begin{bmatrix} \tilde{v}_c \\ \tilde{p}_A \\ \tilde{p}_B \\ \tilde{p}_C \\ \tilde{p}_0 \\ \tilde{p}_x \end{bmatrix} + \begin{bmatrix} 0 \\ 0 \\ \dfrac{k_{qu_{main}}}{C_B} \\ -\dfrac{k_{qu_{main}}}{C_C} \\ -\dfrac{k_{qu_{mainr}}}{C_0} \\ 0 \end{bmatrix} \cdot \tilde{u} \tag{5.85}$$

$$\mathbf{y} = \begin{bmatrix} A_B & 0 & 0 & 0 & 0 & 0 \end{bmatrix} \begin{bmatrix} \tilde{v}_c \\ \tilde{p}_A \\ \tilde{p}_B \\ \tilde{p}_C \\ \tilde{p}_0 \\ \tilde{p}_x \end{bmatrix} \tag{5.86}$$

5.2.4 Transfer Function

The transfer function is calculated based on the state space model as shown in eq. 2.29 in Section 2.3.7. As there are six states in the state space model is the denominator of the transfer function a 6th order polynomial. An analytic investigation of the stability is in this case very unhandy. Parameter values from Chapter 3 are therefore implemented in order to ease the representation. Further is the influence τ has on the stability investigated for certain values of x_c and u. The transfer function is therefore represented as shown in eq. 5.87 where N_1 - N_4 and D_1 - D_6 are functions of τ, and N_0 and D_0 are constants.

$$G(s) = \frac{N_4(\tau) \cdot s^4 + N_3(\tau) \cdot s^3 + N_2(\tau) \cdot s^2 + N_1(\tau) \cdot s + N_0}{D_6(\tau) \cdot s^6 + D_5(\tau) \cdot s^5 + D_4(\tau) \cdot s^4 + D_3(\tau) \cdot s^3 + D_2(\tau) \cdot s^2 + D_1(\tau) \cdot s + D_0} \qquad (5.87)$$

5.2.5 Routh-Hurwitz Stability Criterion

In order for a system to be stable must all poles be in the left half plane. As the denominator is a 6th order polynomial is this investigated by Routh-array, Table 2.1 in Section 2.3.8. A system is considered stable when the sign of the values in the first column of Table 2.1 is the same, as each sign change represents a pole in the right half plane. Further is the sign of the value in each row of the first column of Table 2.1 investigated for $u = 0.15$ and $x_c = 50$ mm with respect to τ. The result is shown in Figure 5.6.
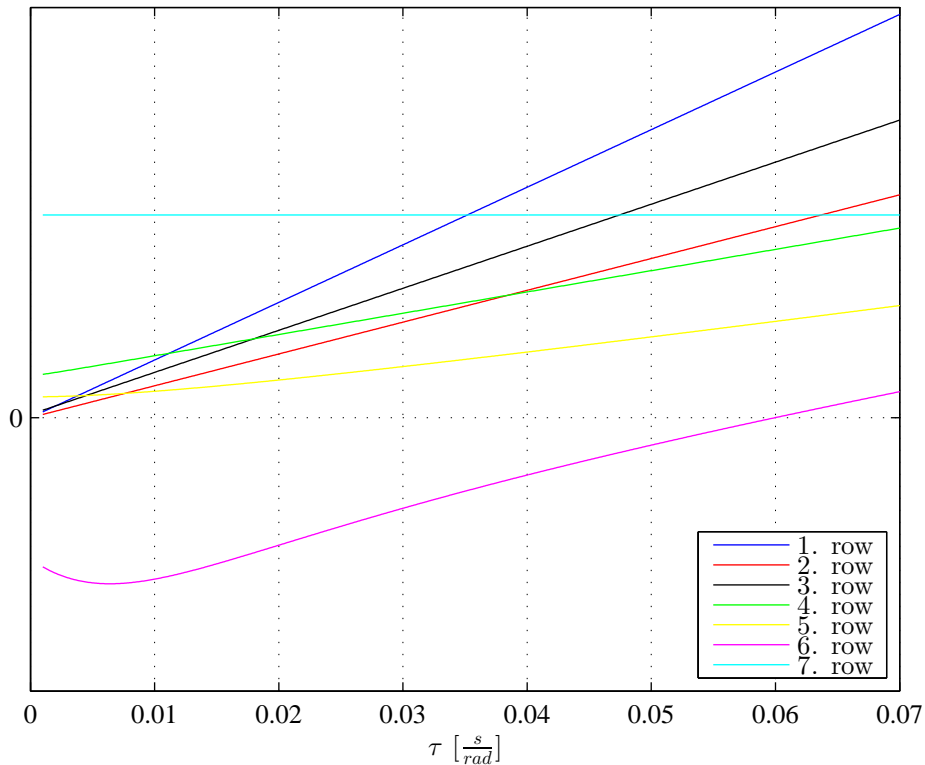

Figure 5.6: The sign of the value in each row of the first column of Table 2.1 for $u = 0.15$ and $x_c = 50$ mm with respect to τ

Figure 5.6 shows that the 6. row is the only row which changes sign. This can be shown to be the case for all the investigated cylinder piston positions, $x_c = 50$ mm, $x_c = 150$ mm, $x_c = 250$ mm, $x_c = 350$ mm and $x_c = 450$ mm. Figure 5.6 shows that the system with $u = 0.15$ and $x_c = 50$ mm is stable for $\tau > 0.06 \frac{\text{s}}{\text{rad}}$. Further is the sign of the first value in the 6. row of Table 2.1 of the investigated cylinder positions plotted with respect to τ in Figure 5.7.
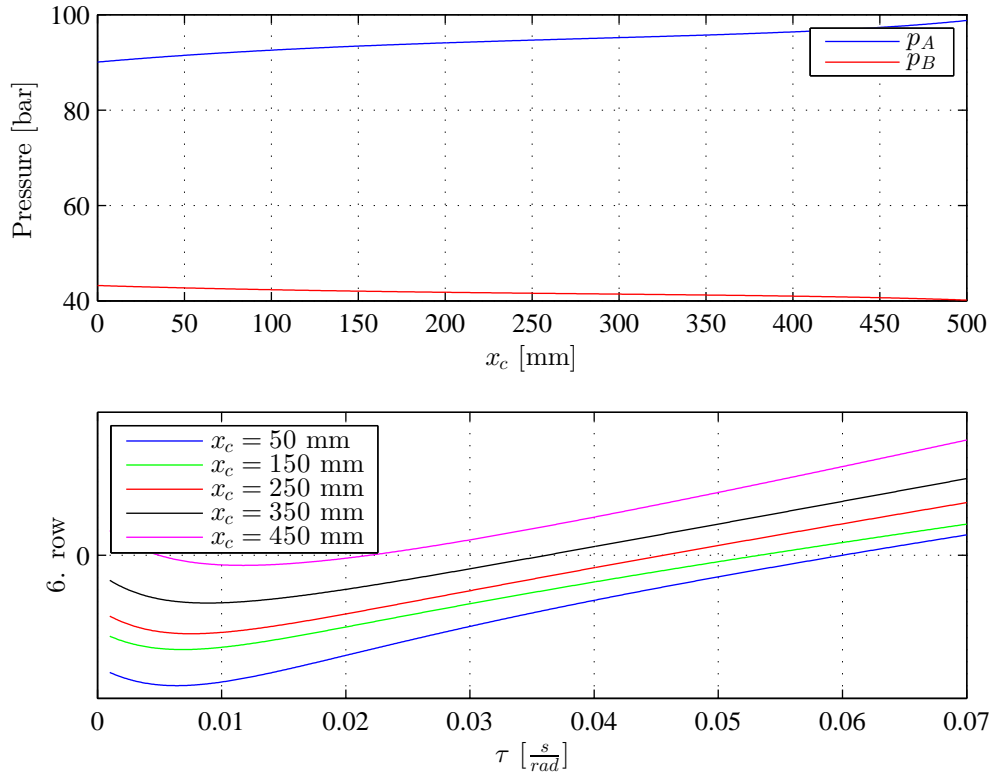
Figure 5.7: System pressures and the sign of the first value in the 6. row of Table 2.1 for Setting 1 with respect to τ

Discussion

Please recall that a higher value of τ means that a lower cutoff frequency of the low pass filter is required. On the other hand, a very low value of τ means that a low pass filter is almost unnecessary. Figure 5.7 shows that the highest value of τ is required when the cylinder is fully extended, and that the value decreases as the cylinder is contracted. This is the same as what was seen for the simplified system in Figure 5.2. Also note that the requirement of τ is very similar compared to the simplified system.

5.2.6 Step Response

Further is the step response of the system investigated for two values of τ, namely $0.5 \frac{\text{s}}{\text{rad}}$ and $10 \frac{\text{s}}{\text{rad}}$. The step responses are shown in Figure 5.8 and Figure 5.9, respectively. In each figure is the step response of five cylinder piston position shown. It is seen from the figures that τ got a miner influence on the step response. A lower value of τ results in higher oscillations and a slight increase in settling time, while the risce time remains the same. It can therefore be said that Setting 1 stabilizes the system, and that τ affects the magnitude of the oscillations and its settling time. τ should therefore be selected carefully.

5.2.7 Validation of the Simplification

The step response for $x_c = 50$ mm and $x_c = 250$ mm for Setting 1 with and without the simplification are compared in Figure 5.10. The figure shows a quite good match, although the results deviates some as the cylinder in contracted. Both the comparison of Figure 5.7 and Figure 5.2, and Figure 5.10 shows that the simplified investigation corresponds well with this investigation.
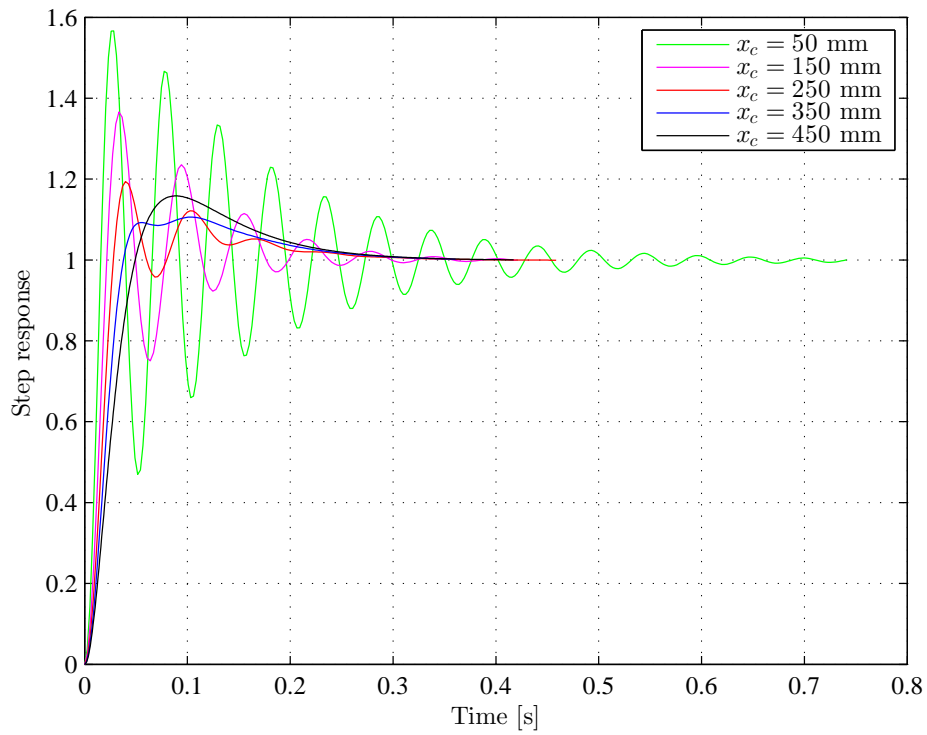
Figure 5.8: Setting 1 step response $\tau = 0.5\,\frac{\mathrm{s}}{\mathrm{rad}}$, $u = 0.15$
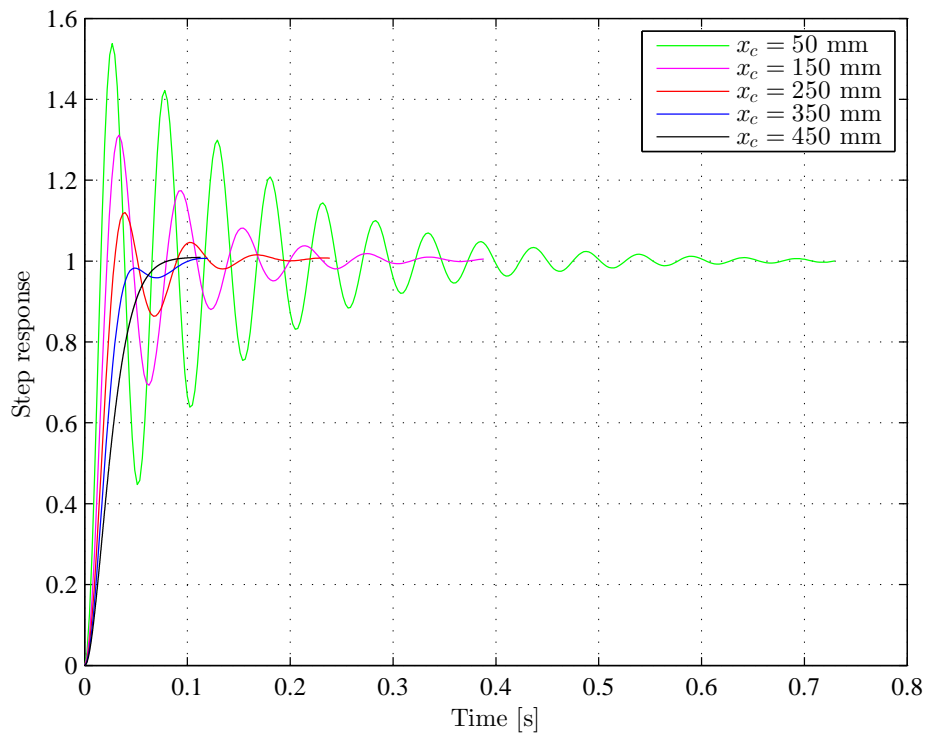
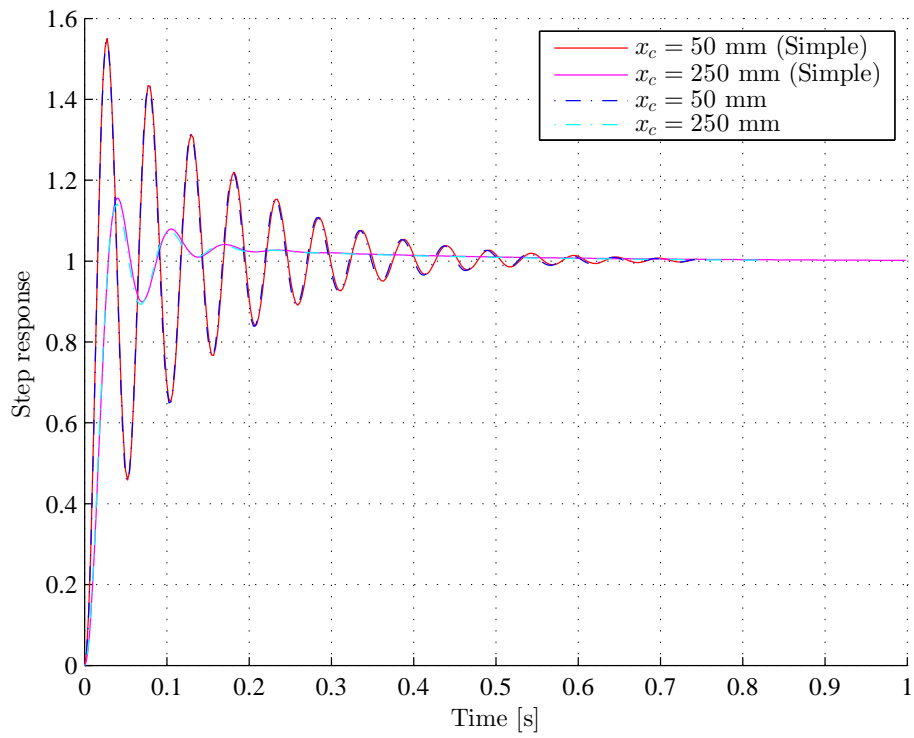Figure 5.9: Setting 1 step response $\tau = 10\,\frac{\mathrm{s}}{\mathrm{rad}}$, $u = 0.15$

57

Figure 5.10: Compare Complex model vs Simple model, step response, $\tau = 1.59 \frac{\text{s}}{\text{rad}}$

5.3 Investigation of Setting 2

In this section is Setting 2 investigated. The initial steps of this investigation is similar to those performed for Setting 1. Only the basic equations which differentiate from those in Setting 1 are therefore presented and linearized in this section. Please recall Section 5.2.1 and Section 5.2.2. An illustration of the circuit investigated in this section is shown in Figure 5.11.
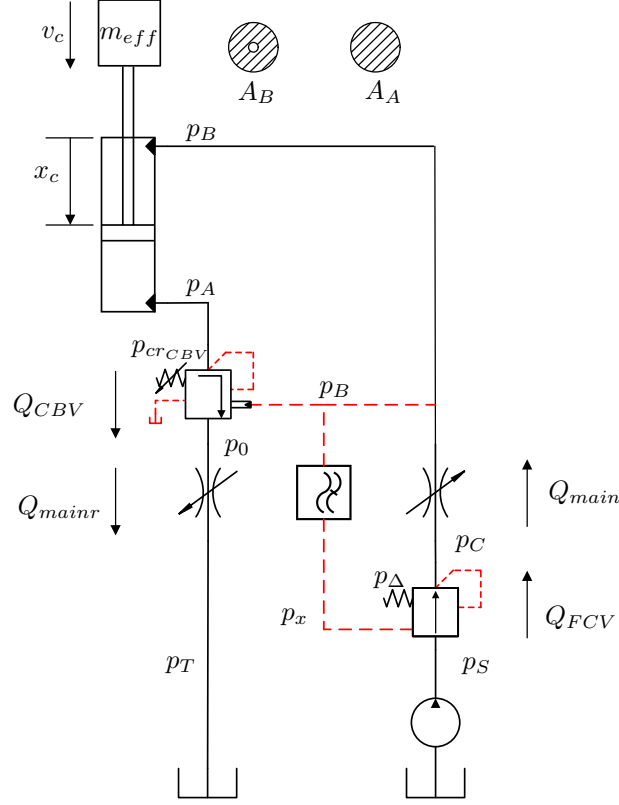
Figure 5.11: Simplified hydraulic circuit Setting 2

What differentiate this system from the system investigated for Setting 1 is that the low pass filtered pressure p_x is assigned to the FCV instead of the CBV. Recall Figure 5.5.

5.3.1 Basic Equations

All the differential equations and flow equations are equal compared to those presented for Setting 1. Recall eq. 5.49 - 5.58. The rate of opening of the CBV and the FCV are calculated as shown in eq. 5.88 and eq. 5.89, based on Figure 5.11, Section 2.2.2 and Section 2.2.1.

$$u_{CBV} = \frac{p_B \cdot \rho_p + p_A - p_{cr_{CBV}}}{\Delta P_{open_{CBV}}} \tag{5.88}$$

$$u_{FCV} = \frac{p_x + p_\Delta - p_C}{\Delta P_{open_{FCV}}} \tag{5.89}$$

5.3.2 Linearization

Further are the basic equations linearized around a certain steady state point. The linearization is performed as described in eq. 2.22 in Section 2.3.5. Equation 5.90 and eq. 5.91 shows the linearization of eq. 5.88 and eq. 5.89. For the remaining linearized equations please recall eq. 5.61 - 5.70.

$$\tilde{u}_{CBV} = \frac{\tilde{p}_B \cdot \rho_p + \tilde{p}_A}{\Delta p_{open_{CBV}}} \tag{5.90}$$

$$\tilde{u}_{FCV} = \frac{\tilde{p}_x - \tilde{p}_C}{\Delta p_{open_{FCV}}} \tag{5.91}$$

5.3.3 State Space Model

The state space model is arranged based on the linearized differential equations, eq. 5.61 - 5.66 from Section 5.2.2 and eq. 5.90 - 5.91. This is performed as in eq. 2.27 and eq. 2.28 in Section 2.3.6. The state space model is a SISO-system with six states. The states are $\tilde{p}_A$, $\tilde{p}_B$, $\tilde{p}_C$, $\tilde{p}_x$, $\tilde{p}_0$ and $\tilde{v}_c$. $\tilde{u}$ is the input signal and $A_B \cdot \tilde{v}_c$ is the output signal. In order to be arranged in the state space model are the linearized differential equations re-organized as shown in eq. 5.92 - 5.97.

$$\dot{\tilde{v}}_c = -\frac{\rho_c \cdot A_B}{m_{eff}} \cdot \tilde{p}_A + \frac{A_B}{m_{eff}} \cdot \tilde{p}_B \tag{5.92}$$

$$\dot{\tilde{p}}_A = \frac{\rho_c \cdot A_B}{C_A} \cdot \tilde{v}_c - \left(\frac{k_{qp_{CBV}}}{C_A} + \frac{k_{qu_{CBV}}}{\Delta p_{open_{CBV}} \cdot C_A} \right) \cdot \tilde{p}_A - \frac{k_{qu_{CBV}} \cdot \rho_p}{\Delta p_{open_{CBV}} \cdot C_A} \cdot \tilde{p}_B + \frac{k_{qp_{CBV}}}{C_A} \cdot \tilde{p}_0 \tag{5.93}$$

$$\dot{\tilde{p}}_B = -\frac{A_B}{C_B} \cdot \tilde{v}_c - \frac{k_{qp_{main}}}{C_B} \cdot \tilde{p}_B + \frac{k_{qp_{main}}}{C_B} \cdot \tilde{p}_C + \frac{k_{qu_{main}}}{C_B} \cdot \tilde{u} \tag{5.94}$$

$$\dot{\tilde{p}}_C = \frac{k_{qp_{main}}}{C_C} \cdot \tilde{p}_B - \left(\frac{k_{qp_{main}}}{C_C} + \frac{k_{qp_{FCV}}}{C_C} + \frac{k_{qu_{FCV}}}{\Delta p_{open_{FCV}} \cdot C_C} \right) \cdot \tilde{p}_C + \frac{k_{qu_{FCV}}}{\Delta p_{open_{FCV}} \cdot C_C} \cdot \tilde{p}_x - \frac{k_{qu_{main}}}{C_C} \cdot \tilde{u} \tag{5.95}$$

$$\dot{\tilde{p}}_0 = \left(\frac{k_{qp_{CBV}}}{C_0} + \frac{k_{qu_{CBV}}}{\Delta p_{open_{CBV}} \cdot C_0} \right) \cdot \tilde{p}_A + \frac{k_{qu_{CBV}} \cdot \rho_p}{\Delta p_{open_{CBV}} \cdot C_0} \cdot \tilde{p}_B - \left(\frac{k_{qp_{CBV}}}{C_0} + \frac{k_{qp_{mainr}}}{C_0} \right) \cdot \tilde{p}_0 - \frac{k_{qu_{mainr}}}{C_0} \cdot \tilde{u} \tag{5.96}$$

$$\dot{\tilde{p}}_x = \frac{K}{\tau} \cdot \tilde{p}_B - \frac{1}{\tau} \cdot \tilde{p}_x \tag{5.97}$$

The state space model is finally arranged in eq. 5.98 and eq. 5.99, based on eq. 5.92 - 5.97.

$$
\begin{bmatrix} \dot{\tilde{v}}_c \\ \dot{\tilde{p}}_A \\ \dot{\tilde{p}}_B \\ \dot{\tilde{p}}_C \\ \dot{\tilde{p}}_0 \\ \dot{\tilde{p}}_x \end{bmatrix}
=
\begin{bmatrix}
0 & -\dfrac{\rho_c \cdot A_B}{m_{eff}} & \dfrac{A_B}{m_{eff}} & 0 & 0 & 0 \\[2ex]
\dfrac{\rho_c \cdot A_B}{C_A} & -\left(\dfrac{k_{qp_{CBV}}}{C_A} + \dfrac{k_{qu_{CBV}}}{\Delta p_{open_{CBV}} \cdot C_A}\right) & -\dfrac{k_{qu_{CBV}} \cdot \rho_p}{\Delta p_{open_{CBV}} \cdot C_A} & 0 & \dfrac{k_{qp_{CBV}}}{C_A} & 0 \\[2ex]
-\dfrac{A_B}{C_B} & 0 & -\dfrac{k_{qp_{main}}}{C_B} & \dfrac{k_{qp_{main}}}{C_B} & 0 & 0 \\[2ex]
0 & 0 & \dfrac{k_{qp_{main}}}{C_C} & -\left(\dfrac{k_{qp_{main}}}{C_C} + \dfrac{k_{qp_{FCV}}}{C_C} + \dfrac{k_{qu_{FCV}}}{\Delta p_{open_{FCV}} \cdot C_C}\right) & 0 & \dfrac{k_{qu_{FCV}}}{\Delta p_{open_{FCV}} \cdot C_C} \\[2ex]
0 & \left(\dfrac{k_{qp_{CBV}}}{C_0} + \dfrac{k_{qu_{CBV}}}{\Delta p_{open_{CBV}} \cdot C_0}\right) & \dfrac{k_{qu_{CBV}} \cdot \rho_p}{\Delta p_{open_{CBV}} \cdot C_0} & 0 & -\left(\dfrac{k_{qp_{CBV}}}{C_0} + \dfrac{k_{qp_{mainr}}}{C_0}\right) & 0 \\[2ex]
0 & 0 & \dfrac{K}{\tau} & 0 & 0 & -\dfrac{1}{\tau}
\end{bmatrix}
\cdot
\begin{bmatrix} \tilde{v}_c \\ \tilde{p}_A \\ \tilde{p}_B \\ \tilde{p}_C \\ \tilde{p}_0 \\ \tilde{p}_x \end{bmatrix}
+
\begin{bmatrix} 0 \\ 0 \\ \dfrac{k_{qu_{main}}}{C_B} \\ -\dfrac{k_{qu_{main}}}{C_C} \\ -\dfrac{k_{qu_{mainr}}}{C_0} \\ 0 \end{bmatrix}
\cdot \tilde{u}
\tag{5.98}
$$

$$
y = \begin{bmatrix} A_B & 0 & 0 & 0 & 0 & 0 \end{bmatrix}
\begin{bmatrix} \tilde{v}_c \\ \tilde{p}_A \\ \tilde{p}_B \\ \tilde{p}_C \\ \tilde{p}_0 \\ \tilde{p}_x \end{bmatrix}
\tag{5.99}
$$

5.3.4   Transfer Function

The transfer function is calculated based on the state space model as shown in eq. 2.29 in Section 2.3.7. As there are six states in the state space model is the denominator of the transfer function a 6th order polynomial. An analytic investigation of the stability is in this case very unhandy. Parameter values from Chapter 3 are therefore implemented in order to ease the representation. Further is the influence τ has on the stability investigated for certain values of x_c and u. The transfer function is therefore represented as shown in eq. 5.100 where N_1 - N_4 and D_1 - D_6 are functions of τ, and N_0 and D_0 are constants.

$$G(s) = \frac{N_4(\tau) \cdot s^4 + N_3(\tau) \cdot s^3 + N_2(\tau) \cdot s^2 + N_1(\tau) \cdot s + N_0}{D_6(\tau) \cdot s^6 + D_5(\tau) \cdot s^5 + D_4(\tau) \cdot s^4 + D_3(\tau) \cdot s^3 + D_2(\tau) \cdot s^2 + D_1(\tau) \cdot s + D_0} \qquad (5.100)$$

5.3.5   Routh-Hurwitz Stability Criterion

In order for a system to be stable must all poles be in the left half plane. As the denominator is a 6th order polynomial is this investigated by Routh-array, Table 2.1 in Section 2.3.8. A system is considered stable when the sign of the values in the first column of Table 2.1 is the same, as each sign change represents a pole in the right half plane. It can be shown that the 6. row is the only row that changes sign with respect to τ for $u = 0.15$. This is similar as for Setting 1, recall Section 5.2.5. The sign of the first value in the 6. row of Table 2.1 for the investigated cylinder positions for this system is therefore plotted with respect to τ in Figure 5.12.
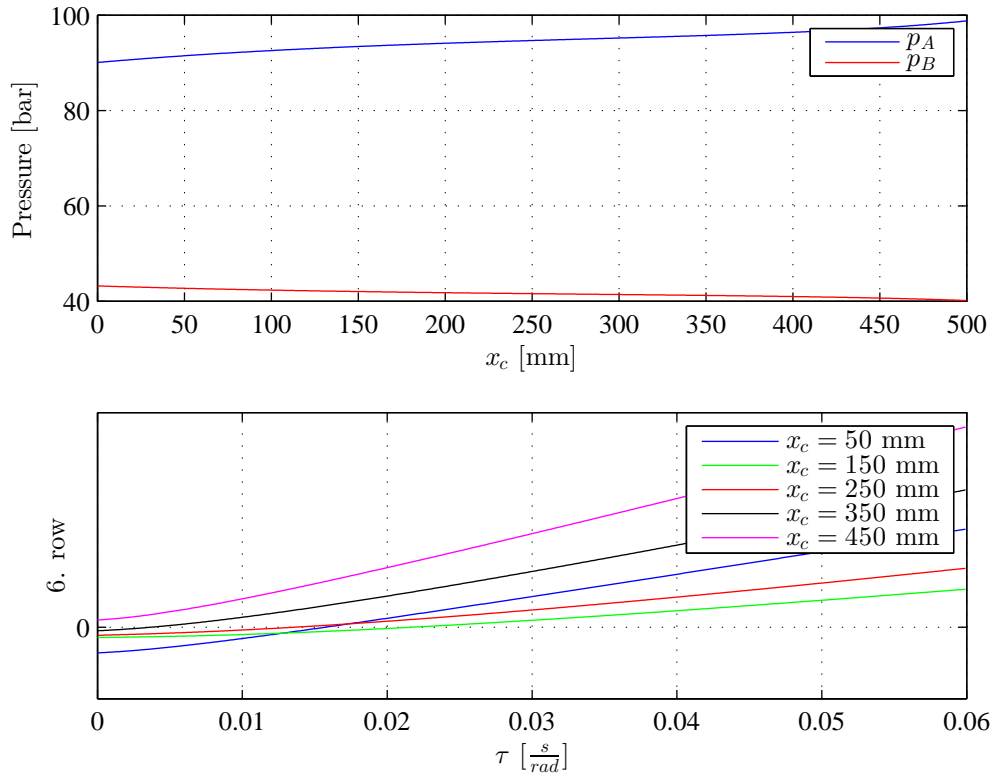

Figure 5.12: System pressures and the sign of the first value in the 6. row of Table 2.1 for Setting 2 with respect to τ

Discussion

Please recall that a higher value of τ means that a lower cutoff frequency of the low pass filter is required. On the other hand, a very low value of τ means that a low pass filter is almost unnecessary. Figure 5.12

shows that the system with $u = 0.15$ is stable through out the motion if $\tau > 0.022\,\frac{\text{s}}{\text{rad}}$. The figure also shows that the system is stable at $x_c = 450$ mm regardless of the value of τ. Note that the figure shows that the highest value of τ is required at $x_c = 150$ mm.

5.3.6 Step Response

Further is the step response of the system investigated for two values of τ, namely $0.1\,\frac{\text{s}}{\text{rad}}$ and $1\,\frac{\text{s}}{\text{rad}}$. The step responses are shown in Figure 5.13 and Figure 5.14, respectively. In each figure is the step response of five cylinder piston position shown. It is seen from the figures that τ got a great influence on the step response. A lower value of τ results in a quicker system as compared to a higher value. Also note that the system with a higher value of τ quickly reaches 80% of the input signal but then slows down for the last 20%. It can therefore be said that Setting 2 stabilizes the system, and that τ got a great influence on the step response and should therefore be selected carefully.
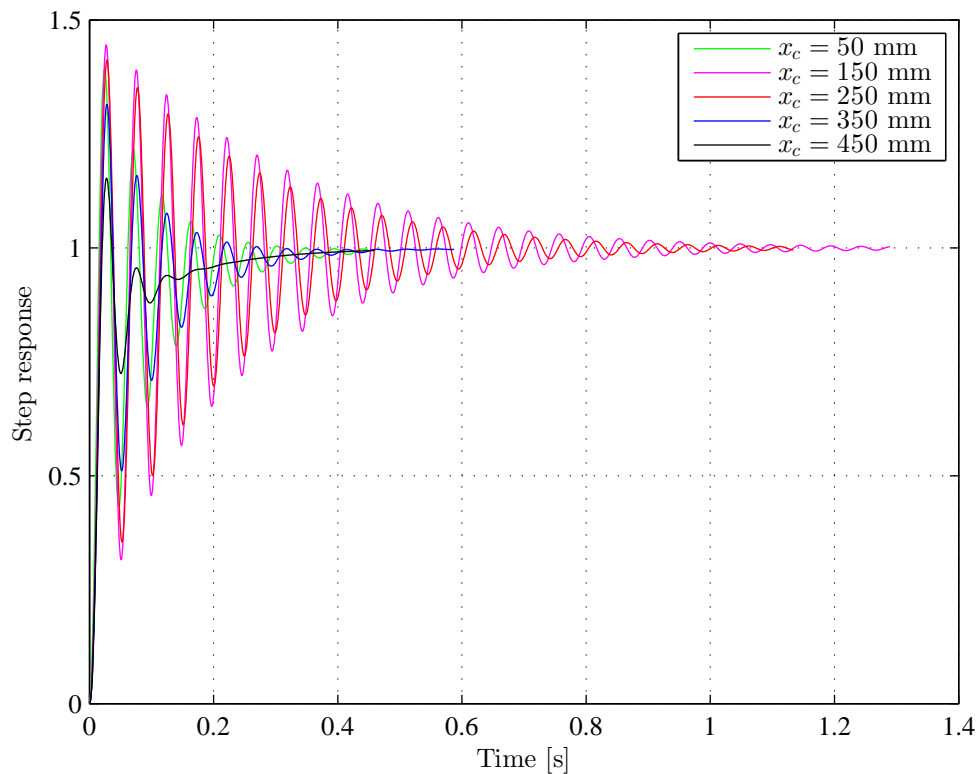
Figure 5.13: Setting 2 step response $\tau = 0.1\,\frac{\text{s}}{\text{rad}}$, $u = 0.15$
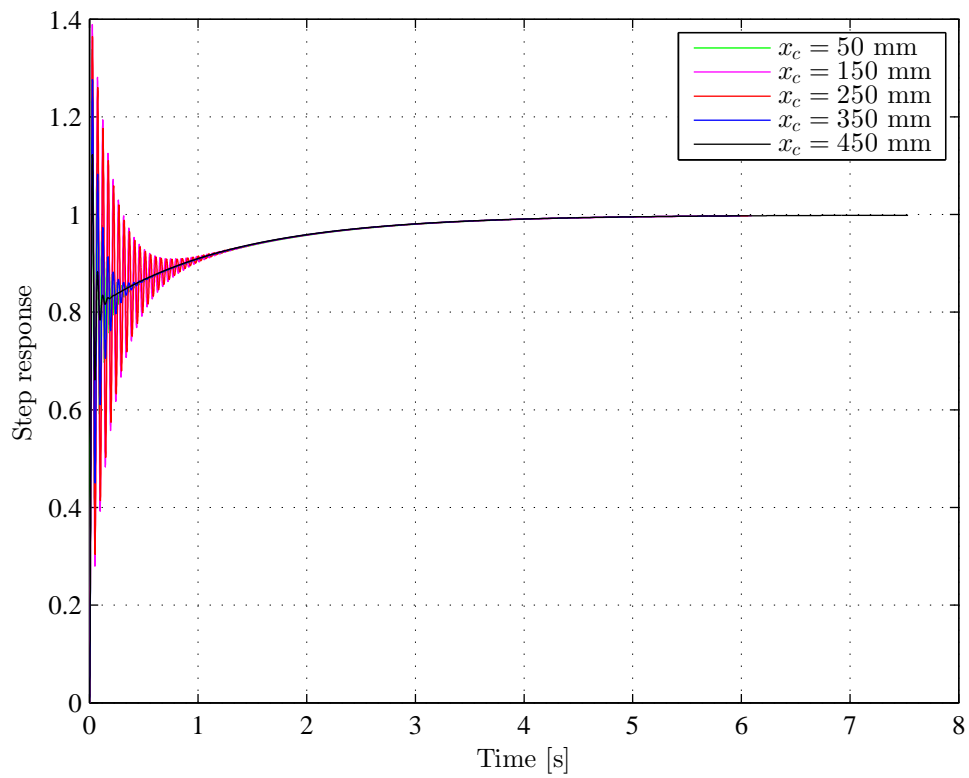
Figure 5.14: Setting 2 step response $\tau = 1\,\frac{\text{s}}{\text{rad}}$, $u = 0.15$

5.4 Investigation of Setting 3

In this section is Setting 3 investigated. The initial steps of this investigation is similar to those performed for Setting 1. Only the basic equations which differentiate from those in Setting 1 are therefore presented and linearized in this section. Please recall Section 5.2.1 and Section 5.2.2. An illustration of the circuit investigated in this section is shown in Figure 5.15.
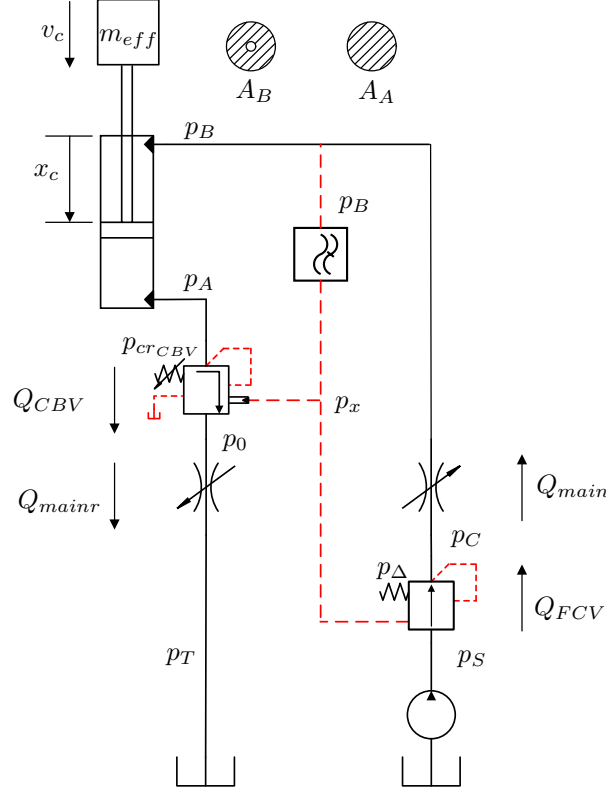

Figure 5.15: Simplified hydraulic circuit, p_x connected to DCV and CBV

What differentiate this system from the system investigated for Setting 1 is that the low pass filtered pressure p_x is assigned both to the FCV and the CBV. Recall Figure 5.5.

5.4.1 Basic equations

All the differential equations and flow equations are equal compared to those presented for Setting 1. Recall eq. 5.49 - 5.58. The rate of opening of the CBV and the FCV are calculated as shown in eq. 5.101 and eq. 5.102, based on Figure 5.15, Section 2.2.2 and Section 2.2.1.

$$u_{CBV} = \frac{p_x \cdot \rho_p + p_A - p_{cr_{CBV}}}{\Delta P_{open_{CBV}}} \tag{5.101}$$

$$u_{FCV} = \frac{p_x + p_\Delta - p_C}{\Delta P_{open_{FCV}}} \tag{5.102}$$

5.4.2 Linearization

Further are the basic equations linearized around a certain steady state point. The linearization is performed as described in eq. 2.22 in Section 2.3.5. Equation 5.103 and eq. 5.104 shows the linearization of eq. 5.101 and eq. 5.102. For the remaining linearized equations please recall eq. 5.61 - 5.70.

$$\tilde{u}_{CBV} = \frac{\tilde{p}_x \cdot \rho_p + \tilde{p}_A}{\Delta p_{open_{CBV}}} \tag{5.103}$$

$$\tilde{u}_{FCV} = \frac{\tilde{p}_x - \tilde{p}_C}{\Delta p_{open_{FCV}}} \tag{5.104}$$

5.4.3 State Space Model

The state space model is arranged based on the linearized differential equations, eq. 5.61 - 5.66 from Section 5.2.2 and eq. 5.103 - 5.104. This is performed as in eq. 2.27 and eq. 2.28 in Section 2.3.6. The state space model is a SISO-system with six states. The states are $\tilde{p}_A$, $\tilde{p}_B$, $\tilde{p}_C$, $\tilde{p}_x$, $\tilde{p}_0$ and $\tilde{v}_c$. $\tilde{u}$ is the input signal and $A_B \cdot \tilde{v}_c$ is the output signal. In order to be arranged in the state space model are the linearized differential equations re-organized as shown in eq. 5.105 - 5.110.

$$\dot{\tilde{v}}_c = -\frac{\rho_c \cdot A_B}{m_{eff}} \cdot \tilde{p}_A + \frac{A_B}{m_{eff}} \cdot \tilde{p}_B \tag{5.105}$$

$$\dot{\tilde{p}}_A = \frac{\rho_c \cdot A_B}{C_A} \cdot \tilde{v}_c - \left(\frac{k_{qp_{CBV}}}{C_A} + \frac{k_{qu_{CBV}}}{\Delta p_{open_{CBV}} \cdot C_A} \right) \cdot \tilde{p}_A + \frac{k_{qp_{CBV}}}{C_A} \cdot \tilde{p}_0 - \frac{k_{qu_{CBV}} \cdot \rho_p}{\Delta p_{open_{CBV}} \cdot C_A} \cdot \tilde{p}_x \tag{5.106}$$

$$\dot{\tilde{p}}_B = -\frac{A_B}{C_B} \cdot \tilde{v}_c - \frac{k_{qp_{main}}}{C_B} \cdot \tilde{p}_B + \frac{k_{qp_{main}}}{C_B} \cdot \tilde{p}_C + \frac{k_{qu_{main}}}{C_B} \cdot \tilde{u} \tag{5.107}$$

$$\dot{\tilde{p}}_C = \frac{k_{qp_{main}}}{C_C} \cdot \tilde{p}_B - \left(\frac{k_{qp_{main}}}{C_C} + \frac{k_{qp_{FCV}}}{C_C} + \frac{k_{qu_{FCV}}}{\Delta p_{open_{FCV}} \cdot C_C} \right) \cdot \tilde{p}_C + \frac{k_{qu_{FCV}}}{\Delta p_{open_{FCV}} \cdot C_C} \cdot \tilde{p}_x - \frac{k_{qu_{main}}}{C_C} \cdot \tilde{u} \tag{5.108}$$

$$\dot{\tilde{p}}_0 = \left(\frac{k_{qp_{CBV}}}{C_0} + \frac{k_{qu_{CBV}}}{\Delta p_{open_{CBV}} \cdot C_0} \right) \cdot \tilde{p}_A - \left(\frac{k_{qp_{CBV}}}{C_0} + \frac{k_{qp_{mainr}}}{C_0} \right) \cdot \tilde{p}_0 + \frac{k_{qu_{CBV}} \cdot \rho_p}{\Delta p_{open_{CBV}} \cdot C_0} \cdot \tilde{p}_x - \frac{k_{qu_{mainr}}}{C_0} \cdot \tilde{u} \tag{5.109}$$

$$\dot{\tilde{p}}_x = \frac{K}{\tau} \cdot \tilde{p}_B - \frac{1}{\tau} \cdot \tilde{p}_x \tag{5.110}$$

The state space model is finally arranged in eq. 5.111 and eq. 5.112, based on eq. 5.105 - 5.110.

$$
\begin{bmatrix} \dot{\tilde{v}}_c \\ \dot{\tilde{p}}_A \\ \dot{\tilde{p}}_B \\ \dot{\tilde{p}}_C \\ \dot{\tilde{p}}_0 \\ \dot{\tilde{p}}_x \end{bmatrix} =
\begin{bmatrix}
0 & -\frac{\rho_c \cdot A_B}{m_{eff}} & \frac{A_B}{m_{eff}} & 0 & 0 & 0 \\[2mm]
\frac{\rho_c \cdot A_B}{C_A} & -\left(\frac{k_{qp_{CBV}}}{C_A} + \frac{k_{qu_{CBV}}}{\Delta p_{open_{CBV}} \cdot C_A}\right) & 0 & 0 & \frac{k_{qp_{CBV}}}{C_A} & -\frac{k_{qu_{CBV}} \cdot \rho_p}{\Delta p_{open_{CBV}} \cdot C_A} \\[2mm]
-\frac{A_B}{C_B} & 0 & -\frac{k_{qp_{main}}}{C_B} & \frac{k_{qp_{main}}}{C_B} & 0 & 0 \\[2mm]
0 & 0 & \frac{k_{qp_{main}}}{C_C} & -\left(\frac{k_{qp_{main}}}{C_C} + \frac{k_{qp_{FCV}}}{C_C} + \frac{k_{qu_{FCV}} \cdot C_C}{\Delta p_{open_{FCV}}}\right) & 0 & \frac{k_{qu_{FCV}} \cdot C_C}{\Delta p_{open_{FCV}}} \\[2mm]
0 & \left(\frac{k_{qp_{CBV}}}{C_0} + \frac{k_{qu_{CBV}}}{\Delta p_{open_{CBV}} \cdot C_0}\right) & 0 & 0 & -\left(\frac{k_{qp_{CBV}}}{C_0} + \frac{k_{qp_{mainr}}}{C_0}\right) & \frac{k_{qu_{CBV}} \cdot \rho_p}{\Delta p_{open_{CBV}} \cdot C_0} \\[2mm]
0 & 0 & \frac{K}{\tau} & 0 & 0 & -\frac{1}{\tau}
\end{bmatrix}
\cdot
\begin{bmatrix} \tilde{v}_c \\ \tilde{p}_A \\ \tilde{p}_B \\ \tilde{p}_C \\ \tilde{p}_0 \\ \tilde{p}_x \end{bmatrix}
+
\begin{bmatrix} 0 \\ 0 \\ \frac{k_{qu_{main}}}{C_B} \\ -\frac{k_{qu_{main}}}{C_C} \\ -\frac{k_{qu_{mainr}}}{C_0} \\ 0 \end{bmatrix}
\cdot u
$$

(5.111)

$$
y = \begin{bmatrix} A_B & 0 & 0 & 0 & 0 & 0 \end{bmatrix}
\begin{bmatrix} \tilde{v}_c \\ \tilde{p}_A \\ \tilde{p}_B \\ \tilde{p}_C \\ \tilde{p}_0 \\ \tilde{p}_x \end{bmatrix}
$$

(5.112)

5.4.4 Transfer Function

The transfer function is calculated based on the state space model as shown in eq. 2.29 in Section 2.3.7. As there are six states in the state space model is the denominator of the transfer function a 6th order polynomial. An analytic investigation of the stability is in this case very unhandy. Parameter values from Chapter 3 are therefore implemented in order to ease the representation. Further is the influence τ has on the stability investigated for certain values of x_c and u. The transfer function is therefore represented as shown in eq. 5.113 where N_1 - N_4 and D_1 - D_6 are functions of τ, and N_0 and D_0 are constants.

$$G(s) = \frac{N_4(\tau) \cdot s^4 + N_3(\tau) \cdot s^3 + N_2(\tau) \cdot s^2 + N_1(\tau) \cdot s + N_0}{D_6(\tau) \cdot s^6 + D_5(\tau) \cdot s^5 + D_4(\tau) \cdot s^4 + D_3(\tau) \cdot s^3 + D_2(\tau) \cdot s^2 + D_1(\tau) \cdot s + D_0} \qquad (5.113)$$

5.4.5 Routh-Hurwitz Stability Criterion

In order for a system to be stable must all poles be in the left half plane. As the denominator is a 6th order polynomial is this investigated by Routh-array, Table 2.1 in Section 2.3.8. A system is considered stable when the sign of the values in the first column of Table 2.1 is the same, as each sign change represents a pole in the right half plane. It can be shown that the 6. row is the only row that changes sign with respect to τ for $u = 0.15$. This is similar as for Setting 1, recall Section 5.2.5. The sign of the first value in the 6. row of Table 2.1 for the investigated cylinder positions for this system is therefore plotted with respect to τ in Figure 5.16.

Figure 5.16: System pressures and the sign of the first value in the 6. row of Table 2.1 for Setting 3 with respect to τ

Discussion

Please recall that a higher value of τ means that a lower cutoff frequency of the low pass filter is required. On the other hand, a very low value of τ means that a low pass filter is almost unnecessary. Figure 5.16

shows that the system with $u = 0.15$ is stable through out the motion if $\tau > 0.02 \, \frac{\text{s}}{\text{rad}}$. The figure also shows that the system is stable at $x_c = 450$ mm regardless of the value of τ. Note that the figure shows that the highest value of τ is required at $x_c = 150$ mm.

5.4.6 Step Response

Further is the step response of the system investigated for two values of τ, namely $0.1 \, \frac{\text{s}}{\text{rad}}$ and $1 \, \frac{\text{s}}{\text{rad}}$. The step responses are shown in Figure 5.17 and Figure 5.18, respectively. In each figure is the step response of five cylinder piston position shown. It is seen from the figures that τ got a great influence on the step response. A lower value of τ results in a quicker system as compared to a higher value. Also note that the system with a higher value of τ quickly reaches 50% of the input signal but then slows down for the last 50%. It can therefore be said that Setting 3 stabilizes the system, and that τ got a great influence on the step response and should therefore be selected carefully.
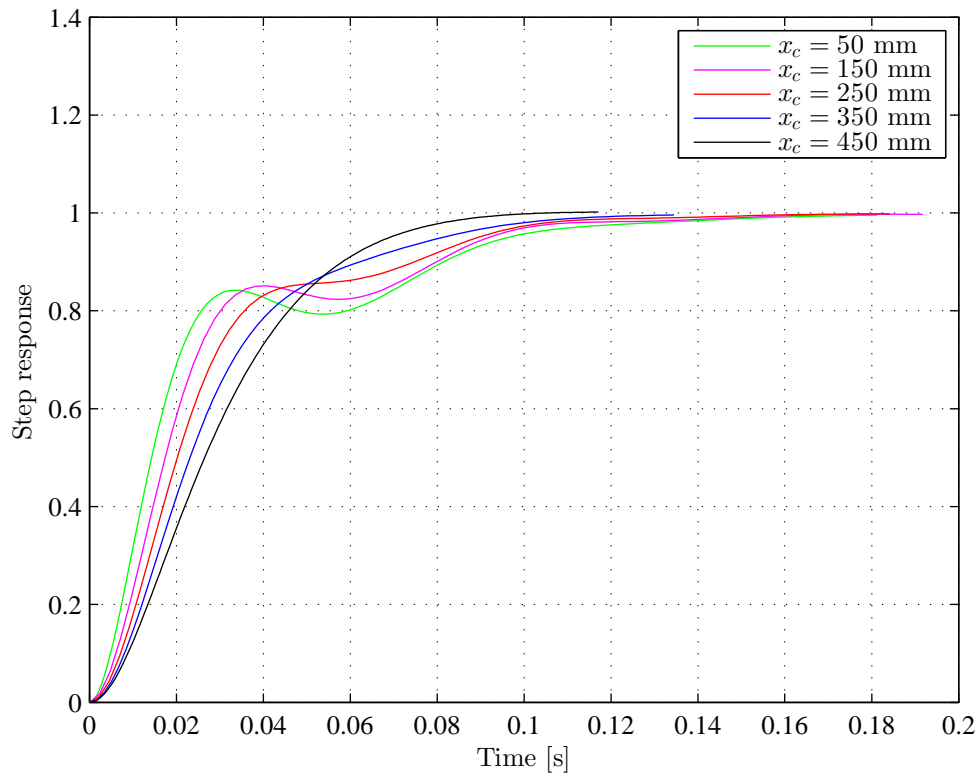
Figure 5.17: Setting 3 step response $\tau = 0.1$, $u = 0.15$
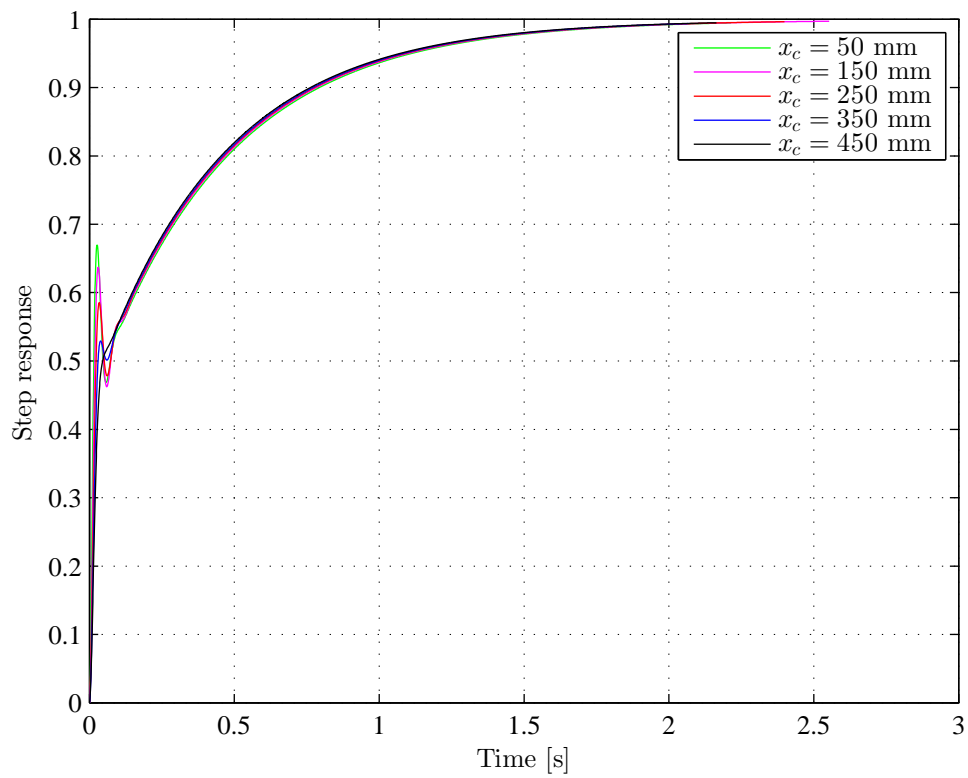
Figure 5.18: Setting 3 step response $\tau = 1$, $u = 0.15$

5.5 Conclusion

It is seen from the linear models that all the settings have a good basis for making the system stable. This is seen as each of the settings is found stable by Routh-Hurwitz stability criterion for obtainable values of τ, or cutoff frequencies. Recall that a higher value of τ means that a lower cutoff frequency of the low pass filter is required. On the other hand, a very low value of τ means that a low pass filter is almost unnecessary. It is found that Setting 1 requires the lowest cutoff frequency. For Setting 2 and Setting 3 is it seen that the cutoff frequency have a great influence on the step response. A high cutoff frequency results in a quick response but will also make the system unstable if set too high. The simplified investigation of Setting 1 shows that the stability is dependent of the volume in chamber A and B. This again means that the cylinder piston position is important. A lower cutoff frequency is therefore required when the cylinder fully extracted as compared to fully retracted. For Setting 2 and Setting 3, on the other hand, is the most critical cylinder piston position for to be around $x_c = 150$ mm. Also, for these systems, are $x_c = 450$ mm found to be stable regardless of the value of the cutoff frequency.

Chapter 6

Time Domain Simulation

In addition to the linear investigation of each setting are time domain simulations carried out. In this chapter is a general introduction to time domain simulation followed up by a step by step description of the simulations performed. The simulation model is then described, before results are presented and conclusions are drawn. Time domain simulations may give the user a better understanding of the behavior of the system, as it provides the possibility to map the systems behavior through a certain motion in time. Both SimulationX and MATLAB are used in this investigation. The main reasons for this are that using two different methods provides an unique opportunity to cross examine the results and strengthens the simulations validity.

6.1 General Introduction

Time domain simulation is a technique used to numerically approximate the solution of ordinary differential equations (ODEs) in a defined time span. In order to find an explicit solution must the initial values of the time derivatives be known, making it an initial value problem (IVP). Two widely used simulations tools are MATLAB and SimulationX. Time domain simulations in MATLAB might be considered more difficult compared to SimulationX for complex systems, as the simulation loop and the ODEs have to be designed by the user itself. On the contrary, using SimulationX, the user defines the system by means of visual programming and the program itself determines the ODEs. The latter may help the user to get an accurate simulation as the program will ask for all the parameters needed to determine the ODEs and solve the IVP.

6.2 Step by Step Description

MATLAB is used as the main simulation tool in this investigation. SimulationX is used to cross examine the results during the investigation process and are therefore not further included. Figure 6.1 is a flow chart showing the stages of the time domain simulation performed in MATLAB.

6.2.1 Define/Calculate constants

In order to find an explicit solution must all the constants used in the simulation be defined. Examples of such constants can be: lengths, angles, pressures, areas, gravitational acceleration, parameters of the hydraulic components and more. Some constants can also be calculated based on other constants.

6.2.2 Determine Initial Conditions

The next step is to determine the initial conditions. These can be determined by steady state calculation. Examples are: initial time, initial position, initial speed of the mechanical parts and initial pressures in the hydraulics.

6.2.3 Define End Time and Step Time

The end time determines for how long the motion of the system will be simulated. The step time or step size determines the size of the time leap from one calculation point to the next. The step time must be set
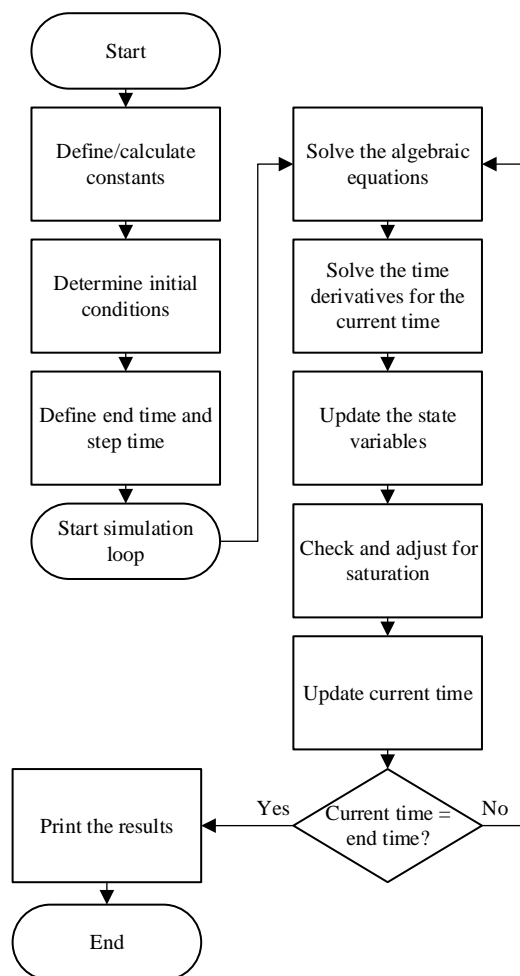
Figure 6.1: Flow chart of time domain simulation in MATLAB

in accordance to the desired accuracy and simulation method.

6.2.4 Update Algebraic Equations

This is the first stage in the simulation loop, meaning that the calculations will be performed for each time step until the end time is reached. This may be considered a redundant step, but is introduced in order to simplify the expressions used to calculate the time derivatives. Examples of such variables are: angle, length, flow, volume, valve opening and more.

6.2.5 Solve Time Derivatives for Current Time

The time derivatives of the system (ODEs) are solved for the current step. The time derivatives can be acceleration and speed of the mechanical system, pressure gradients of the hydraulics, and more.

6.2.6 Update State Variables

The state variables are updated according to the time derivatives in a manner dependent of the chosen simulation method. There exist several methods for this, where some of them are: Forward Euler, Trapezoidal method, Runge-Kutta methods and more. Forward Euler is used in this project as follows. Note that the description is inspired by [6]. Assume the state variable y and its time derivative $\dot{y}$, shown in eq. 6.1, is to be approximated from the start time t_0.

74

$$\dot{y}(t) = f(t, y(t)) \tag{6.1}$$
$$y(t_0) = y_0 \tag{6.2}$$

where

$$
\begin{array}{ll}
y(t) & \text{State variable} \\
\dot{y}(t) & \text{Time derivative} \\
t_0 & \text{Initial time} \\
y_0 & \text{Initial value}
\end{array}
$$

The solving is discretized according to eq. 6.3 and eq. 6.4.

$$t_n = t_0 + n \cdot h \tag{6.3}$$
$$t_{n+1} = t_n + h \tag{6.4}$$

where

$$
\begin{array}{ll}
t_n & \text{Current time} \\
t_{n+1} & \text{Current time for the next step} \\
t_0 & \text{Initial time} \\
n & \text{Current step} \\
h & \text{Step time}
\end{array}
$$

Forward Euler method is used as shown in eq. 6.5 for as many steps as needed to reach the desired end time.

$$y_{n+1} = y_n + h \cdot f(t_n, y_n) \tag{6.5}$$

where

$$
\begin{array}{ll}
y_{n+1} & \text{Estimated value of the state variable for the next step} \\
y_n & \text{Current value of the state variable} \\
h & \text{Step time} \\
f(t_n, y_n) & \text{Rate of change at the current time}
\end{array}
$$

6.2.7 Check and Adjust for Saturation

Any adjustments of the calculated value of the state variable is done in this stage. If, for instance, the hydraulic pressure saturates or any mechanical parts has reached its end position.

6.2.8 Update Current Time

When all the state variables are calculated for the current time, the time for the next step is calculated. This is done as shown in eq. 6.4. The simulation will stop if the time for the next step is equal to the end time, if not, the simulation will continue repeating its calculations until the desired end time is reached.

6.2.9 Print Results

Finally, when the desired end time of the simulation is reached, the results are printed or saved as desired.

6.3   Simulation Model

Further are the simulation models used to investigate the three settings described. The models are quite similar, as only the calculation of u_{CBV} and u_{FCV} differentiates them. A combined description of the three models are therefore presented with the differences pointed out. The investigation is based on the description of the test rig provided in Chapter 3 and Chapter 4. An illustration of the hydraulic circuits used for this investigation is shown in Figure 6.2
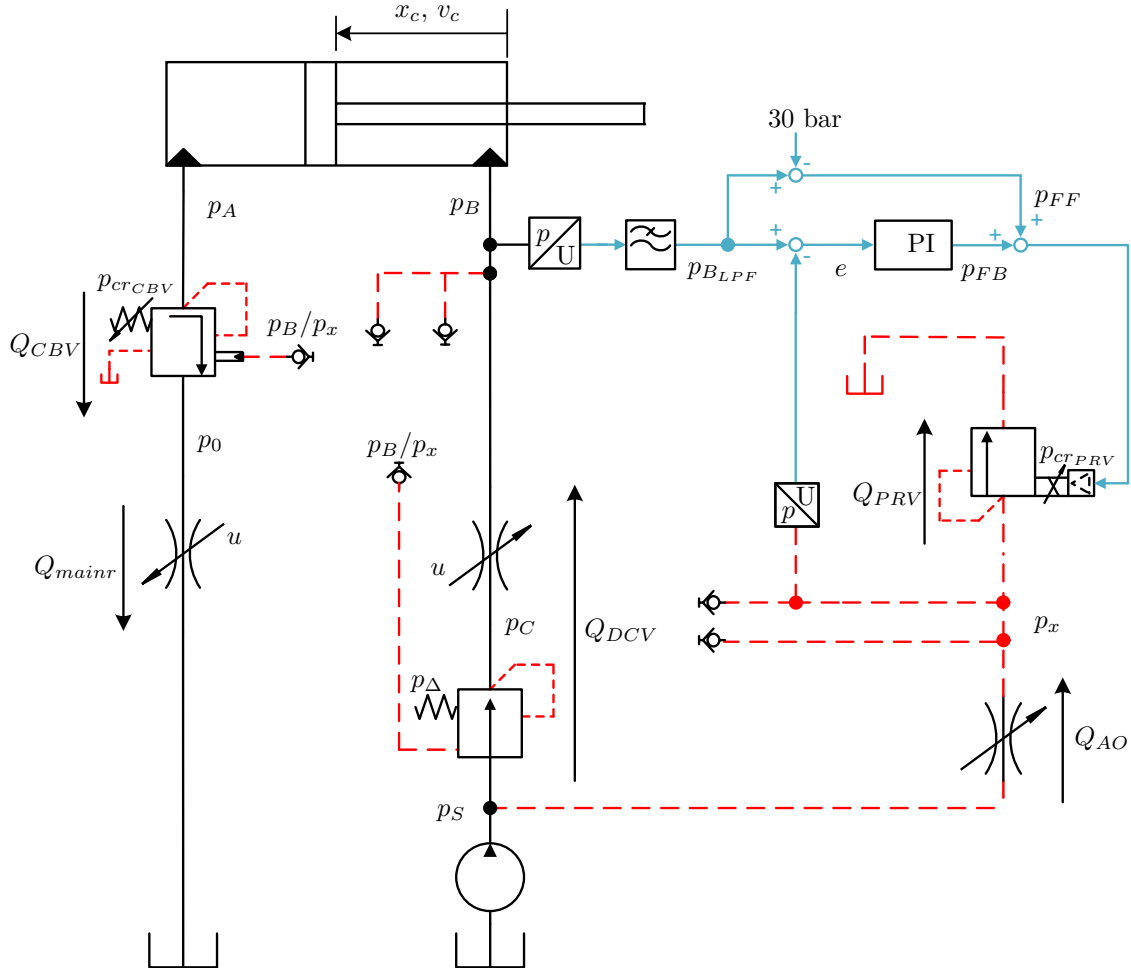
Figure 6.2: Hydraulic circuit for simulation

Please note that the pressure compensated DCV is modeled as one effective orifice. This means that the pressure buildup in the volume between the FCV and the main spool is considered infinitely fast.

6.3.1   Constants

The constants used in this investigation are presented in Chapter 3. They are also listed in Table A.1. Some of the constants are calculated prior to the investigation. These are listed in Table A.2. The parameters of the low pass filter and the PI controller are changed according to the setting and are listed in Table 6.1

6.3.2   Initial Conditions

The initial pressure in chamber A are calculated as described in Section 3.4. The remaining pressures are initially 0 bar as an open-center main spool is used. Note that the initial pressure for p_x is set to 0 bar. This is chosen as the desired pressure in p_x is 0 bar when p_B is 0 bar. The cylinder piston starts at rest with an initial position of 50 mm. All the initial values are listed in Table 6.2.

Table 6.1: Constants depending of the investigated setting

Parameter	Value			Unit	Description
Low pass filter	Setting 1	Setting 2	Setting 3		
f_c	0.1	3	3	Hz	Cut-off frequency
τ	1.59	0.0531	0.0531	$\frac{\text{s}}{\text{rad}}$	Time constant
k	1	1	1	-	Filter gain
PI controller					
G	100	100	100	-	Proportional gain
Ti	0.1	0.1	0.1	s	Integral time

Table 6.2: Initial values

Parameter	Value	Unit	Description
θ	29.8	°	Initial cylinder position
$\dot{\theta}$	0	$\frac{\text{rad}}{\text{s}}$	Initial cylinder speed
p_A	61.1	bar	Initial pressure in V_A
$\dot{p}_A$	0	$\frac{\text{Pa}}{\text{s}}$	Initial pressure gradient V_A
p_B	0	bar	Initial pressure in V_B
$\dot{p}_B$	0	$\frac{\text{Pa}}{\text{s}}$	Initial pressure gradient V_B
p_x	0	bar	Initial pressure in V_x
$\dot{p}_x$	0	$\frac{\text{Pa}}{\text{s}}$	Initial pressure gradient in V_x
p_C	0	bar	Initial pressure in V_C
p_0	0	bar	Initial pressure in V_0
$\dot{p}_0$	0	$\frac{\text{Pa}}{\text{s}}$	Initial pressure gradient in V_0
$p_{B_{LPF}}$	0	bar	Initial value of the low pass filter
$\dot{p}_{B_{LPF}}$	0	$\frac{\text{Pa}}{\text{s}}$	Initial value of the low pass filter gradient
t	0	s	Initial time
n	1	-	Initial step

6.3.3 End Time and Step Time

The end time and step time used in the simulations are listed in Table 6.3.

Table 6.3: Time constants

Parameter	Value	Unit	Description
dt	0.0001	s	Step time
$EndTime$	20	s	Total simulation time

6.3.4 Algebraic Equations

Further are the algebraic equations presented.

Lengths and Angles

The cylinder piston position and speed are calculated as shown in eq. 6.6 and eq. 6.7. For eq. 6.8 - 6.11 recall Section 3.2.3.

$$x_c = 1.272 - \sqrt{l_{BCx}{}^2 + l_{BCy}{}^2} \tag{6.6}$$

$$v_c = -l_{AC} \cdot \dot{\theta} \cdot \cos{(\gamma)} \tag{6.7}$$

where

$$l_{BCx} = l_{AC} \cdot \cos(\theta - \alpha_0) - l_{ABx} \tag{6.8}$$

$$l_{BCy} = l_{ABy} + l_{AC} \cdot \sin(\theta - \alpha_0) \tag{6.9}$$

$$\varphi = \tan^{-1}\left(\frac{l_{BCy}}{l_{BCx}}\right) \tag{6.10}$$

$$\gamma = \theta - \alpha_0 + \frac{\pi}{2} - \varphi \tag{6.11}$$

Volumes

The volume in chamber A and chamber B varies with respect to the cylinder piston position. They are calculated as shown in eq. 6.12 and eq. 6.13, respectively.

$$V_A = (0.5 - x_c) \cdot A_A + V_{A0} \tag{6.12}$$

$$V_B = x_c \cdot A_B + V_{B0} \tag{6.13}$$

Valve Openings

The equations used when calculating the rate of opening of the PRV, CBV and FCV are introduced in Section 2.2. The equations used to calculate the opening of the CBV and the FCV varies with respect to the setting and are therefore presented for each setting. The opening of the PRV is calculated as shown in eq. 6.14. The opening of the CBV is calculated as shown in eq. 6.15, eq. 6.17 and eq. 6.19, for Setting 1, Setting 2 and Setting 3, respectively. The opening of the FCV is calculated as shown in eq. 6.16, eq. 6.18 and eq. 6.20, for Setting 1, Setting 2 and Setting 3, respectively.

$$u_{PRV} = \begin{cases} 1, & u_{PRV} > 1 \\ \frac{p_x - p_{cr_{PRV}}}{\Delta p_{open_{PRV}}}, & 0 \leq u_{PRV} \leq 1 \\ 0, & u_{PRV} < 0 \end{cases} \tag{6.14}$$

Setting 1:

$$u_{CBV} = \begin{cases} 1, & u_{CBV} > 1 \\ \frac{p_x \cdot \rho_p + p_A - p_{cr_{CBV}}}{\Delta p_{open_{CBV}}}, & 0 \leq u_{CBV} \leq 1 \\ 0, & u_{CBV} < 0 \end{cases} \tag{6.15}$$

$$u_{FCV} = \begin{cases} 1, & u_{FCV} > 1 \\ \frac{p_B + p_\Delta - p_C}{\Delta p_{open_{FCV}}}, & 0 \leq u_{FCV} \leq 1 \\ 0, & u_{FCV} < 0 \end{cases} \tag{6.16}$$

Setting 2:

$$u_{CBV} = \begin{cases} 1, & u_{CBV} > 1 \\ \frac{p_B \cdot \rho_p + p_A - p_{cr_{CBV}}}{\Delta p_{open_{CBV}}}, & 0 \leq u_{CBV} \leq 1 \\ 0, & u_{CBV} < 0 \end{cases} \tag{6.17}$$

$$u_{FCV} = \begin{cases} 1, & u_{FCV} > 1 \\ \frac{p_x + p_\Delta - p_C}{\Delta p_{open_{FCV}}}, & 0 \leq u_{FCV} \leq 1 \\ 0, & u_{FCV} < 0 \end{cases} \tag{6.18}$$

Setting 3:

$$u_{CBV} = \begin{cases} 1, & u_{CBV} > 1 \\ \frac{p_x \cdot \rho_p + p_A - p_{cr_{CBV}}}{\Delta p_{open_{CBV}}}, & 0 \leq u_{CBV} \leq 1 \\ 0, & u_{CBV} < 0 \end{cases} \tag{6.19}$$

$$u_{FCV} = \begin{cases} 1, & u_{FCV} > 1 \\ \frac{p_x + p_\Delta - p_C}{\Delta p_{open_{CBV}}}, & 0 \leq u_{FCV} \leq 1 \\ 0, & u_{FCV} < 0 \end{cases} \tag{6.20}$$

Pressure in V_C

As the pressure buildup in V_C is considered infinitely fast is the pressure, p_C, calculated by an algebraic equation as shown in eq. 6.21.

$$p_C = \begin{cases} p_B + \left(\frac{Q_{DCV}}{k_{v_{main}} \cdot u}\right)^2, & p_C > 0 \\ 0, & p_C \leq 0 \end{cases} \tag{6.21}$$

Volume Flows

The flow equations introduced in Section 2.2 are used to calculate the flows in the circuit. The flow trough the CBV and the PRV are calculated shown in eq. 6.22 and eq. 6.23, respectively. The return flow through the main spool are calculated as shown in eq. 6.24 and the flow through the adjustable orifice are calculated as shown in eq. 6.25. As the FCV and main spool are calculated as one effective orifice is the volume flow calculated as shown in eq. 6.26.

$$Q_{CBV} = k_{v_{CBV}} \cdot u_{CBV} \cdot \text{sign}(p_A - p_0) \cdot \sqrt{|p_A - p_0|} \tag{6.22}$$

$$Q_{PRV} = k_{v_{PRV}} \cdot u_{PRV} \cdot \text{sign}(p_x) \cdot \sqrt{|p_x|} \tag{6.23}$$

$$Q_{mainr} = k_{v_{mainr}} \cdot u \cdot \text{sign}(p_0) \cdot \sqrt{|p_0|} \tag{6.24}$$

$$Q_{AO} = k_{v_{AO}} \cdot sign(p_S - p_x) \cdot \sqrt{|p_S - p_x|} \tag{6.25}$$

$$Q_{DCV} = (u \cdot k_{v_{DCV}})_{eff} \cdot \text{sign}(p_S - p_B) \cdot \sqrt{|p_S - p_B|} \tag{6.26}$$

where

$$(u \cdot k_{v_{DCV}})_{eff} = \frac{1}{\sqrt{\frac{1}{\left(k_{v_{FCV}} \cdot u_{FCV}\right)^2} + \frac{1}{\left(k_{v_{main}} \cdot u\right)^2}}} \tag{6.27}$$

and

$$\text{sign}(X) = \begin{cases} 1, & X > 0 \\ 0, & X = 0 \\ -1, & X < 0 \end{cases} \tag{6.28}$$

Control System

The control system is described in Section 4.4. The feed forward signal is calculated as shown in eq. 6.29. The desired crack pressure of the PRV is calculated as shown in eq. 6.30.

$$p_{FF} = p_{B_{LPF}} - 30 \cdot 10^5 \tag{6.29}$$

$$p_{cr_{PRV}} = p_{FF} + p_{FB} \tag{6.30}$$

6.3.5 Time Derivatives

The angular acceleration of the beam is calculated as shown in eq. 6.31. The equation is based on eq. 2.15 in Section 2.3, and the Figures 3.8 - 3.9 in Section 3.2.

$$\ddot{\theta} = \frac{l_{AC} \cdot (p_A \cdot A_A - p_B \cdot A_B) \cdot \cos(\gamma)}{I_A} - \frac{m \cdot g \cdot l_{AG} \cdot \cos(\theta + \alpha_1)}{I_A} \tag{6.31}$$

The pressures gradients in the volumes are calculated as shown in eq. 6.32 - 6.36. These are based on eq. 2.17 in Section 3.2 and Figure 6.2.

$$\dot{p}_x = \frac{\beta}{V_x} \cdot (Q_{AO} - Q_{PRV}) \tag{6.32}$$

$$\dot{p}_0 = \frac{\beta}{V_0} \cdot (Q_{CBV} - Q_{mainr}) \tag{6.33}$$

$$\dot{p}_A = \frac{\beta}{V_A} \cdot (A_A \cdot \dot{x}_c - Q_{CBV}) \tag{6.34}$$

$$\dot{p}_B = \frac{\beta}{V_B} \cdot (Q_{DCV} - A_B \cdot \dot{x}_c) \tag{6.35}$$

$$\dot{p}_C = \frac{\beta}{V_C} \cdot (Q_{FCV} - Q_{DCV}) \tag{6.36}$$

The gradient of the low pass filtered signal is calculated as shown in eq. 6.37 based on eq. 2.19.

$$\dot{p}_{B_{LPF}} = \frac{k \cdot p_B - p_{B_{LPF}}}{\tau} \tag{6.37}$$

The gradient of the feedback signal is calculated as shown in eq. 6.38 based on eq. 2.21 and Figure 6.2.

$$\dot{p}_{FB} = G \cdot \left(\dot{p}_{B_{LPF}} - \dot{p}_x + \frac{p_{B_{LPF}} - p_x}{Ti} \right) \tag{6.38}$$

6.3.6 State Variables and Saturation

The state variables are calculated by means of Forward Euler described in eq. 6.5 in Section 6.2.6. The pressures in the volumes are calculates as shown in eq. 6.39 - 6.42.

$$p_{A_{(n+1)}} = \begin{cases} p_{A_{(n)}} + \dot{p}_A \cdot dt, & p_{A_{(n+1)}} > 0 \\ 0, & p_{A_{(n+1)}} \le 0 \end{cases} \tag{6.39}$$

$$p_{B_{(n+1)}} = \begin{cases} p_{B_{(n)}} + \dot{p}_B \cdot dt, & p_{B_{(n+1)}} > 0 \\ 0, & p_{B_{(n+1)}} \le 0 \end{cases} \tag{6.40}$$

$$p_{x_{(n+1)}} = \begin{cases} p_{x_{(n)}} + \dot{p}_x \cdot dt, & p_{x_{(n+1)}} > 0 \\ 0, & p_{x_{(n+1)}} \le 0 \end{cases} \tag{6.41}$$

$$p_{0_{(n+1)}} = \begin{cases} p_{0_{(n)}} + \dot{p}_0 \cdot dt, & p_{0_{(n+1)}} > 0 \\ 0, & p_{0_{(n+1)}} \le 0 \end{cases} \tag{6.42}$$

The low pass filtered signal is calculated as shown in eq. 6.43 and the feedback signal is calculated as shown in eq. 6.44.

$$p_{B_{LPF(n+1)}} = p_{B_{LPF(n)}} + \dot{p}_{B_{LP}} \cdot dt \tag{6.43}$$

$$p_{FB_{(n+1)}} = p_{FB_{(n)}} + \dot{p}_{FB} \cdot dt \tag{6.44}$$

The angle and angular velocity of the beam are calculated as shown in eq. 6.45 and eq. 6.46, respectively.

$$\dot{\theta}_{(n+1)} = \dot{\theta}_{(n)} + \ddot{\theta} \cdot dt \tag{6.45}$$

$$\theta_{(n+1)} = \begin{cases} 35.42°, & \theta_{(n+1)} > 35.42° \\ \theta_{(n)} + \dot{\theta} \cdot dt, & -17.1° \leq \theta_{(n+1)} \leq 35.42° \\ -17.1°, & \theta_{(n+1)} < -17.1° \end{cases} \tag{6.46}$$

Note that eq. 6.39 - 6.42 and eq. 6.46 are discontinuous. This is done in order for the saturation to be taken into account.

6.3.7 Next Current Time

The current time for the next step and the next step are calculated in eq. 6.47 and eq. 6.48, respectively.

$$t_{(n+1)} = t_{(n)} + dt \tag{6.47}$$

$$n_{(n+1)} = n_{(n)} + 1 \tag{6.48}$$

6.4 Results

This section presents results from the time domain simulations. The settings are simulated with a cutoff frequency which results in a stable lowering of the load. The chosen values might not be optimal, but can be used as a good initial value for the physical testing. The cutoff frequencies are listed in Table 6.1. During the simulation is the input signal ramped from $u = 0$ to $u = 0.15$ within 0.01 seconds.

6.4.1 Setting 1

Figure 6.3 presents the results of the simulation of Setting 1 in three graphs. The first graph shows the cylinder piston position with respect to the simulation time. The second graph shows the cylinder velocity with respect to time. The third graph shows the system pressures, namely p_A, p_B and p_x, with respect to the simulation time.
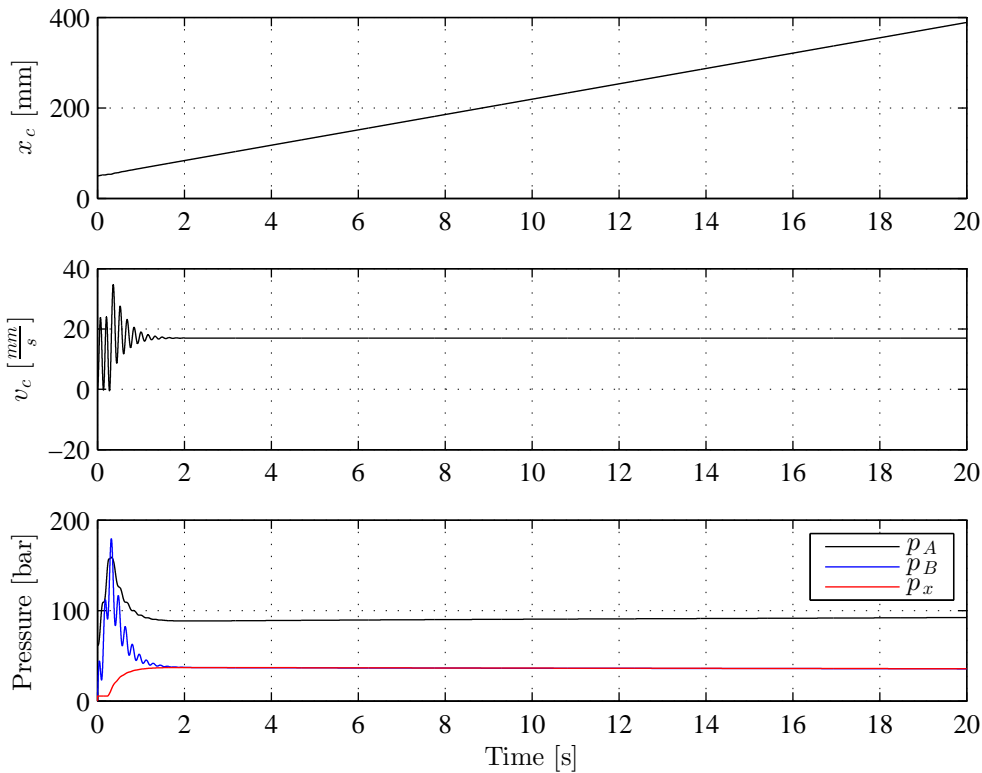
Figure 6.3: Simulation of Setting 1

The simulation shows that Setting 1 stabilizes the lowering sequence, although the pressures and the cylinder velocity oscillates some initially. The pressure in chamber A and chamber B also peaks initially. This is caused by the slow response of the filtered pilot pressure, as the pressure in chamber A rises and opens the CBV. Because of this, is it possible to say that the response time of the system is somewhat unaffected by the cutoff frequency as p_A rises and starts the motion if p_x rises too slow. The cutoff frequency has, on the other hand, influence on the system stability and overshoot of pressure p_A and p_B.

6.4.2 Setting 2

Figure 6.4 presents the results of the simulation of Setting 2 in three graphs. The first graph shows the cylinder piston position with respect to the simulation time. The second graph shows the cylinder velocity with respect to time. The third graph shows the system pressures, namely p_A, p_B and p_x, with respect to the simulation time.
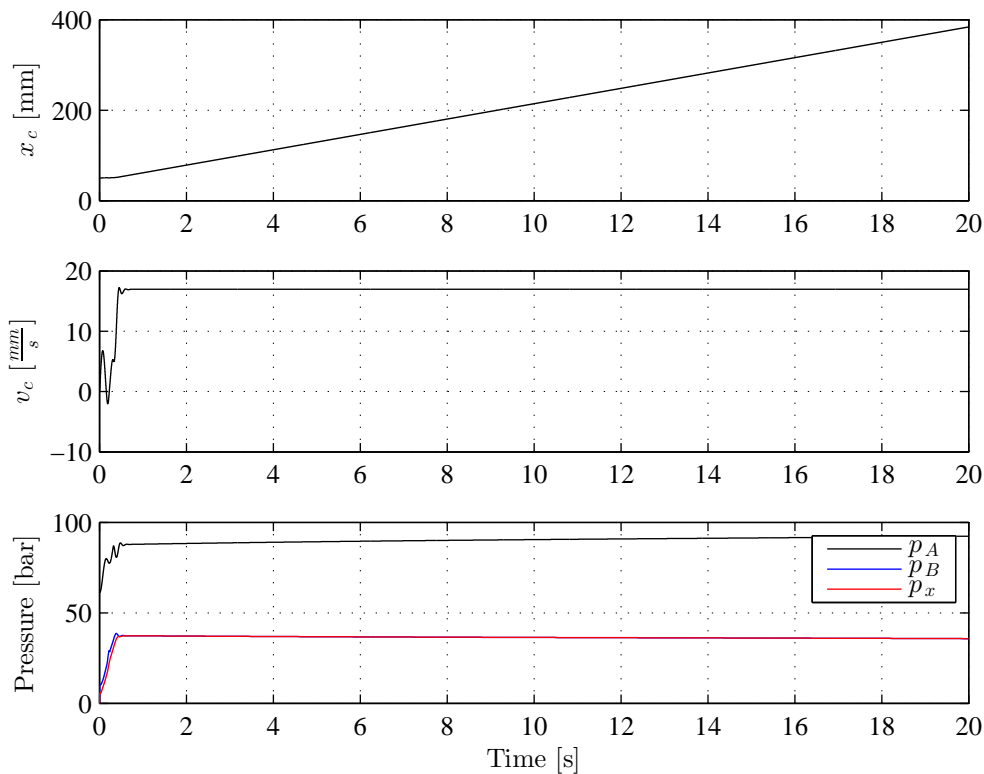
Figure 6.4: Simulation of Setting 2

The simulation shows that Setting 2 stabilizes the lowering sequence. The cylinder velocity and the system pressures reaches steady state after approximately 0.5 seconds with minimum oscillations and overshoot. In this setting is the filtrated pressure, p_x, assigned to the DCV. The pressure tries to open the FCV while the pressure between the FCV and the main spool tries to close the it, recall Figure 2.3. A slow rise of p_x means that the FCV will open slow, which again results in a slow response of the entire system. This is shown in Figure 6.5 where the cutoff frequency is set to 0.1 Hz ($\tau = 1.59 \frac{s}{rad}$). A high cutoff frequency, on the other hand, removes the filtering effect and the system will receive its original characteristic and be unstable.

6.4.3 Setting 3

Figure 6.6 presents the results of the simulation of Setting 3 in three graphs. The first graph shows the cylinder piston position with respect to the simulation time. The second graph shows the cylinder velocity with respect to time. The third graph shows the system pressures, namely p_A, p_B and p_x, with respect to the simulation time. The simulation shows that Setting 3 stabilizes the lowering sequence, although the pressure in chamber A and chamber B oscillates initially for approximately 1.3 seconds. Setting 3 is a combination of Setting 1 and Setting 2 as the low pass filtrated pressure is assigned both to the CBV and the FCV. The same effect when applying a slow filtered pressure to the FCV, as seen for Setting 2, therefore applies for Setting 3. This means that a low cutoff frequency will result in a slow response for the system. The same cutoff frequency are used for Setting 2 and Setting 3 during the simulations. By comparing Figure 6.4 and Figure 6.6 is it seen that Setting 3 tends to oscillate more than Setting 2. These oscillations occurs as the CBV receives a pressure that is filtered by a cutoff frequency of $f_c = 3$ Hz instead of $f_c = 0.1$ Hz, meaning that a cutoff frequency high enough for the system to response quickly also makes the system slightly oscillatory.
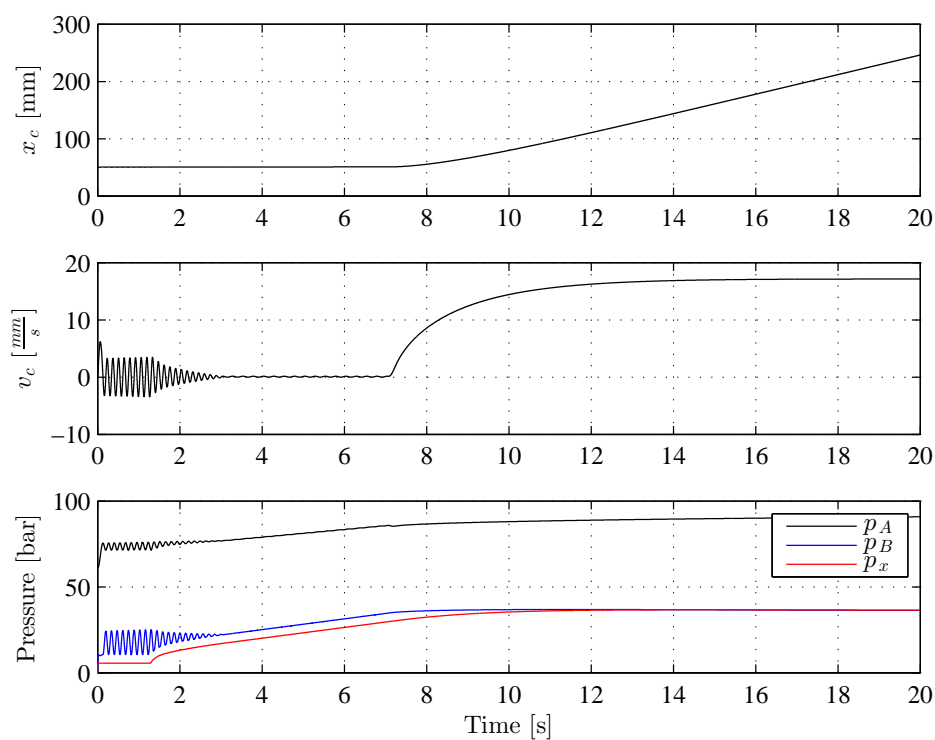
Figure 6.5: Simulation of Setting 2, $\tau = 1.59 \frac{\text{s}}{\text{rad}}$
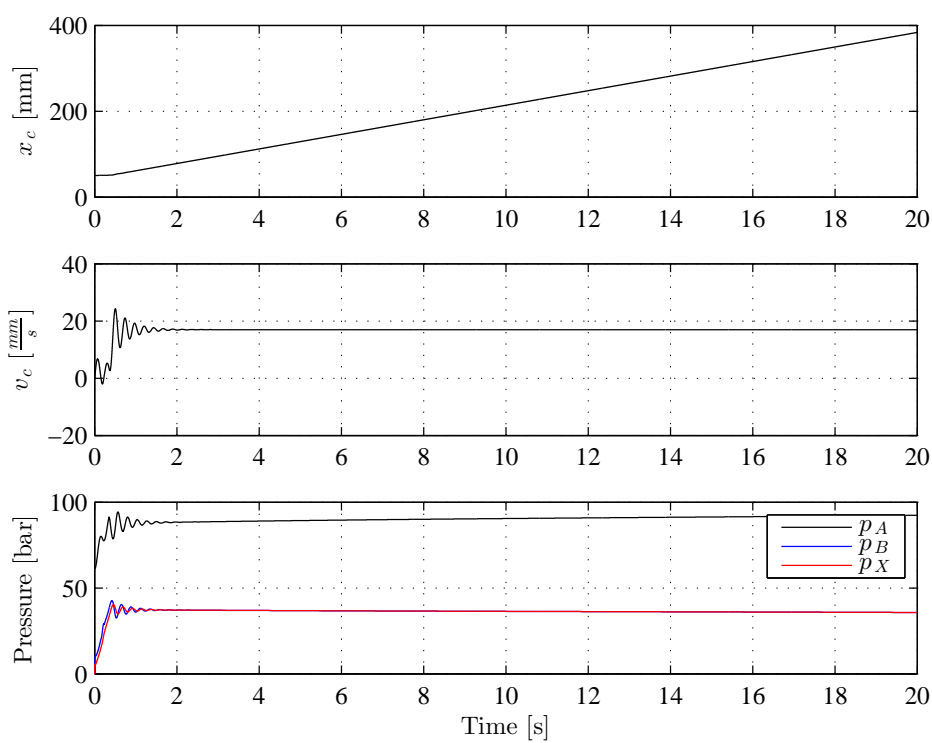
Figure 6.6: Simulation of Setting 3

84

6.5 Conclusion

It is seen from the time domain simulations that all of the three setting have a good basis for making the system stable. They all provides a stable lowering sequence, although Setting 1 and Setting 3 shows some oscillations in the pressure and the velocity initially. For Setting 1 is it seen that the cutoff frequency influences the stability and the overshoot of the pressures. The response of the system, on the other hand, is unaffected by the cutoff frequency as the pressure in chamber A rises and opens the CBV for low cutoff frequencies. Setting 2 shows a minimum of oscillations and overshoot initially. For Setting 2 and Setting 3 is it seen that a low cutoff frequency slows the response of the system as it prevents the FCV from opening. For Setting 3 is it also seen that a compromise for the cutoff frequency must be found as the CBV demands a low cutoff frequency in order for the system to be stable while the FCV demands a higher cutoff frequency in order for the system to be responsive.

Chapter 7

Physical Testing

In this chapter is the stabilizing method investigated by means of physical testing performed on the test rig described in Chapter 3. All three settings are tested. In addition is the original system, called Setting 0, tested once. First is each setting tested with a cutoff frequency, f_c, that results in a satisfactory stable system. These results are then used as basis of comparison for the further tests performed on each setting, which are to be found in Appendix D. In total are seven tests performed on each of the settings. The testing includes:

- Test 1: A test with a satisfactory cutoff frequency (used as basis of comparison)

- Test 2: A test with a cutoff frequency which is higher compared to the satisfactory cutoff frequency

- Test 3: A test with a cutoff frequency which is lower compared to the satisfactory cutoff frequency

- Test 4: A test where the cutoff frequency is equal to the satisfactory cutoff frequency and the load is increased

- Test 5: A test where the cutoff frequency is equal to the satisfactory cutoff frequency and the supply pressure is reduced from 200 bar to 150 during the motion

- Test 6: A test where the cutoff frequency is equal to the satisfactory cutoff frequency and the supply pressure is increased from 150 bar to 200 bar during the motion

- Test 7: A test where an experienced crane operator is asked to manually operate the stabilized test rig

The crane operators were asked to fill in an interview sheet during the testing of each setting. These sheets are to be found in Appendix E. Lastly, in this chapter, is each setting discussed based on the results from the testing. The tests are performed in order to map the characteristics of the stabilizing method when applied to the test rig presented in Chapter 3 under the conditions stated in the each test.

7.1   Presentation of the Test Results

A short test procedure is first presented, and then the results for each setting. For each test is a figure and a table presented. The figure includes three graphs where the first graph shows the cylinder extension, the second graph shows the cylinder speed, and the last graph shows the magnitude of the pressures which are of interest during the testing. All graphs are presented with respect to the time, in seconds. The table includes parameters for the test. The first three elements in the table are the supply pressure, the tank pressure, and the oil temperature. These are assumed to be constant during the test unless otherwise stated. Further are the total motion time, the rise time, and the retardation time listed. Next in the table are the cutoff frequency and the time constant for the low pass filter. The last parameter in the table is the desired valve opening, u_0.

7.2 Test Procedure

In order to obtain comparable results a electrical input signal is used to operate the pressure compensated DCV. Test 1 to test 6 are all performed similarly in 3 steps.

- Step 1: Drive the cylinder to initial position

- Step 2: Wait for pressures to stabilize

- Step 3: Start control signal

Note that Setting 2 and Setting 3 are performed with another DCV compared to Setting 0 and Setting 1, see Appendix C. The control signals are similar in shape but different in magnitude in order to maintain approximately the same volume flow into the circuit, and making the results from the different settings as comparable as possible.

7.2.1 Initial Conditions

In advance of every test, the cylinder is extracted by the same extent in order to obtain the same initial position of the beam. The beam is then kept dormant until the pressures in the system stabilizes. The initial conditions are listed in Table 7.1.

Table 7.1: The initial conditions of the testing

Parameter	Value	Unit
Cylinder extension	450	mm
Cylinder piston velocity	0	$\frac{m}{s}$
Cylinder piston acceleration	0	$\frac{m}{s^2}$
Oil temperature	30 - 50	$^\circ C$

7.2.2 Input signal

Plotting of the test starts after the initial conditions are reach. A trapezoidal input signal is used to control the main spool of the DCV. A typical shape of the signal is shown in Figure 7.1.
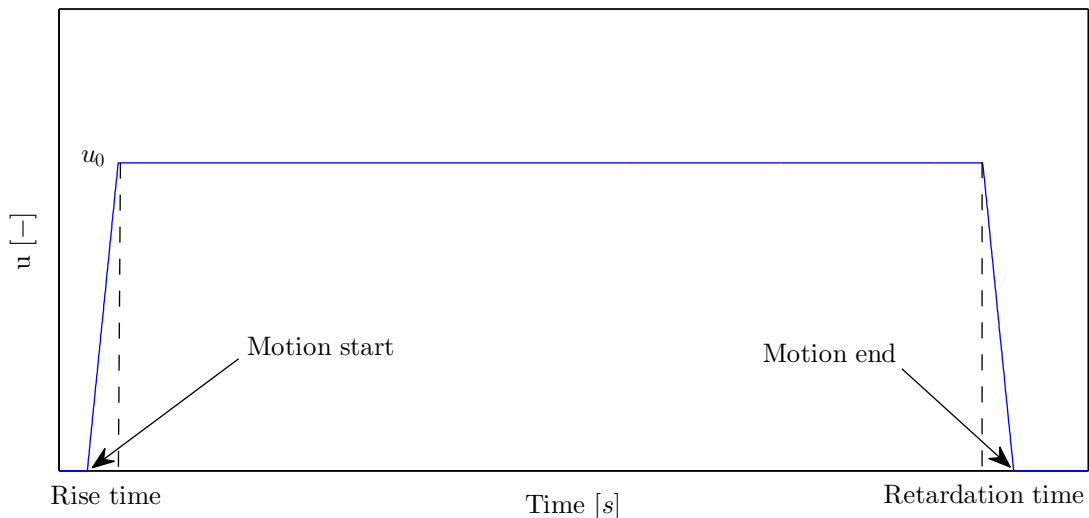
Figure 7.1: Typical control signal used during the testing

The fist part of the motion is called rise time. During the rise time is the control signal gradually increased in a linear manner until the desired valve opening, u_0, is reached. The valve opening is then held constant

at u_0 until the retardation starts. The control signal retardation is carried out during the Retardation time, where the valve opening is linearly reduced until it reaches 0, and the motion is completed. As two different DCVs are used, u_0 depends on which DCV that is used. u_0 is set to 0.15 for Setting 0 and Setting 1, and 0.1 for Setting 2 and Setting 3. The rise time and retardation time is equal for all settings and set to 0.01 seconds. The entire motion takes in total 20.02 seconds.

7.3 Setting 0 (The original system)

In this section is test of the original system, Setting 0, presented. Only one test is performed on this setting. This is the original setup where the pressure in chamber B is assigned both to the pilot line of the CBV and to the pressure compensated DCV. This test is performed in order to demonstrate the instability of the original system. Further conditions of this test are listed in Table 7.2.

Table 7.2: Parameters for the test of Setting 0

Test parameter	Value	Unit
Supply pressure	200	bar
Tank pressure	0	bar
Oil temperature	35	$^\circ C$
Total motion time	20.02	s
Rise time	0.01	s
Retardation time	0.01	s
Cutoff frequency, f_c	-	Hz
Time constant, τ	-	$\frac{\text{s}}{\text{rad}}$
u_0 (Hawe)	0.15	-

Results and Discussion

The results from the test are shown in Figure 7.2. This figure presents the pressure in chamber A (p_A), the pressure in chamber B (p_B), the cylinder contraction (x_c), and the cylinder speed (v_c) during the testing. Test characteristics:

Typical contraction velocity: Oscillatory at about $16 \frac{\text{mm}}{\text{s}}$

Overshoot: A small velocity overshoot in the initial phase of the motion

Settling: Neither the pressures nor the velocity settles during the motion

The test shows that the original system is highly oscillatory and unstable. The beam flexes and is lowered in a jagged manner. Although the jagged motion is hardly seen in the position plot is it made clear in the velocity plot. The pressure plot also shows that the system is highly oscillatory.
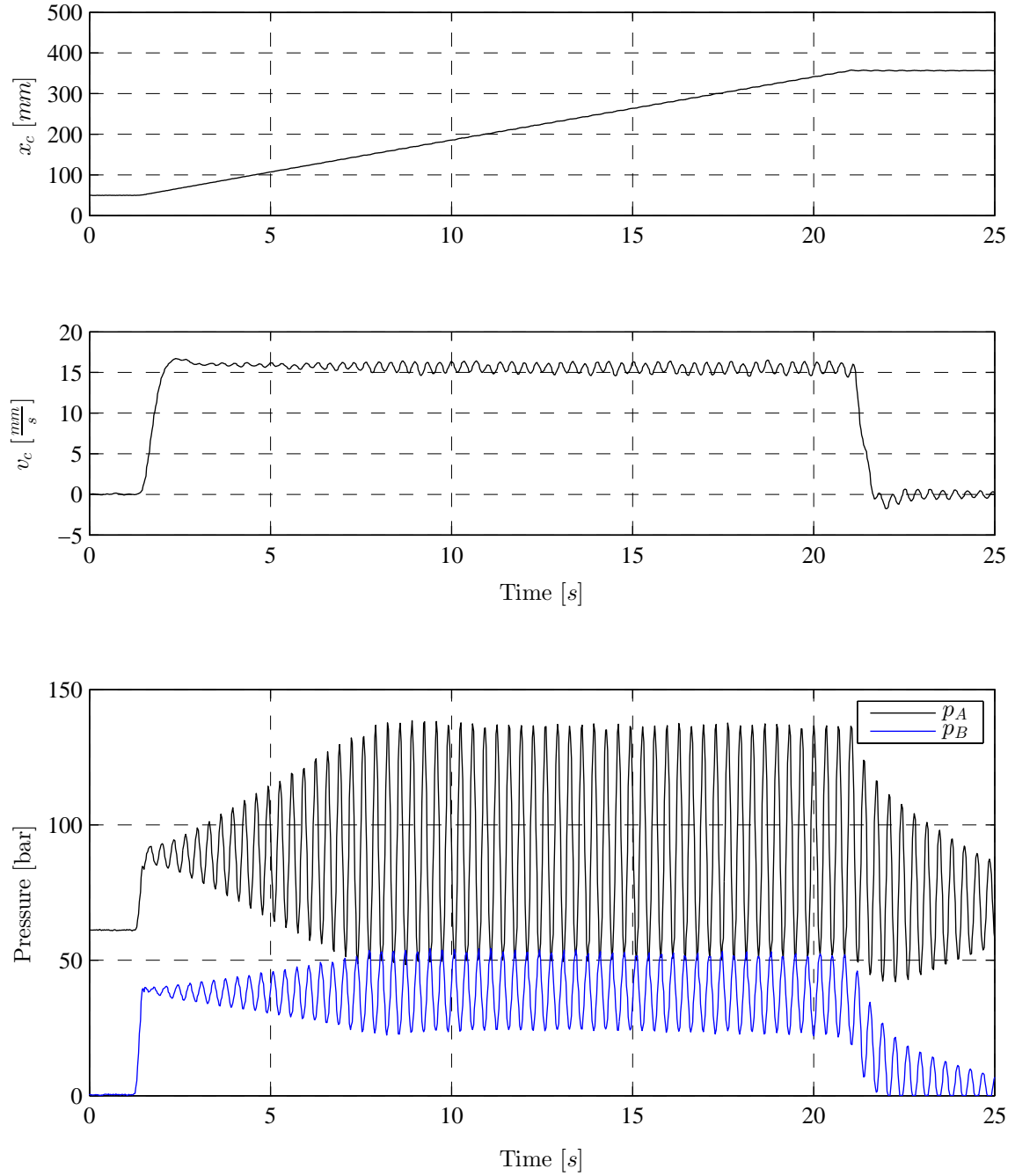
Figure 7.2: Test results Setting 0

7.4 Setting 1

Setting 1 is the setup where the low pass filtered pressure, p_x, is assigned to the pilot line of the CBV while the original pressure in chamber B, p_B, is assigned to the pressure compensated DCV.

In this section, the test of Setting 1 with a satisfactory cutoff frequency is presented. This test is used as basis of comparison for additional tests performed on this setting. These tests are to be found in Appendix D. Lastly in this section, the performances of Setting 1 is discussed. All the tests performed on this setting, also those presented in Appendix D, are background for this discussion.

7.4.1 Test of Setting 1 with a Satisfactory Cutoff Frequency

In this test, the cutoff frequency is chosen to be a value which gives a satisfactory stable and controllable system, namely $f_c = 0.1$. Further conditions of this test are listed in Table 7.3.

Table 7.3: Parameters for the test of Setting 1 with a satisfactory cutoff frequency

Test parameter	Value	Unit
Supply pressure	199	bar
Tank pressure	0	bar
Oil temperature	39	$°C$
Total motion time	20.02	s
Rise time	0.01	s
Retardation time	0.01	s
Cutoff frequency, f_c	0.1	Hz
Time constant, τ	1.592	$\frac{\text{s}}{\text{rad}}$
u_0 (Hawe)	0.15	-

Results and Discussion

The results from the test are shown in Figure 7.3. This figure presents the pressure in chamber A (p_A), the pressure in chamber B (p_B), the low pass filtered pressure (p_x), the cylinder contraction (x_c), and the cylinder speed (v_c) during the testing.
Test characteristics:

Typical contraction velocity: About $17 \frac{\text{mm}}{\text{s}}$ with an overshoot at about $2 \frac{\text{mm}}{\text{s}}$

Overshoot: The pressures overshoots with approximately 70% for p_A and 300% for p_B. The velocity overshoots with approximately 10%

Settling: Settles smoothly after about 2 seconds

This test shows that the pressures gets an oscillatory section in the start of the motion and which later stabilizes. What happens first, after the motion is started, is that the oil starts to enter cylinder chamber B while the CBV is closed and prevents the oil from exiting the cylinder. The first, and highest, spike of p_B indicates that the pressure in chamber B rises quickly while the low pass filtered pressure slowly rises to a level where the CBV starts to open. When the CBV opens is the cylinder forced to accelerate quickly due to the high amount of energy which is stored in the cylinder due to the pressure buildup. This leads to the oscillations detected in the chamber pressures in the first seconds of the motion.
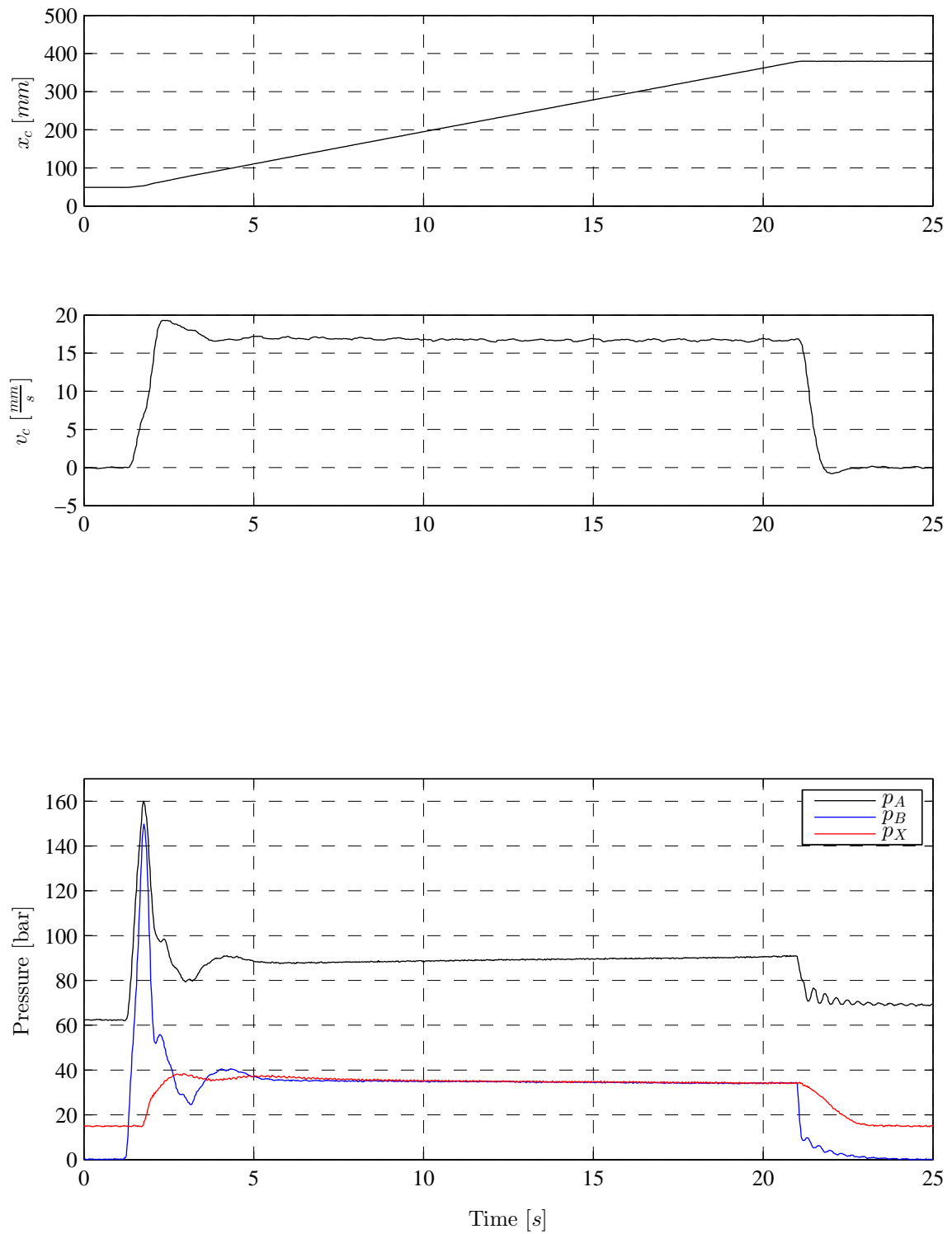
Figure 7.3: Results for Test 1, Setting 1

7.4.2 Discussion of Setting 1 Based on the Testing

Testing shows that Setting 1 stabilizes the lowering sequence, although the cutoff frequency of the low pass filter plays an important role in the stability of the system. The cutoff frequency should be high so that the CBV can react on quick pressure changes in order to avoid a low system efficiency and high pressures in chamber A and chamber B. On the other hand is a certain filtration needed in order for the system to be stable. The response time for the crane is independent of the filter frequency. Sudden changes in the supply pressure seems to affect the cylinder velocity, see Figure D.4 and Figure D.5. Especially when the pressure is reduced. This setting seems to give a safe and stable response when operated manually. Both interviewees claims this to be the best stabilized and most responsive system of the three tested. Manipulation of the CBV can include a safety risk as this valve provides several safety functions. All testing was however performed with an open centered main spool in the DCV (motor spool) without any complications or safety issues.

7.5 Setting 2

Setting 2 is the setup where the low pass filtered pressure, p_x, is assigned to the pressure compensated DCV, while the original pressure in chamber B, p_B, is assigned to the pilot line of the CBV.

In this section, the test of Setting 2 with a satisfactory cutoff frequency is presented. This test is used as basis of comparison for additional tests performed on this setting. These tests are to be found in Appendix D. Lastly in this section, the performances of Setting 2 is discussed. All the tests performed on this setting, also those presented in Appendix D, are background for this discussion.

7.5.1 Test of Setting 2 with a Satisfactory Cutoff Frequency

In this test, the cutoff frequency is chosen to be a value which gives a satisfactory stable and controllable system, namely $f_c = 3$. Further conditions of this test are listed in Table 7.4.

Table 7.4: Parameters for the test of Setting 2 with a satisfactory cutoff frequency

Test parameter	Value	Unit
Supply pressure	200	bar
Tank pressure	0	bar
Oil temperature	39	$°C$
Total motion time	20.02	s
Rise time	0.01	s
Retardation time	0.01	s
cutoff frequency, f_c	3	Hz
Time constant, τ	0.053	$\frac{s}{rad}$
u_0 (Danfoss)	0.1	-

Results and Discussion

The results from the test are shown in Figure 7.4. This figure presents the pressure in chamber A (p_A), the pressure in chamber B (p_B), the low pass filtered pressure (p_x), the cylinder contraction (x_c), and the cylinder contraction speed (v_c) during the testing.
Test characteristics:

Typical contraction velocity: About 17 $\frac{mm}{s}$ with an overshoot at about 0.7 $\frac{mm}{s}$

Overshoot: A small overshoot for both the velocity and pressures

Settling: The cylinder velocity settles quick and smoothly after approximately 0.5 seconds

This test shows a stable and smooth motion. The results shows a small oscillatory section in the pressures in the initial part of the motion. This may be introduced by the compensator as the LS pressure (p_x) at this point is low compared to the actual pressure at the outlet of the DCV (p_B). Another explanation may be that the flow into the circuit is very low and this may affect the CBV in a way so that oscillations are introduced. These oscillations in the pressures are, on the other hand, hardly noticeable in the velocity plot and does not introduce any instabilities in the velocity.
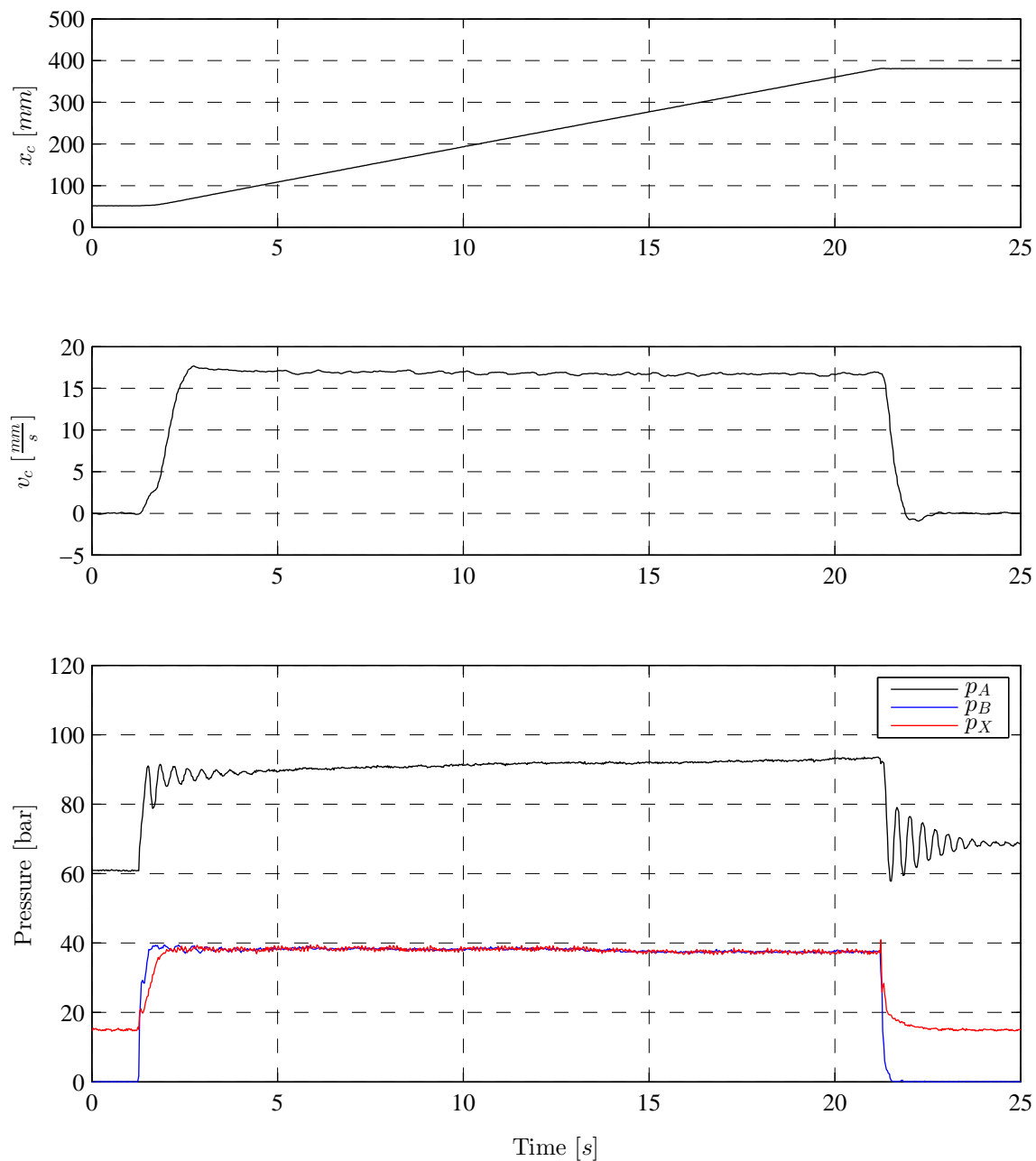
Figure 7.4: Results for Test 1, Setting 2

7.6 Discussion of Setting 2 Based on the Testing

The response time for this setting seems to be highly dependent of the cutoff frequency. The stability, on the other hand, does note make the same demands of the cutoff frequency. With the valve and the opening used in the testing was not the stability dependent of the cutoff frequency. If the cutoff frequency was set low, did the system react very slowly, see Figure D.7. The cylinder velocity did not overshoot in the initial phase of the motion, but an increase in the load resulted in a higher velocity, see Figure D.8. A quick change in the supply pressur introduced a small peak in the cylinder velocity, see Figure D.9 and Figure D.10 . This peak did not introduce any oscillations and the original velocity was quickly maintained. As the CBV is mounted with its original connections, are all the safety functions this valve provides maintained. The first interviewee claims full control over the test rig, while the other interviewee remarks some oscillations. Especially subsequent to an abrupt load lowering. The oscillations indicated may be due to the flexible beam, and may not be instabilities in the hydraulics. The latter interviewee also comments that the system has a too high maximum velocity. This may be due to the fact that a bigger DCV is used in this setting compared to Setting 1.

7.7 Setting 3

Setting 3 is the setup where the low pass filtered pressure, p_x, is assigned both to the pressure compensated DCV and to the pilot line of the CBV.

In this section, the test of Setting 3 with a satisfactory cutoff frequency is presented. This test is used as basis of comparison for additional tests performed on this setting. These tests are to be found in Appendix D. Lastly, in this section, the performances of Setting 3 are discussed. All the tests performed on this setting, also those presented in Appendix D, are background for this discussion.

7.7.1 Test of Setting 3 with a Satisfactory Cutoff Frequency

In this test, the cutoff frequency is chosen to be a value which gives a satisfactory stable and controllable system, namely $f_c = 0.6$. Further conditions of the test are listed in Table 7.5.

Table 7.5: Parameters for the test of Setting 3 with a satisfactory cutoff frequency

Test parameter	Value	Unit
Supply pressure	198	bar
Tank pressure	0	bar
Oil temperature	37	$°C$
Total motion time	20.02	s
Rise time	0.01	s
Retardation time	0.01	s
Cutoff frequency, f_c	0.6	Hz
Time constant, τ	0.265	$\frac{s}{rad}$
u_0 (Danfoss)	0.1	-

Results and Discussion

The results from the test are shown in Figure 7.5. This figure presents the pressure in chamber A (p_A), the pressure in chamber B (p_B), the low pass filtered pressure (p_x), the cylinder contraction (x_c), and the cylinder contraction speed (v_c) during the testing.
Test characteristics:

Typical contraction velocity: About $17 \frac{mm}{s}$ with an oscillatory region initially in the motion with overshoot at about $4.3 \frac{mm}{s}$

Overshoot: Overshoot in the pressure p_B at approximately 15 bar and in the velocity at approximately 4.3 $4.3 \frac{mm}{s}$

Settling: Settles after about 3.5 seconds

This test shows that Setting 3 lowers the load smoothly in most of the motion but struggles to stabilize the system in the initial region of the motion.
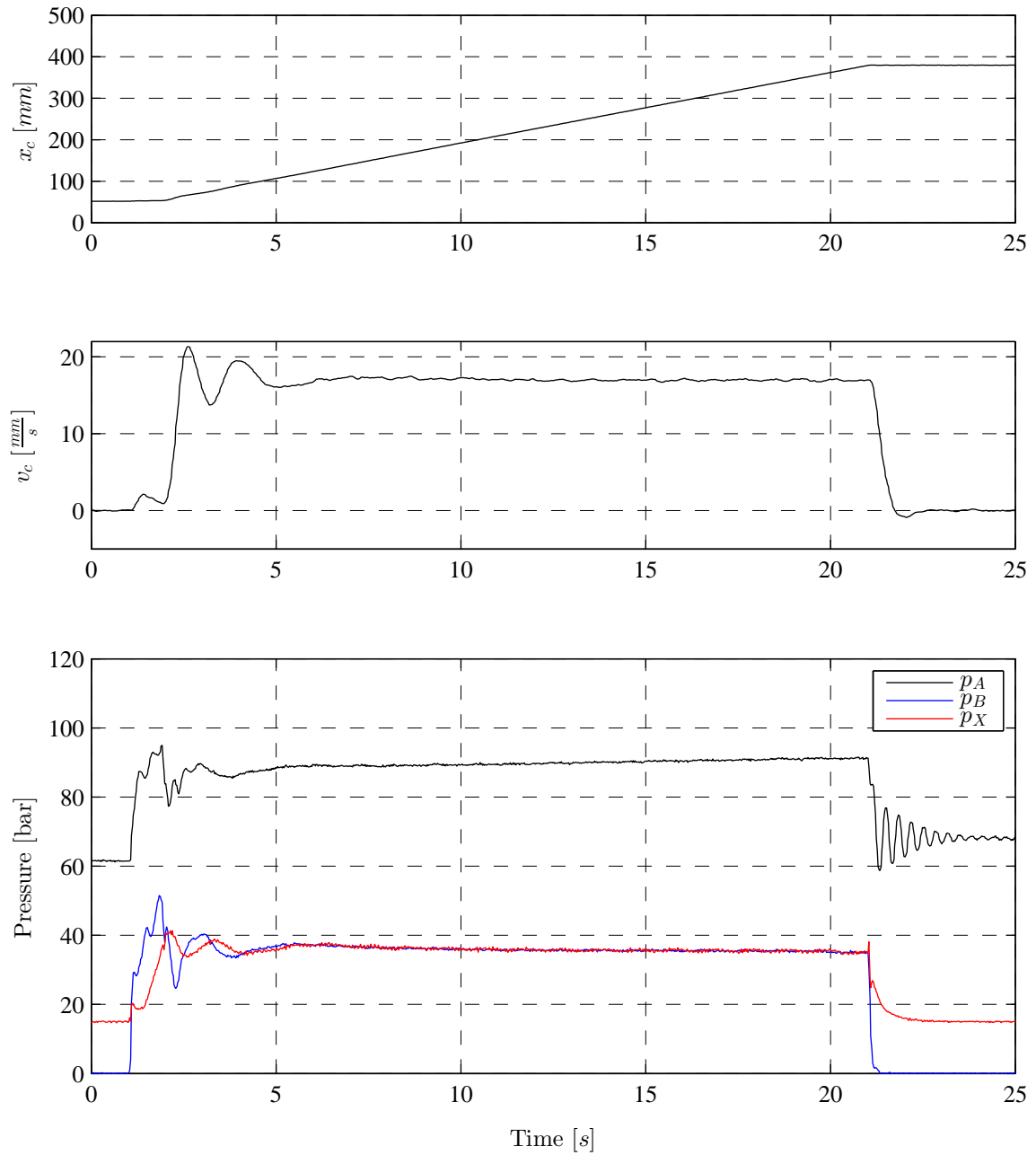
Figure 7.5: Results for Test 1, Setting 3

7.8 Discussion of Setting 3 Based on the Testing

In this setting are both the CBV and the pressure compensated DCV manipulated by the same externally produced pressure. As indicated for Setting 1 does the CBV demand a cutoff frequency which must be high enough for the system to react to abrupt changes, but also low enough to remove oscillations. The DCV, on the other hand, demands a relatively high cutoff frequency as compared to the CBV in order to react satisfactory, as indicated for Setting 2. This compromise leads to a system that may oscillate in the most critical regions. A compromise was found where the system oscillated slightly in the initial phase of the motion and was stable for the rest of the motion. A increase in the cutoff frequency made the system more oscillatory while a lower cutoff frequency made the system reaction time longer, see Figure D.11 and Figure D.12. The increased load did not affect the stability or the contraction velocity, see Figure D.13. Changes in the supply pressure during the motion did however introduce some oscillations at the moment of impact, see Figure D.14 and Figure D.15. Especially when the supply pressure was increased. The oscillations was, however, just temporary. The first interviewee describes the system as stable and controllable, but comments a long reaction time in the initial phase of a motion that starts when the beam is at rest. The latter interviewee comments the high contraction speed available with the lager DCV, the Danfoss DCV, which are used in this setting. Also the oscillations in the beam as a result of its physical structure are commented. Manipulation of the CBV can include a safety risk as this valve provides several safety functions. All testing was however performed with an open centered main spool in the DCV (motor spool) without any complications or safety issues.

7.9 Conclusion

It is seen from the physical testing that all the settings stabilizes the system. This is also backed up by user feedback. All the settings is tested for manual operation by crane operators who found them stable and controllable. The operators pointed out Setting 1 as very satisfactory. This setting is found unstable if the cutoff frequency of the low pass filter is set too high. If the cutoff frequency is set very low, the pressure in chamber A will rise and open the CBV. This setting will therefore remain responsive, but the slow pilot pressure may cause a safety risk. For Setting 2 is the reaction found to be highly dependent of the cutoff frequency. A low cutoff frequency will prevent the FCV from opening. The stability, on the other hand, is found to be unaffected by the cutoff frequency during the testing. For Setting 3, it is shown that a compromise have to be made regarding the cutoff frequency. A cutoff frequency which makes the FCV responsive may also lead to oscillations in the system, and a cutoff frequency which removes the oscillations may slow down the response of the system. None of the settings are found to become unstable for neither an increase in the load nor an abrupt change in the supply pressure. All the testing are performed with an open-center main spool without any complications ors safety issues.

Chapter 8

Discussion

This chapter starts with a short summary. The stabilization method is then discussed. This includes discussion of the implementability, safety and robustness. Further are the main discussions form each investigation brought back up and discussed in the light of the completed research.

8.1 Summary

Through out this thesis is a stabilization method for pressure compensated systems containing counterbalance valves investigated. The investigation starts by a linear stability analysis of the original circuit. This investigation is highly inspired by already published investigations, [10] and [12]. The linear stability analysis of the original system is then followed by linear analyses of the system including the stabilizing method. Three different ways of including the stabilizing method are investigated. These methods are called Setting 1, Setting 2 and Setting 3. First is setting 1 investigated. Two investigations are performed on this setting. For the first investigation is the circuit simplified. The simplification allows for a fully analytic linear stability analysis of this setting. Following this investigation is a linear analysis for each of the three settings. These analyses are partly numerical, as a fully analytic analysis turned out to be very unhandy. Following the linear analysis is the stabilization method investigated by means of time domain simulation. Simulations of each setting are performed. The stabilization method is then investigated by means of physical testing performed on a test rig. Each of the settings are here tested for various situations and impacts from the surroundings. As a final investigation are the settings tested for manual operation by crane operators.

8.2 Stabilization Method

In this section are advantages and disadvantages of the stabilization method presented. First is the ability to implement the method to already existing systems discussed. Then are various failure scenarios and their consequences discussed, followed by a discussion of the robustness of the stabilization method.

8.2.1 Implementability

The investigated stabilization method uses an external circuit in which a desired pressure is designed. This desired pressure is then either assigned to the pilot line of the counterbalance valve, the load-sensing line of the pressure compensated directional control valve, or both. These ways of implementing the stabilization method are called Setting 1, Setting 2 and Setting 3, respectively. Some modifications of the original hydraulic system must be made in order to implement any of these settings. An external circuit must be added to the system in order to create the desired pressure. The main components needed are:

- Flow control valve

- Solenoid operated pressure relief valve

- Two pressure sensors

- Controller

- Hoses and/or tubing

One of the sensors is used to measure a desired pressure in the original circuit. In this case is the pressure on the ring side of the cylinder measured, as this pressure originally is assign both to the CBV and the DCV. The measured signal is then send to the controller where it is low pass filtered. The second pressure sensor is used to measure the pressure in the external circuit. The low pass filtered signal and the measured signal from the external circuit are then send to a control system containing a PI-controller. This control system controls the solenoid operated pressure relief valve, which controls the pressure in the external circuit. The external circuit is supplied by the original circuit through a flow control valve. The flow control valve is used to reduce the flow and the supply pressure.

Setting 1 is the easiest setting to implement. First is the original connection between the pressure on the ring side of the cylinder and the pilot line of the CBV removed. The externally designed pressure is then assign to the CBV. Setting 2 and Setting 3 might be harder to implement as these settings requires a certain type of pressure compensated DCVs. Normally are pressure compensated DCVs equipped with an internal connection between the outlet of the DCV and the internal compensator. Setting 2 and Setting 3 requires a DCV where this internal connection is removed. When a DCV with this feature is acquired, is the externally designed pressure assigned either to this valve alone or in a combination with the CBV.

All Settings requires modifications of the original hydraulic circuit and a power supply for pressure sensors, the solenoid operated PRV and the controller. Setting 2 and Setting 3 may be more expensive as they probably requires a new DCV.

8.2.2 Safety

It is important to consider the safety risks and error causes which may follow a newly developed control technique. Problems may occur if the control technique, or the system it is applied to, should fail or break down. As it is hard to predict every possible error cause and its consequences is strict testing highly recommended. Further are some error causes for this system presented and its consequences discussed in Table 8.1. Note that this table may be imperfect. The measure pressure in the original circuit is p_B and the externally designed pressure is p_x.

The failures presented in Table 8.1 effects the externally designed pressure p_x. The failures are therefore most critical for the settings where p_x is connected to the CBV, as the system will lose many of its important safety functions. For systems where the pressure p_x is assigned to the pressure compensated DCV, are there only consequences during load lowering.

8.2.3 Robustness

The stabilization method must be reliable and safe for all operations. All of the three settings are tested for manual operation. For Setting 1 is it shown that a low flow and a high load pressure is the most critical operating mode. Especially when the cylinder is extracted. The testing indicates that this also applies for Setting 2 and Setting 3. If a cutoff frequency of the low pass filter, which makes the system stable through the entire motion with a high load pressure and a small DCV opening, is chosen. Will this system be stable for all operations.

During the physical testing was the settings tested through various scenarios. The same control signal for the main spool was used during all the tests. The cylinder contraction velocity is kept relatively constant through every test for all settings, except for the test where an extra load is applied. This test affected the velocity of Setting 1 and Setting 2.

It is expected that this stabilization method can be implemented to systems where the load may change from negative to positive during the lowering sequence. An example of such a system is a knuckle boom crane. The stabilization method seems to be robust and safe as long as the controller and the external pressure circuit is operating properly.

Table 8.1: Failure scenarios and consequences

	Lowering sequence	Dormant
Pressure sensor failure		
$p_x >> p_B$	p_x applied to the CBV: No cavitation protection p_x applied to the DCV: No compensator function	p_x applied to the CBV: No leak tight load holding No load holding at pipe burst Drop before lift may occur p_x applied to the DCV: No consequences
$p_x << p_B$	p_x applied to the CBV: High pressure in chamber A and chamber B p_x applied to the DCV: Small opening of the FCV	p_x applied to the CBV: No consequences p_x applied to the DCV: No consequences
Power failure		
Sensor	The pressure sensor signal is equal zero bar. For consequences see pressure sensor failure $p_x << p_B$	The pressure sensor signal is equal zero bar. For consequences see pressure sensor failure $p_x << p_B$
Control system	Zero crack pressure for the PRV, $p_x=$ 15 bar (minimum value), For consequences see pressure sensor failure $p_x << p_B$	Zero crack pressure for the PRV, $p_x=$ 15 bar (minimum value), For consequences see pressure sensor failure $p_x << p_B$
PRV	Zero crack pressure for the PRV, $p_x=$ 15 bar (minimum value), For consequences see pressure sensor failure $p_x << p_B$	Zero crack pressure for the PRV, $p_x=$ 15 bar (minimum value), For consequences see pressure sensor failure $p_x << p_B$

8.3 Linear Analysis

Five linearized stability analysis are performed on the system. First is the stability of the original circuit investigated analytically. The system including Setting 1 are then investigated analytically without the DCV considered. The DCV are then included and all of the three settings are investigated numerically.

8.3.1 The Original Circuit

The stability analysis of the original system is highly inspired by [10] and [12]. [8] states that "the most important asset of a hydraulic system is stability, and therefor stability should be based on hard quantities. Quantities that can be easily identified and determined with fair precision and whose values remain relative constant". In this investigation is the pressure compensated DCV replaced by a constant flow source. The cylinder is assumed ideal with no friction or internal leakage and the dynamics of the CBV are neglected. The original system is in this investigation found unstable, especially if the cylinder is extracted, the load pressure is high and the flow is small. This is later approved by physical testing of the original circuit.

8.3.2 Setting 1 Simplified

For this investigation is the same assumptions and the stabilizing method of Setting 1 applied. Also this system is originally found unstable for high load pressure, small opening of the main spool and the cylinder extracted, but the investigation also shows that the system is stable in all positions if a sufficient cutoff frequency is used in the low pass filter. This is later approved by physical testing of Setting 1.

8.3.3 Setting 1

For this investigations is almost all of the same assumptions applied, but the pressure compensated DCV is included in the investigation. This enlarges the linearized model and the investigation are therefore performed numerically with parameter values from the test rig applied. This investigation shows that Setting 1 stabilizes the system, and that the cutoff frequency of the low pass filter affects the magnitude and the settling time of the oscillations from a step response and must therefore be selected carefully.

8.3.4 Setting 2

The stabilizing method of Setting 2 and the same assumptions as for Setting 1 are applied in this investigation. Also this investigation are performed numerically. The investigation shows that Setting 2 stabilizes the system and that the cutoff frequency must be selected carefully. The stability of this setting is later approved by physical testing.

8.3.5 Setting 3

The stabilizing method of Setting 3 and the same assumptions as for Setting 1 are applied in this investigation. Also this investigation are performed numerically. The investigation shows that Setting 3 stabilizes the system and that the cutoff frequency must be selected carefully. The stability of this setting is later approved by physical testing.

8.4 Time Domain Simulations

The time domain simulations are used as a tool to demonstrate the stabilizing effect of the method and does therefore not provide a perfect model of the test rig. For example is the dynamic of the boom neglected, and only the circuit used for the lowering motion included. Also valve dynamics, leakage in the cylinder, pressure drop in hoses and tubing, volume expansion in hoses, and friction in bearings and cylinder are neglected. The pressure drop in the tubing and hoses are assumed to be small, as the volume flow in the system are low and there are short stretches. Volume expansion in the hoses are assumed insignificant as compared to the volume expansion in cylinder chamber A and chamber B. Friction in the cylinder and the bearings works against the motion. As only the lowering sequence is of interest, the velocity will have a positive value trough the entire sequence. The velocity is relatively constant, and the friction could been included as an extra load. If the velocity changed sign during the motion, would a so called stick slip phenomenon occur and the friction would have been of greater interest. The FCV and the main spool are modeled as one effective orifice. Modeling these as two valves would require a very low step time in order to calculate pressure gradient in the tiny volume between the FCV and the main spool. Assuming infinite fast pressure build up is considered a fair assumption in such tiny volumes.

Figure 8.1 - 8.3 shows simulated and tested results for Setting 1, Setting 2 and Setting 3, respectively. The results are obtained using similar initial pressures, input signal and filter constants. The deviation of results are quite similar for all three settings. In order for the pressures to stabilize at the same values, is the crack pressure of the CBV adjusted from 210 bar to 190 bar in the simulations. In general is it seen that the simulated cylinder velocity rises quicker than the tested, although they stabilizes at the same level. The reason for this might be a deviation in the filtrated pressure signal and the actual pressure in p_x for the test rig, see Figure 8.4. This may be improved by changing the controller gain (G) and integrator gain (Ti). The simulated pressure is created by other PI-controller parameters and an infinite fast PRV. Another improvement for the PI-controller on the test rig might be to improve the feedforward. One way of doing this could be to map the flow characteristics of the adjustable orifice with the desired adjustment, and use the pressure sensors to estimate the flow through the orifice by measuring the pressure drop. The estimated flow through the orifice could then be used to estimate a more exact value of the pressure drop across the PRV, instead of assuming 30 bar. This would lower the requirements of the PI-controller in the feedback loop. The physical control system got a lower limit of 15 bar. If the desired pressure of p_x is lower then 15 bar, is a desired value of 15 bar send to the control system. This is done in order to avoid wind up of the PI controller when the desired pressure is below the lowest pressure possible to design in the circuit. This function is not included in the simulation model, but are assumed to have a neglectable effect on the results, as a pressure in p_B below 15 bar only occurs for a very short moment initially in the simulations. Other

deviations shown from the figures are the oscillation frequency. The simulations are oscillating with a much higher frequency as compared to the test rig. The frequency could have been reduced by including valve and boom dynamics.
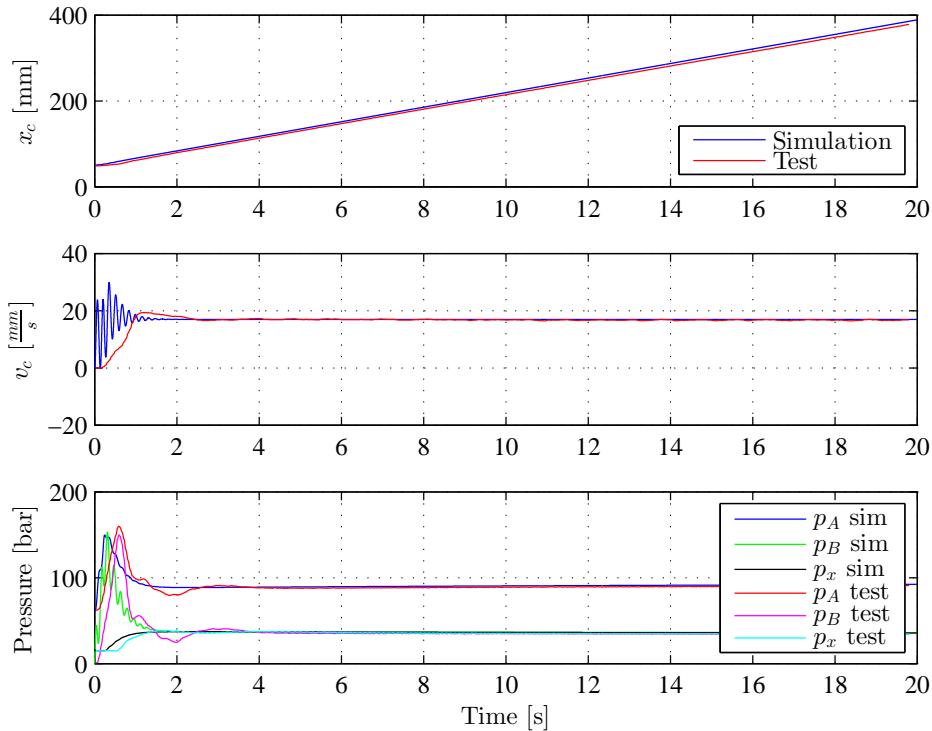
Figure 8.1: Test results vs Time domain simulation, Setting 1

8.5 Physical Testing

In all were four settings tested. The original system was included as Setting 0. One test was performed on this setting in order to investigate the instability of the system. For Setting 1, Setting 2 and Setting 3 were seven tests performed on each setting, and all tests showed that the stabilizing method stabilizes the system. First was each setting tested with a cutoff frequency that resulted in a stable system, and was further used as reference of comparison for other tests. The other tests includes tests with a lower and a higher break frequency, a higher load, an abrupt drop in the supply pressure and an abrupt increase of supply pressure, and user feedback tests where crane operators were asked to manually operate the test rig.

The test of Setting 0 showed heavily oscillations in the cylinder speed and pressure of chamber A and chamber B through the entire motion. The test showed no sign of reduction of oscillations through out the motion. Setting 1 is shown to be characterized by an overshoot in the cylinder velocity due to the high amount of energy in chamber A and chamber B before the CBV is opened. A higher load resulted in a lower cylinder velocity, and quick changes in the supply pressure resulted in small oscillations. The break frequency for the low pass filter is shown to have a great effect on the stability of the system, but have nearly no influence of response time. The response time is almost the same, as a high pressure in chamber A will force the CBV to open and the cylinder will start to move.

Setting 2 is characterized by small or no oscillations in the pressure of chamber A and chamber B, and the cylinder velocity, although a higher load resulted in a higher cylinder velocity and a change in supply pressure resulted in a small peak in velocity. The response time is highly dependent of the cutoff frequency, while the oscillations remains the same. The response time is depending on the cutoff frequency as the
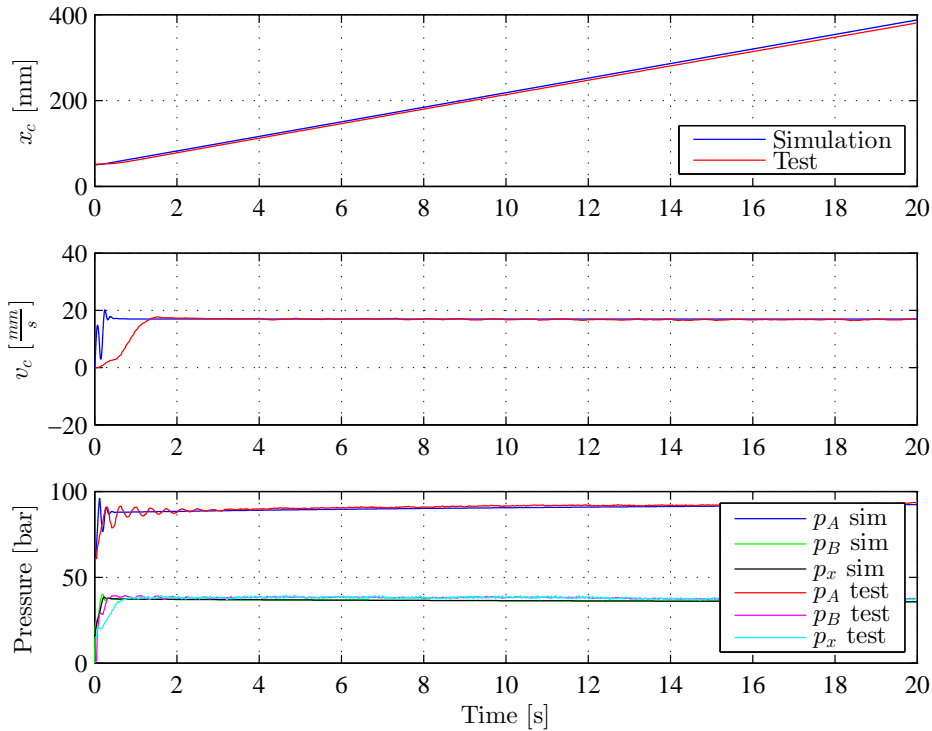
Figure 8.2: Test results vs Time domain simulation, Setting 2

opening of the FCV are directly dependent of the low pass filtrated pressure p_x. A slow pressure build up in p_x leads to a slow opening of the FCV, and a slow response of the system.

Setting 3 is a combination of Setting 1 and Setting 2 in structure and performance. Both the stability and response time are affected by the cutoff frequency. Setting 3 possesses all characteristics of Setting 1 and Setting 2, and the cutoff frequency must be chosen carefully.

In the seventh test was crane operators asked to manually operate the test rig and then be interviewed. Both interviewees claims Setting 1 to give the best performance, both in stability and response. One of the interviewees found the maximum velocity of Setting 2 and Setting 3 too high. This have nothing to do with the stability of the setting, but occurred as Setting 2 and Setting 3 are tested with a larger DCV, see C.

By studying the test results, Setting 2 seems to be the solution which have the highest potential. This setting has never pressures with high overshoot or which is highly oscillating. The cylinder velocity ramps up to a value and is then held relatively constant through out the entire motion. For the test where the load is increased does the velocity increase as compared to the reference test. This error could be compensated for by adding a velocity feedback. The low pass filtrated pressure p_x is not connected to the CBV in this setting and will therefore not affect its safety functions.

8.6 Respect the Unstable

Although the calculations and the test results shows that the system is stable, is it important to remember that the system initially were unstable, and that it is the control technique, the individually designed pressure, which makes the stable lowering possible. Dr. Gunter Stein points out in his Inaugural Bode Prize Lecture [3] and accompanying article [13] that systems with unstable components can only be locally stable, and that the reliability of such a system depends on the reliability of the components used in the control system and the control algorithm itself.
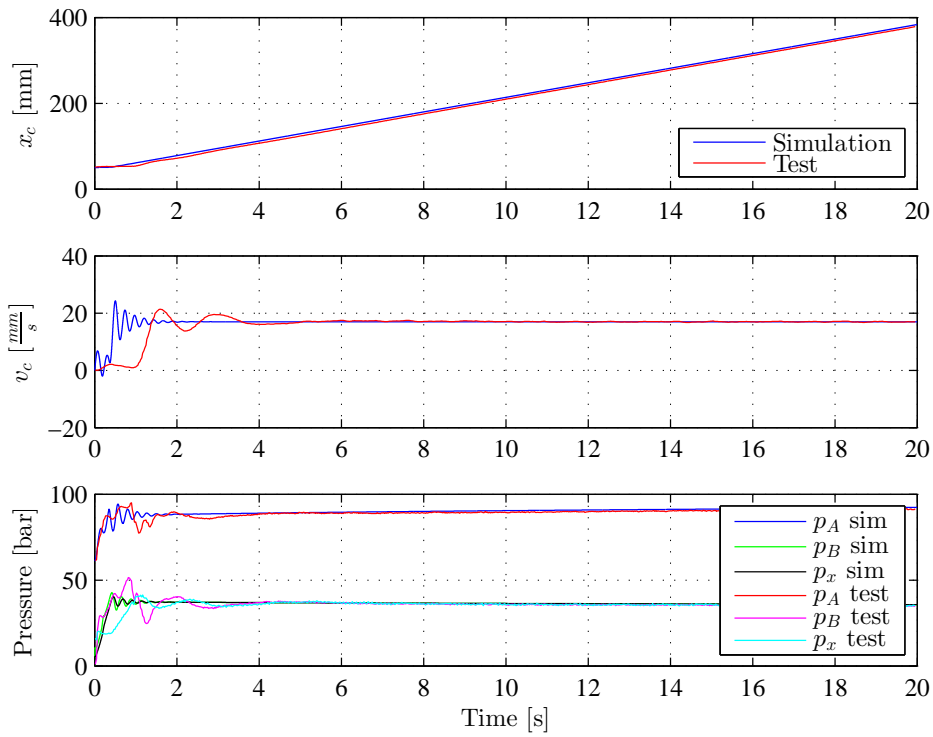
Figure 8.3: Test results vs Time domain simulation, Setting 3
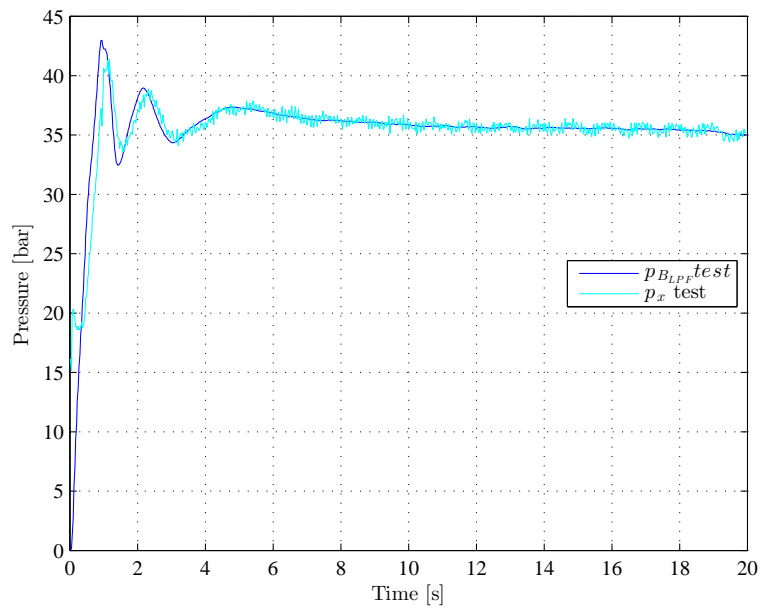
Figure 8.4: Comparison of desired p_x and actual p_x

Chapter 9

Conclusion and Further Work

Through this thesis is a novel method for stabilizing pressure compensated systems containing counterbalance valves investigated. The stabilization method is divided into three different settings, where the settings are different ways of applying the method. The settings are investigated by means of linearized stability analysis, time domain simulation and physical testing. All the settings are found to stabilize the system, and Setting 2 is found to have the greatest potential. This setting is found most stable by the physical testing and is considered the safest solution, as the counterbalance valve is unaffected by this solution.

It would have been of the authors greatest interest to also implement the solution to a system containing a hydraulic motor. A more in depth theoretical investigation of Setting 2 and Setting 3 would also have been interesting, as this may describe why the critical point of stability is moved, as compared to Setting 1. The theoretical investigation would have been possible if the line from the CBV is set directly to tank, and the FCV and the main spool is considered as one effective orifice. This would lead to a state space model of four states, and the stability investigation could have been performed analytically. It would also be interesting to implement one of the settings to an actual crane.

The authors are very satisfied with the results presented in this thesis. Based on the investigations done is it found likely that Setting 1 and Setting 2 can be implemented on to cranes with success.

Bibliography

[1] Counterbalance valves. http://apps.boschrexroth.com/products/compact-hydraulics/pib-catalogs/pdf/counterbalance.pdf.

[2] Danfoss PVG 32 Technical Information. `http://files.danfoss.com/documents/520l0344.pdf`. Accessed: 09.05.2015.

[3] Lecture: Respect the Unstable by Dr. Gunter Stein, 1989. `http://www.ieeecss-oll.org/lectures/1989/respect-unstable`. Accessed: 19.04.2015.

[4] MOBIL DTE 25. `http://www.mobil.com/Norway-English/Lubes/PDS/GLXXENINDMOMobil_DTE_20_Series.aspx`. Accessed: 13.05.2015.

[5] Proportional Pressure Relief Valve. `http://www.kanflu.com/assets/PDFs/PROPORTIONAL-RELIEF-VALVE-DBET-AND-DBETE-WITHOUT-OR-WITH-OBE-RE29162.pdf`. Accessed: 13.05.2015.

[6] Wikipedia article, Euler method. `http://en.wikipedia.org/wiki/Euler_method`. Accessed: 18.05.2015.

[7] Wikipedia article, FPGA. `http://en.wikipedia.org/wiki/Field-programmable_gate_array`. Accessed: 17.04.2015.

[8] Torben Ole Andersen. *Fluid Power Systems Modelling and Analysis*. Aalborg University, 2003.

[9] M. R. Hansen and T. O. Andersen. A design procedure for actuator control system using optimization methods. In *The 7th Scandinavian International Conference on Fluid Power*, Linköping, Sweden, 2001.

[10] M. R. Hansen and T. O. Andersen. Controlling a negative loaded hydraulic cylinder using pressure feedback. In *IASTED Internationak Conference Modelling, Identification and Control*, Innsbruck, Austria, 2010.

[11] M. B. Kjelland and M. R. Hansen. Numerical and experiential study of motion control using pressure feedback. In *The 13th Scandinavian International Conference on Fluid Power*, pages 337–343, Linköping, Sweden, 2013.

[12] M. K. Bak P. A. Nordhammer and M. R. Hansen. A method for reliable motion control of pressure compensated hydraulic actuation with counterbalance valves. In *12th Internationa Conference on Control, Automation and Systems*, pages 759–763, Jeju Island, Korea, 2012.

[13] G. Stein. Respect the unstable. In *IEEE Control Systems Magazine*, 2003.

List of Figures

List of Tables

Abbreviation list

CBV	Counterbalance calve
cRio	CompactRIO (where: RIO = Re-configurable IO Modules)
DCV	Directional control valve
FBD	Free body diagram
FCV	Flow control valve
FPGA	Field-programmable gate array
IVP	Initial value problem
KD	Kinetic diagram
LS	Load-sensing
MATLAB	Matrix laboratory
ODE	ordinary differential equation
PC	Personal computer
PRV	Pressure relief valve
SISO	Single-input single-output

Nomenclature List

Overscores

˙	First derivative with respect to time
¨	Second derivative with respect to time
˜	Linearized variable

Superscripts

(ss)	Steady state

Symbols

Symbol	SI	Description	Comment
A	m^2	Area	
a	$\frac{\text{m}}{\text{s}^2}$	Acceleration	-
$\mathbf{A}$	[-]	System matrix	-
$\mathbf{B}$	[-]	Input matrix	-
$\mathbf{C}$	[-]	Output matrix	-
C	$\frac{\text{m}^3}{\text{Pa}}$	Oil capacitance	$= \frac{V}{\beta}$
C_D	[-]	Discharge Coefficient, orifices equation	-
$\mathbf{D}$	[-]	Direct transmission matrix	-
D	[-]	Denominator	-
F	N	Force	-
G	[-]	Proportional gain	-
$G(s)$	[-]	Transfer function	-
g	$\frac{\text{m}}{\text{s}^2}$	Gravitational acceleration	-
I	kgm^2	Mass moment of inertia	-
K	[-]	Filter gain low pass filter	-
K_c	[-]	Propotional gain (academic PI controller)	-
k_v	$\frac{\text{m}^3}{\text{s}\cdot\sqrt{\text{Pa}}}$	Flow coefficient	-

Symbol	SI	Description	Comment
l	m	Length	-
m	kg	Mass	-
M	Nm	Moment	-
N	[-]	Numerator	-
p	Pa	Pressure	-
p_{cr}	Pa	Crack pressure	-
p_Δ	Pa	Desired pressure drop across main valve	-
r	m	Radius	-
s	$\frac{1}{s}$	Complex frequency variable	-
Ti	s	Integral time	-
T_i	s	Integral time (Academic PI controller)	-
Q	$\frac{m^3}{s}$	Volume flow	-
Q_{ref}	$\frac{m^3}{s}$	Reference volume flow	-
u	[-]	Rate of valve opening	-
$U(s)$	[-]	Output signal laplace domain	-
U	V	Voltage	-
V	m^3	Volume	-
v	$\frac{m}{s}$	Speed	-
x	m	Position	-
$Y(s)$	[-]	Input laplace domain	-
β	Pa	Bulk modulus	-
Δp	Pa	Pressure drop	-
Δp_{open}	Pa	Pressure needed to fully open a spring loaded valve	-
Δp_{ref}	Pa	Reference pressure drop	-
ρ	$\frac{kg}{m^3}$	Mass density	-
ρ_c	[-]	Piston area ratio	-
ρ_p	[-]	Pilot ratio, CBV	-
τ	$\frac{s}{rad}$	Time constant	-
$\theta, \ \phi, \ \gamma$	°	Angels	-
$\phi(s)$	[-]	State transmission matrix	$(I \cdot s - \mathbf{A})^{-1}$
ν	[-]	Input signal	-

Appendix A

List of Constants

Table A.1: Simulation constants

General			
g	9.80665	$\frac{\text{m}}{\text{s}^2}$	Acceleration of gravity
β	1.5	GPa	Bulk modulus
m	402	kg	Mass
I_A	4251.2	$\text{kg} \cdot \text{m}^2$	Mass moment of inertia
p_S	200	bar	Pump pressure
u_0	0.15	[-]	Rate of opening compensated DCV
Valves			
$Q_{ref_{main}}$	16	$\frac{\text{l}}{\text{min}}$	Reference volume flow main valve
$\Delta p_{ref_{main}}$	6	bar	Reference pressure drop main valve
$Q_{ref_{mainr}}$	50	$\frac{\text{l}}{\text{min}}$	Reference volume flow mainr
$\Delta p_{ref_{mainr}}$	7	bar	Reference pressure drop mainr
$Q_{ref_{FCV}}$	210	$\frac{\text{l}}{\text{min}}$	Reference volume flow FCV
$\Delta p_{ref_{FCV}}$	5	bar	Reference pressure drop FCV
p_Δ	6	bar	Desired pressure drop FCV
$\Delta p_{open_{FCV}}$	6	bar	Pressure needed to fully open the FCV
$Q_{ref_{CBV}}$	60	$\frac{\text{l}}{\text{min}}$	Reference volume flow CBV
$\Delta p_{ref_{CBV}}$	16	bar	Reference pressure drop CBV
$p_{cr_{CBV}}$	210	bar	Crack pressure CBV
$\Delta p_{open_{CBV}}$	400	bar	Pressure needed to fully open the CBV
ρ_p	3	[-]	Pilot ratio
$Q_{ref_{PRV}}$	2	$\frac{\text{l}}{\text{min}}$	Reference volume flow PRV
$\Delta p_{ref_{PRV}}$	5.75	bar	Reference pressure drop PRV
$\Delta p_{open_{PRV}}$	280	bar	Pressure needed to fully open the PRV
$Q_{ref_{AO}}$	2	$\frac{\text{l}}{\text{min}}$	Reference volume flow adjustable orifice
$\Delta p_{ref_{AO}}$	200	bar	Reference pressure drop adjustable orifice
Cylinder			
d_p	65	mm	Piston diameter
d_r	35	mm	Rod diameter
Lengths			
l_{ABx}	0.42	m	Length between point A and ponit B in local x-direction
l_{ABy}	1.055	m	Length between point A and ponit B in local y-direction
l_{ACx}	0.55	m	Length between point A and ponit C in local x-direction
l_{ACy}	0.13	m	Length between point A and ponit C in local y-direction
l_{AGx}	3.139	m	Length between point A and center of mass in local x-direction
l_{AGy}	0.064	m	Length between point A and center of mass in local y-direction
Volumes			
V_{A0}	0.2	l	Dead volume chamber A including tubes and hoses
V_{B0}	0.25	l	Dead volume chamber B including tubes and hoses
V_{C0}	$1.0 \cdot 10^{-4}$	l	Internal volume in compensated DCV, between FCV and main valve
V_0	0.1	l	Volume between CBV and mainr
V_X	0.1	l	Volume between variable orifice and PRV

Table A.2: Calculated simulation constants

Valves				
$k_{v_{main}}$	$\frac{Q_{ref_{DCV}}}{p_{ref_{DCV}}}$	$3.44 \cdot 10^{-7}$	$\frac{\text{m}^3}{\text{s}\cdot\text{Pa}}$	Flow coefficient main
kv_{mainr}	$\frac{Q_{ref_{DCVr}}}{p_{ref_{DCVr}}}$	$9.96 \cdot 10^{-7}$	$\frac{\text{m}^3}{\text{s}\cdot\text{Pa}}$	Flow coefficient mainr
kv_{FCV}	$\frac{Q_{ref_{FCV}}}{p_{ref_{FCV}}}$	$4.95 \cdot 10^{-7}$	$\frac{\text{m}^3}{\text{s}\cdot\text{Pa}}$	Flow coefficient FCV
kv_{CBV}	$\frac{Q_{ref_{CBV}}}{p_{ref_{CBV}}}$	$7.906 \cdot 10^{-7}$	$\frac{\text{m}^3}{\text{s}\cdot\text{Pa}}$	Flow coefficient CBV
kv_{PRV}	$\frac{Q_{ref_{PRV}}}{p_{ref_{PRV}}}$	$4.4 \cdot 10^{-8}$	$\frac{\text{m}^3}{\text{s}\cdot\text{Pa}}$	Flow coefficient CBV
kv_{AO}	$\frac{Q_{ref_{AO}}}{p_{ref_{AO}}}$	$7.45 \cdot 10^{-9}$	$\frac{\text{m}^3}{\text{s}\cdot\text{Pa}}$	Flow coefficient adjustable orifices
Cylinder				
A_A	$\frac{\pi \cdot d_p{}^2}{4}$	0.0033	m^2	Piston area in chamber A
A_B	$\frac{\pi \cdot (d_p{}^2 - d_r{}^2)}{4}$	0.0024	m^2	Piston area chamber B
Lengths				
l_{AB}	$\sqrt{l_{ABx}{}^2 + l_{ABy}{}^2}$	1.136	m	Length between point A and point B
l_{AC}	$\sqrt{l_{ACx}{}^2 + l_{ACy}{}^2}$	0.565	m	Length between point A and point C
l_{AG}	$\sqrt{l_{AGx}{}^2 + l_{AGy}{}^2}$	3.126	m	Length between point A and center of gravity
Angles				
α_0	$\tan^{-1}\left(\frac{l_{ACy}}{l_{ACx}}\right)$	13.3	°	See Figure 3.8
α_1	$\tan^{-1}\left(\frac{l_{AGy}}{l_{AGx}}\right)$	1.2	°	See Figure 3.8
α_2	$\tan^{-1}\left(\frac{l_{ABy}}{l_{ABx}}\right)$	68.3	°	See Figure 3.8

Appendix B

Simplified Data Sheets

B.1 Proportional Directional Spool Valve

Manufacturer	Hawe Hydraulik
Type	Proportional directional spool valve
Series	PSV
Original Sheet	D 7700-2

Model code:

PSV 3 . 1 . /D250 - 2

        - A 1 L 25/16 /EA WA /2 AN265 BN265

        - A 2 L 25/16 A200 B200 S1 /EA WA /2 AN265 BN265

        - A 2 O 25/16 A200 B200 S1 /EA WA /2 AN265 BN265

                                                - E 1 - G 24

Size	2
Flow for Outlet A / B	25/16 l/min
Control pressure	Approx. 6 bar
Power supply	12V DC
Control current ratio I/I_N	min. approx. 0.2 max. approx. 1
Viscosity Range	$4\,\mathrm{mm}^2/\mathrm{s}$ to $1500\,\mathrm{mm}^2/\mathrm{s}$
Preferable Viscosity	$10\,\mathrm{mm}^2/\mathrm{s}$ to $500\,\mathrm{mm}^2/\mathrm{s}$
Ambient Temperature	$-40°C$ to $+80°C$
Oil Temperature	$-25°C$ to $+80°C$
Max. Pressure	420 bar

Key words

- Internal inflow controller

- Load-Sensing principle

- Pressure limiting valve factory set to 250 bar

- Integrated pressure reducing valve

- Electro-hydraulic and manual actuated

- Integrated travel indicator via a Hall-sensor
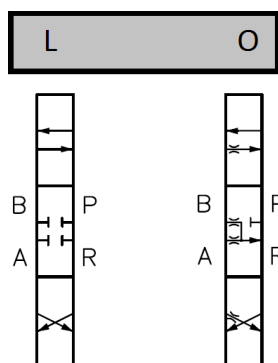
- External control oil return to the tank

Figure B.1: Coding for flow pattern

Diagram for the inflow controller, spool stroke characteristics and position sensor characteristics are to be found on next page.
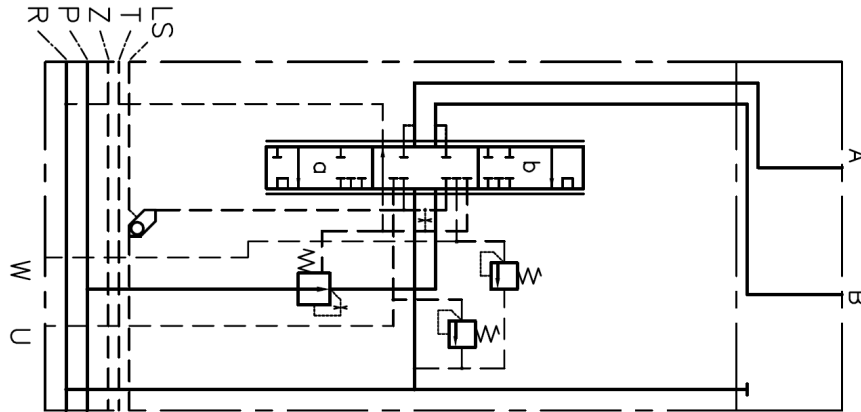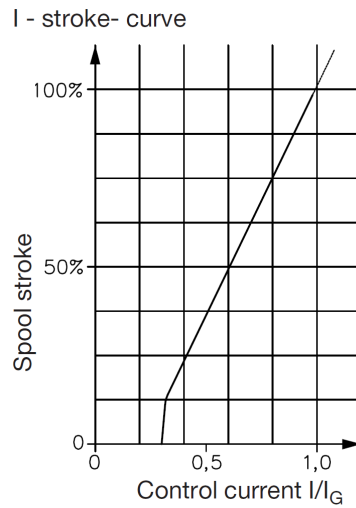
Figure B.2: Diagram for inflow controller

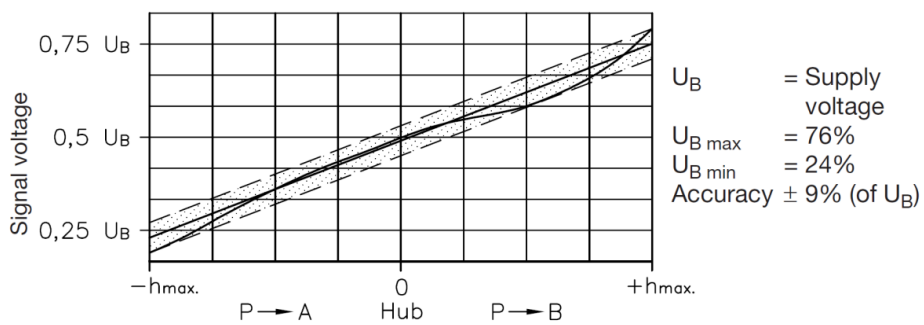Figure B.3: Spool stroke characteristics with respect to control current

Figure B.4: Position sensor signal characteristics with respect to spool stroke

B.2 Counterbalance Valve, 4-port vented

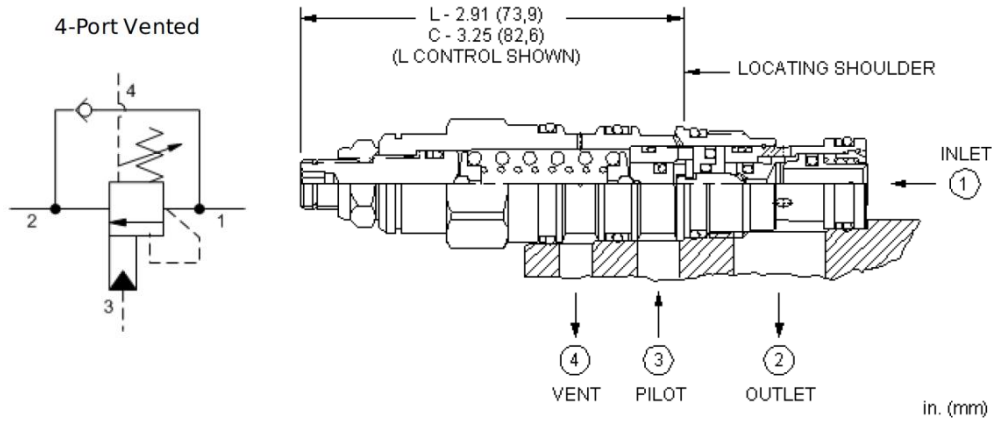|	
Manufacturer	Sun Hydraulics
Model Code	CWCA-LHN
Original Sheet	CWCA
Capacity	60 l/min
Pilot Ratio	3 : 1
Setting Range	70 - 280 bar
Standard Setting	210 bar
Cavity	T-21A
Maximum Setting	280 bar
Maximum Recommended Load Pressure at max. Setting	215 bar
Maximum Valve Leakage at Reseat	0.3 cc/min
Manifold	MAV/S
Check Crack Pressure	2.8 bar
Model Weight	0.19 kg

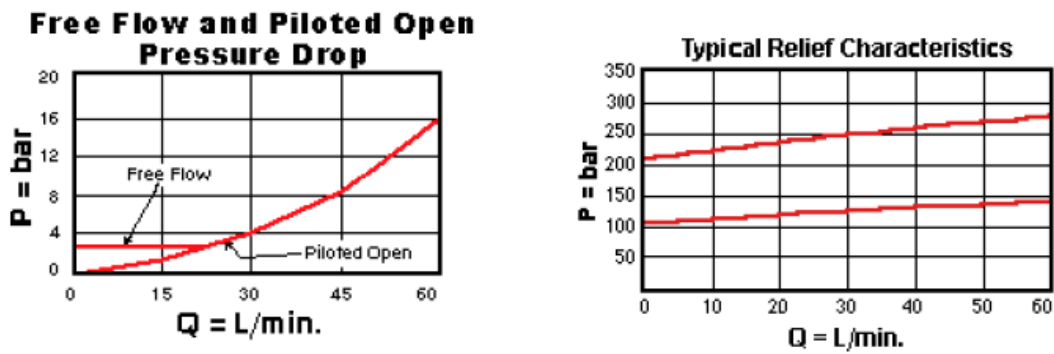Figure B.5: Symbol and illustration of a 4-port vented CBV

Figure B.6: Performance curves

B.3 Hydraulic Cylinder 25 CA

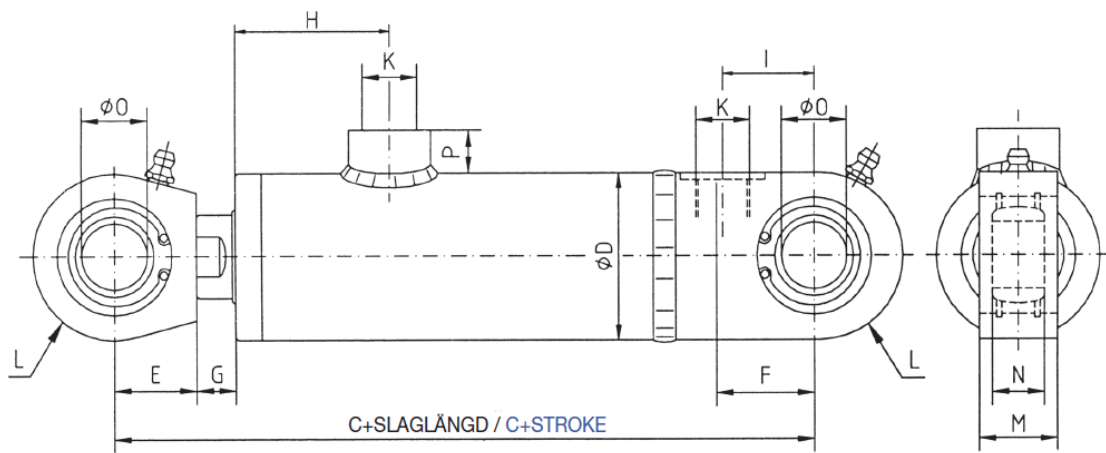|	
Manufacturer	PMC Cylinders
Model Code	25CAL-65/35-0500/85
Original sheet	25CA_Broschyr_20_sid
Stroke	500 mm
Piston rod diameter	35 mm
Cylinder diameter	65 mm
Max working pressure	200 bar
Maximum velocity	0.5 m/s
Temperature range	$-30°C$ to $+80°C$
Push Area	33.1 cm^2
Pull Area	23.6 cm^2
Weight 0 stroke / 100 mm	5.6/1.6

Figure B.7: Cylinder dimensions

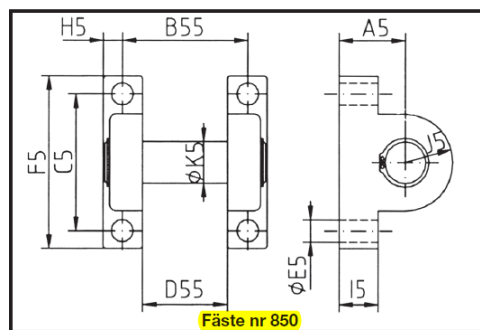| C	D	E	F	G	H	I	K	L	M	N	O	P
272	75	35	40	15	54	32	$G1/2$"	35	30 ± 0.5	20	25	18

Figure B.8: Attachment dimensions

Ø Cyl	A5	B55	B56	C5	D55	D56	E5	F5	G5	H5	I5	J5	K5
65	38	62	132	88	40	110	13	110	106	11	25	28	25

B.4   Proportional Pressure Relief Valve

General

Manufacturer	Bosch Rexroth AG
Model Code	DBETE-61/315G24K31A1V
Original Sheet	RE 29162/07.08
Type	DBETE
Max Pressure Rating	315 bar
Internal Pilot Oil Drain	Yes
Supply Voltage	24 V DC
Command Value	0 V to 10 V
Weight	2.15 kg
Storage Temperature Range	$-20°C$ to $+80°C$
Ambient Temperature Range	$-20°C$ to $+50°C$

Symbol

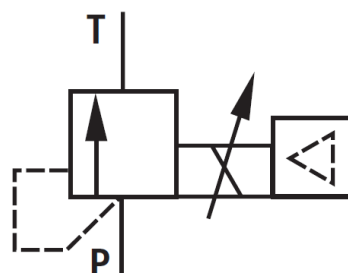Figure B.9: Proportional PRV with integrated electronics (type DBETE) and internal pilot oil drain

Hydraulic

Maximum Flow	2 l/min
Hydraulic Fluid	Mineral oil (HL, HLP) to DIN 51524
Hydraulic Fluid Temperature Range	$-20°C$ to $+80°C$
Viscosity Range	$20\,\text{mm}^2/\text{s}$ to $380\,\text{mm}^2/\text{s}$
Preferable Viscosity	$30\,\text{mm}^2/\text{s}$ to $46\,\text{mm}^2/\text{s}$
Hysteresis	$< 4\%$ of set max. pressure
Range of inversion	$< 0.5\%$ of set max. pressure
Response sensitivity	$< 0.5\%$ of set max. pressure
Linearity (flow 0.8 l/min)	$\pm 3\%$ of set max. pressure

Characteristic curves are to be found on next page.

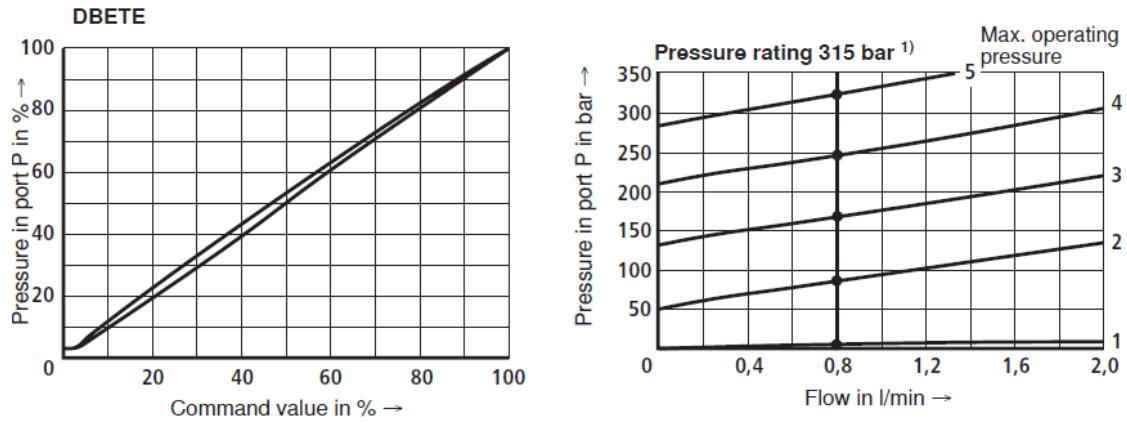**Pressure in port P in dependence on command value** (flow = 0.8 l/min)

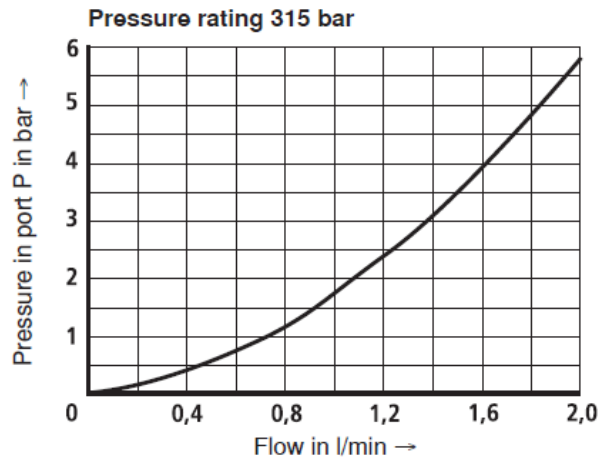Figure B.10: Pressure in port P in dependence on command value or flow

Figure B.11: Min. set pressure in port P at command value 0 V or 4 mA in dependence on flow

B.5   Flow Control Valve

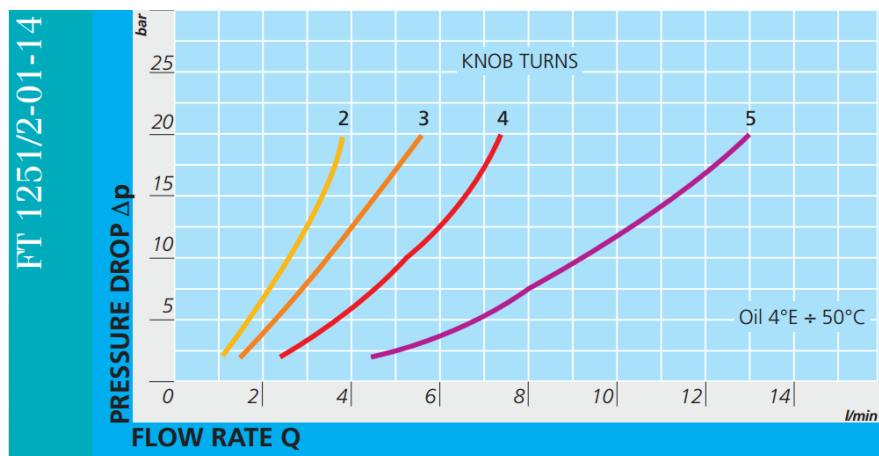|	
Manufacturer	Tognella
Type	Flow control
Series	FT
Model Code	FT 1251/2-01-14
Original Sheet	FT 1251/2-01
Max. Working Pressure	210 bar
Working Temperature	$-20°C$ to $+100°C$
Flow SQ mm^2	12.57
Filtration Grade	25 μm

Figure B.12: Flow control vale symbol

Figure B.13: Pressure drop curve

B.6 Ball Valve

Manufacturer	Pister
Type	Ball Valve
Series	BKH
Model Code	BKHG1/4 06 1113 0 PN500
Original Sheet	PISTER Ball Valves
Working Temperature	$-10°C$ to $+100°C$
Connection	G 1/4 BSP Female

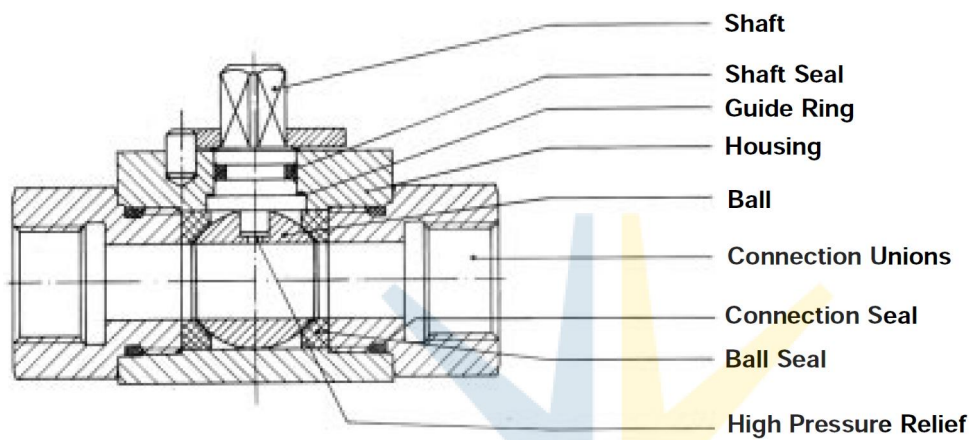|	
Body	Steel
Ball	Steel nickel pl.
Stem	Steel zinc pl.
Ball sealing	Polyamide
Steam sealing	NBR

Figure B.14: Ball valve physical construction

B.7 Pressure Sensor

Manufacturer	Parker
Type	Pressure Sensor
Series	SCP01
Model Code	SCP01-400-44-07
Original Sheet	4083-3/UK

Pressure Range	0 - 400 bar
Response Time	≤ 1 ms
Load Change	> 20 million
Weight	Approx. 80 g
MTTfd	> 100 years
Housing Material	Stainless Steel 1.4404
Output Signal	0 to 10 V

Accuracy	Type $\leq \pm 0.25\%$FS
	Max. $\leq \pm 0.5\%$FS

Total Error at 0 to $85°C$	$\leq 1\%$FS

Ambient Temperature Range	$-40°C$ to $+85°C$
Fluid Temperature Range	$-40°C$ to $+125°C$
Storage Temperature Range	$-40°C$ to $+125°C$
Vibration Resistance	IEC 60068-2-6: 20 g
Shock Resistance	IEC 60068-2-27: 500 g

Eroding Milling	0.6 mm
Tightening Toque	Max 35 Nm

PIN

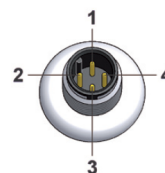|	
1	V_+
2	P signal
3	0 V / GND
4	Not connected

Figure B.15: Circular connector M12x1 4-pole

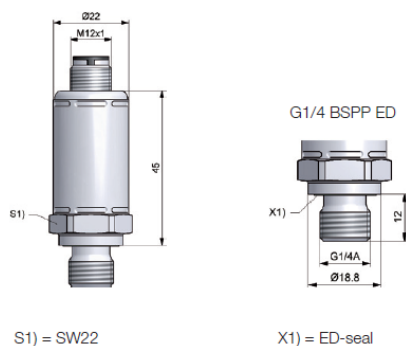
Figure B.16: Pressure sensor dimension drawing

B.8 Flow sensor

Manufacturer	Parker
Type	Flow Sensor
Series	SCQ
Model Code	SCQ-150-10-07
Original Sheet	4083-3/UK

Measurement Range, Q_N	-150 to +150 l/min
Max Flow, Q_{max}	-165 to +165 l/min
Weight	Approx. 1050 g
Tightening Torque	30 Nm

Response Time	≤ 2 ms
Characteristic Curve Deviation	$\pm 2\%$ FS @ 46cSt.
Thermal Drift	$\pm 0.05\%$ FS/$^{\circ}C$
Repeat Accuracy	$\pm 0.5\%$ FS

Pressure Range	3 to 420 bar
Working Pressure, P_N	315 bar
Overload Pressure, P_{max}	420 bar

Working Temperature Range	$+10^{\circ}C$ to $+60^{\circ}C$
Storage Temperature Range	$-20^{\circ}C$ to $+80^{\circ}C$
Max Temperature Fluid, T_{max}	$+80^{\circ}C$
Filtration	25 μm
Viscosity Range	15 to 100 cSt.
Protection Class	IP67 DIN EN 60529

Plug-in Connector	M12x1; 4-pole
Supply Voltage	+18 to +30 VDC
Current Consumption	40 mA
Output	0 to 20 mA = -FS to +FS (10 mA = 0 l/min)
Working Resistance	$\leq 150 \ \Omega$
Signal Noise	< 5 mV

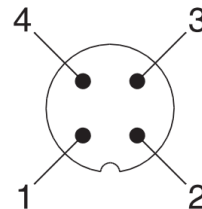| **PIN**	
1	V_+
2	Q signal
3	0 V / GND
4	Not connected

Figure B.17: Circular connector M12x1 4-pole

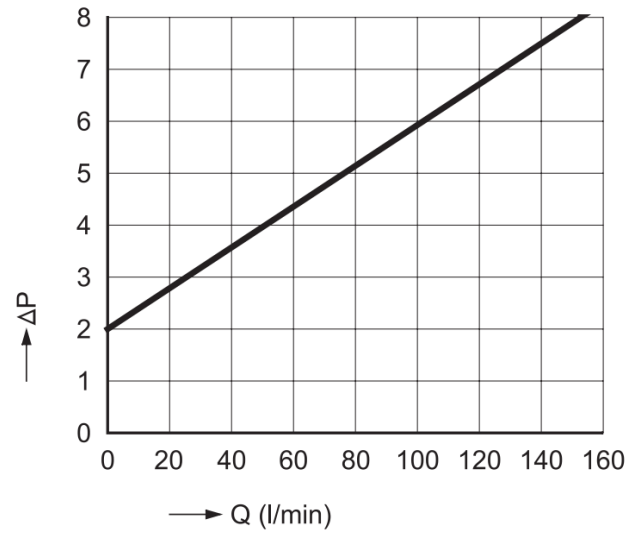**Pressure drop characteristics and dimensions are to be found on next page.**
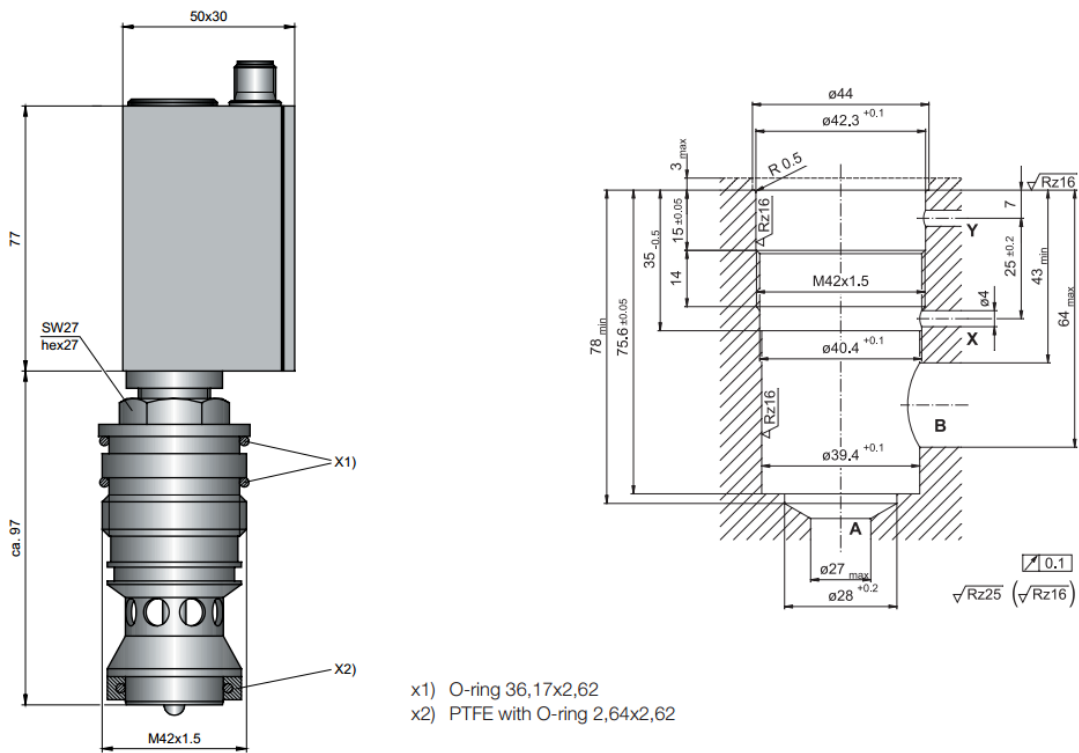
Figure B.18: Flow sensor pressure drop

x1) O-ring 36,17x2,62
x2) PTFE with O-ring 2,64x2,62

Figure B.19: Flow sensor dimensions

B.9 Cylinder Position Sensor

Manufacturer	Regal
Type	Potentiometer
Series	PS6300
Model Code	PS6310
Original Sheet	PS6300

Supply Voltage	Recommended	10 V_{DC}
	Maximum	40 V_{DC}
Independent Linearity	± 0.4 mm	
Repeatably	$< \pm 0.013$ mm	
Resolution	Unlimited	
Operating Speed	< 2 m/s	
Temperature	$-40^\circ C$ to $+125^\circ C$	
Working Pressure	350 bar	
Life Time	< 100 million movements	
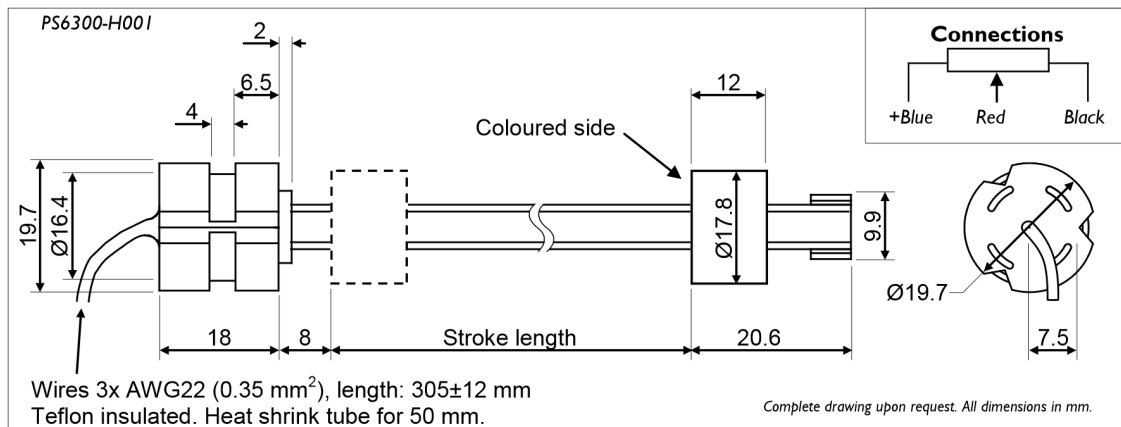
Figure B.20: Potentiometer dimensions

B.10 Digital Module Amplifier

Manufacturer	HCS
Type	Universal Digital Module Amplifier
Series	DMA-22-05
Model Code	DMA-22-05-050-x-SHPR5C
Original Sheet	R02

Keywords

- For one valve with feedback or process value feedback

- Adaptation possible to all kinds of Hawe proportional valves (series PSL/PSV)

- Optimized for current range of existing twin solenoids and feedback signals

- Full digital PI current controller

- Full digital multifunctional controller for valve or process control systems

Appendix C

DCV Modifications for Setting 2 and Setting 3

When setting 2 or setting 3 is used is the pressure from the external pressure circuit assigned to the pressure compensated DCV. Testing of the Hawe DCV, described in Section 3.3.2, revealed an internal connection between the outlet of the DCV and the external load sensing (LS) pressure. This internal connection is needed for the pressure compensation to work when no external LS pressure is applied. In order for setting 2 and setting 3 to function properly must only the externally applied pressure affect the pressure compensator. As no pressure compensated DCV with this feature was available during the testing was an available DCV modified. The modification performed is shown in Figure C.1 where a) shows a diagram of the modified DCV including the internal compensator and b) shows the modified main spool.

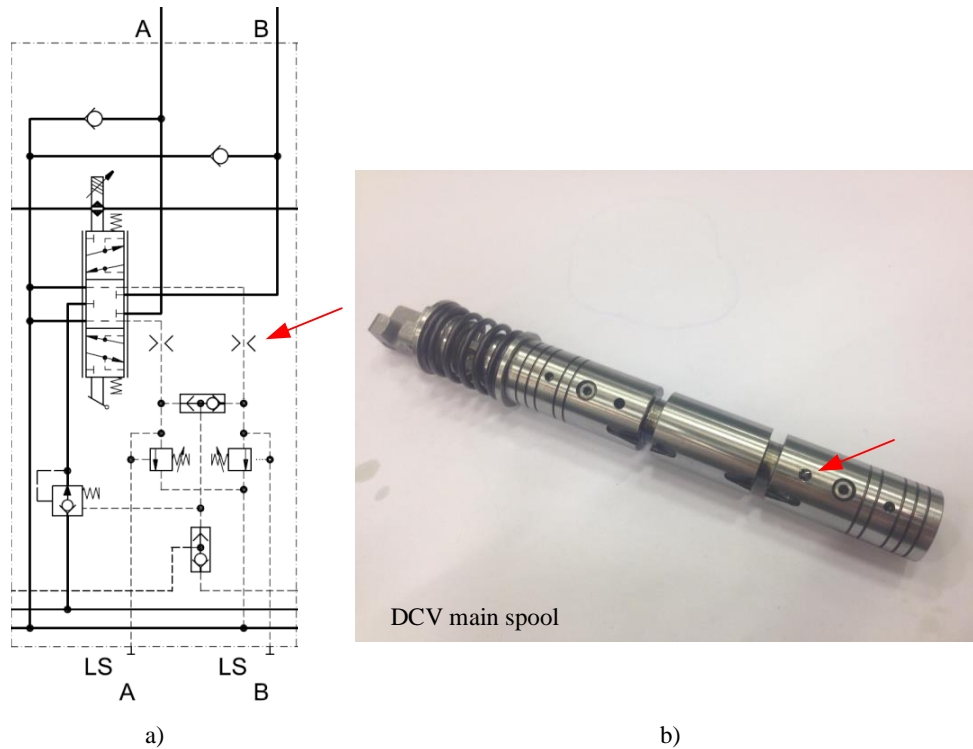a)   b)

Figure C.1: a) Diagram of the DCV and the internal compensator [2] b) The DCV main spool

The DCV which is modified is a pressure compensated DCV called PVG 32 delivered by Danfoss, technical information available at [2]. Also this DCV had the internal connection. Removing this connection meant blocking the orifice pointed out by the red arrow in Figure C.1. The main difference between the Hawe DCV and the Danfoss DCV is the size. The PVG can deliver a slightly higher flow as compared to the Hawe DCV. The rated opening of the valve, u_0, presented in the results will therefore vary according to which DCV that is used for the test.

Appendix D

Results From Further Physical Testing

D.1 Setting 1

In this section are results from test 2, test 3, test 4, test 5 and test 6 for Setting 1 presented.

D.1.1 Test 2: High Cutoff Frequency

In this test is the cutoff frequency chosen to $f_c = 0.3$. This is expected to be to high cut off frequency, meaning that the filter will not completely remove the oscillations and thereby send an oscillating pressure to the pilot line of the CBV. Further conditions of this test are listed in Table D.1.

Table D.1: Parameters for the test of setting 1 with a high cutoff frequency

Test parameter	Value	Unit
Supply pressure	198	bar
Tank pressure	0	bar
Oil temperature	37	$^\circ C$
Total motion time	20.02	s
Rise time	0.01	s
Retardation time	0.01	s
Cutoff frequency, f_c	0.3	Hz
Time constant, τ	0.531	$\frac{s}{rad}$
u_0 (Hawe)	0.15	-

Results and Discussion

The results from the test are shown in Figure D.1. This figure presents the pressure in chamber A (p_A), the pressure in chamber B (p_B), the low pass filtered pressure (p_X), the cylinder contraction (x_c), and the cylinder contraction speed (v_c) during the testing.
Test characteristics:

Typical contraction velocity: Oscillatory at about $16.5 \frac{mm}{s}$

Overshoot: A high velocity peak in the start of the motion

Settling: The velocity and pressures oscillates throughout the motion

The test shows that a higher cutoff frequency results in a more oscillatory motion for setting 1. The start up peak pressure in chamber A and chamber B are lower as compared to the comparison test but the pressures never settles.
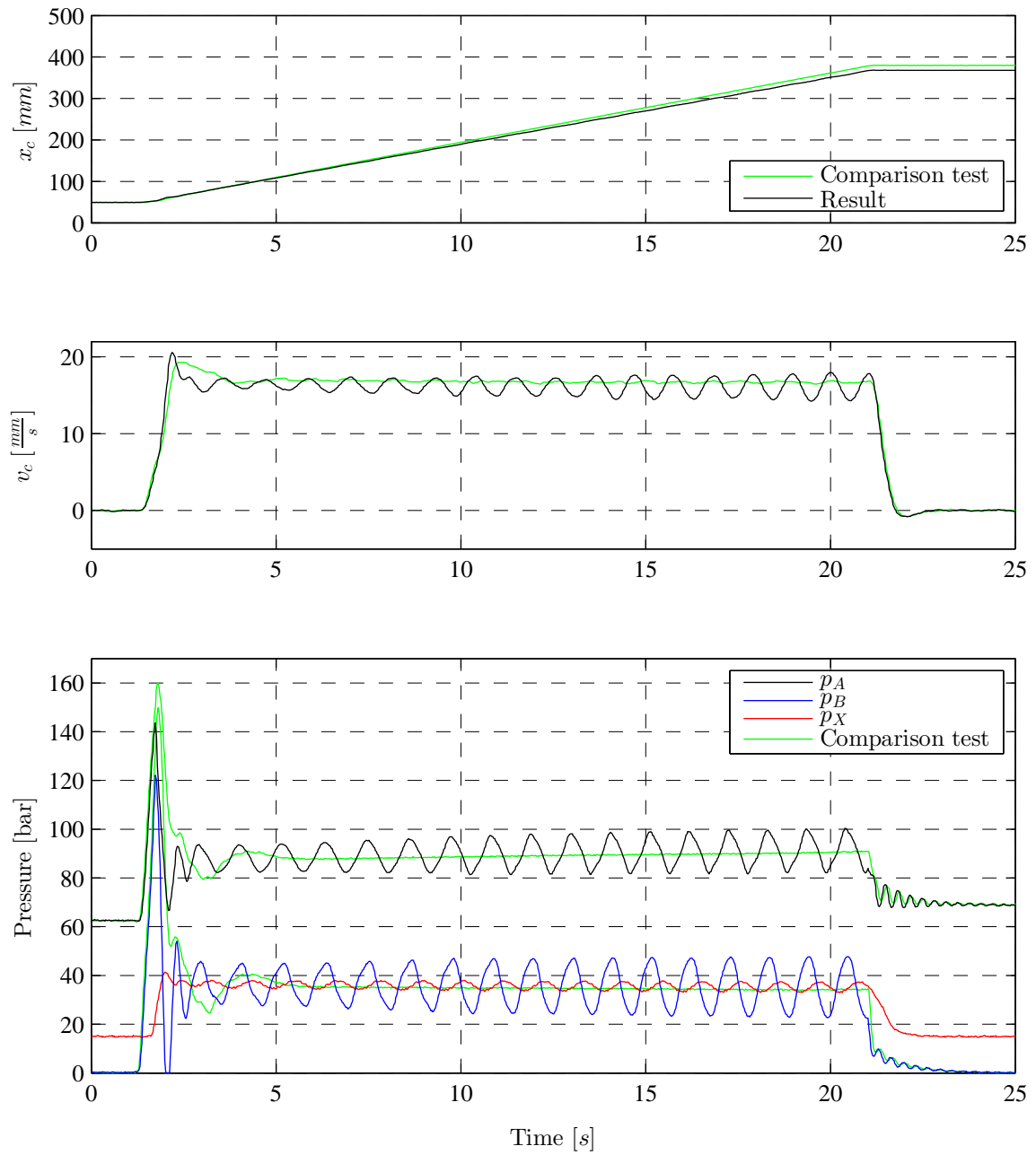
Figure D.1: Test 2 Setting 1

147

D.1.2 Test 3: Low Cutoff Frequency

In this test is the cutoff frequency chosen to $f_c = 0.01$. This is expected to be to low, meaning that the filter will not only remove the oscillations but also slow down pressure changes resulting in a stable but slow pilot pressure. Further conditions of this test are listed in Table D.2.

Table D.2: Parameters for the test of setting 1 with a low cutoff frequency

Test parameter	Value	Unit
Supply pressure	198	bar
Tank pressure	0	bar
Oil temperature	39	$^\circ C$
Total motion time	20.02	s
Rise time	0.01	s
Retardation time	0.01	s
Cutoff frequency, f_c	0.01	Hz
Time constant, τ	15.92	$\frac{\text{s}}{\text{rad}}$
u_0 (Hawe)	0.15	-

Results and Discussion

The results from the test are shown in Figure D.2. This figure presents the pressure in chamber A (p_A), the pressure in chamber B (p_B), the low pass filtered pressure (p_X), the cylinder contraction (x_c), and the cylinder contraction speed (v_c) during the testing.
Test characteristics:

Typical contraction velocity: About 17 $\frac{\text{mm}}{\text{s}}$

Overshoot: None

Settling: The velocity rises slow and stable

This test shows that a low cutoff frequency for setting 1 results in a slow pilot pressure for the CBV. This means that the CBV will open slowly but steady. The start up is slow but stable, and the motion is very stable.
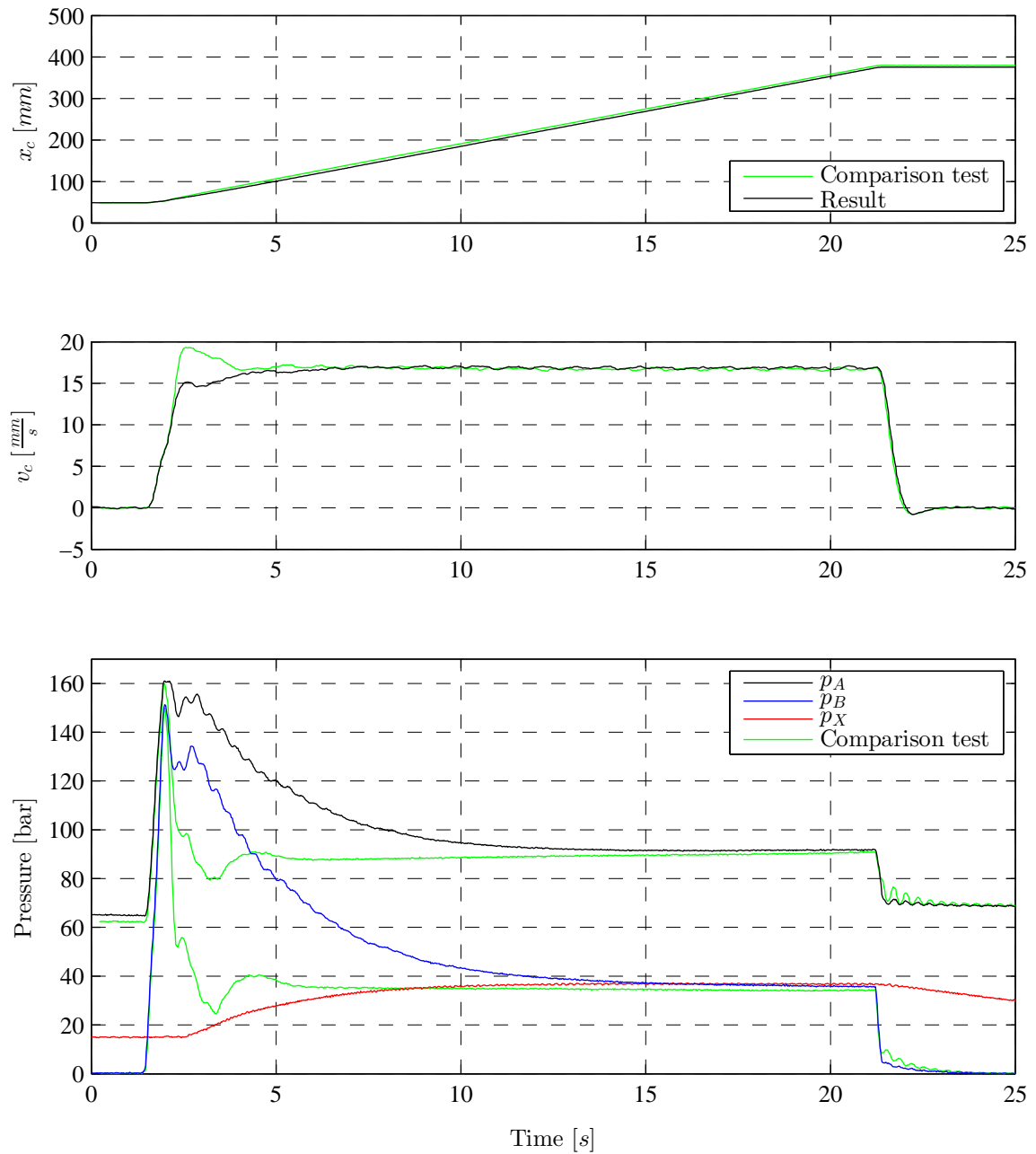
Figure D.2: Test 3 Setting 1

D.1.3 Test 4: Increased in Load

In this test is 77 kg added to the ballast stack to increase the load. The cutoff frequency is the same as in Chapter 7. Some higher system pressures are expected, but the system behavior through out the motion is expected to be stable. Further conditions of this test are listed in Table D.3.

Table D.3: Parameters for the test of setting 1 with a higher load

Test parameter	Value	Unit
Supply pressure	199	bar
Tank pressure	0	bar
Oil temperature	38	$^\circ C$
Total motion time	20.02	s
Rise time	0.01	s
Retardation time	0.01	s
Cutoff frequency, f_c	0.1	Hz
Time constant, τ	1.592	$\frac{\text{s}}{\text{rad}}$
u_0 (Hawe)	0.15	-

Results and Discussion

The results from the test are shown in Figure D.3. This figure presents the pressure in chamber A (p_A), the pressure in chamber B (p_B), the low pass filtered pressure (p_X), the cylinder contraction (x_c), and the cylinder contraction speed (v_c) during the testing.
Test characteristics:

Typical contraction velocity: 15.6 $\frac{\text{mm}}{\text{s}}$

Overshoot: A peak in the start motion

Settling: A velocity peak in the start which settles after some seconds

This test shows that a heavier load results in a slower cylinder contraction. The pressure in chamber A is higher for this load as compared to the comparison test. This is due to the heavier load.
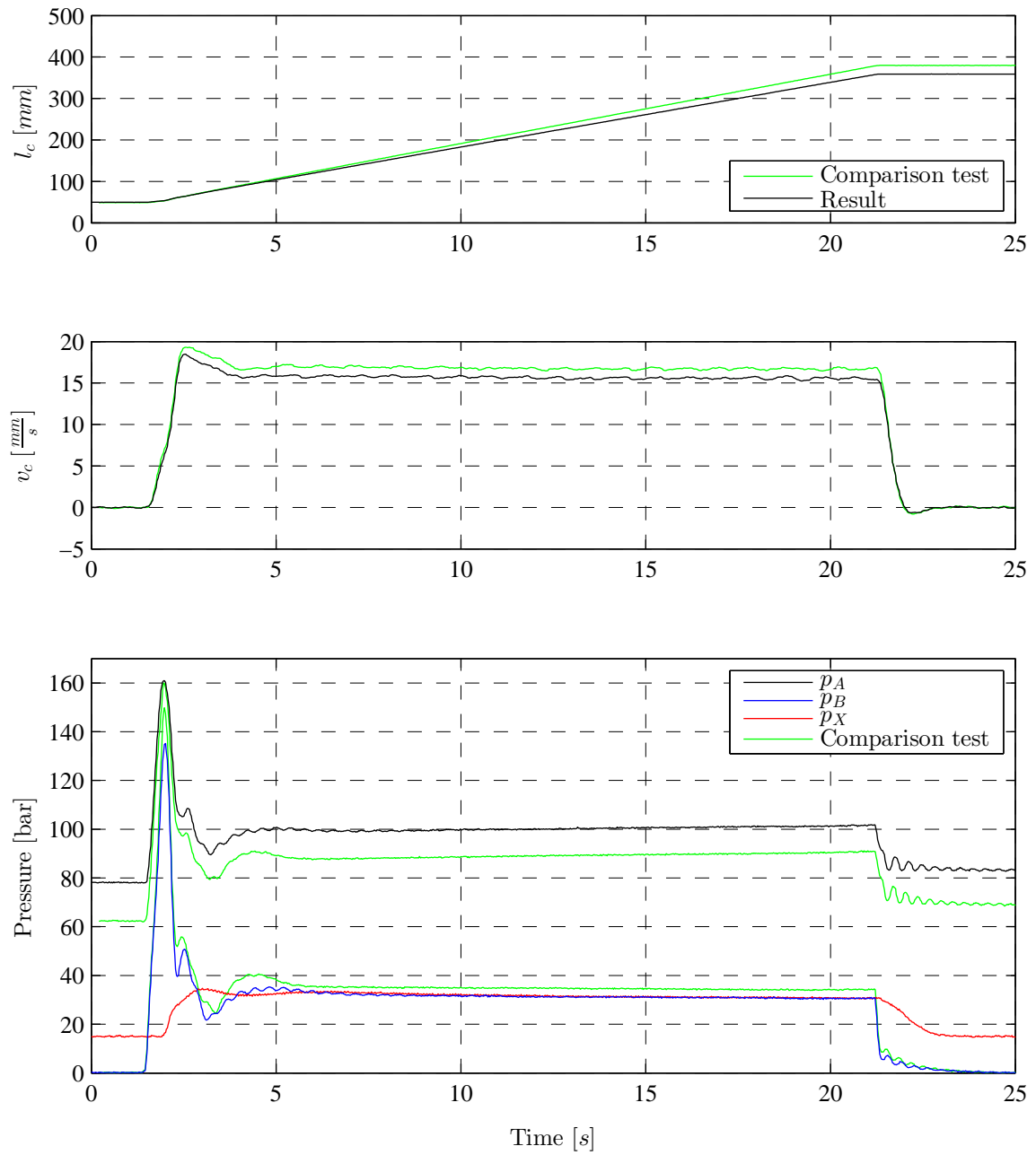
Figure D.3: Test 4 Setting 1

D.1.4 Test 5: Drop in Supply Pressure

In this test is the supply pressure quickly reduced from 200 bar to 150 bar during the motion. This test is carried out in order to map how this affects the stability of the lowering. Further conditions of this test are listed in Table D.4.

Table D.4: Parameters for the test of setting 1 with the supply pressure changed form 200 bar to 150 bar

Test parameter	Value	Unit
Supply pressure	$200 - 150$	bar
Tank pressure	0	bar
Oil temperature	40	$^{\circ}C$
Total motion time	20.02	s
Rise time	0.01	s
Retardation time	0.01	s
Cutoff frequency, f_c	0.1	Hz
Time constant, τ	1.591	$\frac{\text{s}}{\text{rad}}$
u_0 (Hawe)	0.15	-

Results and Discussion

The results from the test are shown in Figure D.4. This figure presents the pressure in chamber A (p_A), the pressure in chamber B (p_B), the low pass filtered pressure (p_X), the cylinder contraction (x_c), and the cylinder contraction speed (v_c) during the testing.
Test characteristics:

Typical contraction velocity: About 16.5 $\frac{\text{mm}}{\text{s}}$ at 200 bar and about 15.5 $\frac{\text{mm}}{\text{s}}$ at 150 bar

Overshoot: The pressure change results in a quick reduction in the contraction velocity for a short period

Settling: Uses about 3 seconds to settle after the pressure change

This test shows that setting 1 is affected by a drop in the supply pressure. The motion is oscillatory for a short period of time after the change and the lower supply pressure slows the motion.
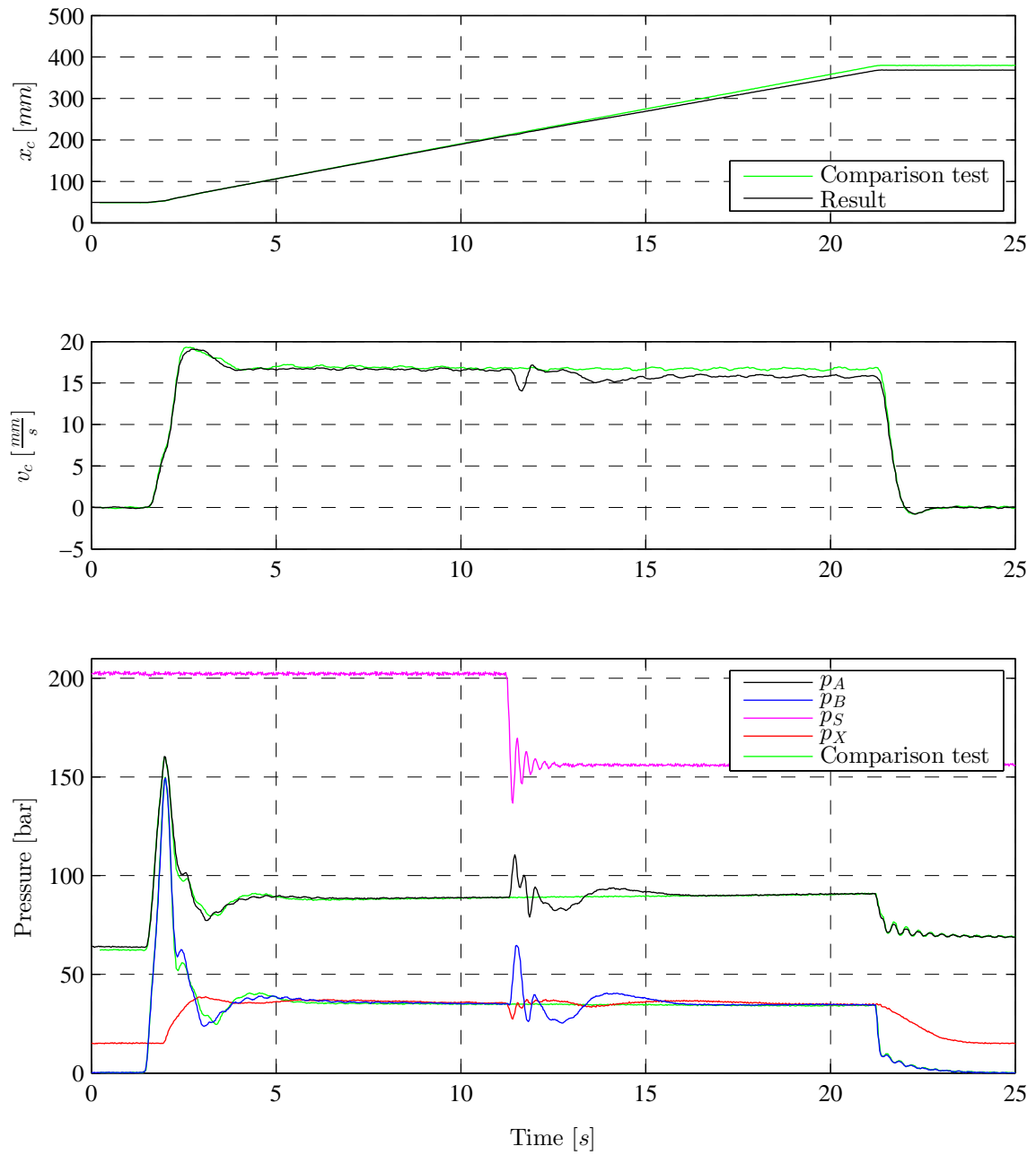
Figure D.4: Test 5 Setting 1

153

D.1.5 Test 6: Quick Increase of Supply Pressure

In this test is the supply pressure quickly increased from 150 bar to 200 bar during the motion. This test is carried out in order to map how this affects the stability of the lowering. Further conditions of this test are listed in Table D.5.

Table D.5: Parameters for the test of setting 1 with the supply pressure changed form 150 bar to 200 bar

Test parameter	Value	Unit
Supply pressure	$150 - 200$	bar
Tank pressure	0	bar
Oil temperature	40	$^{\circ}C$
Total motion time	20.02	s
Rise time	0.01	s
Retardation time	0.01	s
Cutoff frequency, f_c	0.1	Hz
Time constant, τ	1.591	$\frac{\text{s}}{\text{rad}}$
u_0 (Hawe)	0.15	-

Results and Discussion

The results from the test are shown in Figure D.5. This figure presents the pressure in chamber A (p_A), the pressure in chamber B (p_B), the low pass filtered pressure (p_X), the cylinder contraction (x_c), and the cylinder contraction speed (v_c) during the testing.
Test characteristics:

   Typical contraction velocity: About 17 $\frac{\text{mm}}{\text{s}}$ but a short oscillation at pressure change

   Overshoot: The pressure change results in an oscillation where the velocity first is increased, then reduced, and then settles

   Settling: Settles quickly after the pressure change

This test shows the contraction velocity is affected by the pressure change at the moment when the change is conducted. On the other hand is the velocity after the impact quickly stabilized at the same value as before the impact.
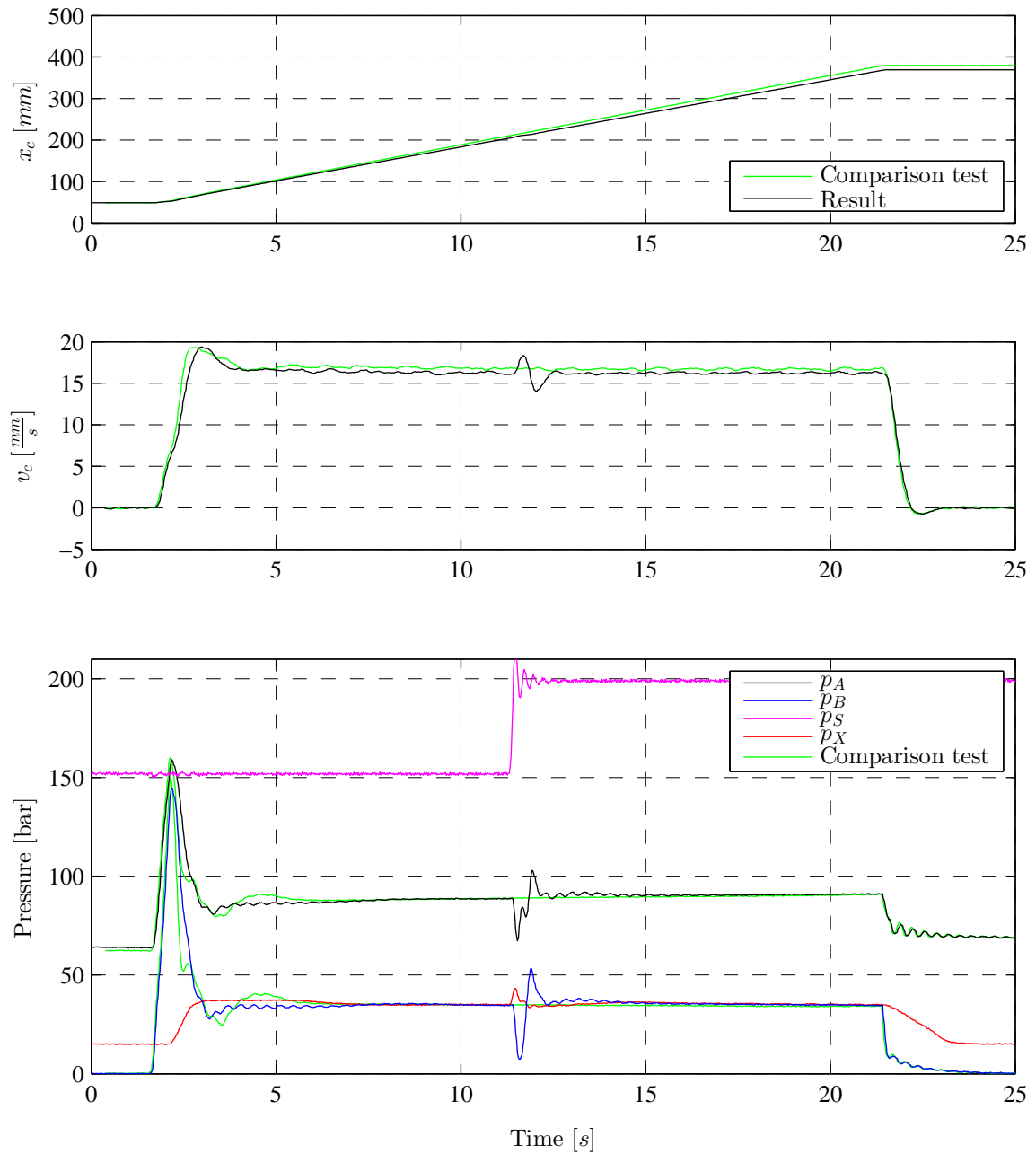
Figure D.5: Test 6 Setting 1

D.2 Setting 2

In this section are results from test 2, test 3, test 4, test 5 and test 6 for Setting 2 presented.

D.2.1 Test 2: High Cutoff Frequency

In this test is the cutoff frequency chosen to $f_c = 1000$. This is expected to be to high, meaning that the filter will not completely remove the oscillations and thereby send an oscillating pressure to the pressure compensator. Further conditions of this test are listed in Table D.6.

Table D.6: Parameters for the test of setting 2 with a high cutoff frequency

Test parameter	Value	Unit
Supply pressure	200	bar
Tank pressure	0	bar
Oil temperature	45	$^{\circ}C$
Total motion time	20.02	s
Rise time	0.01	s
Retardation time	0.01	s
Cutoff frequency, f_c	1000	Hz
Cutoff frequency, τ	0.000159	$\frac{\text{s}}{\text{rad}}$
u_0 (Danfoss)	0.1	-

Results and Discussion

The results from the test are shown in Figure D.6. This figure presents the pressure in chamber A (p_A), the pressure in chamber B (p_B), the low pass filtered pressure (p_X), the cylinder contraction (x_c), and the cylinder contraction speed (v_c) during the testing.
Test characteristics:

Typical contraction velocity: $17 \frac{\text{mm}}{\text{s}}$

Overshoot: none

Settling: Smooth motion

This test shows that an increase in the cutoff frequency for setting 2 results in a quick rise and a smooth motion. Some oscillations in the system pressures occurs for the first 4 seconds of the motion. The high cutoff frequency does, however, not introduce any oscillations in the motion for the system tested.
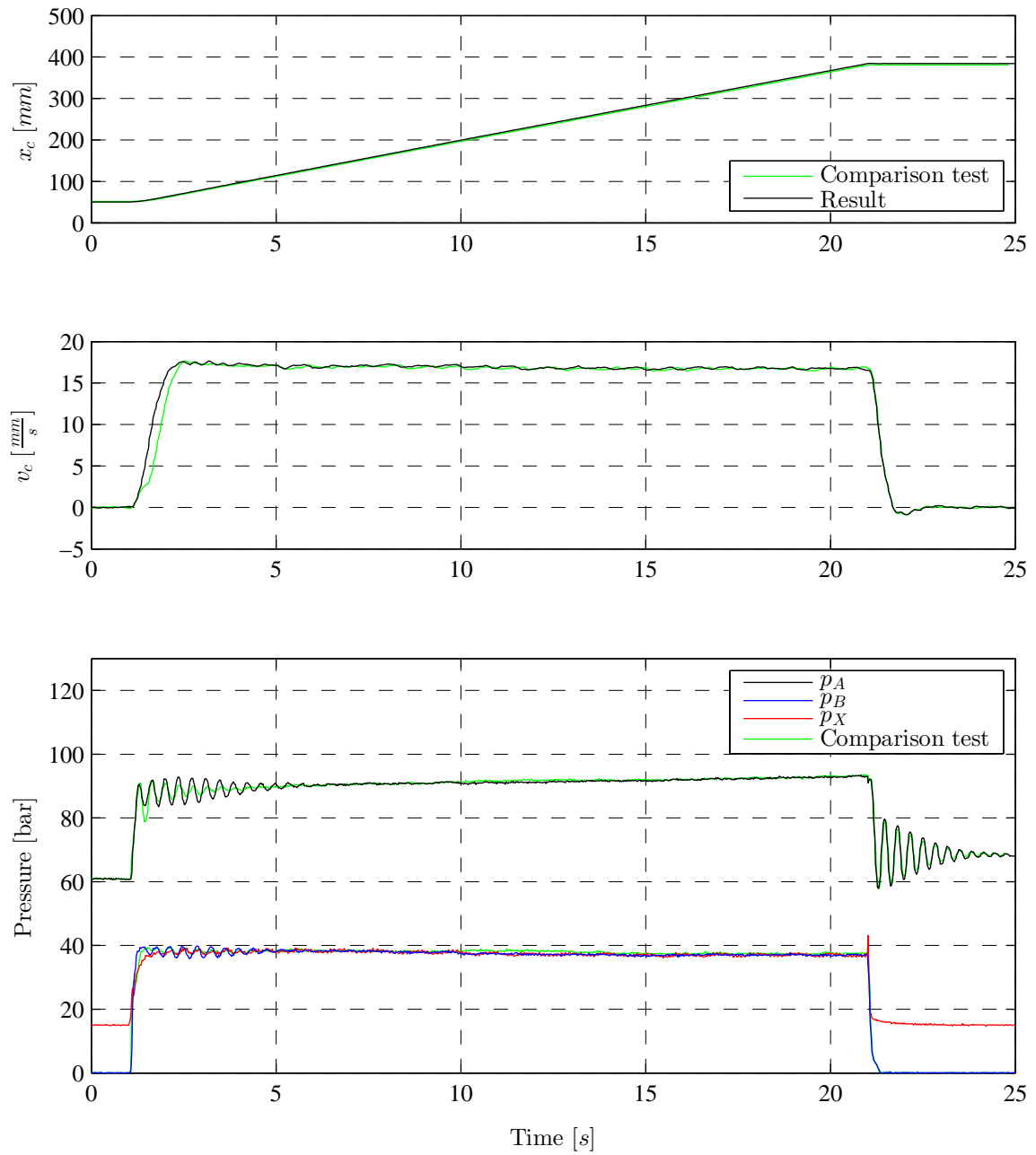
Figure D.6: Test 2 Setting 2

D.2.2 Test 3: Low Cutoff Frequency

In this test is the cutoff frequency chosen to $f_c = 0.1$. This is expected to be to low, meaning that the filter will not only remove the oscillations but also slow down pressure changes resulting in a stable but slow pressure compensator. Further conditions of this test are listed in Table D.7.

Table D.7: Parameters for the test of setting 2 with a low cutoff frequency

Test parameter	Value	Unit
Supply pressure	199	bar
Tank pressure	0	bar
Oil temperature	35	$^\circ C$
Total motion time	20.02	s
Rise time	0.01	s
Retardation time	0.01	s
Cutoff frequency, f_c	0.1	Hz
Cutoff frequency, τ	1.592	$\frac{\text{s}}{\text{rad}}$
u_0 (Danfoss)	0.1	-

Results and Discussion

The results from the test are shown in Figure D.7. This figure presents the pressure in chamber A (p_A), the pressure in chamber B (p_B), the low pass filtered pressure (p_X), the cylinder contraction (x_c), and the cylinder contraction speed (v_c) during the testing.
Test characteristics:

Typical contraction velocity: A slow rise up to 17 $\frac{\text{mm}}{\text{s}}$

Overshoot: none

Settling: A very slow but controlled rise

This test shows that a low cutoff frequency on setting 2 results in a slow rise in the velocity until the desired velocity is reached. The pressures in chamber A and chamber B oscillated during the start up. This might effect the stability of the motion in that section.
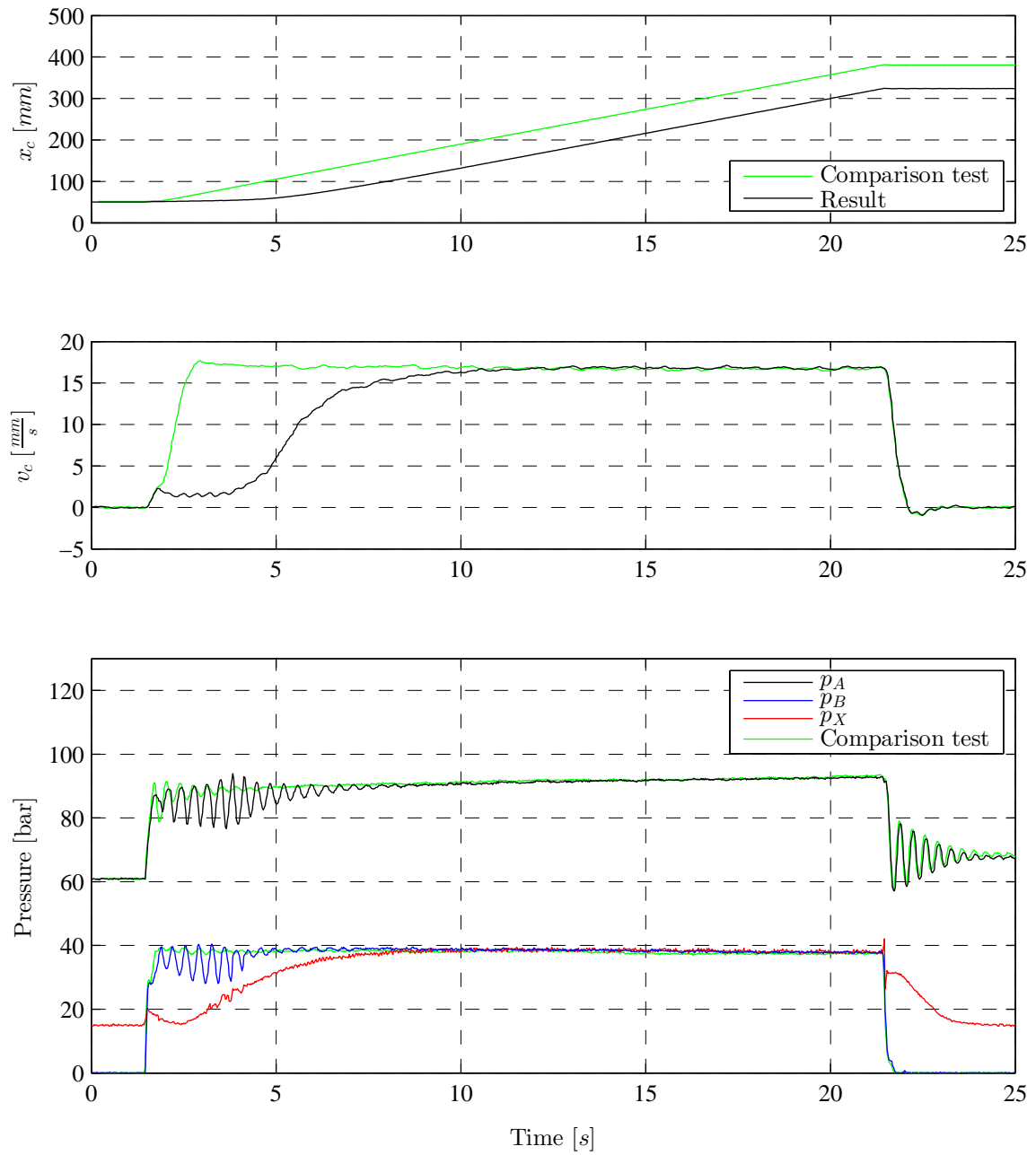
Figure D.7: Test 3 Setting 2

159

D.2.3   Test 4: Increase in Load

In this test is 77 kg added to the ballast stack to increase the load. The cutoff frequency is the same as in Chapter 7. Some higher system pressures are expected, but the system behavior through out the motion is expected to be stable. Further conditions of this test are listed in Table D.8.

Table D.8: Parameters for the test of setting 2 with a higher load

Test parameter	Value	Unit
Supply pressure	199	bar
Tank pressure	0	bar
Oil temperature	39	$^\circ C$
Total motion time	20.02	s
Rise time	0.01	s
Retardation time	0.01	s
Cut-off frequency, f_c	3	Hz
Cut-off frequency, τ	0.053	$\frac{\text{s}}{\text{rad}}$
u_0 (Danfoss)	0.1	-

Results and Discussion

The results from the test are shown in Figure D.8. This figure presents the pressure in chamber A (p_A), the pressure in chamber B (p_B), the low pass filtered pressure (p_X), the cylinder contraction (x_c), and the cylinder contraction speed (v_c) during the testing.
Test characteristics:

Typical contraction velocity: 19 $\frac{\text{mm}}{\text{s}}$

Overshoot: Almost none

Settling: A quick and stable rise

This test show that the stability of setting 2 is unaffected by the load enhancement. On the other hand is the cylinder contraction velocity affected. The test shows that the load is lowered with a higher velocity when the load in increased. The pressure in chamber A is also increased with a heavier load.
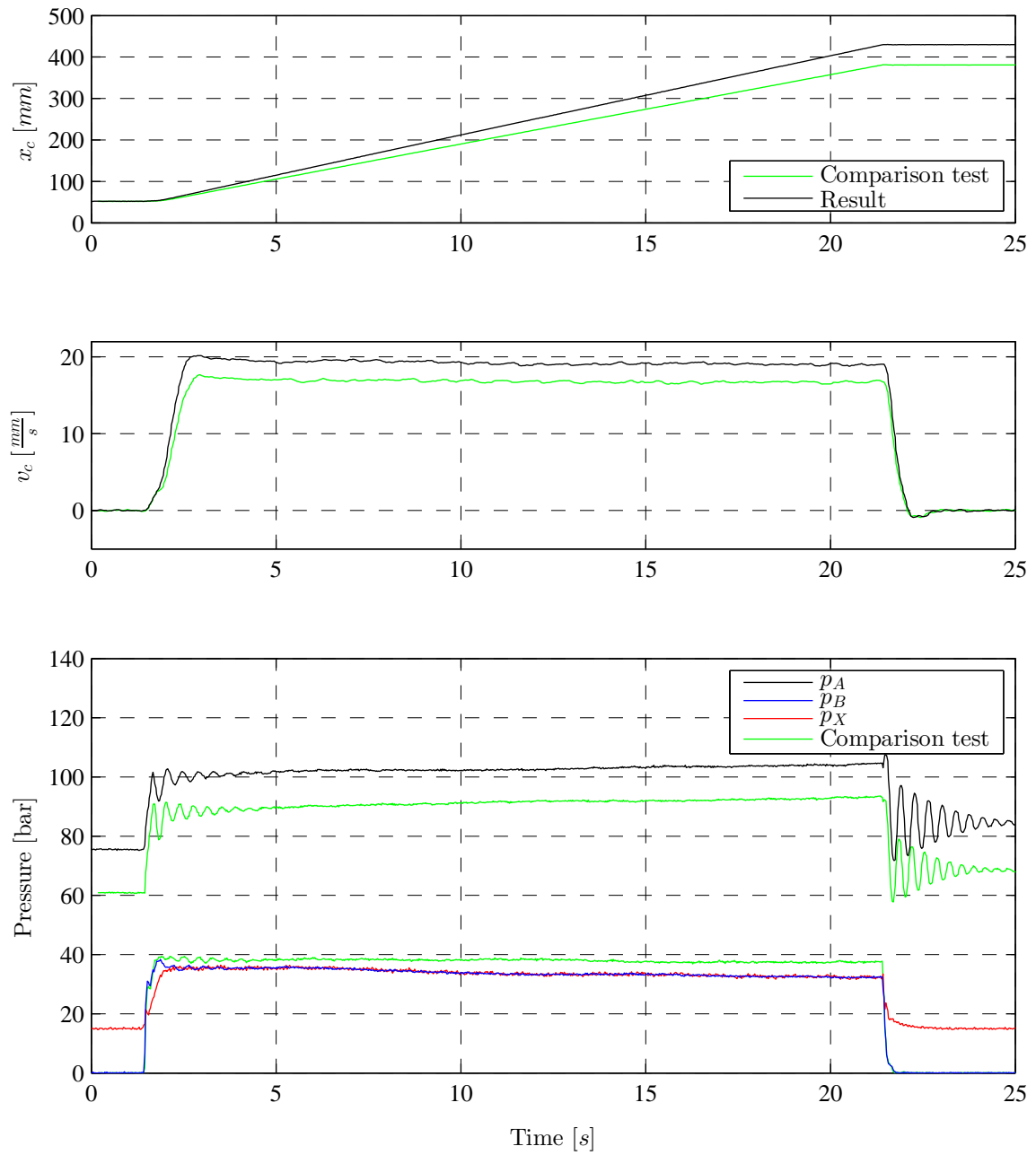
Figure D.8: Test 4 Setting 2

D.2.4 Test 5: Drop in Supply Pressure

In this test is the supply pressure quickly reduced from 200 bar to 150 bar during the motion. This test is carried out in order to map how this affects the stability of the lowering. Further conditions of this test is listed are Table D.9.

Table D.9: Parameters for the test of setting 2 with the supply pressure changed form 200 bar to 150 bar

Test parameter	Value	Unit
Supply pressure	$200 - 150$	bar
Tank pressure	0	bar
Oil temperature	38	$^\circ C$
Total motion time	20.02	s
Rise time	0.01	s
Retardation time	0.01	s
Cut-off frequency, f_c	3	Hz
Cut-off frequency, τ	0.053	$\frac{s}{rad}$
u_0 (Danfoss)	0.1	-

Results and Discussion

The results from the test are shown in Figure D.9. This figure presents the pressure in chamber A (p_A), the pressure in chamber B (p_B), the low pass filtered pressure (p_X), the cylinder contraction (x_c), and the cylinder contraction speed (v_c) during the testing.
Test characteristics:

Typical contraction velocity: About 17.5 $\frac{mm}{s}$ during the motion, with a short reduction at the moment of impact of the pressure change

Overshoot: The velocity is slowed down for a short period when the changes hits

Settling: Settles quickly after the pressure change

This test shows that the cylinder pressures are almost not affected by the change in supply pressure. The contraction velocity, on the other hand, are slightly reduced at the moment of impact of the pressure reduction.
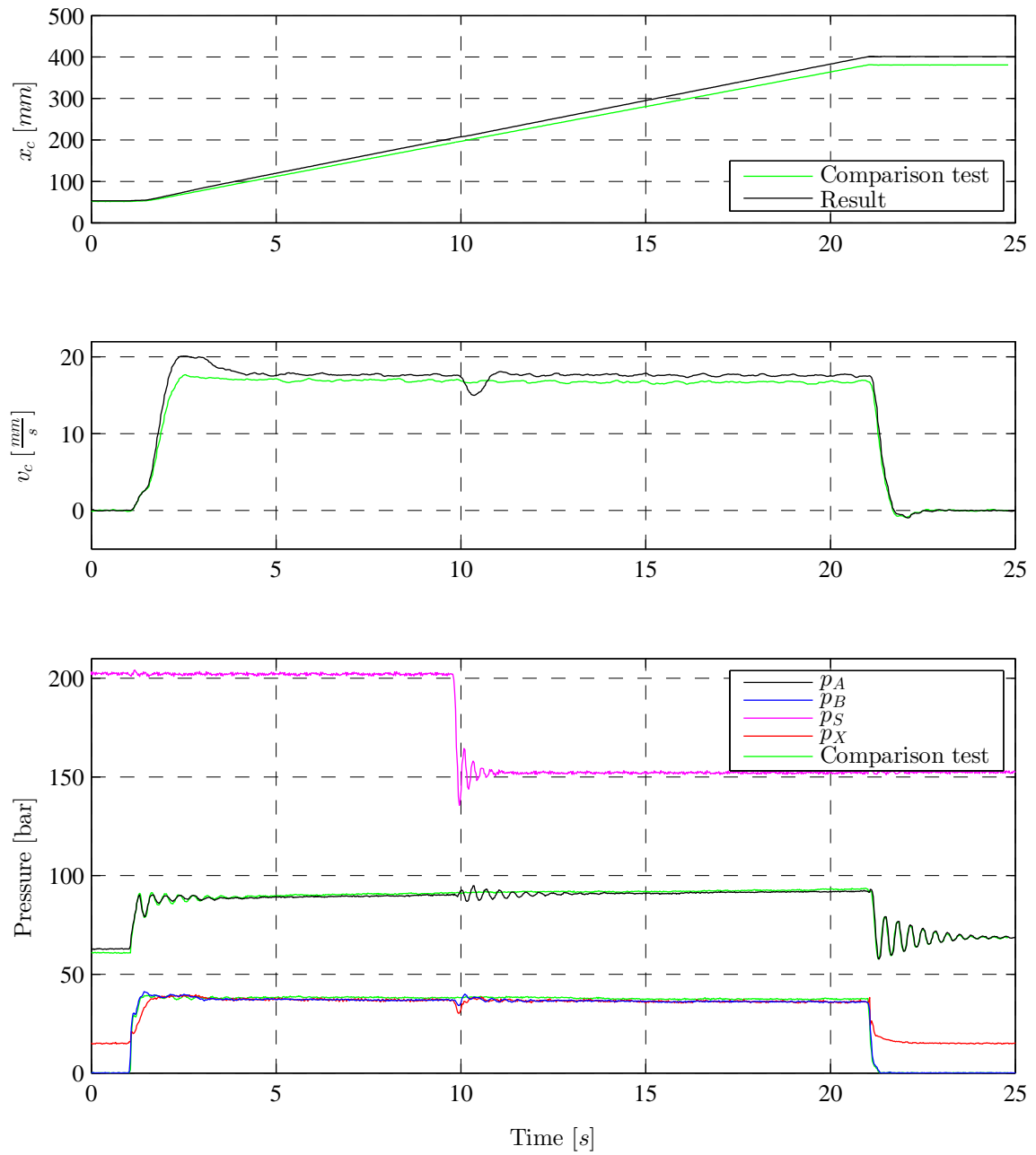
Figure D.9: Test 5 Setting 2

D.2.5   Test 6: Quick Increase of Supply Pressure

In this test is the supply pressure quickly increased from 150 bar to 200 bar during the motion. This test is carried out in order to map how this affects the stability of the lowering. Further conditions of this test are listed in Table D.10.

Table D.10: Parameters for the test of setting 2 with the supply pressure changed form 150 bar to 200 bar

Test parameter	Value	Unit
Supply pressure	$150 - 200$	bar
Tank pressure	0	bar
Oil temperature	38	$^\circ C$
Total motion time	20.02	s
Rise time	0.01	s
Retardation time	0.01	s
Cut-off frequency, f_c	3	Hz
Cut-off frequency, τ	0.053	$\frac{\text{s}}{\text{rad}}$
u_0 (Danfoss)	0.1	-

Results and Discussion

The results from the test are shown in Figure D.10. This figure presents the pressure in chamber A (p_A), the pressure in chamber B (p_B), the low pass filtered pressure (p_X), the cylinder contraction (x_c), and the cylinder contraction speed (v_c) during the testing.
Test characteristics:

Typical contraction velocity: About $17.5 \frac{\text{mm}}{\text{s}}$ with an increase in the velocity at the moment of impact of the pressure change

Overshoot: The velocity is increased for a short period when the pressure change hits

Settling: Settles quickly after the pressure change

This test shows that setting 2 is little affected by the pressure change. Some disturbance in the velocity does occur at the moment of impact of the pressure change.
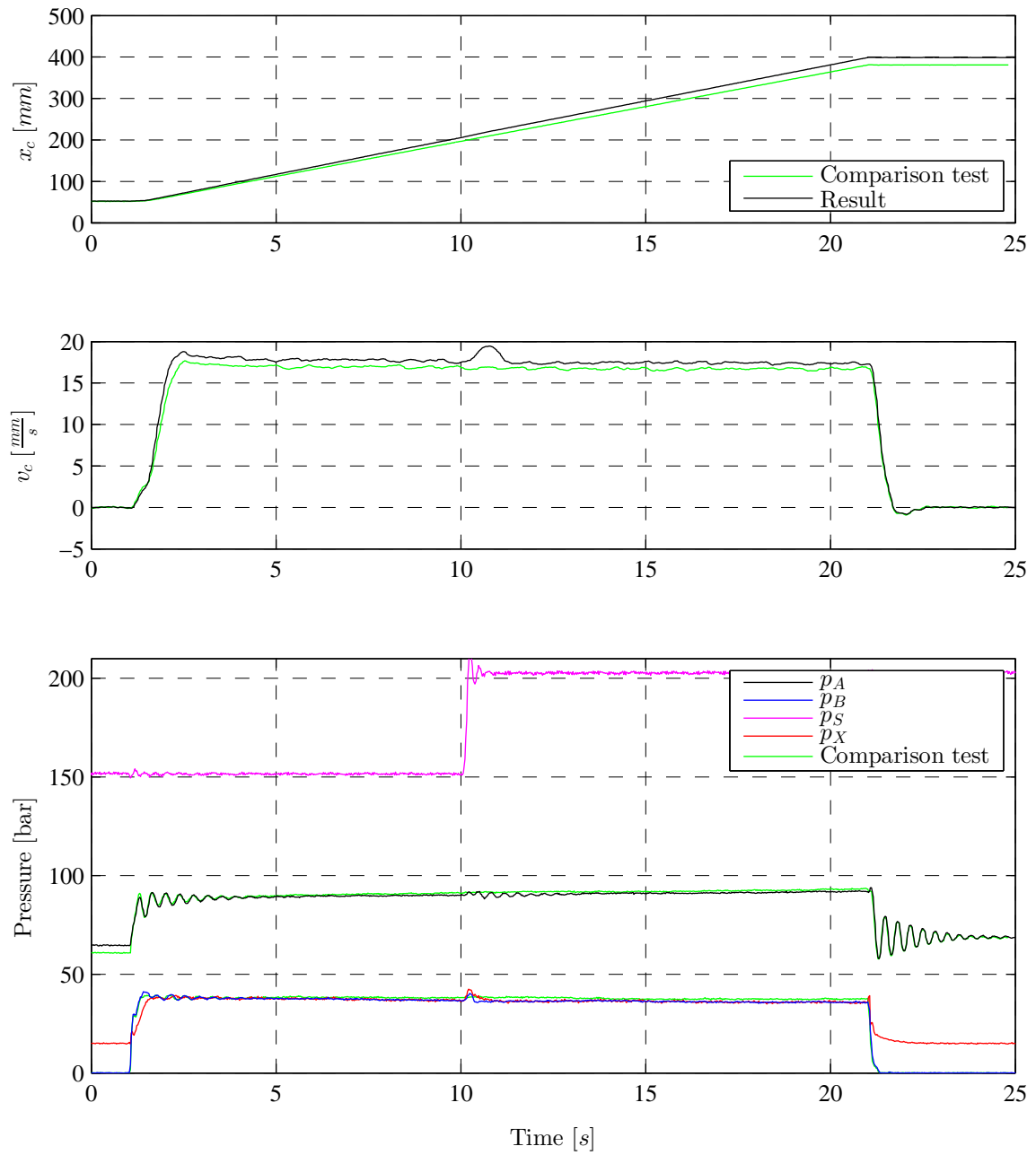
Figure D.10: Test 6 Setting 2

D.3 Setting 3

In this section are results from test 2, test 3, test 4, test 5 and test 6 for Setting 3 presented.

D.3.1 Test 2: High Cutoff Frequency

In this test is the cutoff frequency chosen to $f_c = 3$. This is expected to be to high, meaning that the filter will not completely remove the oscillations and thereby send an oscillating pressure to the pilot line of the CBV and the pressure compensator. Further conditions of this test are listed in Table D.11.

Table D.11: Parameters for the test of setting 3 with a high cutoff frequency

Test parameter	Value	Unit
Supply pressure	199	bar
Tank pressure	0	bar
Oil temperature	38	$°C$
Total motion time	20.02	s
Rise time	0.01	s
Retardation time	0.01	s
Cutoff frequency, f_c	3	Hz
Cutoff frequency, τ	0.053	$\frac{\text{s}}{\text{rad}}$
u_0 (Danfoss)	0.1	-

Results and Discussion

The results from the test are shown in Figure D.11. This figure presents the pressure in chamber A (p_A), the pressure in chamber B (p_B), the low pass filtered pressure (p_X), the cylinder contraction (x_c), and the cylinder contraction speed (v_c) during the testing.
Test characteristics:

Typical contraction velocity: A long oscillatory section in the beginning of the motion at about 16 $\frac{\text{mm}}{\text{s}}$ followed by a stable section at about 17 $\frac{\text{mm}}{\text{s}}$

Overshoot: The peak of the overshoot in the velocity is low but frequent

Settling: Oscillatory through the first half of the motion. Settles very late.

This test shows that a high cutoff frequency for setting 3 makes the system react quicker but also makes the system unstable for large parts of the motion. The high cutoff frequency makes the compensator in the DCV react quicker which makes the system response good. On the other are there still oscillations in the pilot pressure which makes the system oscillatory.
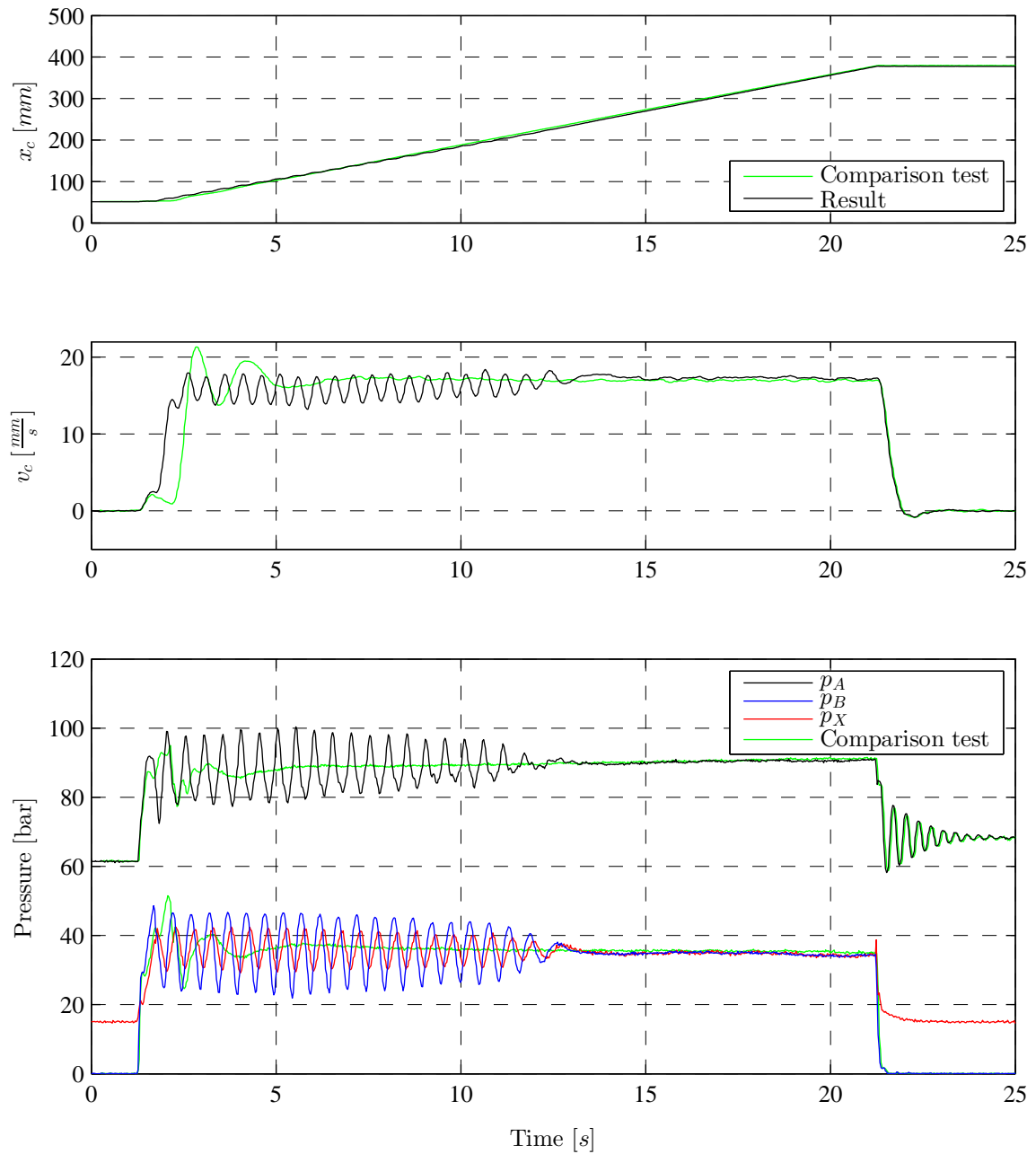
Figure D.11: Test 2 Setting 3

D.3.2 Test 3: Low Cutoff Frequency

In this test is the cutoff frequency chosen to $f_c = 0.01$. This is expected to be to low, meaning that the filter will not only remove the oscillations but also slow down pressure changes resulting in a stable but slow pressure compensator and CBV. Further conditions of this test are listed in Table D.12.

Table D.12: Parameters for the test of setting 3 with a low cutoff frequency

Test parameter	Value	Unit
Supply pressure	199	bar
Tank pressure	0	bar
Oil temperature	38	$°C$
Total motion time	20.02	s
Rise time	0.01	s
Retardation time	0.01	s
Cutoff frequency, f_c	0.01	Hz
Cutoff frequency, τ	15.92	$\frac{s}{rad}$
u_0 (Danfoss)	0.1	-

Results and Discussion

The results from the test are shown in Figure D.12. This figure presents the pressure in chamber A (p_A), the pressure in chamber B (p_B), the low pass filtered pressure (p_X), the cylinder contraction (x_c), and the cylinder contraction speed (v_c) during the testing.
Test characteristics:

Typical contraction velocity: A very slow rise up to 17 $\frac{mm}{s}$ at the end of the motion.

Overshoot: None

Settling: Settles at the very end of the motion

This test shows that a low cutoff frequency makes setting 3 react very slow. The low cutoff frequency makes both the CBV and the DCV open slow but steady. The system does therefore react very slow but the motion is smooth and steady.
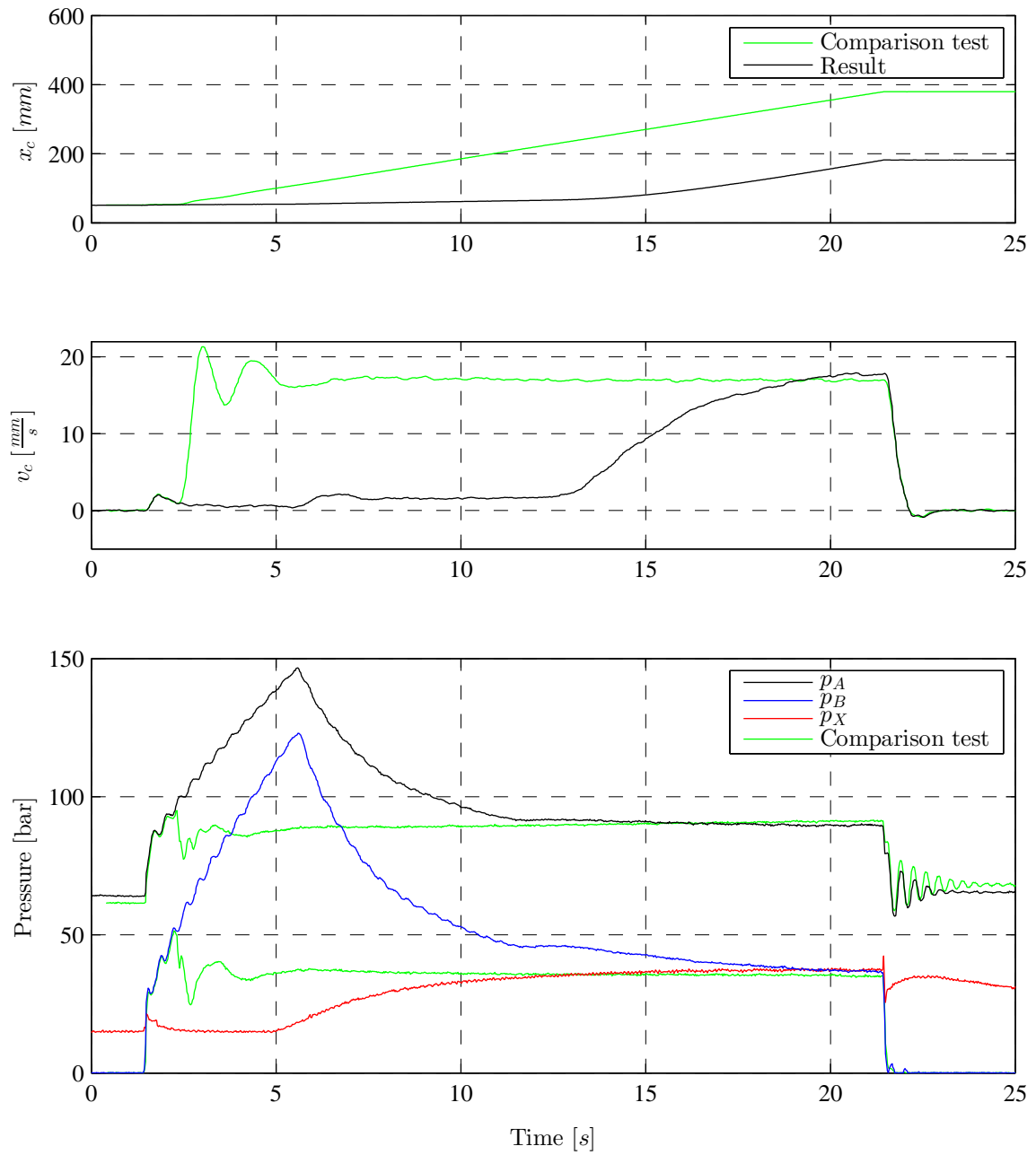
Figure D.12: Test 3 Setting 3

D.3.3   Test 4: Increase in load

In this test is 77 kg added to the ballast stack to increase the load. The cutoff frequency is the same as in Chapter 7. Some higher system pressures are expected, but the system behavior through out the motion is expected to be stable. Further conditions of this test are listed in Table D.13.

Table D.13: Parameters for the test of setting 3 with a higher load

Test parameter	Value	Unit
Supply pressure	200	bar
Tank pressure	0	bar
Oil temperature	39	$^{\circ}C$
Total motion time	20.02	s
Rise time	0.01	s
Retardation time	0.01	s
Cut-off frequency, f_c	0.6	Hz
Cut-off frequency, τ	0.265	$\frac{\text{s}}{\text{rad}}$
u_0 (Danfoss)	0.1	-

Results and Discussion

The results from the test are shown in Figure D.13. This figure presents the pressure in chamber A (p_A), the pressure in chamber B (p_B), the low pass filtered pressure (p_X), the cylinder contraction (x_c), and the cylinder contraction speed (v_c) during the testing.
Test characteristics:

Typical contraction velocity: An oscillatory start which stabilizes at about 17 $\frac{\text{mm}}{\text{s}}$

Overshoot: High overshoot in the start of the motion

Settling: A quite long oscillatory start which then settles

This test shows that setting 3 gets an oscillatory start. These oscillations are on the other hand also present in the satisfactory stable test. Further shows the test results that the contraction speed is almost unaffected by the load enhancement. The pressure in chamber A is increased with a heavier load.
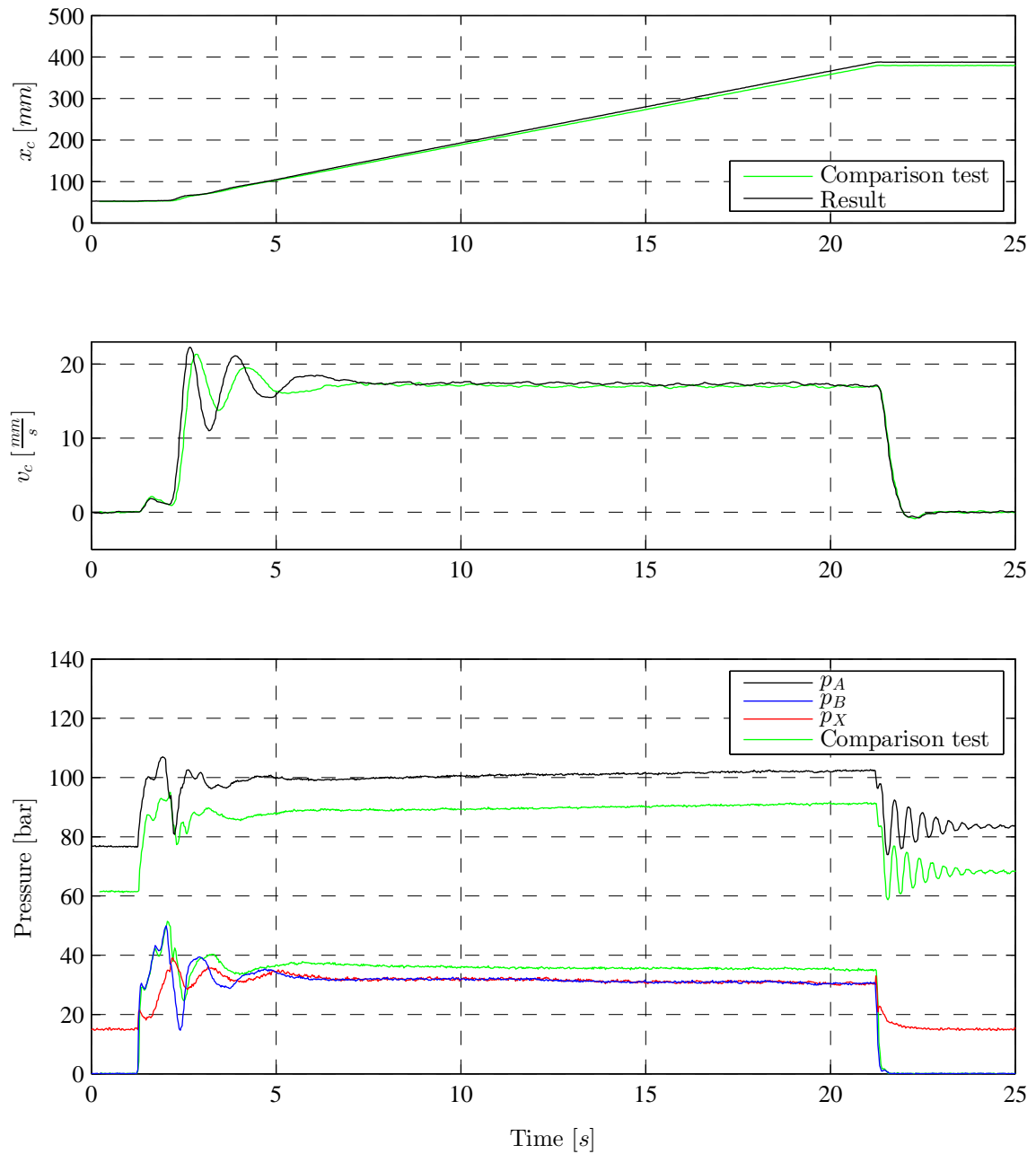
Figure D.13: Test 4 Setting 3

D.3.4   Test 5: Drop in Supply Pressure

In this test is the supply pressure quickly reduced from 200 bar to 150 bar during the motion. This test is carried out in order to map how this affects the stability of the lowering. Further conditions of this test are listed in Table D.14.

Table D.14: Parameters for the test of setting 3 with the supply pressure changed form 200 bar to 150 bar

Test parameter	Value	Unit
Supply pressure	$200 - 150$	bar
Tank pressure	0	bar
Oil temperature	38	$°C$
Total motion time	20.02	s
Rise time	0.01	s
Retardation time	0.01	s
Cut-off frequency, f_c	0.6	Hz
Cut-off frequency, τ	0.265	$\frac{s}{rad}$
u_0 (Danfoss)	0.1	-

Results and Discussion

The results from the test are shown in Figure D.14. This figure presents the pressure in chamber A (p_A), the pressure in chamber B (p_B), the low pass filtered pressure (p_X), the cylinder contraction (x_c), and the cylinder contraction speed (v_c) during the testing.
Test characteristics:

Typical contraction velocity: About $17 \frac{mm}{s}$ with some oscillations in the initial phase and at the moment of impact of the pressure change

Overshoot: The pressure change makes the velocity oscillate some

Settling: Settles about 3 seconds after the pressure change

This test shows that setting 3 oscillates at the moment of impact of the pressure reduction but stabilizes after some seconds.
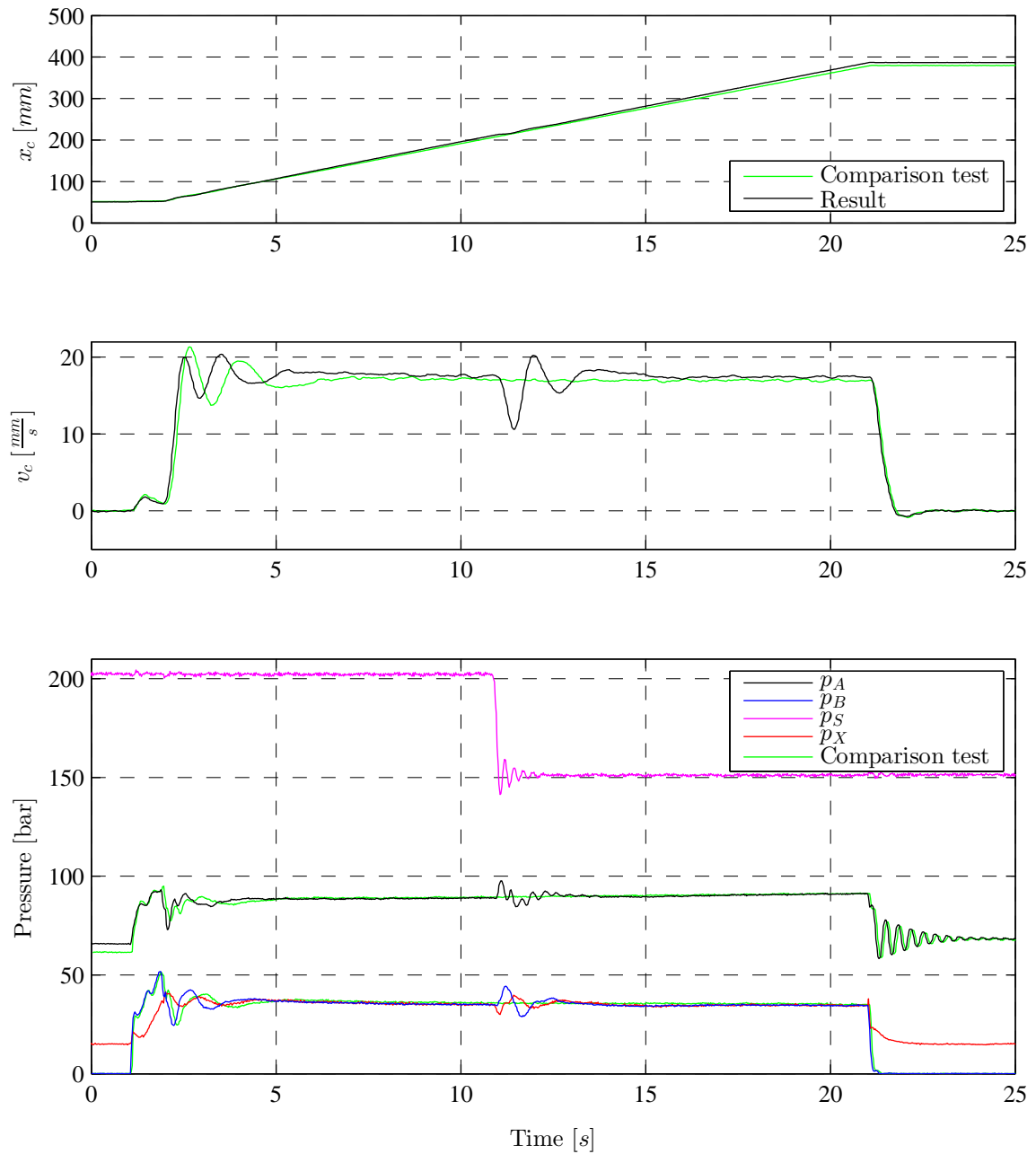
Figure D.14: Test 5 Setting 3

D.3.5   Test 6: Quick Increase of Supply Pressure

In this test is the supply pressure quickly increased from 150 bar to 200 bar during the motion. This test is carried out in order to map how this affects the stability of the lowering. Further conditions of this test are listed in Table D.15.

Table D.15: Parameters for the test of setting 3 with the supply pressure changed form 150 bar to 200 bar

Test parameter	Value	Unit
Supply pressure	$150 - 200$	bar
Tank pressure	0	bar
Oil temperature	38	$°C$
Total motion time	20.02	s
Rise time	0.01	s
Retardation time	0.01	s
Cut-off frequency, f_c	0.6	Hz
Cut-off frequency, τ	0.265	$\frac{s}{rad}$
u_0 (Danfoss)	0.1	-

Results and Discussion

The results from the test are shown in Figure D.15. This figure presents the pressure in chamber A (p_A), the pressure in chamber B (p_B), the low pass filtered pressure (p_X), the cylinder contraction (x_c), and the cylinder contraction speed (v_c) during the testing.
Test characteristics:

Typical contraction velocity: About $17\,\frac{mm}{s}$ with some oscillations in the initial phase and at the moment of impact of the pressure change

Overshoot: The pressure change makes the velocity oscillate with a high amplitude

Settling: Settles about 5 seconds after the pressure change

This test shows that setting 3 oscillates at the moment of impact of the pressure increase. The velocity oscillations gets a quite high amplitude but is stabilized after about 5 seconds.
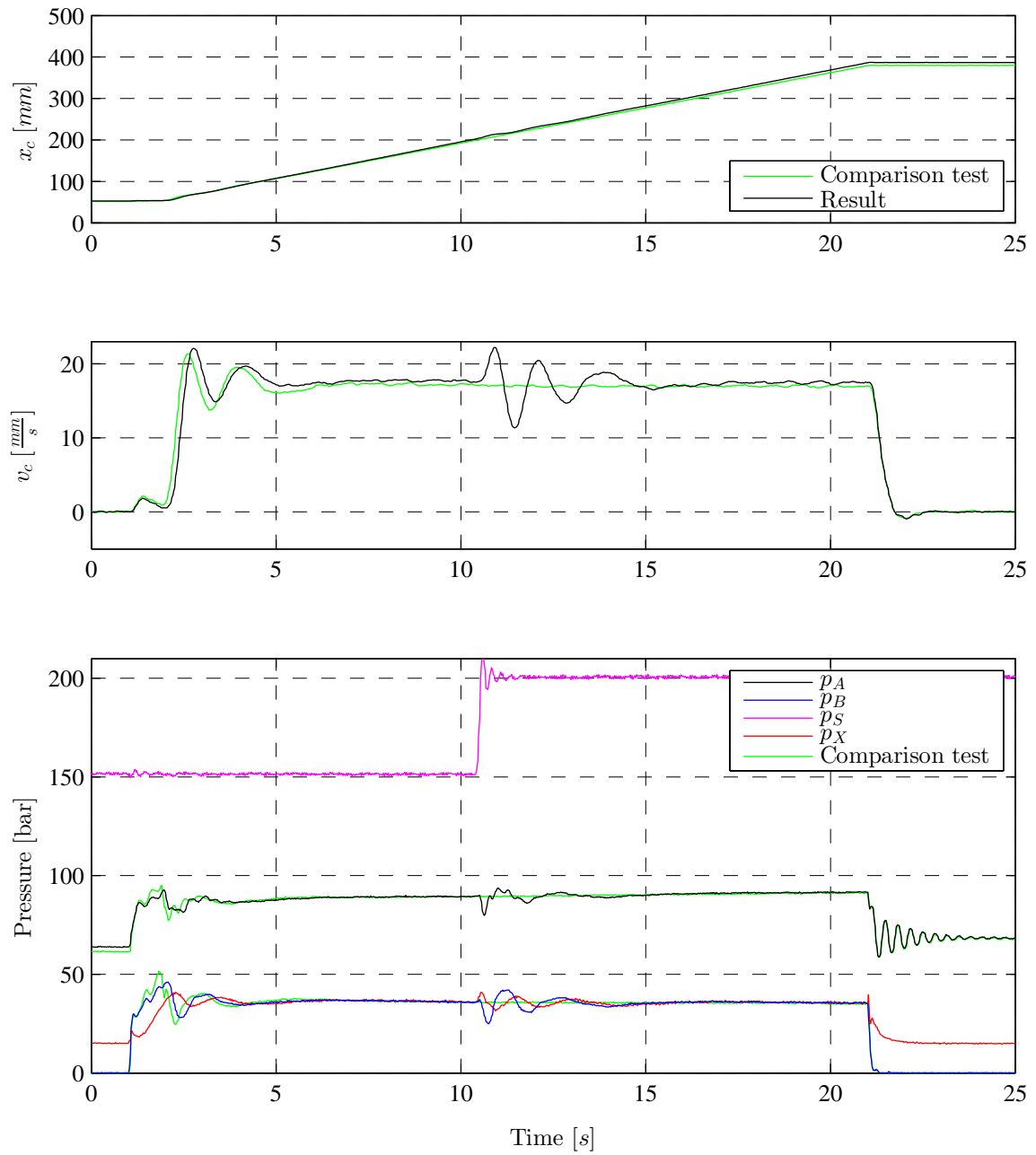
Figure D.15: Test 6 Setting 3

Appendix E

Interview sheets

Interview sheet #1 Setting:1

Oil temp = 47°C

$\eta = 1{,}591$ $f_c = 0{,}1$

Candidate's Name: Jan Andreas Holm

- Address: Subbernes, 4780 Brekkesto

- Telephone number: +47 905 36 905

- Email address: janateig @ online.no

Interviewed By: Rune Husveg

Date/Place: 11/05-2015 / UiA

- Short: what is your profession, how experienced would you say you are as a crane operator, and what type of cranes are you experienced with?

Chief Engineer Hydraulics Mechatronic lab.
Excavators, offshore- and onshore cranes, Roughnecks etc

- How would you describe the stability of the crane?

Satisfactory

- How would you describe the response time of the crane?

Satisfactory

- How would you describe the speed of the crane?

Satisfactory

- How would you describe the over all feeling of the crane?

Satisfactory

- Comments and suggestions:

Candidate's signature: Jan A. Holm

Interviewer's signature: Rune Husveg

Interview sheet #2 Setting: 2

Oil temp = 33°C

~~Viscosity~~ , ~~temp~~

Candidate's Name: Jan A. Holm $x = 0,053$, $f_c = 3$

- Address: Subbernes, 4780 Brekkestø

- Telephone number: +47 905 36 905

- Email address: janateig@online.no

Interviewed By: Rune Husveg

Date/Place: 06.05.2015 / Via

- Short: what is your profession, how experienced would you say you are as a crane operator, and what type of cranes are you experienced with?

Chief Engineer Hydraulics & Mechatronics lab ViA.
Excavators, offshore - and onshore cranes

- How would you describe the stability of the crane?

Satisfactory

- How would you describe the response time of the crane?

Satisfactory

- How would you describe the speed of the crane?

Satisfactory (prop. valve functioned very well)

- How would you describe the over all feeling of the crane?

Total control over the situation / in load case.

- Comments and suggestions:

Candidate's signature: Jan A. Holm

Interviewer's signature: Rune Husveg

Interview sheet #3 Setting:3

$Oil\ temp = 34°C$

$\chi = 0,265 \qquad f_c = 0,6$

Candidate's Name: Jan Andreas Holm

- Address: Subbernes, 4700 Brekkestø

- Telephone number: + 47 905 36 905

- Email address: janakig @ online.no

Interviewed By: Rune Husveg

Date/Place: 06/05/15 ; UiA

- Short: what is your profession, how experienced would you say you are as a crane operator, and what type of cranes are you experienced with?

Chief Engineer Hydraulics Mechatronic lab UiA
Excavators, offshore - and onshore cranes

- How would you describe the stability of the crane?

Satisfactory

- How would you describe the response time of the crane?

Command down: Delay at startup but 100% responsive when variations in command

- How would you describe the speed of the crane?

Satisfactory for marine (onshore) operations but not for offshore operations.

- How would you describe the over all feeling of the crane?

Satisfactory

- Comments and suggestions:

Candidate's signature: Jan A. Holm

Interviewer's signature: Rune Husveg

Interview sheet #4 Setting:1

$Oil\ temp = 24°C$

$\gamma = 1,591$, $f_c = 0,1$

Candidate's Name: Steve Schading

- Address: U.A

- Telephone number:

- Email address: steve.schading@uia.no

Interviewed By: Rune Husveg

Date/Place: 7/5. 2015 UiA Grimstad

- Short: what is your profession, how experienced would you say you are as a crane operator, and what type of cranes are you experienced with?

Profession: senior engineer for renewable energies
→ experience with overhead cranes

- How would you describe the stability of the crane?

→ stability feels quite good in comparison to the arm-length

- How would you describe the response time of the crane?

→ very good → exellent possibility to change position of the arm in a very accurate way

- How would you describe the speed of the crane?

→ speed is ok → very good and smooth

- How would you describe the over all feeling of the crane?

→ very good - nothing else to mention

- Comments and suggestions:

→ would be good if speed would adjust automaticaly to lower and very low speed while adjusting arm position down shortly before reaching lowest position

Candidate's signature:

Interviewer's signature:

Rune Husveg

Interview sheet #5 Setting:2

Oil temp $= 34\,^{\circ}C$
$z = 0,053$ $fc = 3$

Candidate's Name: Steve Schading

- Address: 4,17

- Telephone number:

- Email address: steve.schading @ uia.no

Interviewed By: Rune Husveg

Date/Place: 7/5. 2015   UiA   Grimstad

- Short: what is your profession, how experienced would you say you are as a crane operator, and what type of cranes are you experienced with?

  See sheet #4

- How would you describe the stability of the crane?

  good in upwards movement → more unstable in downwards movement. Quite big swinging after downwards movement

- How would you describe the response time of the crane?

  response time is fast but still not very comftable than in the very first setup

- How would you describe the speed of the crane?

  depending on usage speed is a little to high to feel comftable

- How would you describe the over all feeling of the crane?

  nearly like in setup nr:3 but as named before not that good than in setup nr. 1

- Comments and suggestions:

  ⇒ setup 1 was most comftable in stability, speed, response time and overall feeling

Candidate's signature:

Interviewer's signature:

Rune Husveg

Interview sheet #6 Setting:3

Oil temp = 31 °C

$\gamma = 0,265$ $f_c = 0,6$

Candidate's Name: Steve Schading

- Address: UiA

- Telephone number:

- Email address: steve.schading@uia.no

Interviewed By: Rune Husveg

Date/Place: 7/5.2015   UiA Grimstad

- Short: what is your profession, how experienced would you say you are as a crane operator, and what type of cranes are you experienced with?

  See sheet #4

- How would you describe the stability of the crane?

  Less stability than before especially while lowering of crane-arm. Upwards adjustment is still ok.

- How would you describe the response time of the crane?

  response of the arm is faster than before as same as movement speed, so it is more difficult to "fine"-adjust arm-position

- How would you describe the speed of the crane?

  quite high speed, which makes it more difficult to handle the crane → swings more than before

- How would you describe the over all feeling of the crane?

  still quite good, but not that comftable than before

- Comments and suggestions:

  problems in stopp at lowest position are bigger than before → very hard stopp and course of that bigger swinging of the arm

Candidate's signature:

Interviewer's signature:
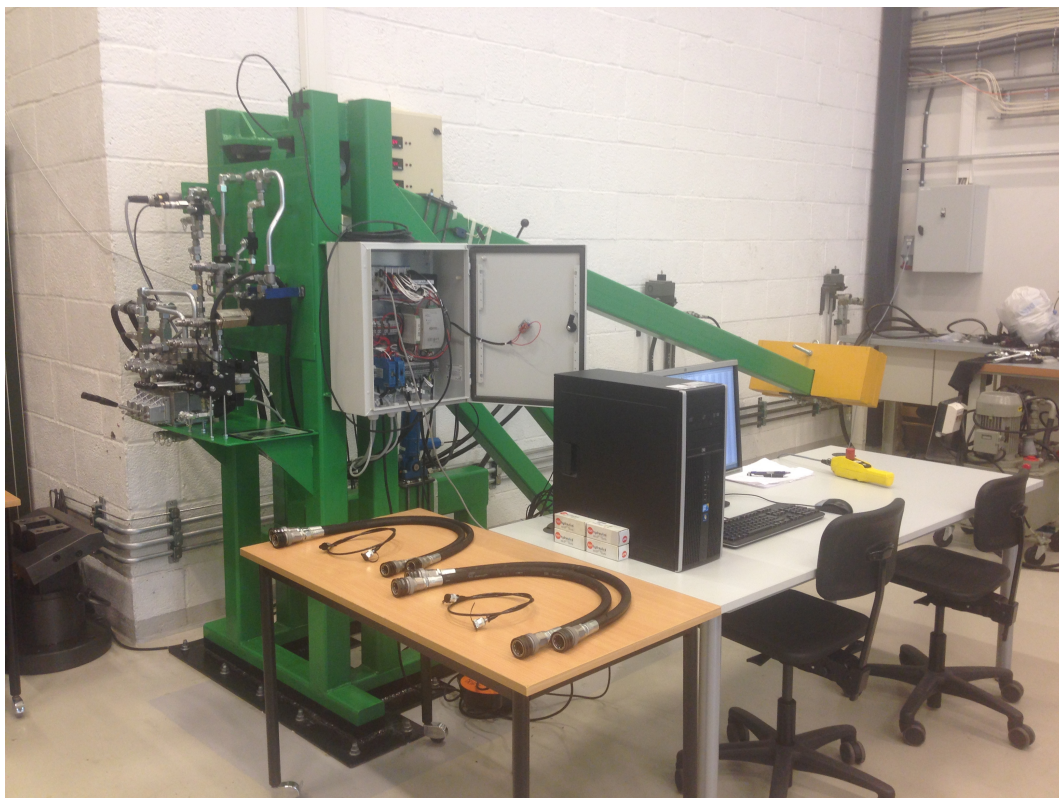
Rune Husveg

Appendix F

Pictures of the Test Rig
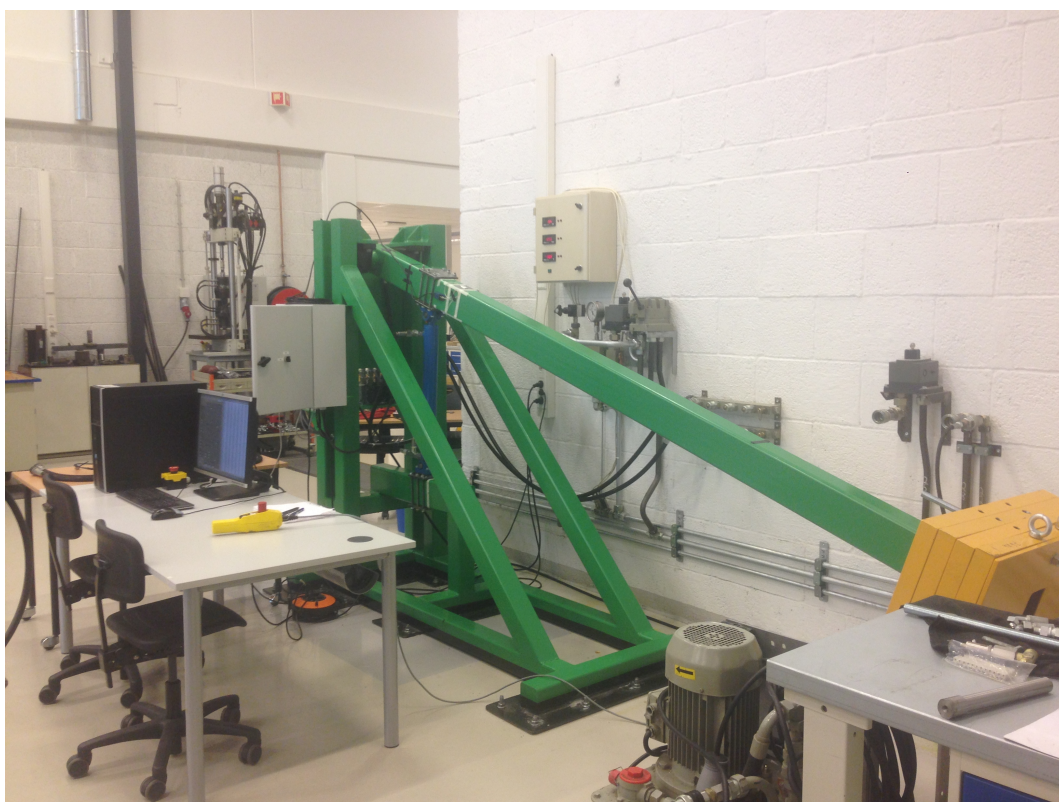
Figure F.1: Test rig overview 1
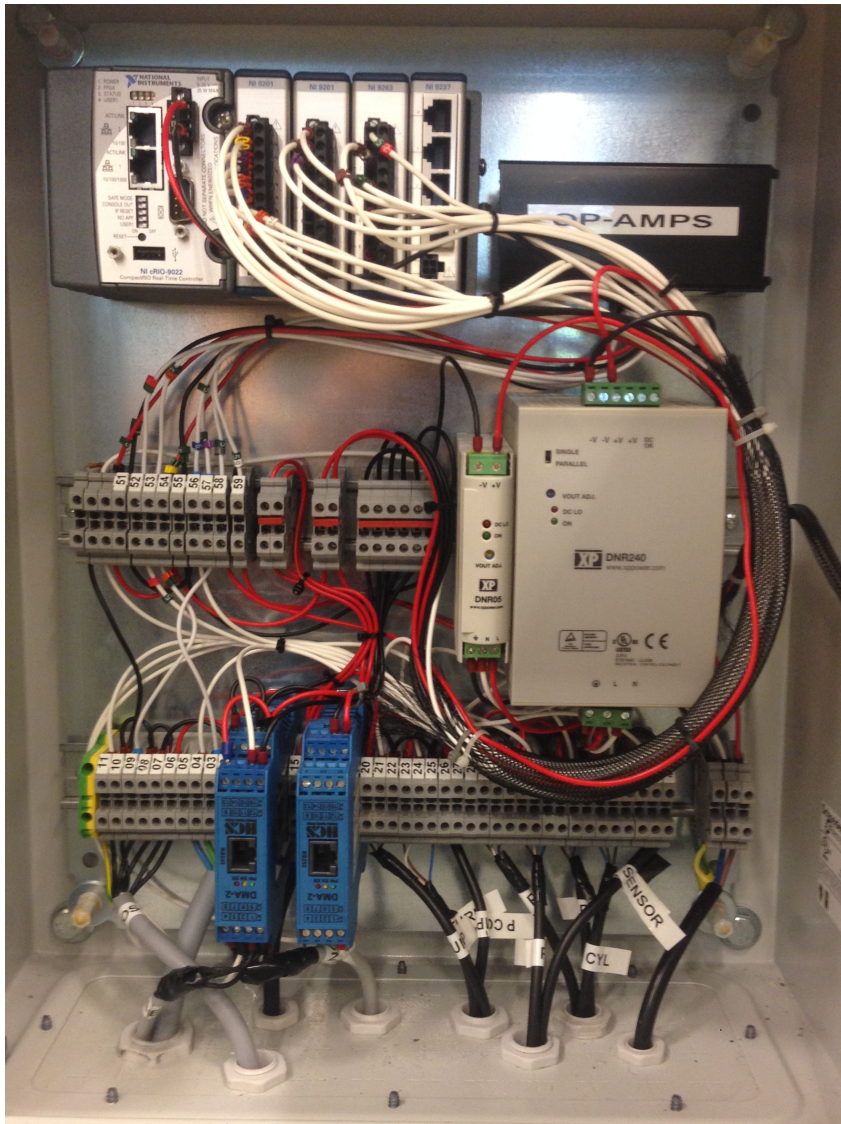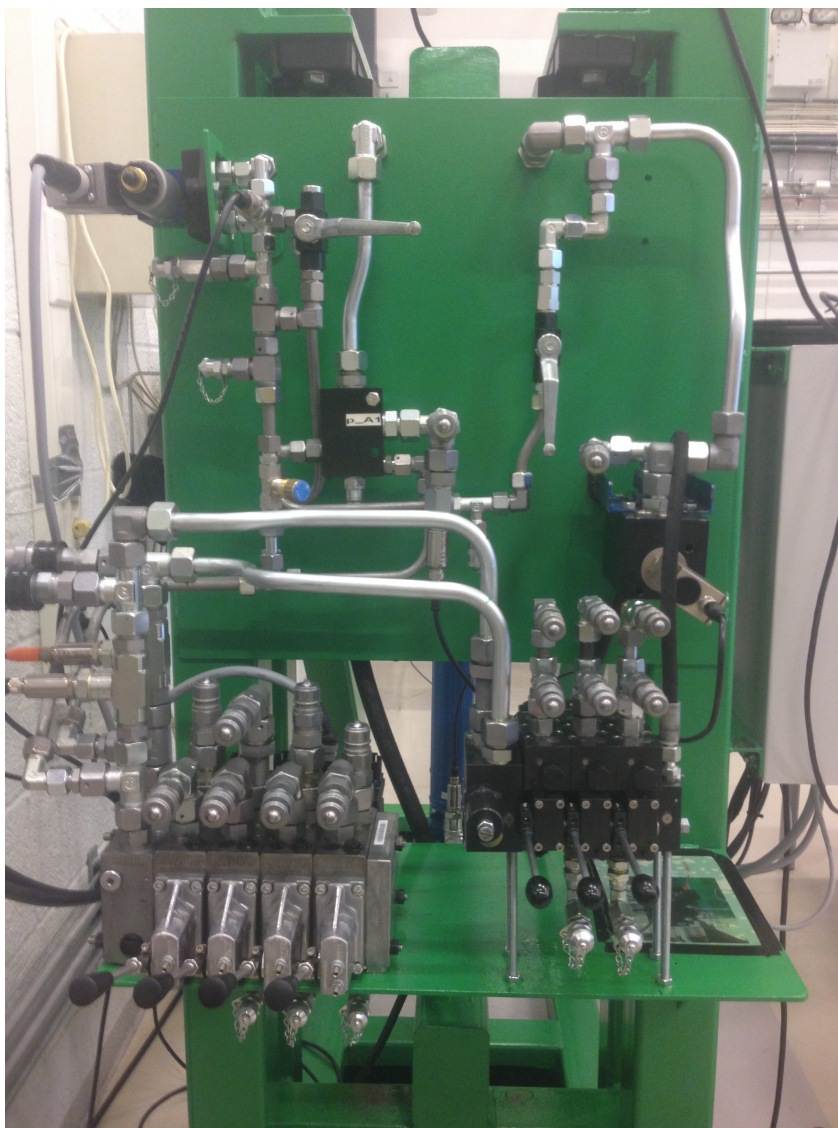

Figure F.2: Test rig overview 2

Figure F.3: Electrical cabinet

Figure F.4: Hydraulic components